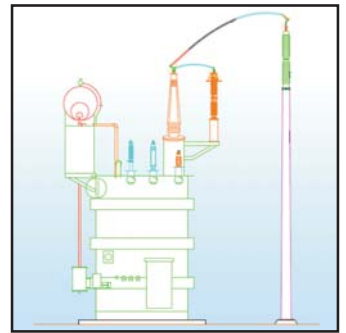
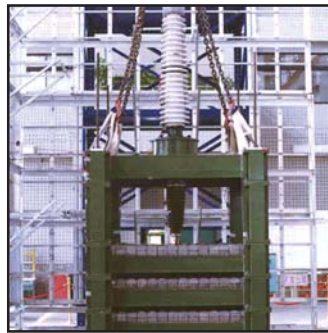
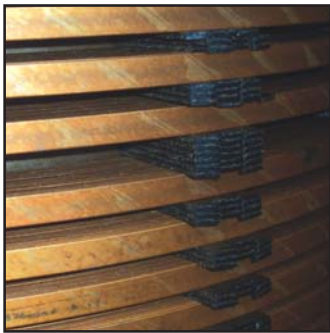


Seismic Evaluation and Rehabilitation of Critical Components of Electrical Power Systems

by
Selahattin Ersoy, Bakhtiar Feizi, Ali Ashrafi and
M. Ala Saadeghvaziri



Technical Report MCEER-08-0011

March 17, 2008

NOTICE

This report was prepared by the New Jersey Institute of Technology as a result of research sponsored by MCEER through a grant from the Earthquake Engineering Research Centers Program of the National Science Foundation under NSF award number EEC-9701471 and other sponsors. Neither MCEER, associates of MCEER, its sponsors, the New Jersey Institute of Technology, nor any person acting on their behalf:

- a. makes any warranty, express or implied, with respect to the use of any information, apparatus, method, or process disclosed in this report or that such use may not infringe upon privately owned rights; or
- b. assumes any liabilities of whatsoever kind with respect to the use of, or the damage resulting from the use of, any information, apparatus, method, or process disclosed in this report.

Any opinions, findings, and conclusions or recommendations expressed in this publication are those of the author(s) and do not necessarily reflect the views of MCEER, the National Science Foundation, or other sponsors.

Seismic Evaluation and Rehabilitation of Critical Components of Electrical Power Systems

by

Selahattin Ersoy,¹ Bakhtiar Feizi,² Ali Ashrafi³ and M. Ala Saadeghvaziri⁴

Publication Date: March 17, 2008
Submittal Date: February 8, 2008

Technical Report MCEER-08-0011

Task Number 10.1.1

NSF Master Contract Number EEC 9701471

- 1 Technical Director, Rua Engineering, Istanbul, Turkey; Former Ph.D. Student, Department of Civil and Environmental Engineering, New Jersey Institute of Technology
- 2 Ph.D. Student, Department of Civil and Environmental Engineering, New Jersey Institute of Technology
- 3 Senior Engineer, Thornton Tomasetti, New York, NY; Former Ph.D. Student, Department of Civil and Environmental Engineering, New Jersey Institute of Technology
- 4 Professor, Department of Civil and Environmental Engineering, New Jersey Institute of Technology

MCEER

University at Buffalo, The State University of New York

Red Jacket Quadrangle, Buffalo, NY 14261

Phone: (716) 645-3391; Fax (716) 645-3399

E-mail: mceer@buffalo.edu; WWW Site: <http://mceer.buffalo.edu>

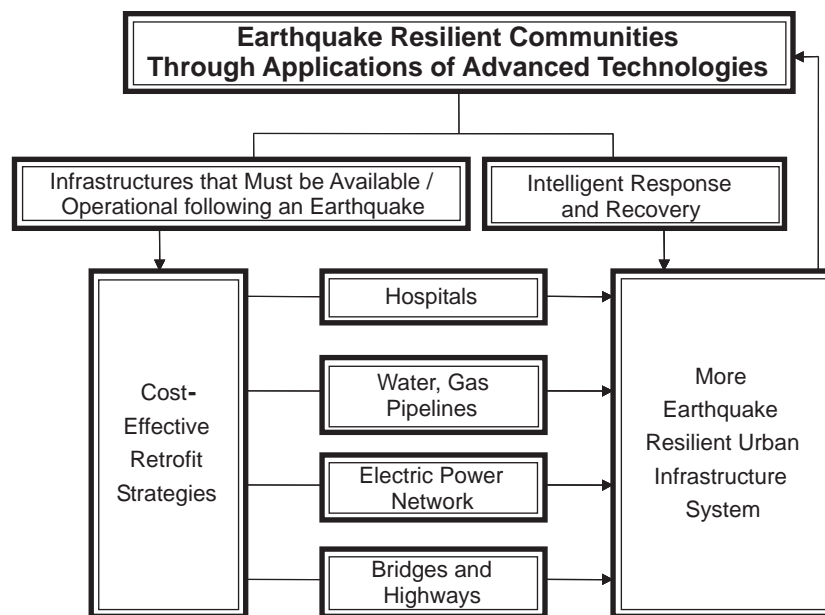
Preface

The Multidisciplinary Center for Earthquake Engineering Research (MCEER) is a national center of excellence in advanced technology applications that is dedicated to the reduction of earthquake losses nationwide. Headquartered at the University at Buffalo, State University of New York, the Center was originally established by the National Science Foundation in 1986, as the National Center for Earthquake Engineering Research (NCEER).

Comprising a consortium of researchers from numerous disciplines and institutions throughout the United States, the Center's mission is to reduce earthquake losses through research and the application of advanced technologies that improve engineering, pre-earthquake planning and post-earthquake recovery strategies. Toward this end, the Center coordinates a nationwide program of multidisciplinary team research, education and outreach activities.

MCEER's research is conducted under the sponsorship of two major federal agencies: the National Science Foundation (NSF) and the Federal Highway Administration (FHWA), and the State of New York. Significant support is derived from the Federal Emergency Management Agency (FEMA), other state governments, academic institutions, foreign governments and private industry.

MCEER's NSF-sponsored research objectives are twofold: to increase resilience by developing seismic evaluation and rehabilitation strategies for the post-disaster facilities and systems (hospitals, electrical and water lifelines, and bridges and highways) that society expects to be operational following an earthquake; and to further enhance resilience by developing improved emergency management capabilities to ensure an effective response and recovery following the earthquake (see the figure below).



A cross-program activity focuses on the establishment of an effective experimental and analytical network to facilitate the exchange of information between researchers located in various institutions across the country. These are complemented by, and integrated with, other MCEER activities in education, outreach, technology transfer, and industry partnerships.

The overall goal of this study was to assess the seismic performance of electrical power substations and develop rehabilitation measures for existing substations using advanced technologies. A comprehensive study was conducted that included detailed finite element analyses of different types of transformers and bushings, as well as parameter and experimental studies of the friction pendulum system for use as a possible mitigation approach. Based on the results of the finite element analysis, simplified models were developed and interaction among transformer-bushing and interconnecting equipment was investigated. Internal packaging of transformers was also evaluated and its seismic performance was qualitatively assessed. Experimental studies of critical substation components were performed in collaboration with the National Center for Earthquake and Research (NCREE) in Taiwan, which identified important parameters that may impact the response of transformer-bushing systems. Furthermore, results demonstrate that base isolation using a friction pendulum system is a viable rehabilitation option for substations.

ABSTRACT

Substations, key components of electric power systems, are susceptible to significant damage under seismic events. The overall goals of this study was assessment of seismic performance of substations and development of rehabilitation measure for existing substations using advanced technologies to reduce the likelihood of failure and/or to enhance the probability of post-earthquake system functionality in a timely manner. It will also ensure long-term reliability and longevity of critical equipment, which is essential in light of ever increasing dependence of modern societies on electrical power. Substation equipment are designed and qualified for a specified level of base excitation. If the design level is exceeded or if their interaction aggravates the seismic response, as in the case of recent strong earthquakes in California and abroad, damage of the equipment are almost certain. Additionally, electrical equipment such as transformers have delicate internal packaging with specific design requirements on parameters such as gaps, clearances, tolerances, etc. Seismic forces can have significant effects on these parameters with adverse and chronic impact on long term electromagnetic performance of transformers. For example, LADWP has reportedly lost unexpectedly many transformers in the years after the San Fernando earthquake of 1971. This can result in direct and indirect loss and significantly impact the regional economy. Raising the design force level is not practical neither technologically nor economically. Furthermore, the complicated dynamic interaction among various electrical components is not well understood and cannot simply be addressed through an increase in the design forces. That is, raising the design force level by itself will not remedy the situation even if it was feasible to do so. Thus, there was the need for research to (1) identify critical components in the power system, (2) assess and enhance our understanding of seismic performance of various substation components as well as their interaction in light of the system response (3) develop advanced but practical and cost-effective strategies for rehabilitation of the most critical elements, (4) perform case-studies, and (5) disseminate successful results for wider applications including improvements and expansion to IEEE 693-1997. Thus, this research included both analytical and experimental studies on critical substation components to better understand their dynamic characteristics and to evaluate their seismic response in order to develop effective rehabilitation strategies. Results have identified important parameters affecting response of transformer-bushing system that can be used in development of next generation seismic guidelines and codes. Furthermore, results demonstrate that base-isolation is a viable rehabilitation option.

ACKNOWLEDGEMENTS

This work was supported primarily by the Earthquake Engineering Research Centers Program of the National Science Foundation under Award Number EEC-9701471 to the Multidisciplinary Center for Earthquake Engineering Research. Any opinions, findings, and conclusions or recommendations expressed in this material are those of the author(s) and do not necessarily reflect the views of the National Science Foundation.

TABLE OF CONTENTS

SECTION	TITLE	PAGE
1	INTRODUCTION	1
1.0	Background and Objectives	1
1.1	Power Systems and Power Transformers	1
1.2	Past Earthquake Performance	4
1.3	Literature Review	6
1.4	Report Organization	8
2	FINITE ELEMENT STUDY OF TRANSFORMER-BUSHING SYSTEM	11
2.1	IEEE Seismic Qualification Procedures for Transformers and Bushings	12
2.2	Modeling and Analysis Issues for the Transformer and Bushing	13
2.3	Response Criteria for Transformer and Bushing	18
2.4	Finite Element Analysis Results	19
2.4.1	Dynamic Response of Transformers	20
2.4.2	Dynamic Response of Bushing	28
3	STUDY OF THE FRICTIONAL PENDULUM SYSTEM	33
3.1	Friction Pendulum System	33
3.1.1	Geometric Description and Technical Characteristics	35
3.2	Formulation of the Equation of Motion for the Friction Pendulum System	36
3.2.1	Numerical Solution of the Equation of Motion for FPS	39
3.2.2	Input Parameters for Numerical Solution	40
3.2.3	Ground Motion Input	41
3.3	Parametric Study Results	42
3.3.1	Results of 1-D Analyses	43
3.3.2	Results of 2-D Analyses and Response Combinations	45
3.3.3	Effect of Vertical Motion	51
3.3.4	Ground Motion Characteristics	54
3.4	FPS System for Large Displacement Assumption and Results	56
3.5	Force Displacement Response of FPS Model	60
3.6	Finite Element of FPS Behavior	61
3.7	Behavior of Fixed and Isolated Primary-Secondary Systems	64
4	EXPERIMENTAL STUDY OF FRICTIONAL PENDULUM SYSTEM	77
4.1	Earthquake Simulator	77
4.2	Instrumentation	77
4.3	Transformer Model and Bushing	78
4.4	Modal Analysis of Transformer Model and Bushing	79
4.5	Results	81
4.6	Force/Displacement Response of Transformer Model	90

TABLE OF CONTENTS (cont'd)

SECTION	TITLE	PAGE
5	SIMPLIFIED MODEL APPROACH	93
5.1	Simplified Model Analysis Results	95
5.2	Simplified Model for Interaction Study	109
5.3	FPS Graphs to Select FPS Radius and Cable Slack	125
5.4	Practical Aspects and Design Recommendations	129
6	EVALUATING THE APPLICATION OF BASE-ISOLATION: A CASE STUDY	133
6.1	Transformers and Bushings Characteristics	133
6.2	Modeling	133
6.3	Seismic Forces Based on IEEE	135
6.4	Results of Time History Analyses	136
6.4.1	Transformer Responses	136
6.4.1.1	Fixed Base Case	136
6.4.1.2	Base Isolated	138
6.4.2	Bushings Responses	142
6.4.2.1	Fixed Base	142
6.4.2.2	Base Isolated	145
6.5	Additional Slack Required	146
6.6	Check for Uplift	150
6.7	Foundation Seismic Forces	151
7	INTERNAL COMPONENTS OF HIGH-POWER CORE-FORM ELECTRICAL TRANSFORMERS	153
7.1	Components of the Internal Structure	154
7.1.1	Core	154
7.1.2	Transformer Cooling	156
7.1.3	Windings	156
7.1.4	Insulating Structure	158
7.1.5	Structural Elements	161
7.2	Mechanical Design of Internal Components	163
7.2.1	Force Calculations	164
7.2.2	Stress Analysis	165
7.2.2.1	Compressive Stress in Key Spacers	166
7.2.2.2	Axial Bending Stress per Strand	166
7.2.2.3	Tilting Strength	167
7.2.2.4	Stress in Tie-Plates	168
7.2.2.5	Stress in Pressure Rings	169
7.2.2.6	Hoop Stress	169
7.2.2.7	Radial Bending Stress	170
7.2.3	Radial Buckling Strength	172
7.2.4	Points About the Mechanical Design	173

TABLE OF CONTENTS (cont'd)

SECTION	TITLE	PAGE
7.3	Behavior of Internal Components under Earthquake	174
7.3.1	Possible Failure Modes of Internal Components	174
7.3.1.1	Sliding of Key Space	174
7.3.1.2	Movements or Separation of Leads	176
7.3.1.3	Decrease or Loss of Safe Clearance between Layers of Conductors Due to Seismic Excitations	177
7.3.1.4	Loss of Close Fitting Tolerances between Limbs and Yokes Causing Long-Term Electrical Loss	178
7.3.2	The Analytical Model	178
7.3.2.1	The Geometric and Mechanical Details	178
7.3.2.2	The Mechanical Properties of Material	180
7.3.3	The Results	181
8	EFFECT OF ISOLATION ON FOUNDATION DESIGN OF TRANSFORMERS	191
8.1	Seismic Design of Foundations in Electrical Substations	191
8.2	Foundation Design Results	193
9	CONCLUSIONS	199
10	REFERENCES	203
APPENDIX A	STATIC CALCULATIONS FOR TRANSFORMERS	209
APPENDIX B	FORTTRAN CODE FOR FPS	211
APPENDIX C	IMPLEMENTATION OF A FPS IN ADINA	215

LIST OF ILLUSTRATIONS

FIGURE	TITLE	PAGE
1-1	Typical Substation	2
1-2	Typical Power Transformer and its Components	3
1-3	Typical Bushing and its Components	3
1-4	Damage to a Rail-Mounted Transformer	4
1-5	Transformer Turned Over	5
1-6	Damage to a Transformer Foundation	5
1-7	Bushing Failure at the Flange	6
1-8	Experimental Setup for Testing 550 kV Bushing at PEER	7
2-1	Mesh of Transformer and Element Types	14
2-2	Views of Gasket Model	15
2-3	Acceleration Response Spectra for Components of El-Centro Record and IEEE High Performance Level	16
2-4	Acceleration Response Spectra for Components of Hollister Airport Record and IEEE High Performance Level	16
2-5	Acceleration Response Spectra for Components of Pacoima Dam Record and IEEE High Performance Level	17
2-6	Acceleration Response Spectra for Components of Lake Hughes Array #4 Record and IEEE High Performance Level	17
2-7	Determination of Rayleigh Damping Coefficients for Analysis	18
2-8	Monitored Nodes on Transformer Model	19
2-9	Points Monitored on Bushing Finite Element Model	20
2-10	Displacement, Acceleration Responses and Normalized Power Spectrum at SW5 of TT2 for El-Centro Record in X-direction	27
2-11	Displacement, Acceleration Responses and Normalized Power Spectrum at SW5 of TT2 for El-Centro Record in Y-direction	27
2-12	Displacement, Acceleration Responses and Normalized Power Spectrum at SW5 of TT2 for El-Centro Record in Z-direction	28
2-13	Displacement, Acceleration Responses and Normalized Power Spectrum at BUC12 of TT2 for El-Centro Record in X-direction	29
2-14	Displacement, Acceleration Responses and Normalized Power Spectrum at BUC12 of TT2 for El-Centro Record in Y-direction	29
2-15	Displacement, Acceleration Responses and Normalized Power Spectrum at BUC12 of TT2 for El-Centro Record in Z-direction	30
2-16	Gap in the Bushing Gasket Mounted on TT3 for Lake Hughes Array # 4 Record	31
3-1	Photograph of a FPS Isolator	36
3-2	Typical Elevation and Section of FPS	36
3-3	Force Diagram of FPS	37
3-4	A Time History for Variable Z	38
3-5	Variation of Coefficient of Sliding Friction	40
3-6	Acceleration Time Histories for an Example Case	43

LIST OF ILLUSTRATIONS (cont'd)

FIGURE	TITLE	PAGE
3-7	Displacement-Inertia Reduction Chart for PGA of 0.25g	44
3-8	Displacement-Inertia Reduction Chart for PGA of 0.50g	44
3-9	Displacement-Inertia Reduction Chart for PGA of 1.00g	45
3-10	Comparison of 1-D and Corresponding Component of a 2-D Case for PGA of 0.25g	46
3-11	Comparison of 1-D and Corresponding Component of a 2-D Case for PGA of 0.50g	46
3-12	Comparison of 1-D and Corresponding Component of a 2-D Case for PGA of 1.00g	47
3-13	Comparison of Displacement Responses for Combination Methods with 2-D Case for PGA of 0.25g	47
3-14	Comparison of Displacement Responses for Combination Methods with 2-D Case for PGA of 0.50g	48
3-15	Comparison of Displacement Responses for Combination Methods with 2-D Case for PGA of 1.0g.	48
3-16	Comparison of Inertia Reduction Responses for Combination Methods with 2-D Case for PGA of 0.25g	49
3-17	Comparison of Inertia Reduction Responses for Combination Methods with 2-D Case for PGA of 0.50g	49
3-18	Comparison of Inertia Reduction Responses for Combination Methods with 2-D Case for PGA of 1.00g	50
3-19	Effect of Vertical Motion on Displacements for PGA of 0.25g and 0.5g (3-D Analyses)	51
3-20	Effect of Vertical Motion on Displacements for PGA of 0.75g and 1.0g (3-D Analyses)	52
3-21	Effect of Vertical Motion on Inertia Reduction for PGA of 0.25g and 0.5g (3-D Analyses)	52
3-22	Effect of Vertical Motion on Inertia Reduction for PGA of 0.75g and 1.0g (3-D Analyses)	53
3-23	Displacements Time Histories with (Sinusoidal) and without Vertical Motion	54
3-24	Comparison of Rock and Soil Displacements for PGA of 0.25g and 0.50g	54
3-25	Comparison of Rock and Soil Displacements for PGA of 0.75g and 1.0g	55
3-26	Comparison of Rock and Soil Inertia Reduction for PGA of 0.25g and 0.50g	55
3-27	Comparison of Rock and Soil Inertia Reduction for PGA of 0.75g and 1.0g	56
3-28	Comparison of Displacements Based on Small and Large Displacement Assumptions for PGA of 0.25g	57

LIST OF ILLUSTRATIONS (cont'd)

FIGURE	TITLE	PAGE
3-29	Comparison of Displacements Based on Small and Large Displacement Assumptions for PGA of 0.50g	58
3-30	Comparison of Displacements Based on Small and Large Displacement Assumptions for PGA of 1.0g	58
3-31	Comparison of Inertia Reductions Based on Small and Large Displacement Assumptions for PGA of 0.25g	59
3-32	Comparison of Inertia Reductions Based on Small and Large Displacement Assumptions for PGA of 0.50g	59
3-33	Comparison of Inertia Reductions Based on Small and Large Displacement Assumptions for PGA of 1.00g	60
3-34	Typical Load-Displacement Hysteresis Loop for FPS Isolator	61
3-35	Diagram of the Forces in FPS	63
3-36	Primary-secondary Model	65
3-37	Bushing Response for TT1	69
3-38	Effect of Vertical Frequency and Support Fixity on Bushing Response	69
3-39	Bushing Response for TT2	70
3-40	Effect of Transformer Frequency on Bushing Response	71
3-41	Vertical Force at Support	71
3-42	Effect of Vertical Frequency and Support Fixity on Shear Force in x-direction	72
3-43	of Vertical Frequency and Support Fixity on Shear Force in y-direction	73
3-44	Shear Force in x-direction for TT1	73
3-45	Shear Force in y-direction for TT1	74
3-46	Effect of Transformer Frequency on Shear Force in Isolated Systems	75
3-47	Effect of Transformer Frequency on Shear Force in Fixed-base Systems	75
4-1	A View of the Transformer Model and Instrumentation	78
4-2	Transformer Model with the Bushing Mounted on the Top	78
4-3	FFT of Testing Frame Response for 1-D Case of Sylmar Record with 0.375g in X direction	80
4-4	FFT of Bushing Response for 1-D Case of Sylmar Record with 0.375g in X Direction	80
4-5	FFT of Bushing Response with Respect to Testing Frame for 1-D case of Sylmar Record with 0.375g in X Direction	81
4-6	Acceleration Maps for Chi-I-Ray-Li Record for 1-D Case	84
4-7	Acceleration Maps for El-Centro Record for 1-D Case	84
4-8	Acceleration Maps for Sylmar Record for 1-D Case	85
4-9	Acceleration Maps for Sylmar Record for 2-D Case in X Direction	85
4-10	Acceleration Maps for Sylmar Record for 2-D Case in Y direction	86

LIST OF ILLUSTRATIONS (cont'd)

FIGURE	TITLE	PAGE
4-11	Acceleration Maps for Sylmar Record for 3-D Case in X-Direction	86
4-12	Acceleration Maps for Sylmar Record for 3-D Case in Y Direction	87
4-13	Acceleration Maps for Sylmar Record for 3-D Case in Z Direction	87
4-14	Comparison of Displacement Responses for Analytical and Experimental Studies	90
4-15	Hysteresis Loop of Northridge-Sylmar Record for PGA of 0.25g in X- Direction	91
4-16	Hysteresis Loop of Northridge-Sylmar Record for PGA of 0.375g in X-Direction and 0.25g in Y-Direction	91
4-17	Hysteresis Loop of Northridge-Sylmar Record for PGA of 0.375g in X-Direction, 0.25g in Y-direction and 0.25g in Z-Direction	92
5-1	Typical Partial Substation	93
5-2	Simplified Model for Partial Substation	94
5-3	Rayleigh's Damping for Simple System	94
5-4	Displacement Responses of Case 1	100
5-5	Force Responses for Case 1	101
5-6	Displacement Responses of Case 12	102
5-7	Force Responses of Case 12	102
5-8	Displacement Response of Bushing and Connecting Equipment for Case 25	106
5-9	Displacement Response of Bushing and Connecting Equipment for Case 41	107
5-10	Relative Displacement of Bushing and Connecting Equipment for Case 25 and Case 41	107
5-11	Force Response of Case 12 with 1/1000 k and 1/1000 m	108
5-12	Force Response of Case 12 with 1000 k and 1000 m	109
5-13	Simplified Model Used in This Study	109
5-14	FPS Displacement Versus Frequency Ratio	111
5-15	Displacement of Interconnecting Equipment Versus Frequency Ratio	112
5-16	Relative Displacement of Bushing Versus Frequency Ratio	112
5-17	Effect of Interconnecting Equipment Mass on FPS Displacement	113
5-18	Effect of Interconnecting Equipment Mass on Relative Displacement of Bushing	113
5-19	History Responses In Simplified Model, Case 1	117
5-20	Relative Displacement of The Cable in Simplified Model, Case 1	117
5-21	FPS Displacement in Simplified Model, Case 1	118
5-22	Relative Displacement of Bushing Versus Slack Ratio	119
5-23	Interconnecting Equipment Displacement Versus Slack Ratio	119
5-24	Cable Force Versus Slack Ratio	120
5-25	FPS Displacement Versus Slack Ratio	120

LIST OF ILLUSTRATIONS (cont'd)

FIGURE	TITLE	PAGE
5-26	Transformer Force Versus Slack Ratio	121
5-27	Bushing Relative Displacement Versus INC Frequency	122
5-28	Interconnecting Equipment Displacement Versus INC Frequency	122
5-29	Transformer Relative Displacement Versus INC Frequency	123
5-30	FPS Displacement Versus INC Frequency	123
5-31	Cable Force Versus INC Frequency	124
5-32	Average FPS Displacement Versus FPS Radius	126
5-33	Average Inertia Reduction Versus FPS Radius	126
5-34	Average FPS Displacements Versus FPS Radius for Rock	127
5-35	Average Inertia Reduction Versus FPS Radius for Rock	128
5-36	Average FPS Displacement Versus FPS Radius for Soil.	128
5-37	Average Inertia Reduction Versus FPS Radius for Soil	129
5-38	Outline View of TT3	130
6-1	Front and Side Elevation of a 433.3 MVA Substation Transformer	135
6-2	Simplified 2-DOF Model	135
6-3	Modeling the FPS as a Bi-linear Hysteretic Element with Kinematic Hardening	136
6-4	Time History of Transformer Acceleration (Case 15-fixed base)	137
6-5	Maximum Acceleration Responses of Transformers (San Fernando - fixed base)	138
6-6	Maximum Acceleration Responses of Transformers (El Centro - fixed base)	138
6-7	Hysteresis Behavior of the FPS During the Application of San Fernando Record	139
6-8	Time History of Transformer Acceleration (Case 15-base isolated)	140
6-9	Reduction in Transformer Accelerations ($f_t=5$ Hz)	141
6-10	Reduction in Transformer Accelerations ($f_t=12$ Hz)	141
6-11	Reduction in Transformer Accelerations ($f_t=15$ Hz)	142
6-12	Maximum Acceleration Responses of Bushings	142
6-13	Maximum Acceleration Responses of Bushings (El Centro - fixed base)	143
6-14	Time History of Bushing Displacement (Case 15 – fixed base)	144
6-15	Maximum Displacements of Bushings (San Fernando - fixed base)	144
6-16	Maximum Displacements of Bushings (El Centro - fixed base)	145
6-17	Reduction in Bushings Acceleration ($F_t=5$ Hz)	145
6-18	Reduction in Bushings Acceleration ($F_t=12$ Hz)	146
6-19	Reduction in Bushings Acceleration ($F_t=15$ Hz)	146
6-20	Time History of Bushing Displacement (Case 15-base isolated)	147
6-21	Maximum Bushings Displacements (El Centro -fixed base)	148
6-22	Maximum Bushings Displacements (El Centro-base isolated)	148

LIST OF ILLUSTRATIONS (cont'd)

FIGURE	TITLE	PAGE
6-23	230kV Bushing to Bus Connection	149
6-24	500kV Bushing to Bus Connection	150
6-25	Boundaries of Rest, Slide and Rock Modes for Height/Width Ration of 2	151
7-1	Core Sections, 7-Step Taped and 14-Step Banded	154
7-2	Four-limb Core in Course of Building (GEC Alsthom)	155
7-3	Three-phase Stepped Core for a Core-form Transformer without the Top Yoke	155
7-4	Two Major Types of Coil Construction for Core-form Power Transformers	157
7-5	Winding in Progress	157
7-6	Continuously Transposed Conductor	158
7-7	Major Insulation Structure Consisting of Multiple Barriers Between Windings	159
7-8	Top View of Two Windings Showing the Major Insulation Structure, Key Spacers, and Sticks	160
7-9	Top View of Clamping Structure for a 3-phase Transformer	163
7-10	Plot of Transformer Leakage Flux.	164
7-11	Types of Wire or Cable Used in Transformer Coils	165
7-12	Geometry of Strand Tilting Due to Axial Compressive Force	167
7-13	Geometry for Determining the Hoop Stress in a Cylinder Acted on by a Radially Inward Pressure	170
7-14	Geometry for Determining the Radial Bending Stresses	171
7-15	Radial Support Structure	172
7-16	Key Spacers Separating Different Layers of Winding	175
7-17	Model of Internal Components Used for Analysis	176
7-18	Wooden Frame Designed to Support the Leads	177
7-19	Dimensions of a Cross-Section of the Model	179
7-20	Maximum Tensile Force in Coil Due to Earthquake	182
7-21	Maximum Tensile Force in Coil Due to Earthquake and Weight	183
7-22	Maximum Tensile Force in Coil Due to Earthquake as a Percentage of Weight	184
7-23	Maximum Tensile Force in Coil Due to Earthquake and Weight as a Percentage of Weigh	185
7-24	Maximum Tensile Force in Coil Under Earthquake for Case 10	186
8-1	Distribution of Lateral Force on Isolated and Fixed Transformers	192
8-2	Effective Area for Foundation	194
8-3	Inclined Load Reduction Factors	195
8-4	Variation of α With Undrained Cohesion of Clay	196

LIST OF TABLES

TABLE	TITLE	PAGE
2-1	Summary of Maximum Displacement and Acceleration Responses for TT1	21
2-2	Summary of Maximum Displacement and Acceleration Responses for TT2	22
2-3	Summary of Maximum Displacements and Acceleration Responses for TT3	23
2-4	Summary of Maximum Support Reactions for TT1	24
2-5	Summary of Maximum Support Reactions for TT2	25
2-6	Summary of Maximum Support Reactions for TT3	26
3-1	Values of Equation (3-6) Constants	41
3-2	Ground Motion Records Employed	42
3-3	Properties of the Primary Systems Studied	66
3-4	Properties of the Secondary Systems Studied	66
3-5	Characteristics of the Primary-Secondary Systems Studied	67
4-1	Characteristics of 161 kV Bushing	79
4-2	Characteristics of the Isolation System	79
4-3	Dynamic Characteristics of the Transformer Model and the Bushing	79
4-4	Responses for Northridge-Sylmar Record (Case 1 through Case 3)	82
4-5	Responses for Northridge-Sylmar Record (Case 4 through Case 7)	83
4-6	Simulated Experimental Cases	89
5-1	FPS Response for El-Centro S90W Record	96
5-2	FPS Response for Taft S69E Record	96
5-3	Simple Model Case 1 through Case 32	97
5-4	Simple Model Case 33 through Case 64	98
5-5	Simple Model Case 65 through Case 96	99
5-6	Simplified Analysis Responses for Case 1 through Case 32	103
5-7	Simplified Analysis Responses for Case 33 through Case 64	104
5-8	Simplified Analysis Responses for Case 65 through Case 96	105
5-9	Interconnecting Equipment Characteristics for Studies on Effects of Frequency Ratio on Interaction	110
5-10	Interconnecting Equipment Characteristics for Studies on Effect of Slack Ratio on Interaction	114
5-11	The Cases Studied on Interaction of Isolated Transformer-Bushing and Interconnecting Equipment	115
5-12	Maximum Results of Interaction of Isolated Transformer-Bushing and Interconnecting Equipment	116
5-13	Earthquake Records Used	125
5-14	Required Slack for FPS Displacements (Moderate Seismic Performance Level)	132

LIST OF TABLES (cont'd)

TABLE	TITLE	PAGE
5-15	Required Slack for FPS Displacements (Moderate Seismic Performance Level)	132
6-1	Properties of the Transformers and the Bushings	134
7-1	Characteristics of the Acceleration Time-Histories Used for the Analyses	181
7-2	Specifications of the Models Used for Each Analysis	182
7-3	Maximum Tensile Forces in the Core and Tie-Plates for Different Analyses	187
7-4	Maximum Tensile Forces in the Coil for Different Analyses	187
8-1	Properties of the Cases Considered for Design of Transformer Foundations	193
8-2	The Design Transformer Foundations	193

SECTION 1 INTRODUCTION

1.0 Background and Objectives

The functionality of electric power network is vital to maintain the welfare of the general public, to sustain the economic activities and to assist in the recovery, restoration, and reconstruction of the seismically damaged environment. Electric substations are among the most important parts of any electric power network and they are susceptible to significant damage under seismic events. Rehabilitation of existing substations using advanced technologies and proper design of new systems will reduce the likelihood of failure and/or will enhance the probability of post-earthquake system functionality in a timely manner. Furthermore, it will ensure long-term reliability and longevity of critical equipments, which is essential in light of ever increasing dependence of modern societies on electrical power. Under this research effort a system approach is employed in order to better understand seismic performance of substations and to evaluate the interaction among transformers, bushings and interconnecting electrical equipment.

Substations sustained significant damage and failure during past earthquakes. Substation equipment are designed and qualified for a specified level of base excitation. If the design level is exceeded or if their interaction aggravates the seismic response, as in the case of recent strong earthquakes in California and abroad, damage of the equipment is almost certain. This would result in direct and indirect loss and significantly impact on the regional economy. Raising the design level is not practical; neither technologically nor economically. Furthermore, we do not understand the complicated interaction among various electrical components during the dynamic response of the entire system to an event. Therefore, raising the design level by itself might not remedy the situation even if it was feasible to do so. Thus, the objectives of this study are to (1) identify critical components in the power system, (2) develop the tools and a framework to evaluate and assess seismic performance of various components as well as their interaction in light of the system response (3) develop advanced but practical and cost-effective strategies for rehabilitation of the most critical elements, (4) perform case-studies, and (5) disseminate successful results for wider applications including improvements and expansion to IEEE 693-1997. Thus, this research included both analytical and experimental studies on critical substation components to better understand their dynamic characteristics and to evaluate their seismic response in order to develop effective rehabilitation strategies.

1.1 Power Systems and Power Transformers

Electric power systems can be divided into five major parts: power generating facilities, transmission and distribution lines, transmission and distribution substations, control and data acquisition systems, and ancillary facilities and functions. This study focuses on two substation components, transformer bushing and a connecting equipment item. (See figure 1-10). Substations perform many functions including [ASCE, 1999]:

1. Protection of transmission and distribution lines and the equipment within the substation.

2. Triggering other devices to isolate the lines or the equipment in case of abnormal system operating conditions.
3. Providing transfer of power between different voltage levels through the use of power transformers.
4. Reconfiguring of the power network by opening transmission lines or partitioning multi section busses.



Figure 1-1 Typical Substation

One of the key components of the substation is the power transformer. A power transformer is the single largest capital item in a substation, comprising almost 60% of the total investment [Woodcock, 2000]. Most of the power transformers (and those discussed here) are core type transformers. The size, shape and installation of transformers vary according to the voltage handled. The basic components of a transformer are the coils, core, tank, oil and bushing. The coils and core are usually enclosed in a steel tank to protect them from the elements, vandalism and, for safety purposes; oil is placed in the tank over the coils and core to provide a means of cooling. Figure 10-2 shows inner and outer parts of a power transformer. A more comprehensive detail about the internal components of transformers is provided in Section 7. Also more information on transformers is given in the literature [Pansini, 1999].

Bushings are insulated conductors providing electrical connections between high voltage lines and oil-filled transformers. They are typically mounted on the top plate of the transformer tank or a turret attached to a transformer tank. Typical bushing and its components are shown in figure 1-3. Bushings take the terminals of the coils through the tank, insulating them from the tank. Typically, they consist of a conductor through an insulating collar, usually porcelain. For higher voltages, the porcelain cylinders may also be filled with oil or contain layers of insulation with metal foil inserted between them to equalize electric stresses among the layers.

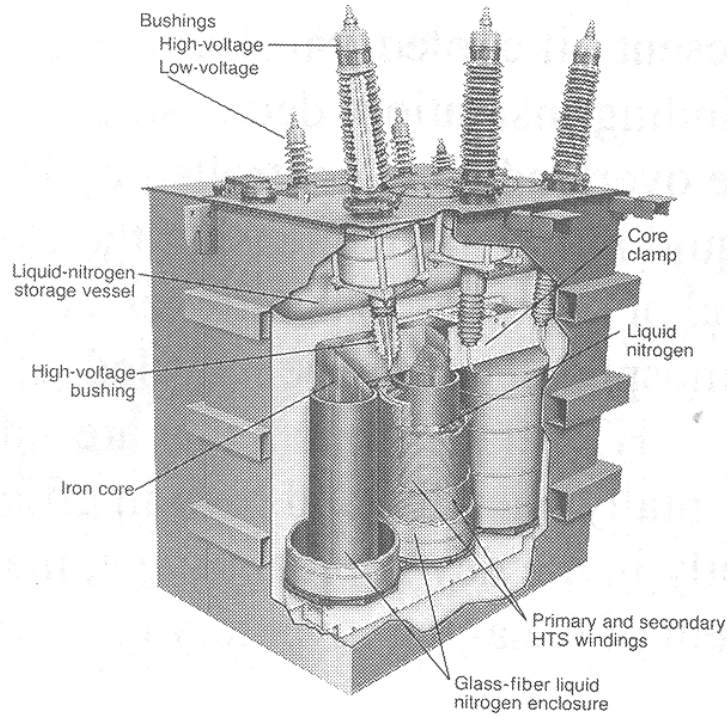


Figure 1-2 Typical Power Transformer and its Components [Pansini, 1999]

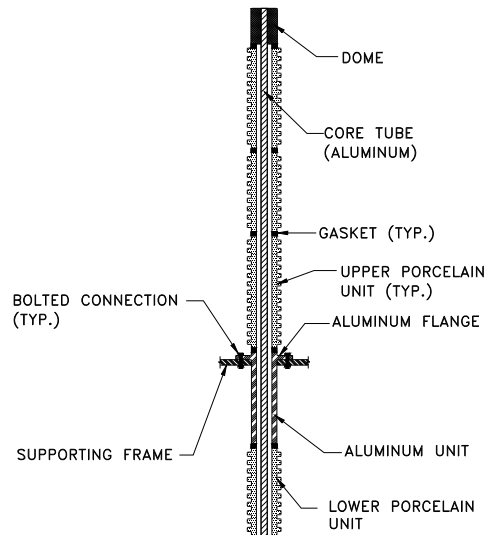


Figure 1-3 Typical Bushing and its Components

Transformer components include: sudden pressure and protective relays, anchorage, radiators, bushings, conservators, lightning arresters, tertiary bushings, and surge arresters. Some transformer installations also have transfer busses so that a spare transformer can quickly replace a unit that must be taken out of service. The effect of the loss of function of a transformer is generally significant, unless a spare transformer is available or there is a second transformer

bank in parallel with the damaged unit. The consequences of transformer damage will depend on system configuration and other system elements that may be damaged or can be out of service. If no damage is observed in an earthquake and earthquake intensity is low to moderate, the transformer will usually be put back into service. If there is any concern regarding an internal fault, a high-potential test of the transformer is performed before it is put back into service.

1.2 Past Earthquake Performance

The failure of electric power systems in the 1994 Northridge earthquake in the United States, the 1999 Izmit earthquake in Turkey, the 1999 Chi-Chi Taiwan Earthquake and other recent earthquakes have demonstrated the critical need for electric power networks during and after an earthquake. Observed failure types of power transformers are categorized as:

1. Failure of unrestrained transformers
2. Anchorage failure of transformers
3. Conservator failure of transformers
4. Foundation failure of transformers
5. Damage to control boxes

The first two are the most common failure types of transformer bodies. Figure 1-4 and 0figure 1-5 show over-turned transformers from recent earthquakes. The most common power transformer failures are those of unrestrained transformers in earthquake prone regions. It is common practice to fix the transformer base to the foundation either by anchor bolts or welds. However, there are many cases of bolt or weld failure during the past earthquakes [ASCE, 1999]. Designing the anchorage at the supports requires consideration of large forces not only due to gravity and seismic forces but also from overturning moments in both directions. In addition to strength, the anchorage must have adequate stiffness to prevent initiation of impact forces that can damage internal elements or excite higher modes that can damage brittle porcelain members.

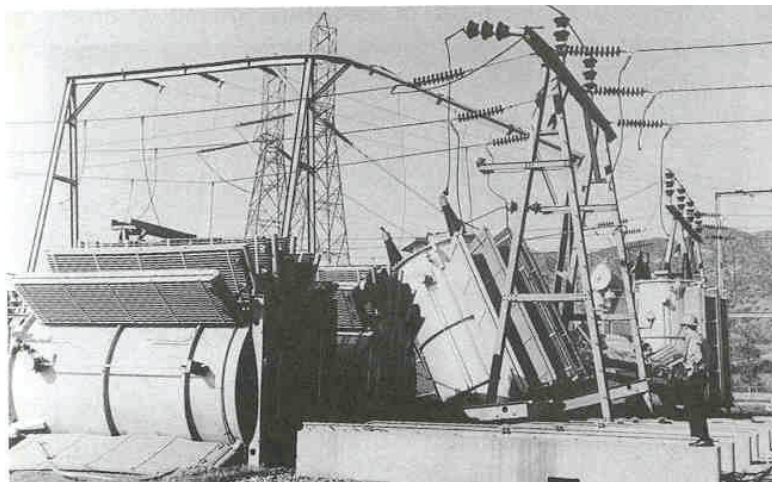


Figure 1-4 Damage to a Rail-Mounted Transformer [ASCE, 1999]

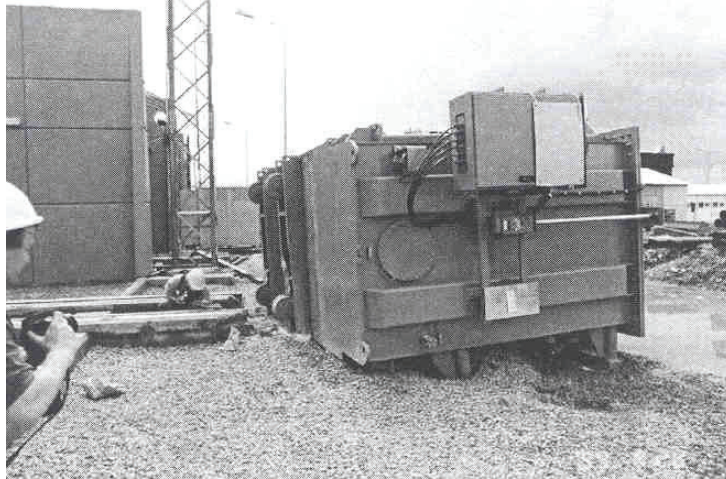


Figure 1-5 Transformer Turned Over [MCEER, 2000]

Figure 1-6 shows foundation failure of a transformer in 1999 Izmit Earthquake. This was an unrestrained transformer placed on top of a foundation pad.



Figure 1-6 Damage to a Transformer Foundation [EERI, 1999]

Bushing failures are classified into two groups:

1. Oil leaks due to gasket failure
2. Fracture of the porcelain body due to lack of slack in the connecting cable between the bushing and the connecting equipment.

Figure 1-7 shows the failure of a bushing at the gasket level. The most vulnerable gasket is the one closest to the flange connecting the bushing to the transformer.



Figure 1-7 Bushing Failure at the Flange [ASCE, 1999]

There are many more examples of power transformer and bushing failures during recent earthquakes [ASCE, 1998, 1999].

1.3 Literature Review

Amplification of the ground motion by the transformer body itself is one of the most important concerns in transformer and bushing response. The latter is the classic case of secondary systems in which the motion of secondary parts can significantly damage the primary. Based on a field study performed at the University of California at Irvine, the dynamic amplification of 500 kV bushings mounted at the top of transformers is in agreement with the amplification factor given in the IEEE Standard 693. However, amplification factor for a 230 kV bushing mounted on a transformer has been observed to exceed the specifications by a factor of almost two [Villaverde, 1999]. Another study has revealed that the dynamic amplification factor between the ground and bushing flange for 160 MVA, 230/135 kV power transformer is over two [Bellorini, 1998].

Besides these studies, the performance of bushings was analyzed through extensive testing in the Pacific Earthquake Engineering Research Center (PEER). They tested 196 kV, 230 kV and 550 kV bushings mounted on a fixed frame at their flange [Gilani, 1998, 1999]. The experimental setup for this testing is shown in figure 1-8. Excellent performance was observed for the 196 kV, 230 kV bushings in spite of their poor performance during the past earthquakes. That is the bushing performed well even though the tests were conducted for a motion with response spectra two times that given in IEEE 693 in order to account for the dynamic amplification of the transformer tank (an IEEE requirement for the qualification of bushings). These tests were conducted using a rigid frame to support the bushings therefore the in-situ effect of the translational motion of transformers is not included. The critical environment for bushings can be either due to the effect of the motion of the transformer body or the interaction of the bushing with the other equipment. Apparently, the fixed frame shown in figure 1-8 used for the qualification of the bushings does not take into account the effect of transformer flexibility. It is thus important to revise the qualification procedures for bushings set by IEEE 693-1997.

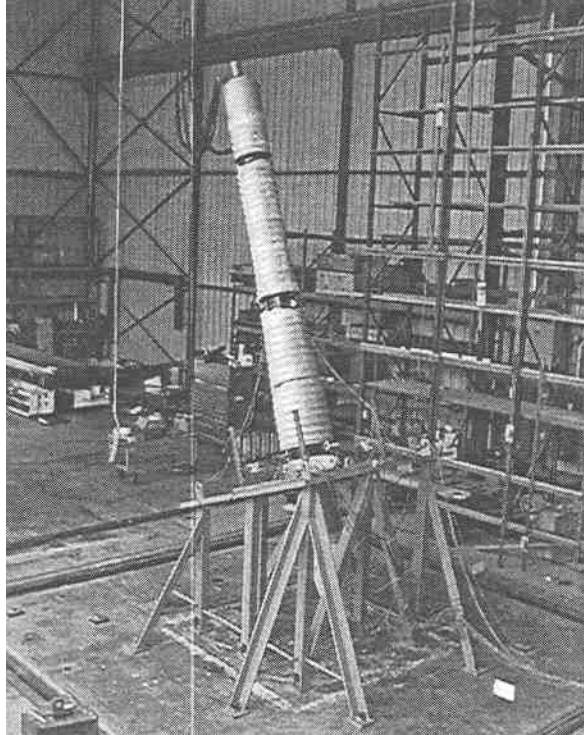


Figure 1-8 Experimental Setup for Testing 550 kV Bushing at PEER

Even though the previously mentioned tests showed excellent performance of bushings, their poor performance during past earthquakes calls for additional studies aimed at developing appropriate remedies. It should be born in mind that one of the reasons of poor performance is interaction of transformer with bushing. Therefore, a suitable remedy for the transformer bushing system can be base isolation of the transformer. One of the most recent base isolation systems to improve the earthquake resistance of structures is Frictional Pendulum System (FPS). Since the period of vibration for structures isolated by FPS is independent of mass, it is an ideal device for the isolation of transformers. FPS will reduce the input acceleration into the bushing and will lessen the interaction between the transformer and the bushing.

FPS has been studied by many researchers in an effort to improve the seismic performance of structures [Al-Hussaini, 1994; Almazan, 1998; Mokha, 1990, 1991]. The FPS system is a base isolation system in which the object being isolated is constrained to move on a spherical surface (FPS is described in detail in Section 3). Some examples of applications of the FPS system are the San Francisco Airport International Terminal, the U.S. Court of Appeals, and the Hayward City Hall [Mokha, 1996]. There are also industrial applications of FPS in systems like natural gas storage tanks and emergency and fire cooling water tanks. There have also been FPS applications to many bridges throughout USA and Canada [Constantinou, 1993]. In another case, FPS bearings were used to retrofit an international airport terminal building in Turkey [Constantinou, 2001]. Recently new generations of FPS has been introduced where uplift is restrained. An uplift-restraining friction pendulum system, termed XY-FP, consists of two orthogonal opposing concave beams interconnected through a sliding mechanism that permits tension to develop in the bearing, thereby preventing uplift [Constantinou, 2006]. Another

recently developed type of frictional pendulum bearings is Double Concave Friction Pendulum (DCFP) bearing which is an adoption of single concave FPS [Constantinou, 2004]. A great advantage of DCFP is its ability to accommodate larger displacements [Constantinou, 2004]. This study considers the use of FPS for power transformers for the first time.

Furthermore a comprehensive experimental study has been carried out on the performance of base-isolated power transformers [Feng et al., 2006] where sliding and rubber bearings are employed. In this study, a triaxial earthquake stimulator was conducted with model transformer and real bushing. The experiment had two phases: In phase 1 the combination of sliding bearings and low-damping bearings was developed and applied as an isolation system. In phase 2 segmented high-damping rubber bearings were developed and applied as an isolation system. In both phases it was observed that base isolations are very effective in reducing the transformer and bushings response. However under triaxial shaking in the first phase the acceleration response of bushing did not decrease and even in some cases it was amplified. Nevertheless in the second phase there was no amplification of bushings under triaxial shaking.

There has also been a study of the interaction of interconnected substation components [Kiureghian, 1999]. This was a theoretical study that was conducted for two equipment items. Studies of multiple equipment items with properties closer to real equipment would lead to a better understanding of interaction of electrical equipment.

1.4 Report Organization

This report is organized into nine sections. Section 2 presents results of a comprehensive finite element analysis of transformer-bushing system. Finite element analysis of power transformers and bushings is performed on three different types of transformers in this section. Section 3 provides background information and parameter study on friction pendulum system (FPS) as a possible rehabilitation strategy for substation transformers. In light of the transformer's weight and the mobility requirements for maintenance purposes, base isolation is identified as a practical technology for their seismic rehabilitation and design charts are developed for this base isolation system [Ersoy, 2001; Saadeghvaziri, 2000]. Finite element formulation of the behavioral characteristics of FPS is presented and the element is used to study primary-secondary (transformer-bushing) interaction vis-à-vis effect of vertical component of ground motion. Details of element implementation into ADINA finite element package are provided. Experimental studies performed in collaboration with National Center for Earthquake and Research (NCEER) in Taiwan are given in Section 4.

Section 5 develops a simplified substation model (of key components) for parameter study on interaction of transformer-bushing-interconnecting equipment. The results are also compared to the results from previous studies with simpler model for FPS. Graphs are provided showing the amount of slack required for different levels of peak ground acceleration and FPS radius. Analytical results and a discussion of the practical aspects of design recommendations and rehabilitation guides are presented therein. The basic work of Section 3 does not take into account transformer and bushing flexibility. In order to include the effect of the flexibility of the transformer on the bushing response, the results of Section 2 are utilized in the development of the simplified model.

Section 6 is on the seismic performance of electric substation transformers, and discusses advantages and considerations in the use of base-isolation as a viable hazard mitigation option. Through an actual case study a simplified model of transformer-bushing will be developed and the results of fixed base case and base isolated case are compared. Moreover, design concepts are investigated.

Section 7 investigates the seismic behavior of internal components of transformers. A fairly detailed explanation of the internal components is presented. Four possible modes of failure/damage are identified for the internal components, two of which are detected to be of more concern. The prestressing force in core is identified as the critical criterion for these failure modes and several analyses are performed to determine the level of ground excitation that can cause loss of prestressing. Again, effect of use of FPS on reducing the hazard of damage to the internal components is studied and it is shown to be an effective rehabilitation option.

Section 8 studies the effects of FPS on foundation design. The design of foundation is done for several cases of isolated transformers. These designs are compared to that of fixed-base transformers. The differences in foundation size and cost are assessed.

Finally Section 9 presents conclusions.

SECTION 2

FINITE ELEMENT STUDY OF TRANSFORMER-BUSHING SYSTEM

The reliability of a power system exposed to earthquake loading is dependent upon the seismic response of its individual components and interaction of these components with each other. Unrestrained or poorly anchored transformers and porcelain transformer bushings have failed in recent earthquakes. Since transformers and their mounted bushings are vital system components which have been damaged in past earthquakes, they are the main focus of the finite element part of this study.

Transformers perform the vital function of transferring power between circuits operating at different voltages. The important components of transformers with regard to earthquake performance are anchorage, bushings, and connections to other equipment. Transformers are usually isolated in case of abnormal operating conditions through the opening of the circuit breakers which are usually located next to the transformers. Power transformers typically have several protective relays that monitor performance and provide electrical protection. Some protective relays may be activated by an earthquake and cause the transformer to be taken offline. These relays can prevent damage to the distribution system in an earthquake. Earthquake induced vibrations can cause distribution lines to swing and adjacent phases to come in contact. This can consequently cause the lines to wrap around each other, to burn down, or to blow fuses and trip circuit breakers. Therefore special care should be given to the slack configurations of the interconnecting equipment.

The anchorage of transformers is another issue that requires special attention. Transformers are usually placed on top of a concrete pad or on rails without anchorage in seismically safe regions. Another anchorage approach is bolting the transformer to a concrete foundation where there is seismic risk. There are many transformer configurations and constraints in designing transformer anchorage retrofits. Cost and materials, as well as geometric constraints, may yield less than optimal designs that are nonetheless adequate. The installation of transformers without anchorage should be avoided because of the significant loss associated with the transformer damage. Base isolation can be provided as a rehabilitation scheme for transformers to lessen the earthquake induced accelerations. However, there have been significant problems with existing base isolation designs that use conical shape disk springs (washer) [IEEE, 1998]. Base isolation requires very careful evaluation to assure that the desired effects are achieved. Large displacements resulting from the base isolation can potentially cause problems with the amount of slack cable between system components. Generous slack can be provided to accommodate the increased demand for flexible conductor connections as long as the electrical clearances provided are sufficient.

Several researchers have performed experimental and finite element studies on transformers and bushings [Gilani, 1998, 1999; Villaverde, 1999]. Most recent tests were performed at PEER (Pacific Earthquake Engineering Research Center) [Gilani, 1998, 1999] and Construction Engineering Research Laboratories of US Army Corp of Engineers [Wilcoski 1997]. Bushings tests were performed using a stiff supporting frame in these cases. Even though the most

vulnerable flange to porcelain gasket detail has been used in these tests, the performance of 196 kV, 230 kV and 550 kV bushings was fairly good in terms of the general response based on the qualification of bushings set forth in IEEE 693-1997. However, many bushings of the same type have failed in past earthquakes. This situation points to the need for reassessment of the current IEEE 693-1997 qualification procedures for both transformer and bushings. Electrical equipment components are typically designed for electrical requirements more than structural performance requirements. Interconnecting substation components can complicate the seismic response. It is likely that significant seismic interaction and equipment damage can occur using either flexible or rigid connectors. Therefore the identification of critical loading environments for bushings using shake table tests alone is not likely. The critical loading of bushings can be either due to dynamic effect of the transformer tank or loads at the terminal end of the bushing due to vibration of the transformer and its connected equipment. Finite element analysis will help to understand the response characteristics of transformer bushing system and to quantify their interaction. Besides, these analyses will provide the knowledge base for development of simplified models of substation equipment.

In this section, the seismic qualification procedures of the most recent code for substations are summarized first. Then, modeling and analysis issues of three different types of transformers follow. Finally, the response criteria and the finite element results are given for analyzed transformer bushing systems. One of the main purposes of this chapter is to provide the necessary input for development of simplified model of a portion of a substation.

2.1 IEEE Seismic Qualification Procedures for Transformers and Bushings

Seismic qualification tests are used to demonstrate through experimentation that a piece of equipment is able to perform its intended function during and after an earthquake. In the United States, electrical equipment is seismically qualified using a standard developed by the Institute of Electrical and Electronic Engineers. The IEEE standard entitled IEEE 693-1997 Recommended Practices for Seismic Design of Substations details procedures for qualification of electrical substation equipment for different seismic performance levels (high, moderate, and low).

For qualification, the transformer and its appendages, except bushings, are required to satisfy static analysis using 0.5g in two horizontal directions and 0.4g simultaneously in the vertical direction. However, IEEE 693-1997 states that bushings rated at 161 kV and above must be qualified using three-component earthquake-simulator tests. Because it is impractical to test bushings mounted on a transformer, IEEE specifies that bushings must be mounted on a rigid stand for earthquake testing and qualification. IEEE 693-1997 identifies several response spectra of identical shape but different amplitudes for the qualification of a transformer bushing on an earthquake simulator.

Performance Levels (PL) for substation equipment are represented by a response spectrum that is anchored to peak ground acceleration (PGA) of 0.5g for Moderate Level qualification and 1.0g for High Level qualification. Since it is often impractical to test components to the PL, IEEE 693-1997 permits equipment to be tested using a reduced level of shaking called the Required Response Spectrum (RRS). RRS corresponds to a PGA of 0.25g and PGA of 0.5g, for Moderate

Level and High Level qualification respectively. To account for the amplification of earthquake motion due to the flexibility of the transformer and the local flexibility, IEEE 693-1997 states that the input motion measured at the bushing flange shall match a spectrum with ordinates twice that of the RRS, termed as the Test Response Spectra for Mounted Equipment (TRSME). The PGA for the TRSME spectrum is therefore 0.5g for Moderate Level qualification and 1.0g for High Level qualification. For this level of shaking, IEEE recommendations are as follows:

1. The stresses in non-ductile components must be less than one-half the ultimate stress
2. The factor of safety against oil leakage must exceed 2.

Since there are no earthquake simulators capable of subjecting equipment to shaking compatible with the spectrum for High Level qualification, a response amplification factor of 2.0 is applied as bushing input.

Anchorage is stated as one of the most cost effective measure to improve the performance of inadequately anchored equipment. Anchorage must withstand the shear, uplift, and compressive forces resulting from the design earthquake. Conductor length determinations are based on the displacements of the equipment that conductor is attached to at each end. The recommended method in IEEE is summation of the equipment displacements multiplied by a factor of 1.5, straight line distance between connection points, and minimum required slack for conductor configuration under consideration. Three basic configurations are given in the IEEE specifications based on the conductor size, equipment differential movement, vertical and horizontal separation of the termination points and voltage.

2.2 Modeling and Analysis Issues for the Transformer and Bushing

A typical power transformer is composed of six parts: transformer tank, radiators, reservoir, core and coil, mineral oil, and bushings. The transformer tank is the main structural component of power transformers. Lateral bracing of the tank wall is provided usually by plates as channels. It has a core and a coil centrally placed within 2/3 of transformer height and the tank is completely filled by mineral oil. Radiators and reservoirs are appendages that are externally attached to the transformer tank.

Three different sizes of power transformers were selected for time history analysis. First transformer type is 25 MVA – 650 HV BIL and it is called transformer type 1 (TT1) in this study. This transformer weighs about 179 kips and does not have a reservoir. The dimensions of this transformer are B=85", L=125", H=170" (B, L, and H represents width, length, and height of the transformer tank, respectively). The second transformer type is 33/44/55 MVA 230/133 HV three phase transformer and it is called transformer type 2 (TT2) in this study. It weighs about 300 kips and the radiators (on the side) and reservoir weigh 27 kips and 9 kips, respectively. The dimensions of this transformer are B=100", L=200", H=200". Third transformer type is 250 MVA 230/119.5 kV and it is called transformer type 3 (TT3) hereafter in this study. Its weight is about 512 kips. The dimensions of this transformer are B=100", L=280", H=180".

The finite element package ANSYS is used for development of the finite element model [ANSYS]. The transformer tank is modeled by shell elements. Braces around the transformer

tank are modeled by offset beam elements. The core and coil inside the transformer are modeled as mass elements. The radiators and the reservoir are modeled by 3-D solid elements. The contained oil inside the transformer was modeled with fluid elements in early stages of this study. Later the contained oil was modeled as a solid with modulus of elasticity equal to the bulk modulus of the fluid since the transformer is filled completely with oil and there is no slashing effect under consideration. The results obtained from both methods were similar, but solid modeling of the contained oil is computationally more efficient. These three types of transformer all support 3-196 kV bushings that are located on top of the transformer tank.

Bushings are composed of several elements, namely; an aluminum support unit, porcelain units, gaskets, aluminum core, and dome. The aluminum support has a built-in flange used to mount the bushing on top of the transformer. The aluminum core runs from the top to the bottom of the bushing and houses the aluminum conductor. Bushings are prestressed through the aluminum core and this prestressing force is distributed evenly to the other components through the dome to hold the units together. There are gaskets located in between the units. Finite element model of one of the transformers with element types and details is shown in Figure 2-1. Schematic view of a portion of a bushing model is shown in Figure 2-2. Based on this information, the analytical models for the bushings were created by beam elements with equivalent density and stiffness to represent the porcelain units, the dome, and the aluminum core. Gaskets between these elements are modeled using linear axial and shear springs. The total axial stiffness is introduced as in equation (2-1).

$$K_a = \frac{AE}{t} \tag{2-1}$$

Moreover the shear stiffness is obtained by equation (2-2).

$$K_s = \frac{AG}{t} \tag{2-2}$$

In these equations, A is the area of the gasket, E is young's modulus, G is the shear modulus and t is the thickness of the gasket.

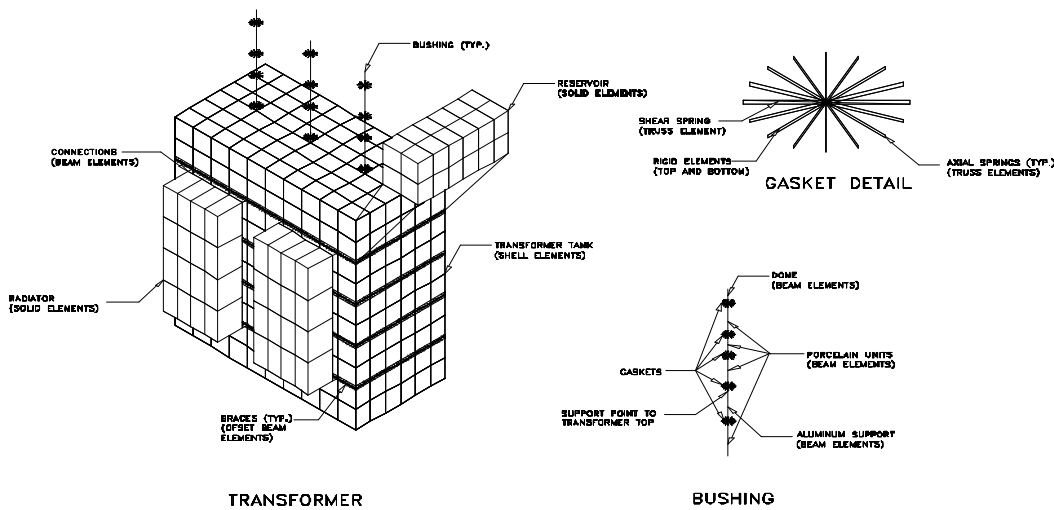


Figure 2-1 Mesh of Transformer and Element Types

Since anchoring of a transformer at its corners is a common practice, the transformer models are fixed at each corner of the transformer.

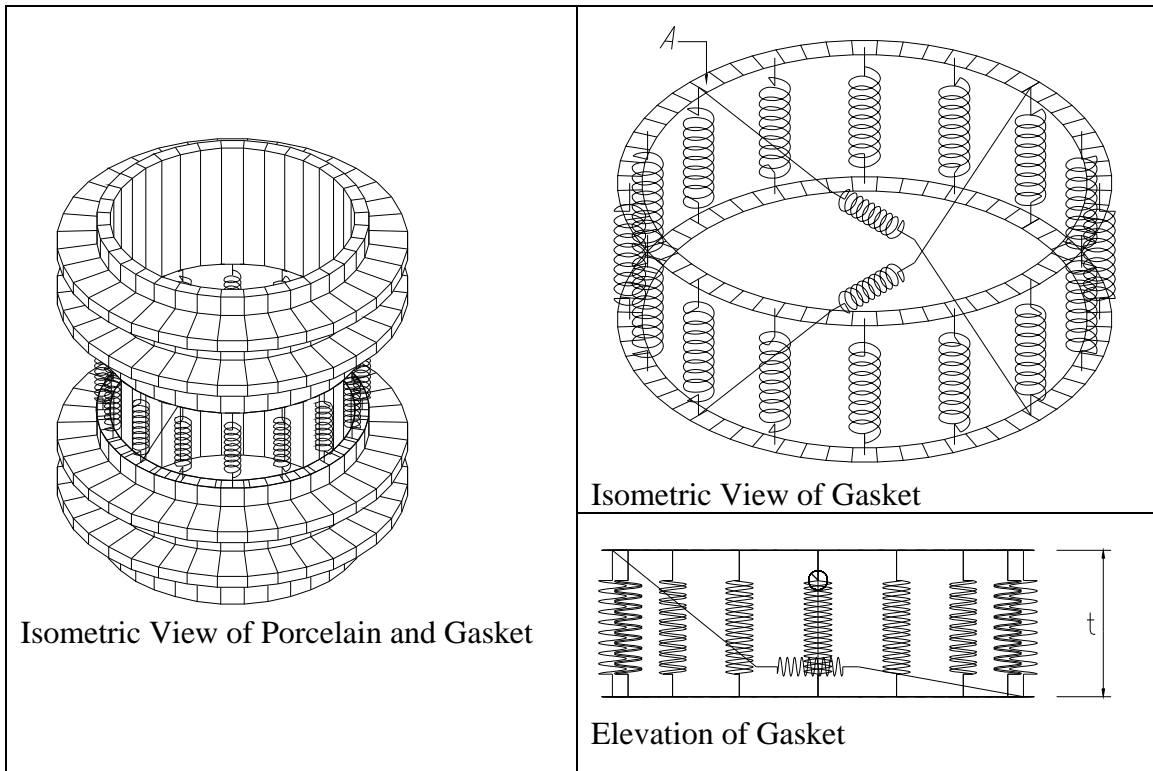


Figure 2-2 Views of Gasket Model

Full time history analyses are performed for ground input with PGA of 1g in orthogonal horizontal directions and PGA of 0.8 g in the vertical direction as per IEEE recommendation. For each transformer type, 2-soil and 2-rock earthquake records are utilized for 3-D time history analysis. The response spectrum of the earthquake motions (soil records) used for orthogonal horizontal components and vertical component together with the IEEE High Performance level spectra are shown in 0figure 2-3 and figure 2-4 for 2 % damping.

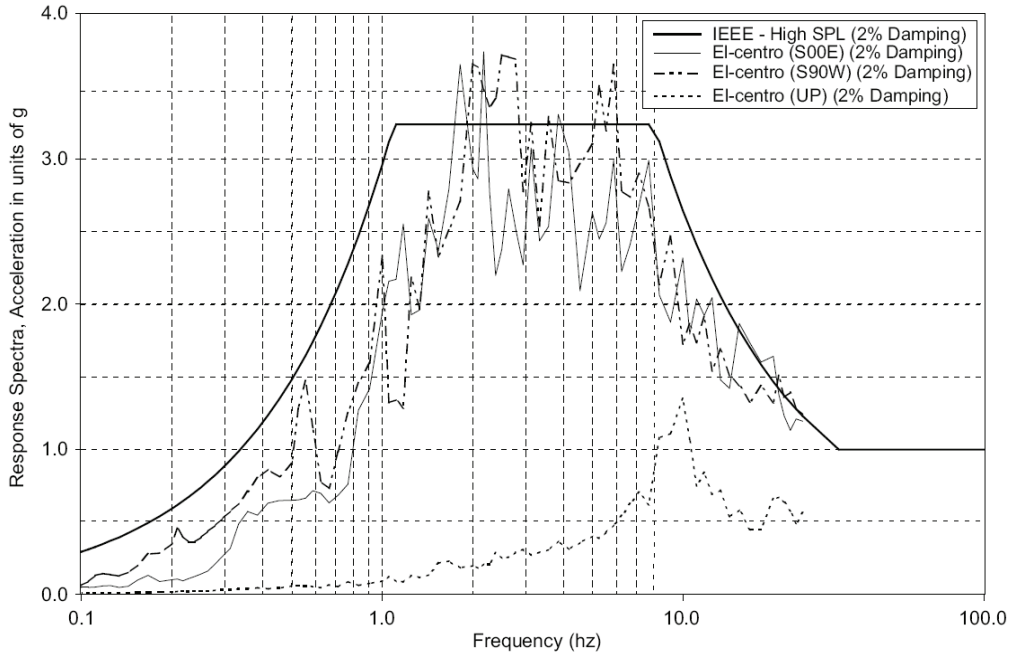


Figure 2-3 Acceleration Response Spectra for Components of El-Centro Record and IEEE High Performance Level

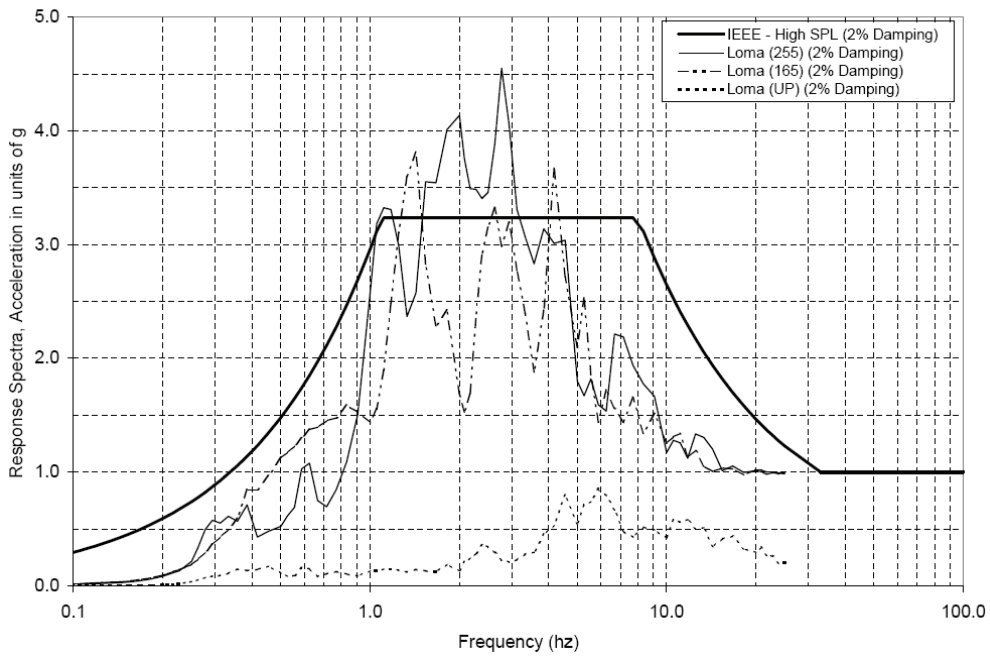


Figure 2-4 Acceleration Response Spectra for Components of Hollister Airport Record and IEEE High Performance Level

The response spectrum of component of the rock records with IEEE High Performance level spectra are shown in 0figure 2-5 and 0figure 2-6 for 2 % damping.

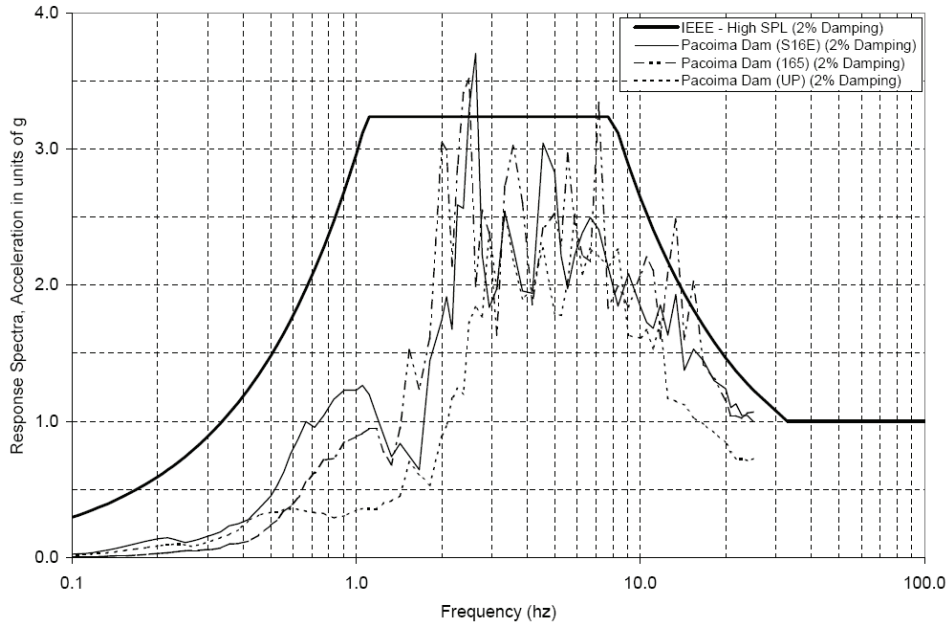


Figure 2-5 Acceleration Response Spectra for Components of Pacoima Dam Record and IEEE High Performance Level

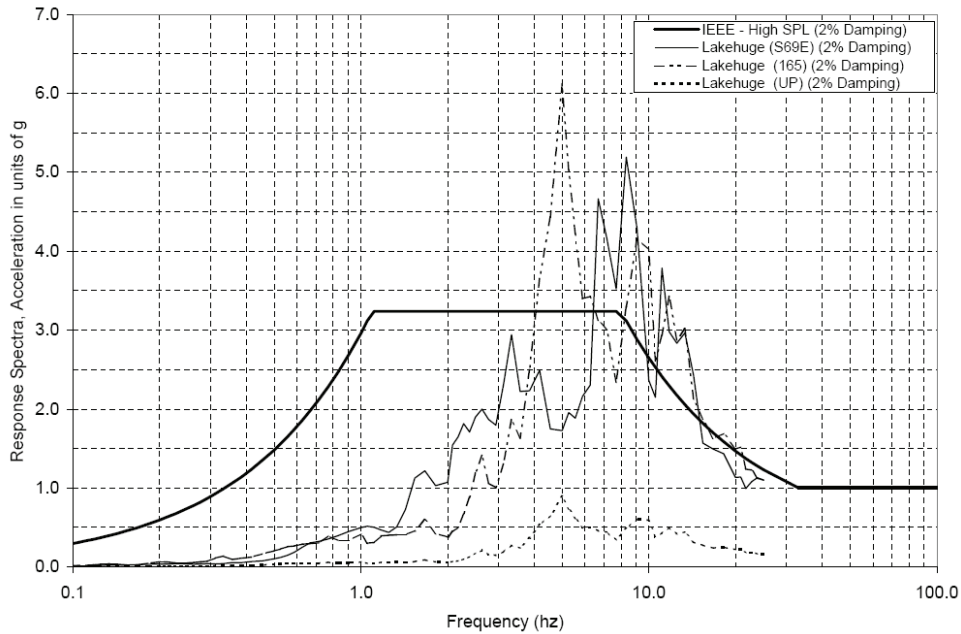


Figure 2-6 Acceleration Response Spectra for Components of Lake Hughes Array #4 Record and IEEE High Performance Level

Based on IEEE 693-1997, 2% damping value was employed in the finite element model. Rayleigh damping is used for all the time history analysis and the Rayleigh damping coefficients were obtained by fixing the damping value at 0.02 for frequencies of 8 Hz and 25 Hz (shown in Ofigure 2-7). These frequency values were selected based on the response frequencies of the transformer bushing systems. The minimum damping value obtained in this frequency range is 1.71 %.

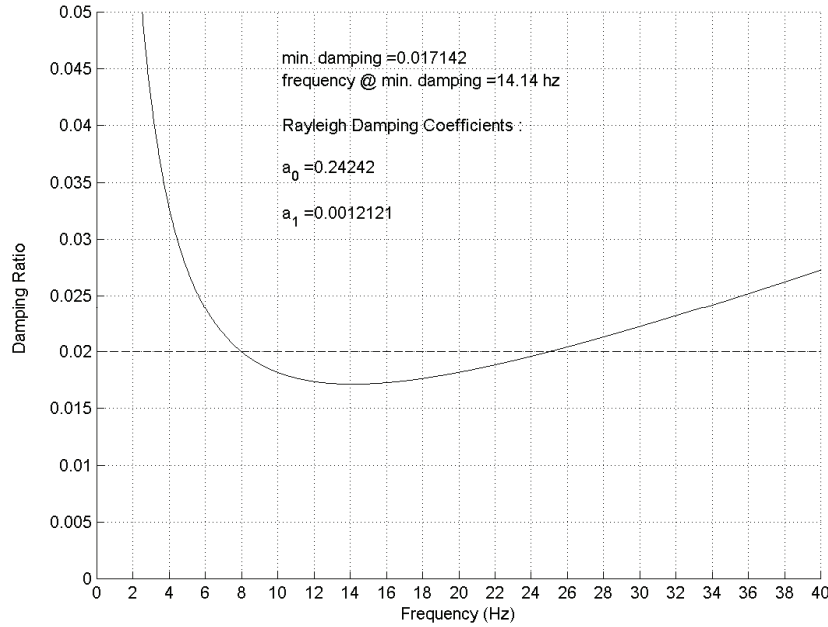


Figure 2-7 Determination of Rayleigh Damping Coefficients for Analysis

2.3 Response Criteria for Transformer and Bushing

Five fragility criteria for bushings were identified in this study:

1. Gap between the porcelain units and/or aluminum components and the gasket.
2. Stress/Strain levels in the gasket.
3. Stress/Strain levels in porcelain units.
4. Top displacement of bushing based on slack.
5. Loss of pre-stress/relaxation.

The first two of these criteria are related to the gasket. The third and fourth items are associated with the strength of the porcelain units, which may cause failure of bushing such as cracking of the porcelain due to high pressure or insufficient slack provided between bushing and the connecting equipment. There have been examples of failures caused by insufficient slack during past earthquakes.

2.4 Finite Element Analysis Results

In this finite element analysis, weak and strong orthogonal horizontal axes are referred to x and y directions, respectively. The vertical axis is referred to as the z direction. Transformer type 1, transformer type 2, and transformer type 3 are described as TT1, TT2, and TT3, respectively.

Finite Element (FE) responses are monitored at several locations throughout the height of the transformer and the bushing. Displacement, velocity and acceleration responses on the transformer tank are obtained for five levels through the height of transformer, at each corner and the center point between the corners. Schematic view of the points monitored is shown in figure 2-80. Displacement, velocity and acceleration responses of 12 points for each of the three bushings are also monitored. Figure 2-9 shows the monitored points on the bushings. These 12 points are top of bushing, bottom of bushing and a total of 10 points at the top and the bottom of 5 gaskets.

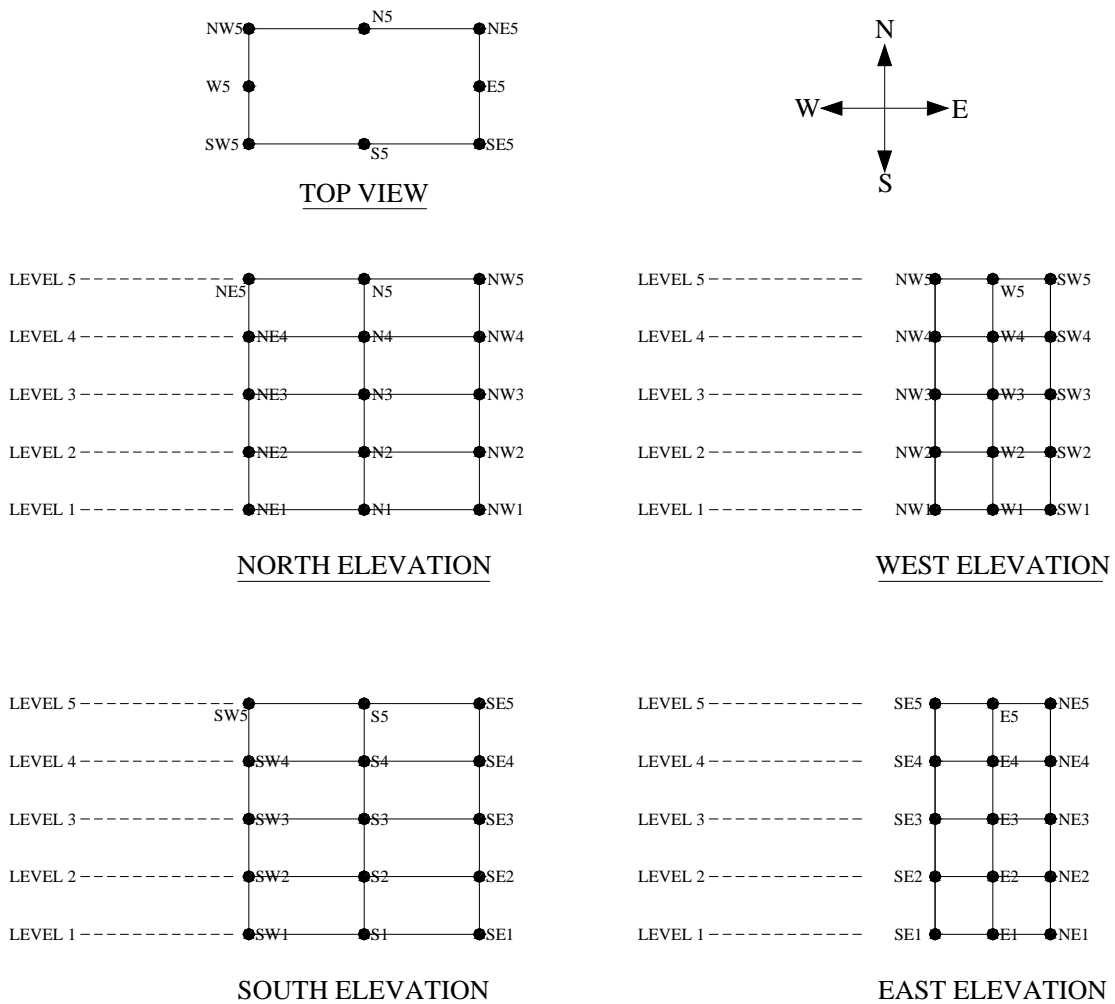


Figure 2-8 Monitored Nodes on Transformer Model

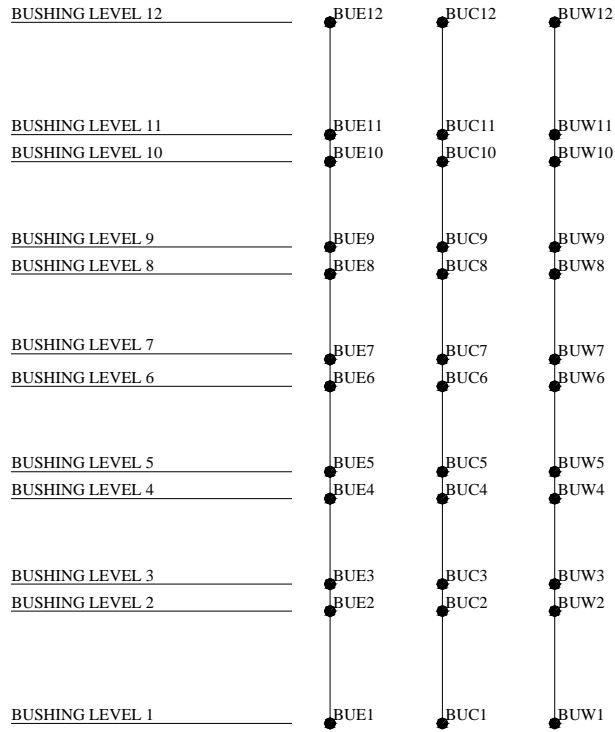


Figure 2-9 Points Monitored on Bushing Finite Element Model

2.4.1 Dynamic Response of Transformers

Modal analyses show that translational modes of the transformers have the highest participation in their response. Frequency of the translational mode of TT1 in x-direction (weak horizontal axis) is 14.1 Hz. That of TT2 and TT3 is 13.8 Hz. and 11.7 Hz., respectively. The maximum relative displacement and total acceleration responses at mid height of transformer, top of transformer and top of bushing for TT1, TT2, and TT3 are tabulated in table 2-1, table 2-2 and table 2-3, respectively (the bushings will be discussed in a following section). The maximum translation at the top of the transformer in x-direction is 0.12 inch for TT1. That of TT2 and TT3 is 0.14 inch and 0.21 inch, respectively. One can note that the translations in y-direction are always smaller than the ones in the x-direction due to higher stiffness of the transformers in the y-direction. Comparison of the displacement values at mid-height of the transformer to those at the top of the transformer shows that mid-height displacement values are one half of the top displacements. It can be deduced that there is almost always a linear relationship for the displacement values throughout the height of the transformer (shear mode deformation of the transformer tank).

Table 2-1 Summary of Maximum Displacement and Acceleration Responses for TT1

Transformer Type	EQ Record	Location	Displacement (in)			Acceleration (g)		
			x	y	z	x	y	z
TT1	El-Centro	Mid level of Transformer	0.045	0.022	0.020	1.011	0.999	0.490
		Top of Transformer	0.091	0.039	0.021	1.383	1.308	0.510
		Top of Bushing	0.550	0.244	0.012	6.179	2.967	0.541
	Hollister Airport	Mid level of Transformer	0.038	0.018	0.017	1.021	1.011	0.185
		Top of Transformer	0.074	0.032	0.018	1.134	1.020	0.193
		Top of Bushing	0.282	0.143	0.011	2.858	1.150	0.419
	Pacoima Dam	Mid level of Transformer	0.046	0.020	0.021	1.092	1.074	0.264
		Top of Transformer	0.093	0.035	0.021	1.532	1.129	0.274
		Top of Bushing	0.600	0.263	0.011	7.975	2.750	0.379
	Lake Hughes Array #4	Mid level of Transformer	0.059	0.022	0.025	1.301	1.116	0.421
		Top of Transformer	0.118	0.038	0.025	2.002	1.293	0.437
		Top of Bushing	0.954	0.372	0.011	10.949	3.962	0.370

The maximum dynamic amplification factor is found to be 2 for TT1. That of TT2 and TT3 is determined to be 2.4 and 2.5, respectively. Therefore it can be stated that the dynamic amplification due to the transformer body stated as 2 by IEEE 693-1997 is not always conservative. The dynamic amplification for smaller transformer, namely TT1 is satisfactory; however, it is not suitable for TT2 and TT3.

Table 2-2 Summary of Maximum Displacement and Acceleration Responses for TT2

Transformer Type	EQ Record	Location	Displacement (in)			Acceleration (g)		
			x	y	z	x	y	z
TT2	El-Centro	Mid level of Transformer	0.059	0.018	0.025	1.056	1.000	0.618
		Top of Transformer	0.120	0.028	0.026	1.495	1.176	0.645
		Top of Bushing	0.597	0.265	0.015	5.449	2.087	0.701
	Hollister Airport	Mid level of Transformer	0.049	0.019	0.022	1.029	1.010	0.235
		Top of Transformer	0.099	0.032	0.023	1.194	1.016	0.245
		Top of Bushing	0.285	0.213	0.014	2.440	1.313	0.485
	Pacoima Dam	Mid level of Transformer	0.054	0.016	0.023	1.154	1.051	0.322
		Top of Transformer	0.105	0.024	0.023	1.724	1.074	0.331
		Top of Bushing	0.577	0.298	0.013	6.737	2.466	0.426
	Lake Hughes Array #4	Mid level of Transformer	0.070	0.019	0.029	1.375	1.083	0.512
		Top of Transformer	0.138	0.030	0.030	2.376	1.195	0.526
		Top of Bushing	0.809	0.433	0.012	8.297	3.722	0.417

Table 2-3 Summary of Maximum Displacements and Acceleration Responses for TT3

Transformer Type	EQ Record	Location	Displacement (in)			Acceleration (g)		
			x	y	z	x	y	z
TT3	El-Centro	Mid level of Transformer	0.086	0.022	0.025	1.265	1.011	0.501
		Top of Transformer	0.175	0.029	0.045	2.038	1.037	0.709
		Top of Bushing	1.229	0.288	0.036	12.386	2.791	0.730
	Hollister Airport	Mid level of Transformer	0.064	0.020	0.031	1.034	1.012	0.457
		Top of Transformer	0.120	0.026	0.032	1.281	1.015	0.474
		Top of Bushing	0.539	0.188	0.037	5.081	1.368	0.567
	Pacoima Dam	Mid level of Transformer	0.090	0.023	0.036	1.311	1.097	0.410
		Top of Transformer	0.168	0.028	0.037	1.787	1.117	0.428
		Top of Bushing	1.156	0.314	0.028	12.118	2.814	0.403
	Lake Hughes Array #4	Mid level of Transformer	0.111	0.024	0.046	1.624	1.146	0.673
		Top of Transformer	0.212	0.030	0.048	2.515	1.187	0.701
		Top of Bushing	1.563	0.497	0.027	18.385	4.544	0.466

Support reactions are given in Otable 2-4, table 2-5, and Otable 2-6 for TT1, TT2, and TT3, respectively, for different earthquake records. The maximum vertical support reaction is 230 kips and the corresponding horizontal reaction is 98 kips in x direction (weak axis), for TT1. Maximum vertical support reaction is 256 kips and corresponding horizontal reaction is 103 kips in x direction, for TT2. Similarly, the maximum vertical support reaction is 440 kips and corresponding horizontal reaction is 246 kips in x direction, for TT3. The maximum reactions were also computed by the static analysis method specified in IEEE recommendations [IEEE 1998]. The center of gravity of for each transformer type is assumed at center of the tank. Acceleration of 0.5g in horizontal direction (weak axis) and 0.4g in vertical direction are applied to the center of gravity for each transformer type. Dimensions of the transformer tanks are given earlier in this section. Self-weight of transformers are not considered in calculation of overturning moments. The vertical static acceleration (0.4g) is applied in upward direction for critical overturning moment. Static calculations are carried out to get vertical and horizontal reactions. Calculations are given in Appendix A of this report. Vertical reaction is 63 kips and horizontal reaction is 22 kips in horizontal weak axis, for TT1. Vertical reaction is 105 kips and horizontal reaction is 38 kips in horizontal weak axis, for TT2. Similarly, vertical reaction is 166 kips and horizontal reaction is 64 kips in horizontal weak axis, for TT3.

In this finite element study, time history analyses are performed for ground input with PGA of 1g in orthogonal horizontal directions and PGA of 0.8 g in the vertical direction. However, static analysis recommended for transformer tanks utilizes 0.5g in horizontal directions and 0.4g in vertical direction, applied to the center of the transformer tank. It is seen that the vertical reaction obtained from the IEEE recommendations is 73% less than the finite element analysis result for TT1. Similarly, the vertical reactions are 59% and 62% less than the finite element analysis results for TT2 and TT3, respectively. It is also noted that the horizontal reaction obtained from the recommendations is 78% less than the finite element analysis result for TT1. Similarly, the horizontal reactions are 63% and 74% less than the finite element analysis results for TT2 and TT3, respectively.

Table 2-4 Summary of Maximum Support Reactions for TT1

Transformer Type	EQ Record	Location	Force (kips)		
			x	y	z
TT1	El-Centro	Support 1	60.6	70.8	132.1
		Support 2	76.4	79.9	159.3
		Support 3	72.6	83.3	173.2
		Support 4	60.4	70.7	130.1
	Hollister Airport	Support 1	77.9	75.3	140.8
		Support 2	71.6	82.7	137.3
		Support 3	73.2	84.7	149.3
		Support 4	73.3	71.5	134.8
	Pacoima Dam	Support 1	88.4	103.8	186.7
		Support 2	70.2	74.3	138.7
		Support 3	56.0	63.4	111.2
		Support 4	98.0	125.9	230.1
	Lake Hughes Array #4	Support 1	79.4	97.0	188.6
		Support 2	90.0	91.6	200.8
		Support 3	89.4	107.5	204.6
		Support 4	85.2	99.1	183.1

Table 2-5 Summary of Maximum Support Reactions for TT2

Transformer Type	EQ Record	Location	Force (kips)		
			x	y	z
TT2	El-Centro	Support 1	87.8	105.1	198.8
		Support 2	90.8	97.5	180.8
		Support 3	90.0	96.0	181.8
		Support 4	74.4	95.6	192.3
	Hollister Airport	Support 1	93.5	94.1	175.7
		Support 2	79.4	103.9	189.6
		Support 3	107.2	107.8	204.9
		Support 4	85.5	78.9	156.3
	Pacoima Dam	Support 1	96.5	114.3	186.3
		Support 2	81.8	89.1	173.2
		Support 3	75.3	64.7	139.0
		Support 4	117.6	134.9	221.5
	Lake Hughes Array #4	Support 1	104.2	112.6	232.9
		Support 2	103.4	109.5	256.3
		Support 3	115.7	111.6	242.5
		Support 4	109.6	113.0	234.0

Table 2-6 Summary of Maximum Support Reactions for TT3

Transformer Type	EQ Record	Location	Force (kips)		
			x	y	z
TT3	El-Centro	Support 1	152.7	182.4	346.5
		Support 2	181.3	199.0	368.9
		Support 3	191.7	203.9	358.0
		Support 4	160.3	161.1	318.5
	Hollister Airport	Support 1	160.8	168.9	241.5
		Support 2	145.3	182.2	224.6
		Support 3	162.7	183.1	257.2
		Support 4	151.3	151.8	235.8
	Pacoima Dam	Support 1	196.9	180.0	339.0
		Support 2	191.7	176.7	339.6
		Support 3	164.9	135.9	262.6
		Support 4	174.7	207.3	282.2
	Lake Hughes Array #4	Support 1	245.5	280.6	440.2
		Support 2	220.0	233.0	375.0
		Support 3	223.5	259.6	383.6
		Support 4	226.2	230.3	387.5

Figure 2-10 through figure 2-12 show relative displacements, acceleration responses, and the normalized power spectra of the acceleration responses at top of transformer at one of the top corners (SW5) for TT2. As an example figure 2-10 contains 2-time history graphs and 1-normalized power spectrum graph. The upper plot shows the relative displacement time history and the second graph in this figure shows the acceleration time history. Normalized power spectra graphs help us better understand the frequency response of the transformer-bushing system. Normalized power spectra are obtained by taking advantage of the Fast Fourier Transformation (FFT). As it is seen in this figure, the response frequency of SW5 point in this graph gives us the value 13.85 Hz and this value is very close to that of mode 7 of TT2 (14.1 Hz). It can be pointed out that the translational modes of transformers have the highest participation in the response at the top of transformers.

Failure of transformer and its components other than bushing was not found in the finite element analysis performed in this study. The stress responses of the transformer tank are below the allowable material stresses. Failure of the transformer bushing system is introduced at the gap between the bushing units. For the fixed case, since the base forces are so high, providing proper

anchorage is a major problem. A base isolation system (FPS) is investigated as a retrofitting scheme under this study and results are presented in the next section. Base isolation of the transformer reduces the base forces of the transformer; therefore, it can be a possible solution for eliminating high anchorage forces.

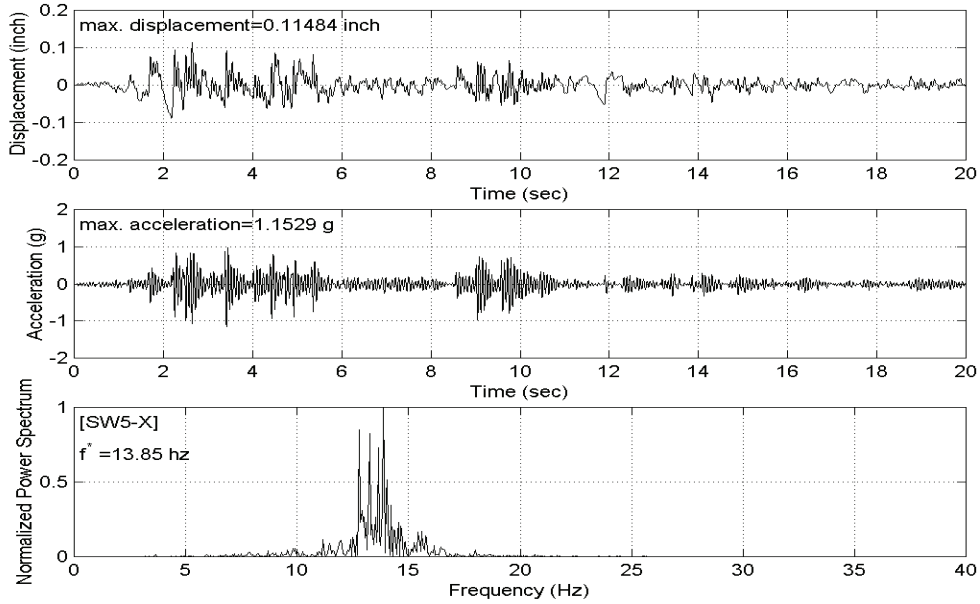


Figure 2-10 Displacement, Acceleration Responses and Normalized Power Spectrum at SW5 of TT2 for El-Centro Record in X-direction

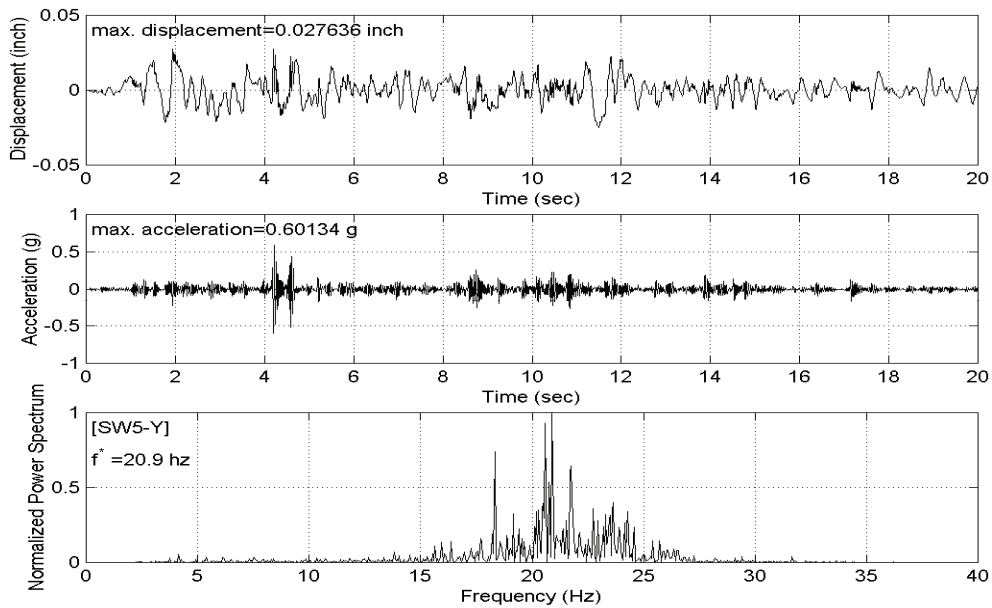


Figure 2-11 Displacement, Acceleration Responses and Normalized Power Spectrum at SW5 of TT2 for El-Centro Record in Y-direction

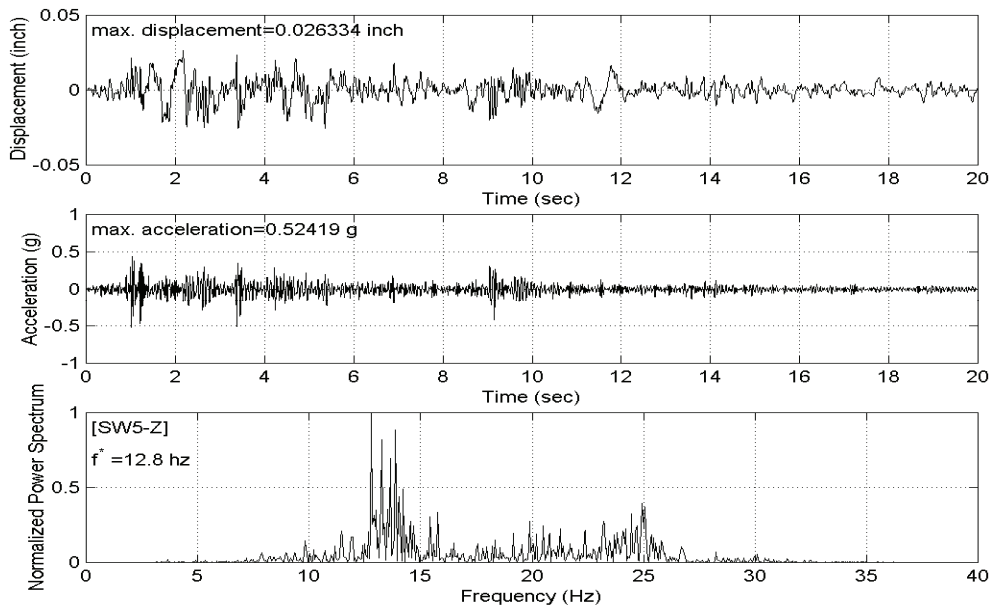


Figure 2-12 Displacement, Acceleration Responses and Normalized Power Spectrum at SW5 of TT2 for El-Centro Record in Z-direction

2.4.2 Dynamic Response of Bushing

The maximum responses at top of bushing mounted on top of transformers TT1, TT2, and TT3 are tabulated in Otable 2-1, Otable 2-2 and Otable 2-3, respectively. These are for four different earthquake records. Ofigure 2-13 through Ofigure 2-15 show relative displacement, acceleration response, and the normalized power spectrum of the acceleration responses at the top of the east bushing (BUE12), center bushing (BUC12), and west bushing (BUW12) mounted on TT2.

As an illustrative example, figure 2-13 contains two time history graphs and one normalized power spectrum graph. The upper plot shows the relative displacement time history and the second graph in this figure shows the acceleration time history. Bushing frequency is obtained as 9.9 Hz from normalized power spectrum. The fundamental frequency of the bushing was obtained as 14.4 Hz from the modal analysis of bushing itself fixed at flange of the bushing. The transformer top plate has an effect on the dynamic characteristics of the bushing. As a general tendency, the translation mode of the transformer affects the input into the bushing by filtering the motion and causing higher mode to be excited. For the bushing mounted on TT1, frequency is reduced to 11 Hz. For the bushing mounted on TT2, frequency is reduced to 10 Hz. And the response frequency of bushing mounted on TT3 is reduced to 10.5 Hz.

The maximum displacement response at the top of the bushing in x-direction (weak horizontal axis) for four earthquake inputs throughout the time history analysis is 0.95 inch for bushing mounted on TT1. That of the bushing mounted on TT2 and TT3 is obtained as 0.81 inch and 1.56 inch, respectively. The maximum total acceleration response at the top of the bushing in x-direction (weak horizontal axis) for four earthquake inputs throughout the time history analysis is

10.9g for bushings mounted on TT1. That of bushings mounted on TT2 and TT3 is obtained as 8.3g and 18.4g, respectively.

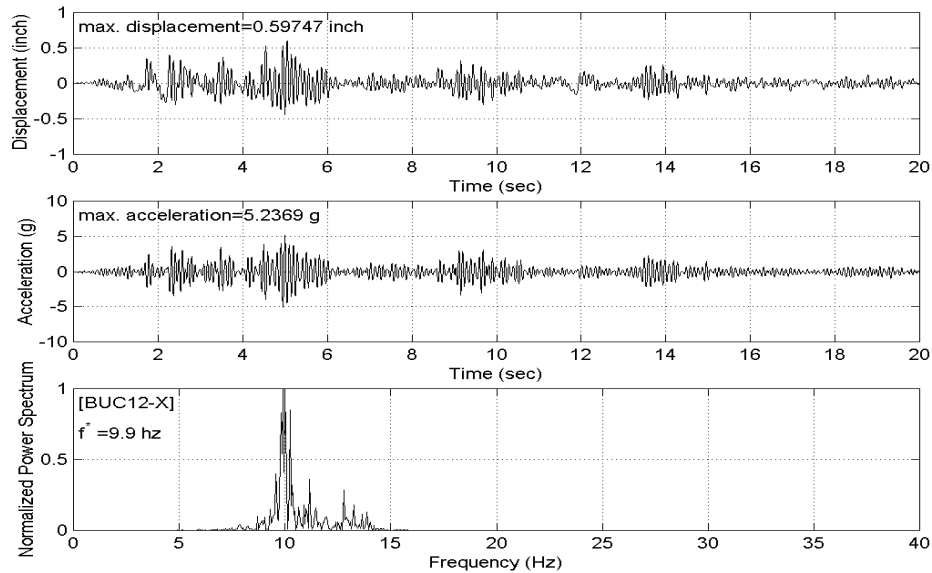


Figure 2-13 Displacement, Acceleration Responses and Normalized Power Spectrum at BUC12 of TT2 for El-Centro Record in X-direction

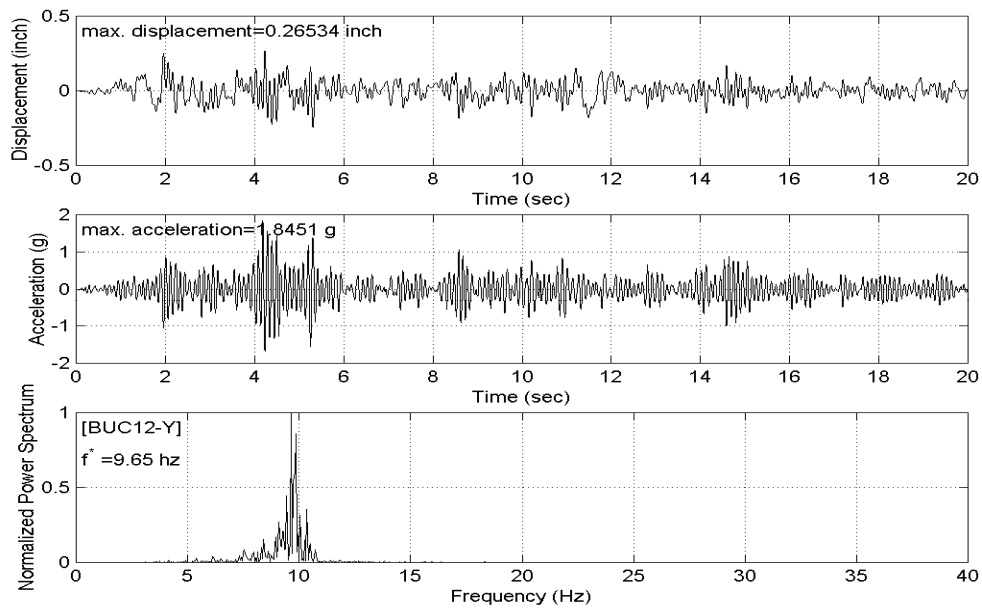


Figure 2-14 Displacement, Acceleration Responses and Normalized Power Spectrum at BUC12 of TT2 for El-Centro Record in Y-direction

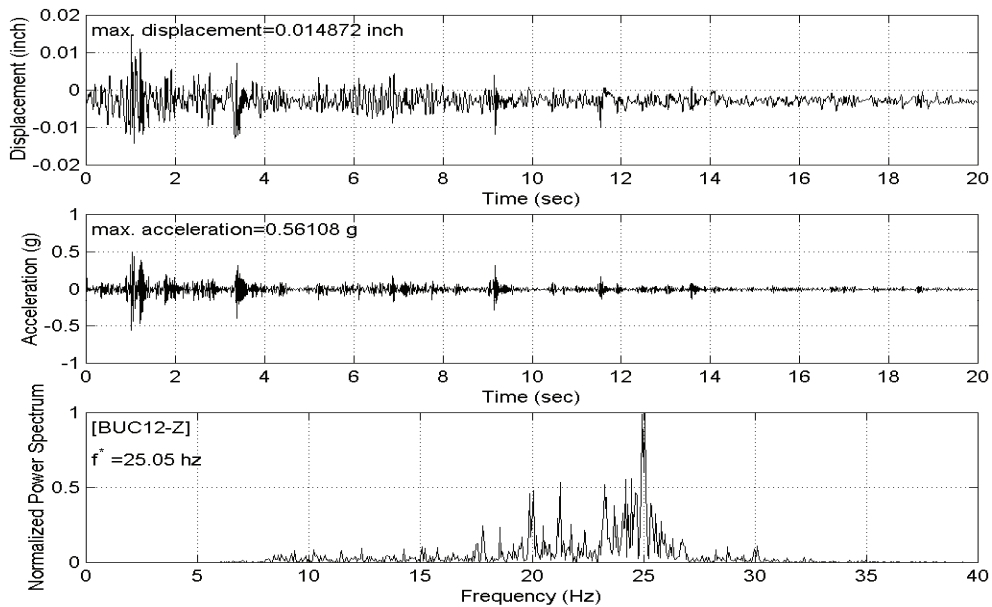


Figure 2-15 Displacement, Acceleration Responses and Normalized Power Spectrum at BUC12 of TT2 for El-Centro Record in Z-direction

Axial responses of bushing gaskets are also analyzed in this section. The seismic response of the bushings is dominated by the behavior of the gaskets between the porcelain units. One of the common failure modes involves movement of the upper porcelain unit relative to its support flange, causing oil leakage. In the following figure two gaskets located right above the flange are referred to as gasket 2 and the first gasket from the top of bushing is referred to as gasket 5. The vertical axis in the graph shows the gap between the gasket and the porcelain components. Since the bushing is prestressed, the gap initially starts from some negative value showing the initial displacement of the gasket under prestress force. The positive gap amount illustrates that there is a gap during the time history loading between the gasket edge and porcelain unit. The positive gap causes oil leakage from the bushing. As one can note from 0figure 2-16 the gap near the aluminum flange of the bushing, called gasket 2 in this study, is always more serious for bushing. The gap forms due to the relative vertical displacements of the units right above and below the gaskets and the rotation of these two units. No formation of a positive gap is observed in time history analyses performed for TT1. However, a gap forms during the analysis of TT2 and TT3. 0Figure 2-16 shows the most critical condition, which occurs for TT3 with Lake Hughes Array #4 record. Since failure is likely some preventive measures are needed.

The porcelain units are brittle and fragile components, therefore, stress and strain levels in these units were also investigated under this study. Based on the previous studies performed on porcelain units, their ultimate axial strain capacity is $4000E-6$ in/in [Gilani, 1998]. It is observed that stress/strain levels in the porcelain units are well below the capacity.

The bushing has an aluminum core housing the copper cables between equipment items and the coils, throughout its length. The bushing is post-tensioned through its aluminum core and the

springs in the metallic dome ensure the uniform distribution of this prestress force. The relaxation effect of the axial dynamic force is also examined. It is found that the effect of axial vibration of the bushing on the prestressing is insignificant, indicating that there has not been any prestress loss.

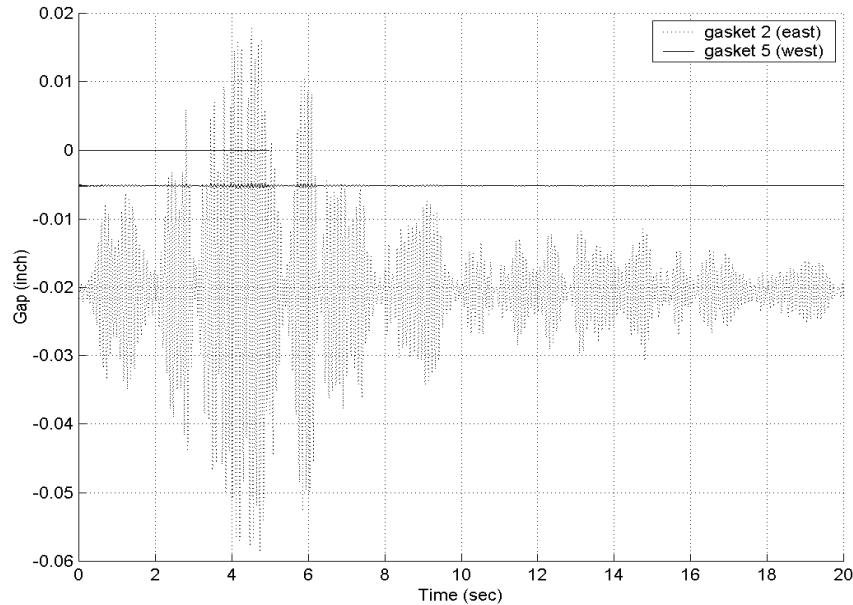


Figure 2-16 Gap in the Bushing Gasket Mounted on TT3 for Lake Hughes Array # 4 Record

As it was stated previously, the transformer models used in the finite element analyses were fixed at each corner of bottom transformer plate. The finite element analyses results show that anchoring of transformer to its base does not prevent the interaction between transformer and bushing and causes bushing failure for some of the cases. For this reason, the implementation of well-designed anchorage for retrofit of existing transformers can be difficult and costly. Furthermore, in many situations, for both new and existing transformers, a well-designed anchorage may only change the mode of failure to the foundation. Boundary gaps due to back and forth motion of transformers and rocking of transformers and their footings due to soil-structure interaction have been observed during past earthquakes [ASCE, 1999]. Therefore, in many cases the use of base-isolation for transformers may be the only suitable remedy to alleviate these problems, especially for existing transformers in high seismic regions. Base-isolation will also reduce the input acceleration into the bushing and will lessen the interaction between the transformer and the bushing, which has been the cause of many bushing failures during past earthquakes. Furthermore, by reducing the inertia forces, base-isolation can also prevent the possibility of internal damage. The after effect of an earthquake on reliability and longevity of a transformer is directly related to the level of shaking of internal elements. High level of uncontrolled shaking may very well reduce the life expectancy and reliability of internal elements.

SECTION 3

STUDY OF THE FRICTIONAL PENDULUM SYSTEM

Base isolation is a simple structural design approach to mitigate or reduce potential earthquake damage. Base isolation reduces the seismic force transmitted to the structure by supporting it with flexible element at the base to elongate the natural period of the structure and decouple it from the ground motion. The first patent regarding base isolation was proposed in early 1900 and the first research paper on the base isolation was published in 1891. Most early publications were limited to the description of the concept. In the last 30 years, however, the base isolation technology has been developed to the point of practical applications with the aid of new materials and computer analysis.

Basically, base isolation systems provide both a restoring force and energy dissipation. The rubber bearings which are made up with layers of alternating rubber and steel plates are the most popular for providing restoring force and energy dissipation. The plates and rubber layers are bonded to each other by strong special adhesive materials and the plates act as confinement for the rubber layers to support vertical load with low horizontal stiffness.

Some of the effective base isolation systems which are being utilized today are listed below. Their system performance characteristics are given in a study by Naeim [Naeim, 1999].

1. Elastomeric-based system
2. Low damping natural and synthetic rubber bearings
3. Lead plug bearings
4. High damping natural rubber bearings
5. Resilient friction natural rubber bearing
6. Friction pendulum system
7. Resilient-friction based isolation system
8. EERC combined system

Among these base isolation methods, the frictional pendulum system is selected for this study to retrofit the power transformer. The frictional pendulum is one of the most effective base isolation methods since it can accommodate larger displacements compared to others systems, and is easy to design. The most important design parameter of this system is the radius of curvature of the bearing.

3.1 Friction Pendulum System

The Friction Pendulum System (FPS) is an effective and practical base isolation technology for reducing the damaging effects of an earthquake on a structure. This base isolation device, which was originally developed by MCEER (Multidisciplinary Center for Earthquake Engineering and Research) researchers, is based on the effective concept of pendulum motion combined with velocity dependent damping characteristics. Typical FPS is shown in figure 2-1 and figure 2-2. This isolation system combines sliding action and restoring force. The FPS isolator shown in

figure 2-2 has an articulated slider that moves on a stainless steel spherical surface. The side of the articulated slider in contact with the spherical surface is coated with a low friction composite material. As the slider moves over spherical surface, it causes the supported mass to rise and provides the gravity induced restoring force for the system. Friction between the articulated slider and the spherical surface provides damping in the isolator. The radius of curvature of the concave surface controls the effective stiffness of the isolator. Geometry and gravity of the FPS achieve the desired seismic-isolation. In light of transformer's weight and the mobility requirements for maintenance purposes, FPS has been identified as a practical technology for their seismic rehabilitation. Result of a parameter study on use of FPS for transformers is presented in this section.

There are a series of experimental studies performed on FPS. A report was published in 1986 on compression-shear testing of model FPS bearings and shake table tests of a model two-story steel frame structures [Zayas, 1987]. This report is followed by another one in 1989 containing feasibility and performance studies on use of FPS for improving seismic behavior of new and existing buildings [Zayas, 1989]. Shake table tests of scaled six-story steel moment frame were performed in 1990 [Mokha, 1990]. Compression-shear testing was done on full size 2.0 second period FPS bearings used in seismic retrofit of a four-story wooden apartment building in 1991 [Zayas, 1991]. Use of Friction Pendulum System for seismic isolation of bridges was studied experimentally and analytically in 1993 [Constantinou, 1993]. A comprehensive study of the behavior of friction surface under different normal force and speeds was performed in 1993 [Zayas, 1993]. FPS was used to perform shake table tests of a quarter model of a seven-story steel moment and braced frames [Al-Hussaini, 1994]. The behavior of computer equipment on FPS was studied in 1994 [Lambrou, 1994]. More extensive compression-shear tests of full size FPS bearings were continued and 20,000-cycle wear tests of the bearing liner were conducted in Earthquake Protection Systems, Inc. in 1996 [Zayas, 1996]. Constantinou performed research on longevity and reliability of sliding seismic isolation systems at the same year [Constantinou, 1996]. A history of all the experimental work done on FPS is presented in a technical report by Earthquake Protection Systems, Inc. [EPS, 1996].

Different approaches have been used to analytically model the behavior of structures isolated with FPS bearings. The most comprehensive program developed having this analytical capability is the series of 3D-BASIS software developed by Reinhorn in MCEER. This software group includes 3D-BASIS [Nagarajaiah, 1989, 1991], 3D-BASIS-M [Tsopelas, 1991], 3D-BASIS-ME [Tsopelas, 1994], and 3D-BASIS-TABS [Nagarajaiah, 1993; Reinhorn, 1994]. These software are designed for analysis of three-dimensional structures isolated using different isolation mechanisms including FPS. Different versions of the software provide for special needs such as analysis of single and multiple structures and liquid storage tanks. They provide the user with a series of options in modeling the structure including inputting the characteristics of the model, or modeling the structure through ETABS [Reinhorn, 1994]. They are, however, restricted to linear structures, condense the structure into 3 degrees of freedom per floor (two lateral displacements and one torsional) and cannot consider the vertical behavior of the structure. Only 3D-BASIS-ME has the option to partially consider the effects of vertical ground motion through modification of the gravity constant g to $g + \ddot{u}_g$ and calculating the normal force change due to overturning moments. However, the effect of structural flexibility on normal force change is

ignored [Tsopelas, 1994]. 3D-BASIS uses pseudo-force method for computing the effects of isolation systems. There have been other direct attempts in finite element modeling of FPS as well. Tsai has done a finite element formulation for friction pendulum seismic isolation systems considering the effect of local bending moments [Tsai, 1997]. Almazan et. al. also have modeled FPS and used their model through MATLAB to study effect of different parameters including vertical excitation in behavior of structures isolated with FPS [Almazan 1998, 2002].

There was a need for additional parameter study on FPS to investigate ground motion characteristics, bi-axial effect, combination rule, large displacement effects, and the effect of vertical component of ground motion. The first part of this section presents the results of the parameter study using an exact formulation of FPS as a single degree of freedom system. Additionally, available analytical tools have shortcomings that justify development of a finite element model of FPS that can be implemented in a finite element package. Study of seismic behavior of isolated transformer-bushing requires a complex nonlinear structural model that is not offered by these tools. The models by Almazan and Tsai are not part of a finite element package allowing such modeling, while the family of 3-D BASIS software permits a linear model that is limited to linear elements and condenses the structure into a model with three degrees of freedom per floor. In addition, 3D-BASIS does not consider the effects of vertical ground excitation and vertical response of the structure (except partially by 3D-BASIS-ME).

The finite element package ADINA provides the user with the capability of defining his own element while offering him access to a rich library of elements and material models [ADINA 2001]. The formulation of FPS presented by Tsai and Almazan is not consistent with the format of the user-defined element subroutine in ADINA. Hence, a special finite element model was developed by under this study [Ashrafi 2003] to be used in ADINA to model behavior of structures isolated with FPS and investigate effect of vertical motion on system response among other parameters.

3.1.1 Geometric Description and Technical Characteristics

Dynamic periods from one to five seconds and displacement capacities up to 48" can be provided. The dynamic coefficient of friction ranges from 3% to 20%. Effective damping ranges from 10 to 50%. Individual capacities up to 12 million pounds can be provided. Bearings can be fitted with enclosing tension restraint plates that carry tension loads. The pendulum properties of FPS make the FPS system particularly effective at minimizing adverse torsional motions that result from accidental mass eccentricities. The bearing's dynamic stiffness is directly proportional to the supported weight; hence the center of lateral stiffness of the bearings always coincides with the center of mass of the structure. Therefore, the stiffness and friction forces automatically adjust for accidental mass eccentricities. The materials used in the FPS bearings can maintain their performance properties for temperatures as low as -100°F. The total assembly height eases the installation of the bearings and the bearing can be installed with the concave surface facing up or down.

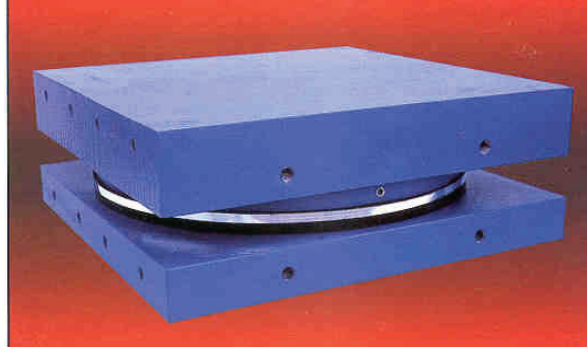
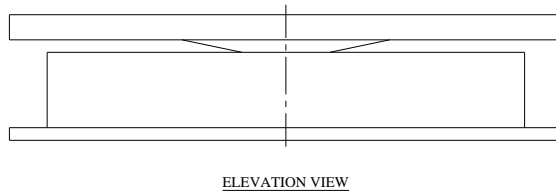
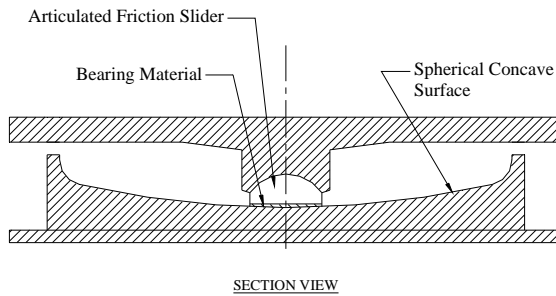


Figure 3-1 Photograph of a FPS Isolator [EPS]



ELEVATION VIEW



SECTION VIEW

Figure 3-2 Typical Elevation and Section of FPS

3.2 Formulation of the Equation of Motion for the Friction Pendulum System

The formulation discussed in this section is based on the assumption of small displacements. As it can be seen in figure 3-3, there are three forces acting on the free body diagram of the FPS bearing. Having θ as angle between initial and displaced positions, the geometric relations imply that:

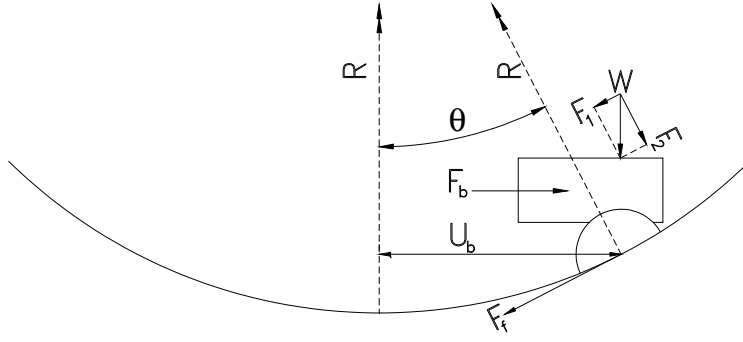


Figure 3-3 Force Diagram of FPS

$$\sin \theta = \frac{F_1}{W} \quad (3-1)$$

$$\sin \theta = \frac{U_b}{R} \quad (3-2)$$

where

W= supported weight

R= the radius of curvature of the bearing

F_1 = restoring force

U_b = bearing displacement.

Restoring force is expressed as,

$$F_1 = W \sin \theta = \frac{W}{R} U_b \quad (3-3)$$

Friction force acts opposite to the motion,

$$F_f = F_2 \mu_s = \mu_s W \cos \theta \quad (3-4)$$

Having $\cos \theta = 1$ for small displacement assumption, and introducing $\text{sgn}(\dot{U}_b)$ for direction of friction force, equation (6) can be rewritten as follows:

$$F_f = \mu_s W \text{sgn}(\dot{U}_b) \quad (3-5)$$

μ_s = the coefficient of friction mobilized during sliding

\dot{U}_b = bearing sliding velocity

F_f = friction force

The model of friction for Teflon-steel interface used in this study is based on principles of theory of viscoplasticity and is referred to as a modified viscoplasticity model [Constantinou, 1990]. This model is based on equation (3-6).

$$Y\dot{Z} + \gamma |\dot{U}_b| Z |Z|^{\eta-1} + \beta \dot{U}_b |Z|^\eta - A \dot{U}_b = 0 \quad (3-6)$$

In this equation β , r , A , and η are dimensionless constants, and Y represents a small elastic displacement for Teflon-steel interfaces before sliding. The frictional force is given by equation (3-7).

$$F_f = \mu_s WZ \quad (3-7)$$

This equation is essentially identical to equation (3-5). It should be noted that during sliding (yielding), Z takes values of ± 1 . A time history graph of Z , for one of the parametric studies performed in this chapter is shown in (4-3)figure . During sticking (elastic behavior) the absolute value of Z is less than unity. The conditions of separation and reattachment are accounted by equation 6-3)). In this respect Z may be regarded as a continuous approximation to the function of $\text{sgn}(\dot{U}_b)$ in equation (3-5). Teflon-steel interfaces undergo some very small elastic displacements before sliding. Experimental observation suggests a value of Y of about 0.005 to 0.02 inch [Constantinou, 1990]. The value of $\eta = 2$, with $A=1$ and $\beta+\gamma=1$ ($\beta=0.1$, $\gamma=0.9$) produces loops of frictional force versus sliding displacement that are in good agreement with experimental results. The lateral force at the isolation level, F_b , is equal to the sum of the restoring force and friction force and it is given in equation (3-8).

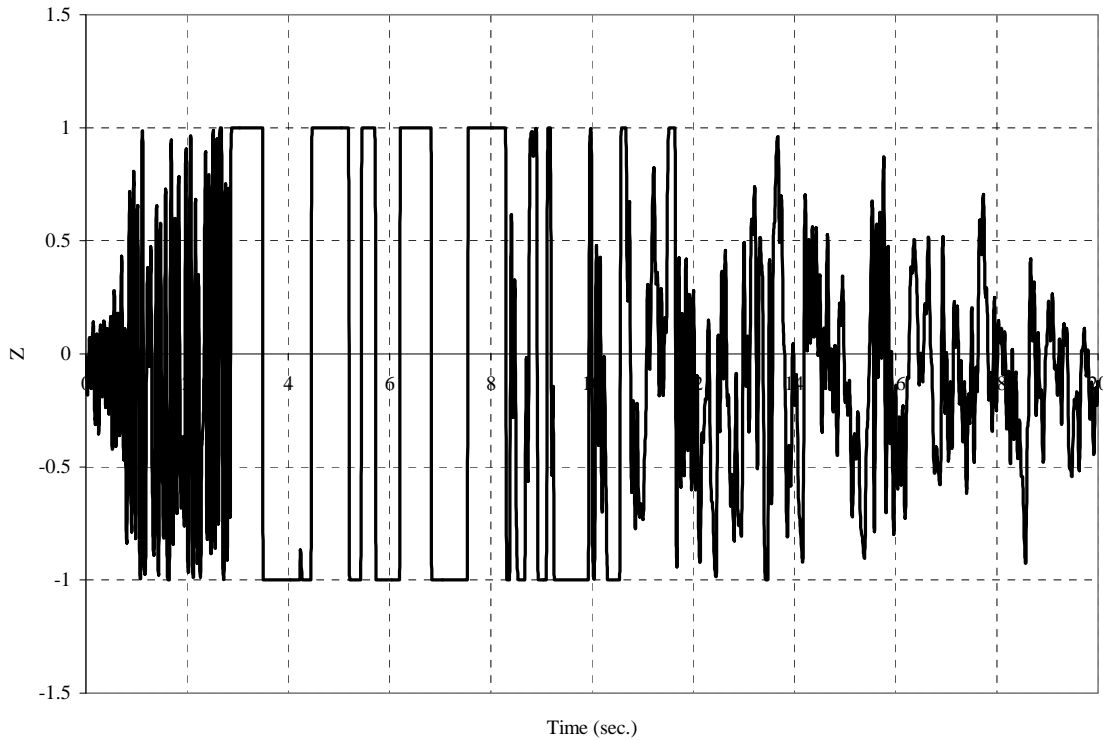


Figure 3-4 A Time History for Variable Z

$$F_b = U_b \frac{W}{R} + \mu_s WZ \quad (3-8)$$

The period of vibration of the structure in its rigid body condition is,

$$T = 2\pi \sqrt{\frac{R}{g}} \quad (3-9)$$

g is the gravitational acceleration. This is the natural period of a pendulum of length R , which shows that the natural period of vibration of a FPS isolated structure is independent of the structure weight. Assuming that the system behaves as a rigid body, dynamic equilibrium in horizontal direction can be expressed as follows:

$$M_b(\ddot{U}_b + \ddot{U}_g) + F_b = 0 \quad (3-10)$$

$$M_b \ddot{U}_b + F_b = -M_b \ddot{U}_g \quad (3-11)$$

$$M_b \ddot{U}_b + \mu_s WZ + \frac{W}{R} U_b = -M_b \ddot{U}_g \quad (3-12)$$

where

\ddot{U}_b = bearing base acceleration

\ddot{U}_g = ground acceleration

M_b = mass of the block

R = the radius of curvature of the bearing

3.2.1 Numerical Solution of the Equation of Motion for FPS

The analysis was performed by employing a Fortran code, which uses an IMSL routine IVPAG. This routine solves an initial-value problem for ordinary differential equations using the Adams-Moulton's method. This Fortran code is provided in Appendix B of this thesis. The formulation for the 1-D case is as follows. Let

$$\dot{U}_b = V \quad (3-13)$$

where

V = bearing sliding velocity

Equations (3-6) and (3-12) can be reduced to a system of first-order differential equations,

$$\dot{V} = -\frac{W}{M_b R} U_b - \mu_s \frac{W}{M_b} Z - \ddot{U}_g \quad (3-14)$$

$$\dot{Z} = -\frac{\gamma}{Y} |V| |Z| |Z|^{\eta-1} - \frac{\beta}{Y} V |Z|^\eta + \frac{A}{Y} V \quad (3-15)$$

Equations (3-13), (3-14) and (3-15) are solved for the 1-D analysis. For 2-D analysis, let

$$\dot{U}_{bx} = V_x \quad (3-16)$$

and

$$\dot{U}_{by} = V_y \quad (3-17)$$

where

V_x = bearing sliding velocity in x-direction

V_y = bearing sliding velocity in y-direction, then

$$\dot{V}_x = -\frac{W}{M_b R} U_{bx} - \mu_s \frac{W}{M_b} Z_x - \ddot{U}_{gx} \quad (3-18)$$

$$\dot{V}_y = -\frac{W}{M_b R} U_{by} - \mu_s \frac{W}{M_b} Z_y - \ddot{U}_{gy} \quad (3-19)$$

The 2-D model is based on the following system of coupled equations [Constantinou, 1990].

$$Y\dot{Z}_x + \gamma|\dot{U}_{bx}Z_x|Z_x + \beta\dot{U}_{bx}Z_x^2 + \gamma|\dot{U}_{by}Z_y|Z_x + \beta\dot{U}_{by}Z_xZ_y - A\dot{U}_{bx} = 0 \quad (3-20)$$

$$Y\dot{Z}_y + \gamma|\dot{U}_{by}Z_y|Z_y + \beta\dot{U}_{by}Z_y^2 + \gamma|\dot{U}_{bx}Z_x|Z_y + \beta\dot{U}_{bx}Z_xZ_y - A\dot{U}_{by} = 0 \quad (3-21)$$

Equations (3-20) and (3-21) are extensions of equation (3-6) for $\eta = 2.0$ then,

$$\dot{Z}_x = -\frac{\gamma}{Y}|\dot{U}_{bx}Z_x|Z_x - \frac{\beta}{Y}\dot{U}_{bx}Z_x^2 - \frac{\gamma}{Y}|\dot{U}_{by}Z_y|Z_x - \frac{\beta}{Y}\dot{U}_{by}Z_xZ_y + \frac{A}{Y}\dot{U}_{bx} \quad (3-22)$$

$$\dot{Z}_y = -\frac{\gamma}{Y}|\dot{U}_{by}Z_y|Z_y - \frac{\beta}{Y}\dot{U}_{by}Z_y^2 - \frac{\gamma}{Y}|\dot{U}_{bx}Z_x|Z_y - \frac{\beta}{Y}\dot{U}_{bx}Z_xZ_y + \frac{A}{Y}\dot{U}_{by} \quad (3-23)$$

Equations (3-16), (3-17), (3-18),(3-19), (3-22), and (3-23) then are solved for 2-D case.

3.2.2 Input Parameters for Numerical Solution

A representative graph of the coefficient of sliding friction is shown in figure 3-5 for a pressure value of 2.5 ksi. As it is observed from figure 3-5, the coefficient of sliding friction at low velocity is smaller than the maximum friction value. As the sliding velocity increases, the amount of friction reaches the maximum. The coefficient of friction used for this parametric study is 0.10, which is a good approximation for bearing pressures of transformer considered in this study. The values of the constants used for solution of equation (3-6) are given in 0table 3-1.

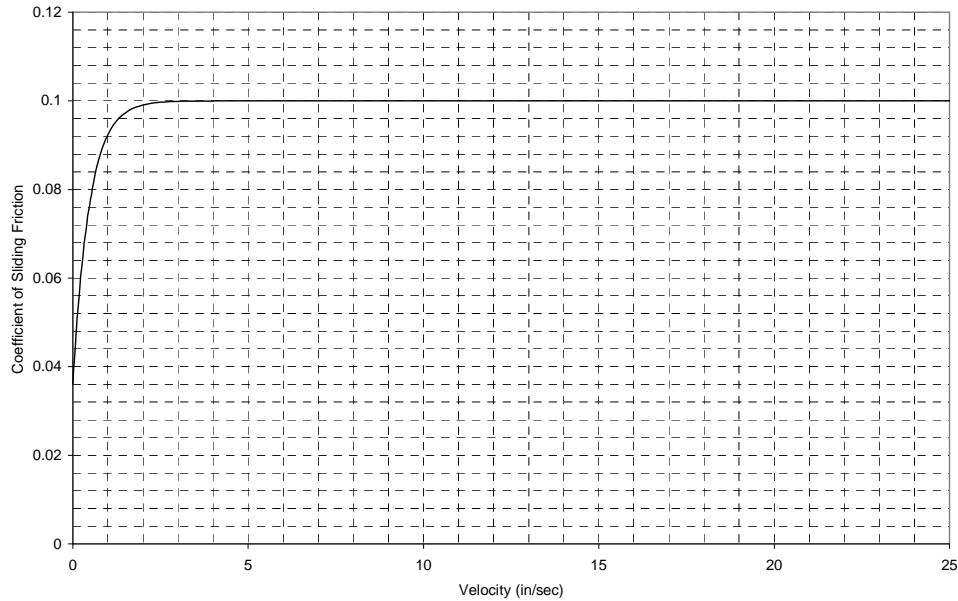


Figure 3-5 Variation of Coefficient of Sliding Friction

Table 3-1 Values of Equation (3-6) Constants

β	0.1
γ	0.9
A	1.0
η	2.0
Y	0.005

3.2.3 Ground Motion Input

Earthquake ground motions are random and irregular. Therefore, earthquake-resistant design is based on the general characteristics of an ensemble of earthquakes. Earthquakes can be classified into four categories [Newmark, 1971]:

1. Single shocks: Motions of this type occur at short distances from the epicenter, on firm ground, and only for shallow earthquakes.
2. Moderately long, extremely irregular motions: Motions of this type occur at moderate distances from the epicenter, on firm ground. They have the characteristics of white noise and have almost equal severity in all directions.
3. Long ground motions exhibiting pronounced prevailing periods of vibration: Motions of this type result from the filtering of earthquakes of the preceding type through layers of soft soils.
4. Ground motions involving larger-scale permanent deformations of the ground: Motions of this type are representative of near-source ground motions.

Earthquakes belonging to the second and third groups cause the seismic hazard in most locations. Therefore, 20 records belonging to these two classes are selected for a parametric study. They are tabulated in table 3-2. These records were scaled based on peak ground acceleration (PGA) throughout this study. For design purposes the average of all records is presented and discussed. In addition, results based on rock and soil records are individually presented in the subsection on ground motion effects in this chapter.

Table 3-2 Ground Motion Records Employed

Type of Motion	Earthquake Name	Station Component	Station Name	PGA (g)
ROCK	San Fernando	S16E	Pacoima Dam	1.170
	San Fernando	S74W	Pacoima Dam	1.075
	San Fernando	S69E	Lake Hughes Array #4	0.172
	San Fernando	S21W	Lake Hughes Array #4	0.146
	Loma Prieta	227	Apeel Array #9	0.108
	Loma Prieta	137	Apeel Array #9	0.117
	Loma Prieta	360	Calaveras Array	0.079
	Loma Prieta	270	Calaveras Array	0.076
	Kern County	S69E	Taft	0.179
	Kern County	N21E	Taft	0.156
SOIL	Northridge	N21E	Sylmar	0.826
	Northridge	N79W	Sylmar	0.492
	Kern County	S00W	Hollywood Storage	0.059
	Kern County	N90E	Hollywood Storage	0.042
	Imperial Valley	S00E	El Centro	0.348
	Imperial Valley	N90W	El Centro	0.214
	Loma Prieta	255	Hollister Airport	0.287
	Loma Prieta	165	Hollister Airport	0.282
	Northridge	90	Norwalk	0.141
	Northridge	360	Norwalk	0.141

3.3 Parametric Study Results

Three different types of parameter studies were conducted: Unidirectional (1-D) analysis, bi-directional (2-D) analysis where two orthogonal horizontal motions were considered, and tri-directional (3-D) analysis to investigate the effect of the vertical component of ground motion on the horizontal responses. These results are discussed in the following sections.

The 1-D analyses were performed for 400 different cases. This consisted of five different bearing radii ($R = 30''$, $60''$, $90''$, $120''$, and $150''$), and four different PGAs (0.25g, 0.5g, 0.75g and 1.0g). The 2-D analyses included 200 cases. Similar to the 1-D case, radius and PGA were the parameters. It consisted of five different bearing radii ($R = 30''$, $60''$, $90''$, $120''$ and $150''$) and four different PGAs (0.25g in x and 0.25 in y, 0.50g in x and 0.50g in y, 0.75g in x and 0.75g in y, 1.0 g in x and 1.0g in y). Using the same parameters another 200 cases were analyzed to investigate the effect of vertical motion.

In the following sections, the criteria used for performance evaluation are the maximum displacement and the inertia reduction. Inertia reduction refers to the decrease in the force at the isolation level, $-M_b(\ddot{U}_b + \ddot{U}_g)$, compared to $-M_b\ddot{U}_g$. It should be noted that the inertia reduction

compared to a fixed base situation (i.e., if FPS was not used) is generally much higher than these numbers. However, under a SDOF idealization such comparison is not possible.

3.3.1 Results of 1-D Analyses

The acceleration time history for one of the case studies is shown in figure 3-6. The parameters used for this particular case are as follows: radius of bearing is 30", and PGA is 1.0g. The maximum response acceleration, as seen from figure 3-6, is equal to 0.41g and the maximum displacement is 10 inches for this example case. Thus, there is about a 60% reduction in system acceleration compared to ground PGA for this particular case.

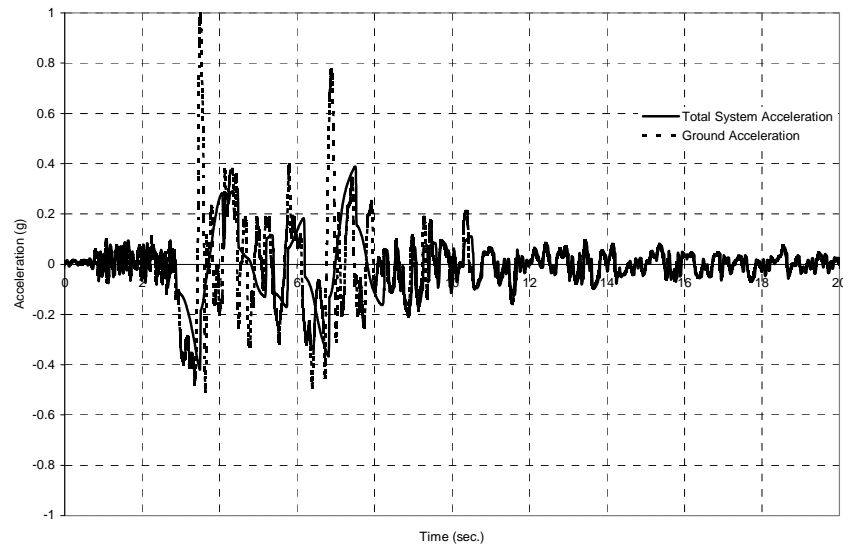


Figure 3-6 Acceleration Time Histories for an Example Case

Considering the parameters used, the period of vibration for this example, using equation (3-9), is equal to 1.75 second. It is instructive to compare the results of this case to that of an equivalent single-degree-of-freedom model. Assuming unit mass, the equivalent stiffness, $K = W/R$ will be 12.88 lb/in. Using these system parameters and the same input motion, several analyses with various damping ratios were performed. The maximum displacement for the equivalent SDOF with 5% damping is equal to 18.3 inches. To get the equivalent damping for the isolated system, other cases of damping were analyzed and it was determined that the equivalent damping for this particular case is 40% of the critical damping. However, the manufacturer's data indicates that the equivalent damping for FPS bearings can be as high as 50%.

Based on the 1-D analyses using all 20 records, the average inertia reduction varies from 40% to 75%. The maximum displacements range from 1" to 22" for different cases. The average maximum displacement and inertia reduction are shown in figure 3-7 through figure 3-9 for a PGA of 0.25g, 0.50g, and 1.0g. Note that the wide difference between the inertia reductions of smaller PGA compared to higher PGA is due to the fact that for lower PGAs the static friction is not exceeded at all times. Therefore, the isolator is more effective for higher PGAs. The charts in figure 3-7 through figure 3-9 can be used in the seismic design of transformers.

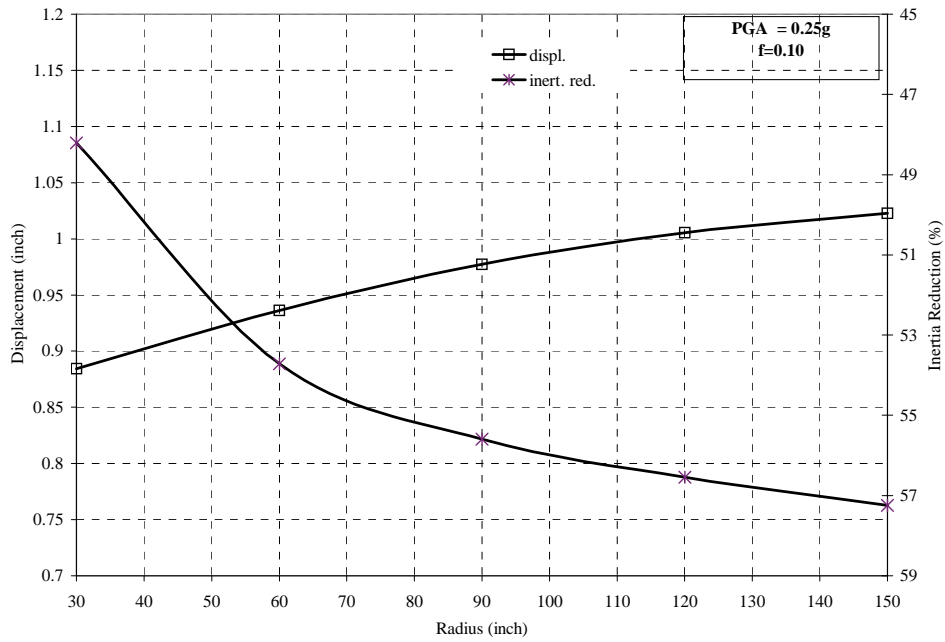


Figure 3-7 Displacement-Inertia Reduction Chart for PGA of 0.25g

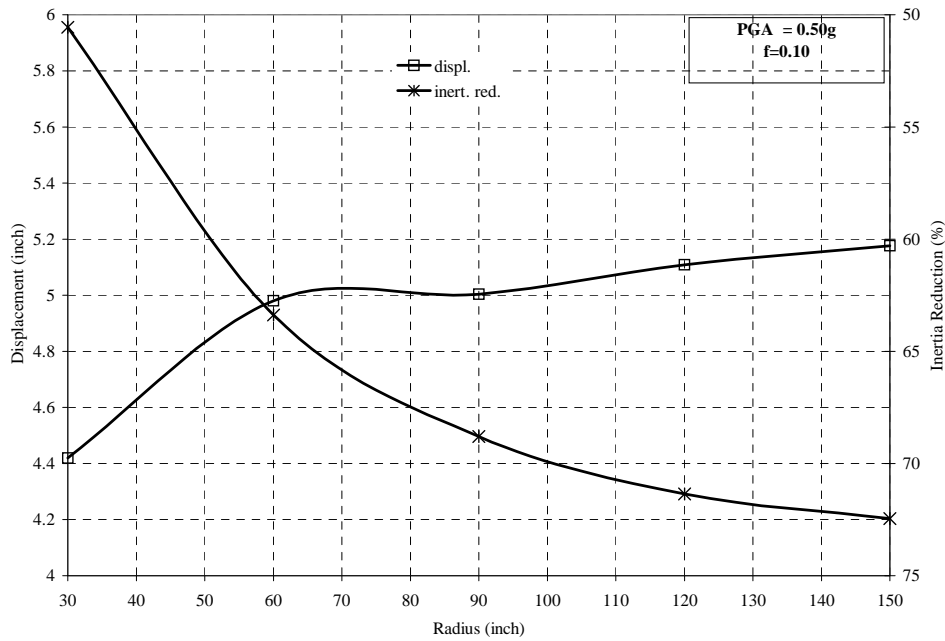


Figure 3-8 Displacement-Inertia Reduction Chart for PGA of 0.50g

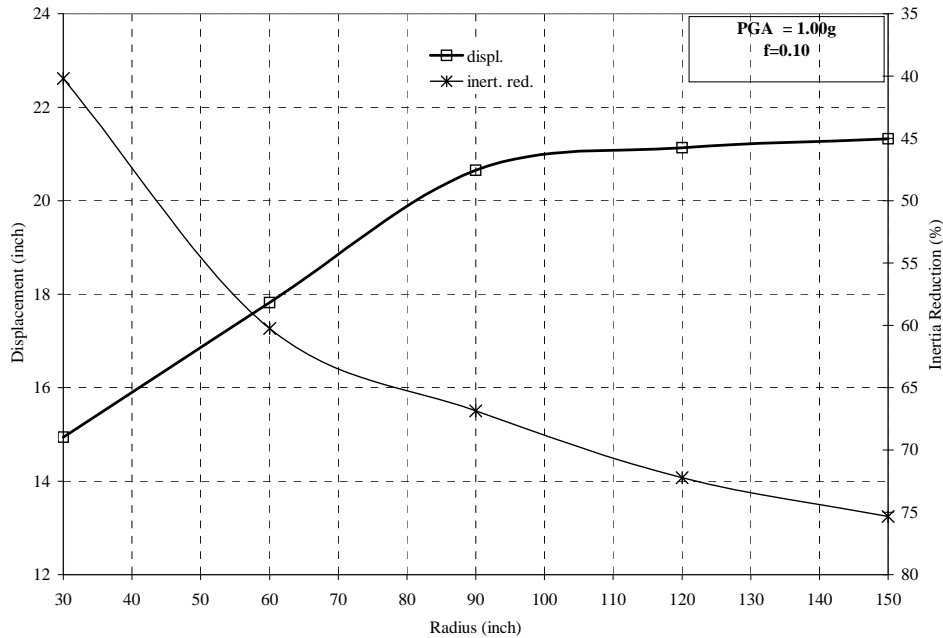


Figure 3-9 Displacement-Inertia Reduction Chart for PGA of 1.00g

The challenge in design will be the selection of radius of curvature of the bearing such that there is a balance between the desired inertia reduction and the displacement limitations.

3.3.2 Results of 2-D Analyses and Response Combinations

A total of 200 cases were analyzed under two orthogonal horizontal earthquake ground motions. The objectives of the 2-D analyses were to investigate the possibility of coupling between responses in the horizontal directions and to determine a suitable combination rule to be used in design. Due to dependency of friction force on total velocity, it is expected that there is coupling between responses in two horizontal directions that needs to be quantified.

Figure 3-10 through figure (3-12) show comparisons of one-dimensional results with the corresponding component of two-dimensional analyses for PGAs of 0.25g, 0.50g, and 1.0g respectively. It can be seen from these figures, both inertia reduction and displacement are affected, however, the effect on displacement is much more pronounced. Furthermore, the effect of coupling is more significant for lower ground accelerations. As mentioned before, this is due to the effect of total velocity on frictional parameters. Consequently, the individual components of a 2-D response are always larger than the responses of two 1-D cases.

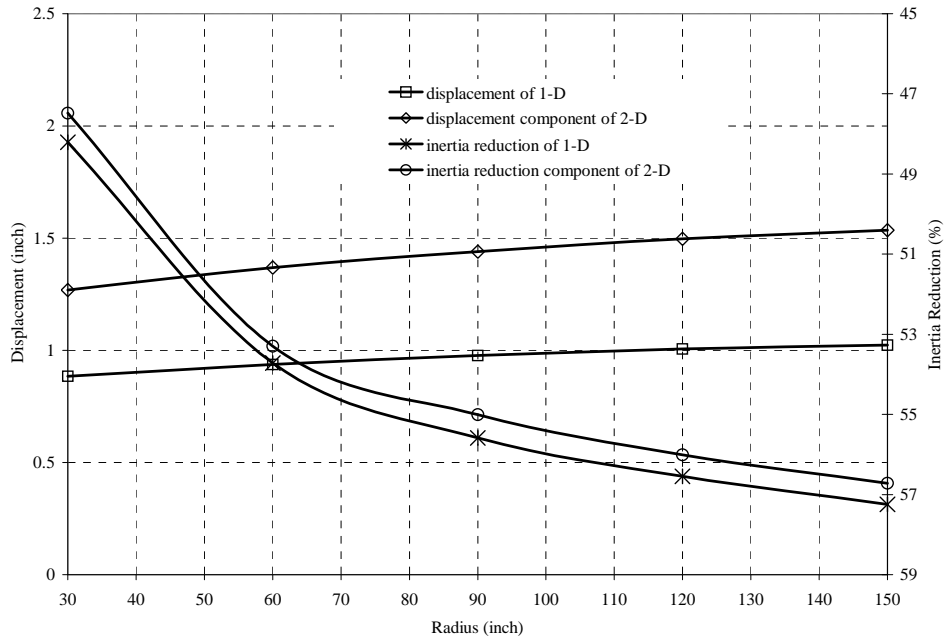


Figure 3-10 Comparison of 1-D and Corresponding Component of a 2-D Case for PGA of 0.25g

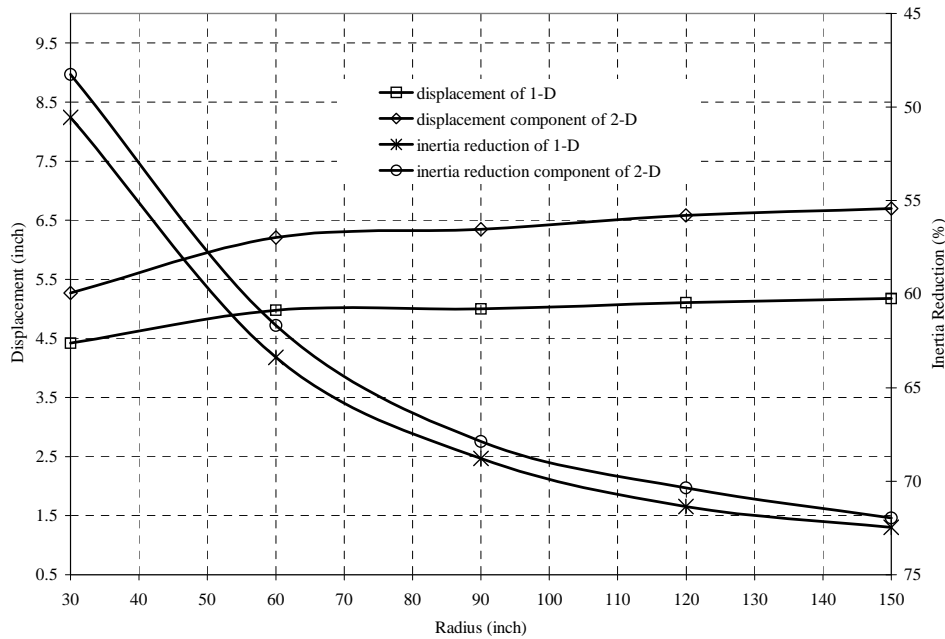


Figure 3-11 Comparison of 1-D and Corresponding Component of a 2-D Case for PGA of 0.50g

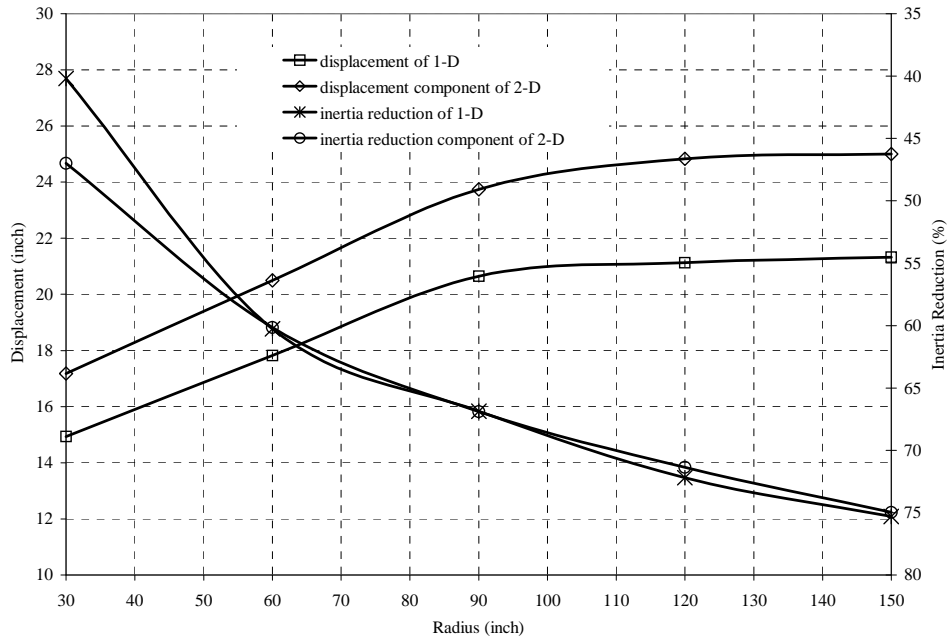


Figure 3-12 Comparison of 1-D and Corresponding Component of a 2-D Case for PGA of 1.00g

The comparison of total displacement responses using the SRSS (square-root-of-sum-of-squares) and CQC (complete quadratic combination) methods of 1-D analysis with 2-D analysis are shown in 0figure 3-13 through 0figure 3-15 for PGA of 0.25g, 0.50g, and 1.0g.

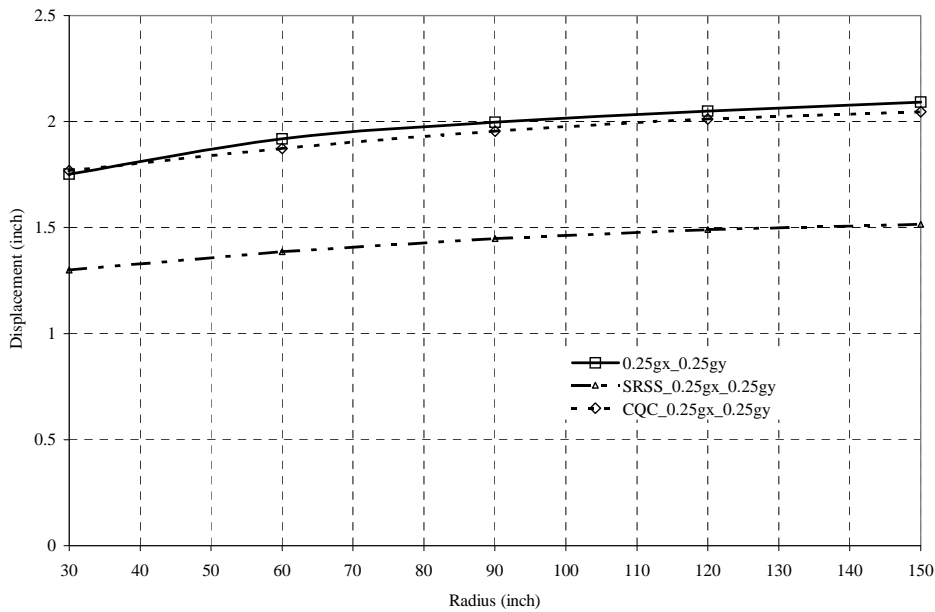


Figure 3-13 Comparison of Displacement Responses for Combination Methods with 2-D Case for PGA of 0.25g

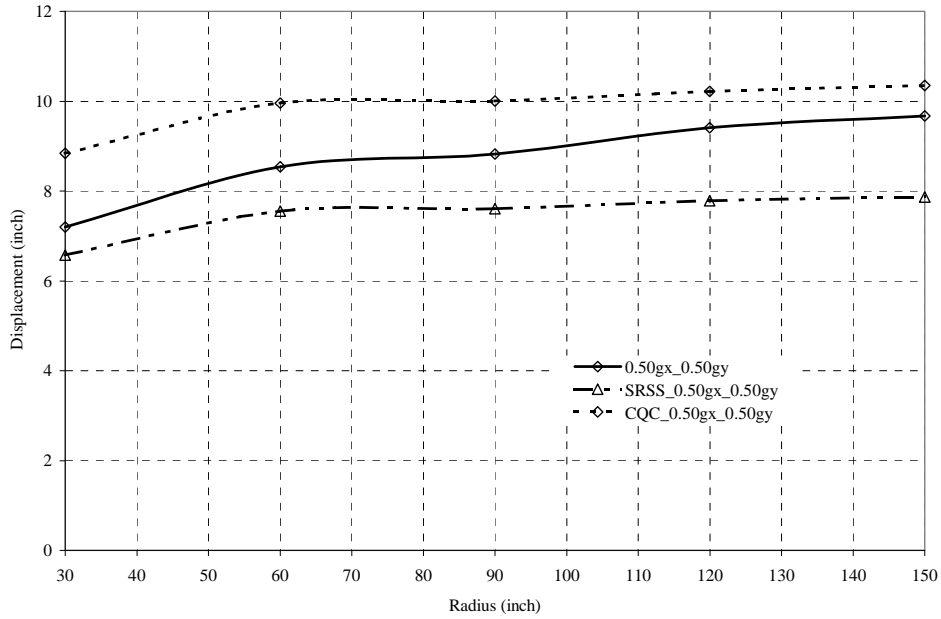


Figure 3-14 Comparison of Displacement Responses for Combination Methods with 2-D Case for PGA of 0.50g

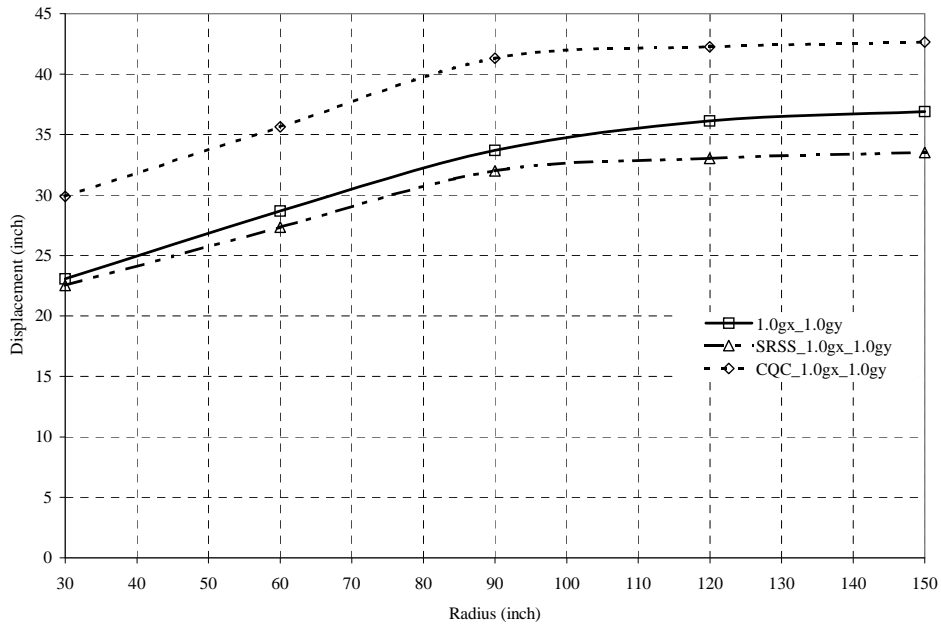


Figure 3-15 Comparison of Displacement Responses for Combination Methods with 2-D Case for PGA of 1.0g.

The comparison of inertia reduction responses using the SRSS and CQC methods of 1-D analysis with 2-D analysis are shown in figure 3-16 through figure 3-18 for PGAs of 0.25g, 0.50g, and 1.0g respectively.

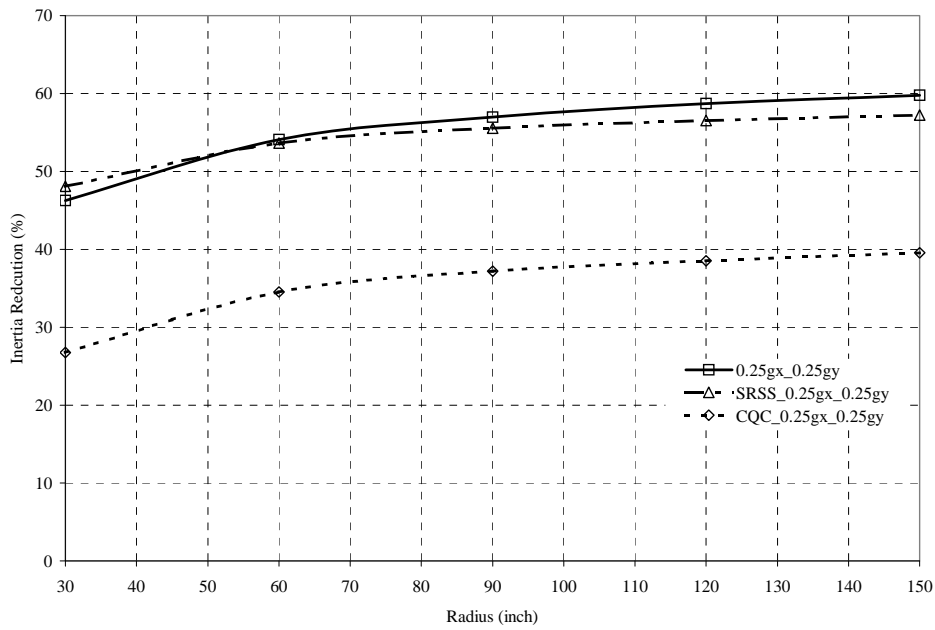


Figure 3-16 Comparison of Inertia Reduction Responses for Combination Methods with 2-D Case for PGA of 0.25g

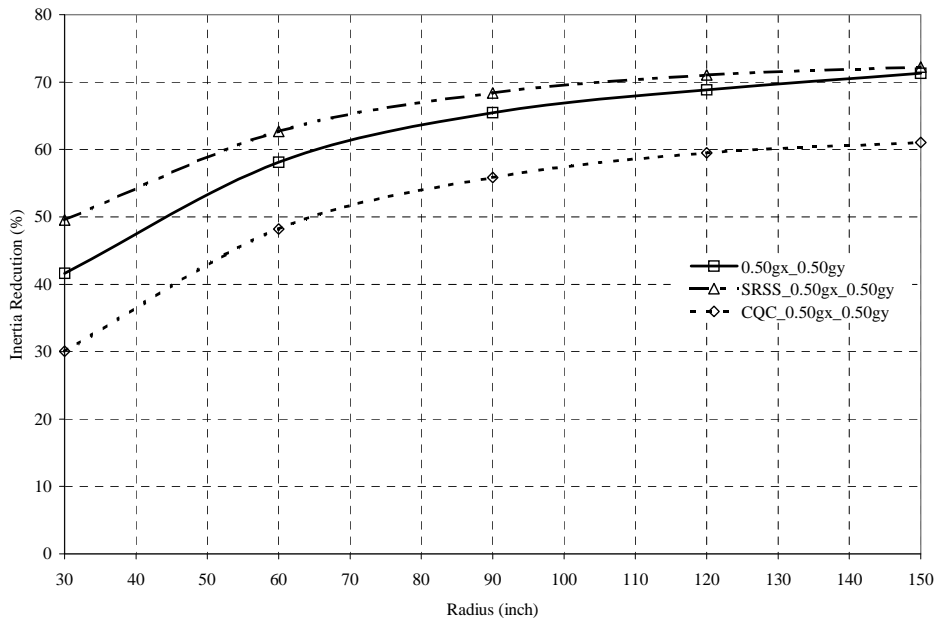


Figure 3-17 Comparison of Inertia Reduction Responses for Combination Methods with 2-D Case for PGA of 0.50g

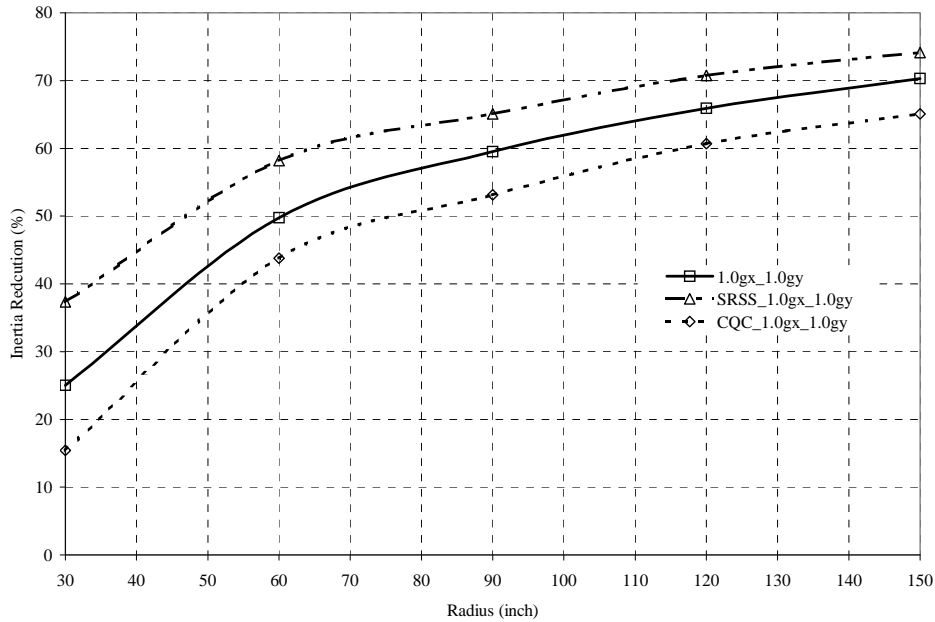


Figure 3-18 Comparison of Inertia Reduction Responses for Combination Methods with 2-D Case for PGA of 1.00g

In these figures, the SRSS and the CQC response values are obtained by combining responses of two orthogonal 1-D cases. The SRSS method is basically the square root of the sum of the squares of the maximum responses in both horizontal directions. The CQC method turns out to be the absolute sum of the responses since FPS is symmetric. The equation for the CQC method is given in equation (3-24) [Chopra, 1995].

$$d_0 \cong \left(\sum_{i=1}^N \sum_{j=1}^N \rho_{in} d_{i0} d_{j0} \right)^{\frac{1}{2}} \quad (3-24)$$

For $N=2$ modes with equal frequencies (FPS is symmetric), $\rho_{in}=1.0$ and the equation reduces to equation (3-25).

$$d_0 \cong d_{10} + d_{20} \quad (3-25)$$

As it is seen from figure (3-16) through (3-18), one can say that the CQC method is always conservative in estimating both displacements and inertia reductions. That is, it overestimates the maximum total displacement and it underestimates the total inertia reduction. However, the SRSS method is almost always un-conservative by underestimating the displacements and overestimating the inertia reductions. Based on these results, which include 40 records (20 sites, 2 orthogonal horizontal component site) and many analysis cases, the use of CQC method is recommended for estimating the total displacement for PGAs less than 0.5g. For higher PGAs, the average of the two methods could be used for displacements in order to reduce the conservatism of the CQC method, which can be as high as 30%. For inertia reductions, the average of the two methods is recommended for all PGAs.

3.3.3 Effect of Vertical Motion

Horizontal responses could be affected by vertical motion since the period of the isolated system which depends on the gravitational and vertical motions also affects the normal contact force. To consider vertical effects, the same FORTRAN code, written for the 2-D case was employed. The weight of the transformer was revised to include the effect of vertical motion for every time step, i.e. $W=M_b (g \pm \ddot{U}_{g,up})$. To study the former factor, 200 cases were analyzed using earthquake records. Note that for all sites the actual vertical acceleration record was used. With regard to the latter factor, the frictional characteristics of the isolator are affected as a result of the changes in pressure. However, for typical transformer weights the change in pressure is not large enough to have noticeable effect on the response. Results for displacement with and without the vertical motion are shown in figure 3-19 and figure 3-21 for different PGAs. For lower PGA values, effect of vertical is negligible. For higher PGA values, however, the effect of vertical on the response of FPS is more pronounced. On the average, the displacement responses are affected by about $\pm 10\%$.

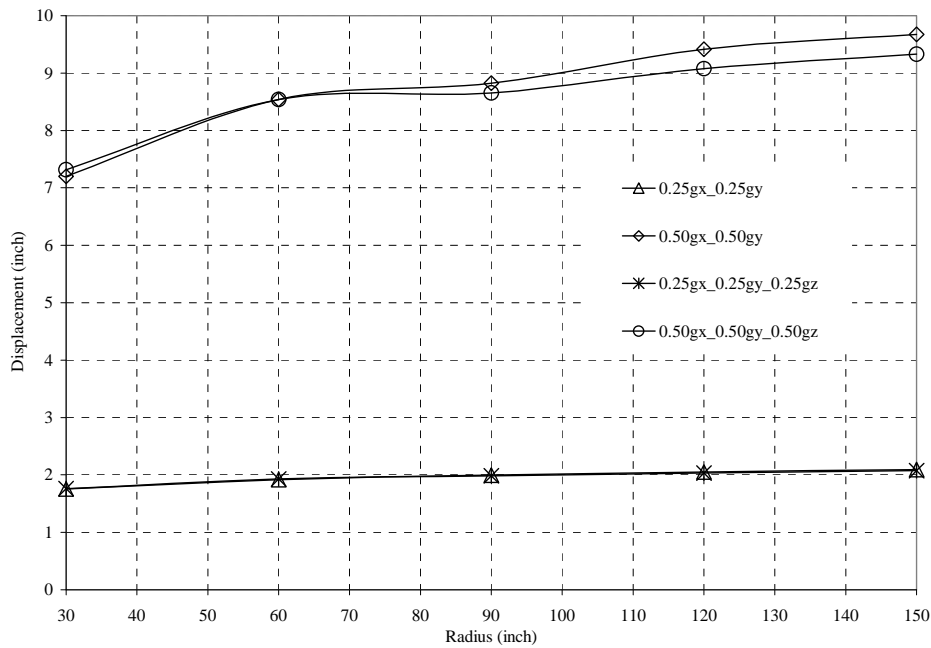


Figure 3-19 Effect of Vertical Motion on Displacements for PGA of 0.25g and 0.5g (3-D Analyses)

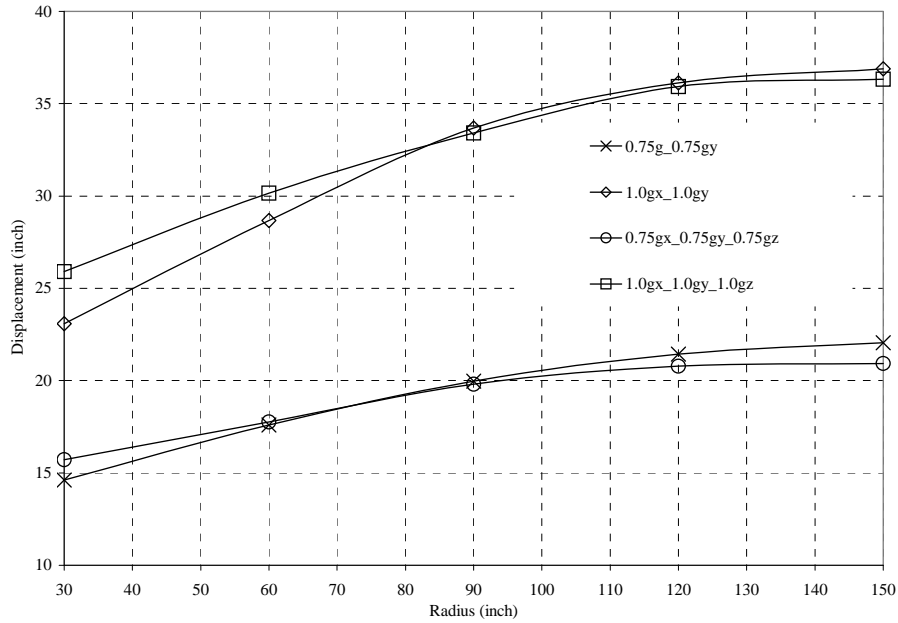


Figure 3-20 Effect of Vertical Motion on Displacements for PGA of 0.75g and 1.0g (3-D Analyses)

Results for inertia reduction with and without the vertical motion are shown in figure 3-21 and figure 3-22 for different PGAs. It can be seen from these figures that effect of vertical motion changes from marginal to significant, depending on response parameter under consideration. It is noted that the vertical ground acceleration has a considerable adverse effect on system performance in reducing the inertia forces. The inertia reductions attained without consideration

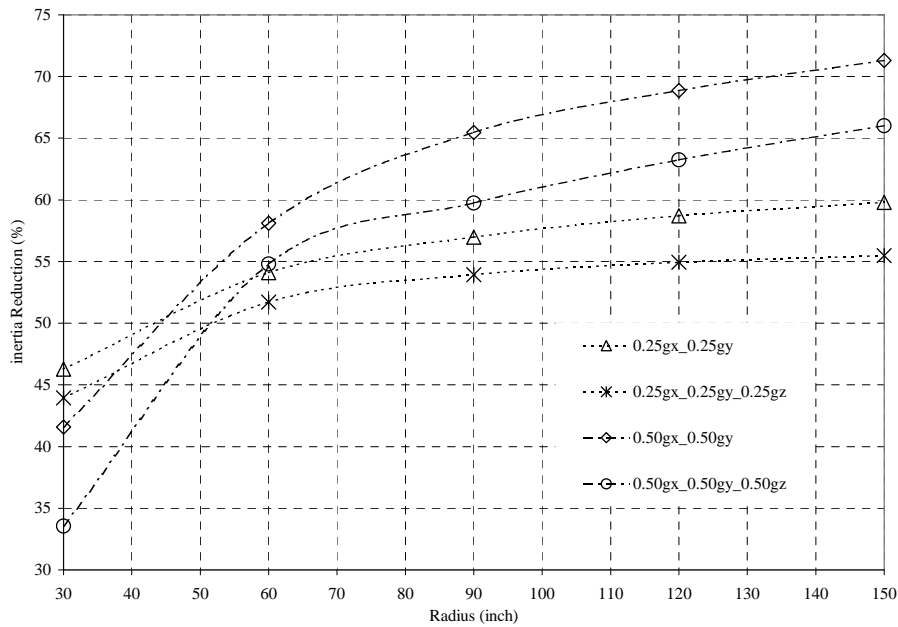


Figure 3-21 Effect of Vertical Motion on Inertia Reduction for PGA of 0.25g and 0.5g (3-D Analyses)

to vertical motion were higher, in some cases by as much as 40%. This adverse effect of vertical motion becomes more pronounced for higher PGAs.

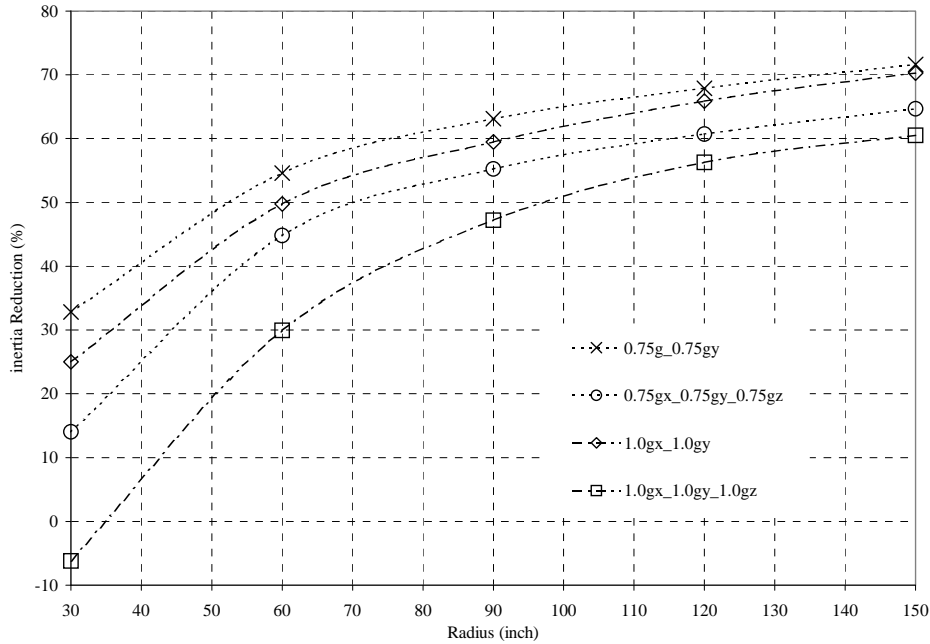


Figure 3-22 Effect of Vertical Motion on Inertia Reduction for PGA of 0.75g and 1.0g (3-D Analyses)

Furthermore, for vertical acceleration records of higher periods (i.e., lower frequency content) the effect of this component of ground motion becomes more evident. This is because vertical motion of a higher period has enough time to significantly alter the system period. To elaborate on this point one of the previous cases is analyzed with sinusoidal vertical acceleration. The period of the sinusoidal vertical motion is assumed to be equal to $2T_{bearing}$ and $5T_{bearing}$, with PGA of 1g. As can be seen from figure 3-23, vertical motions of higher period significantly affect the horizontal responses by influencing both amplitude and frequency content. It should be noted that vertical records are generally rich in frequency and normally of higher frequency content than the horizontal ones. This example is provided only to more clearly demonstrate the effect of vertical motion. Nevertheless, it is recommended that for sites where the motion can be filtered through layers of soft soils, the effect of vertical motion be explicitly considered in design.

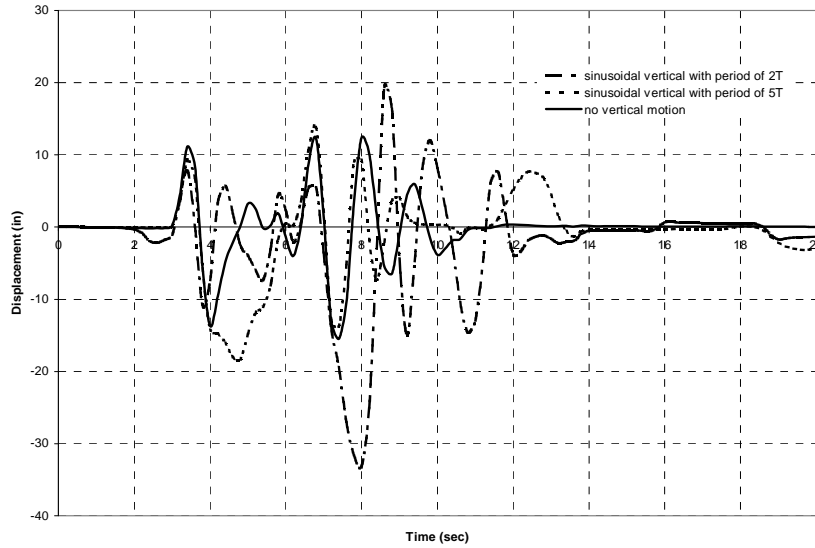


Figure 3-23 Displacements Time Histories with (Sinusoidal) and without Vertical Motion

3.3.4 Ground Motion Characteristics

The effect of ground motion characteristics on the response of FPS has been investigated for 10 soil and 10 rock earthquake records. Displacement results for soil and rock sites are given in figure 3-24 and figure 3-25 respectively. It is noted that the soil records on the average cause more displacement than the rock records for every PGA employed. This is due to lower frequency content of soil records in general.

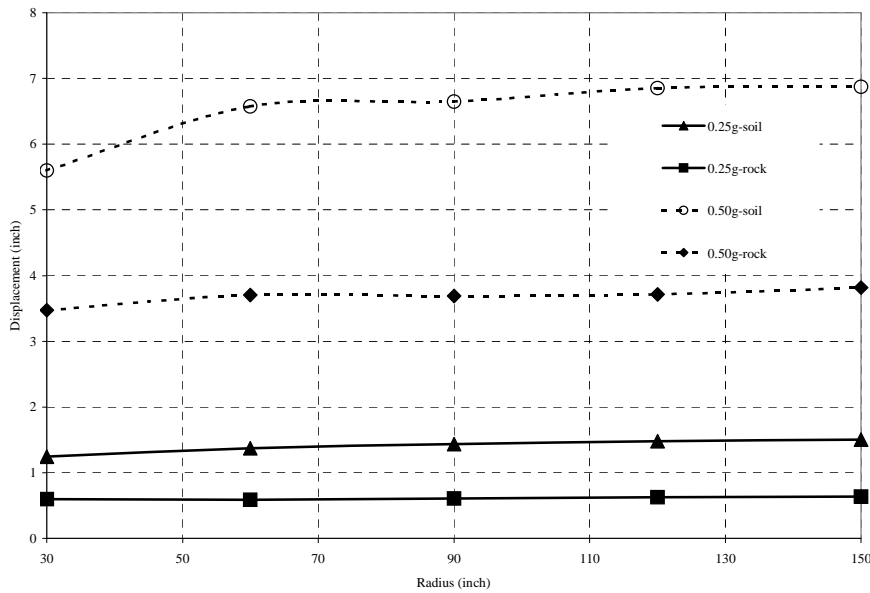


Figure 3-24 Comparison of Rock and Soil Displacements for PGA of 0.25g and 0.50g

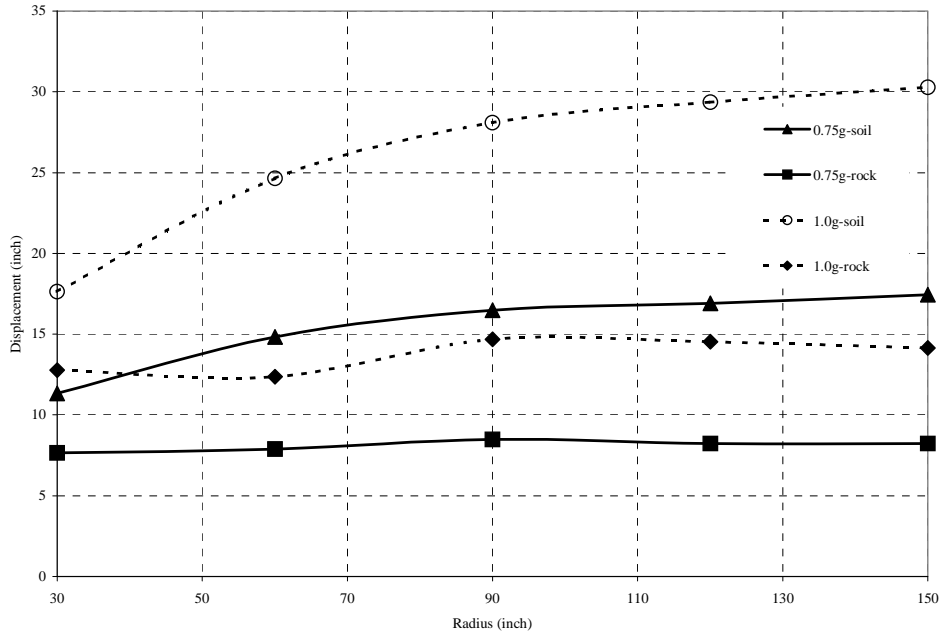


Figure 3-25 Comparison of Rock and Soil Displacements for PGA of 0.75g and 1.0g

Figure 3-26 and figure 3-27 show the variation between the inertia reduction responses of soil and rock records. Rock records attained more inertia reduction, i.e., the acceleration values for all PGA input are less than the soil acceleration levels.

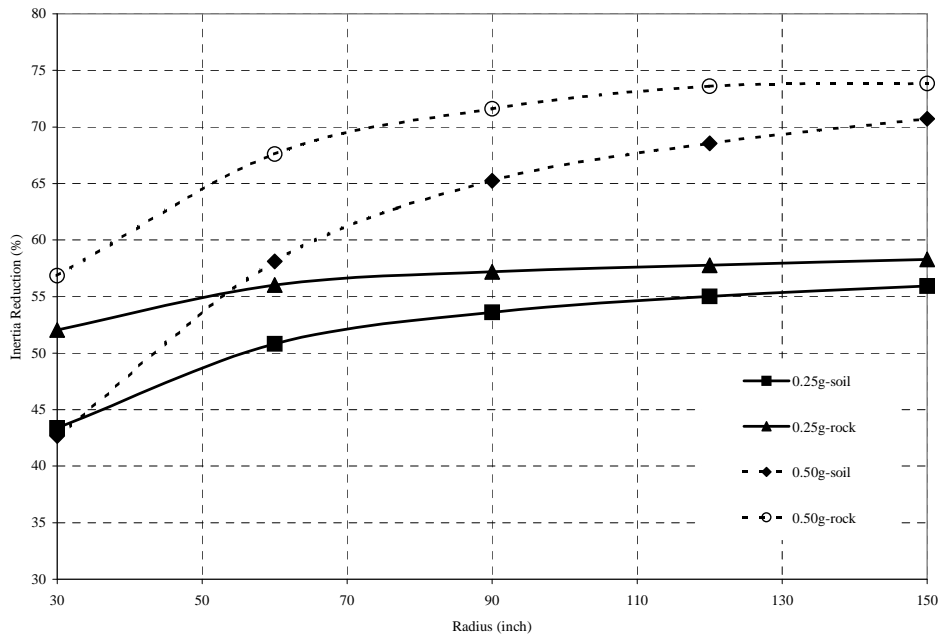


Figure 3-26 Comparison of Rock and Soil Inertia Reduction for PGA of 0.25g and 0.50g

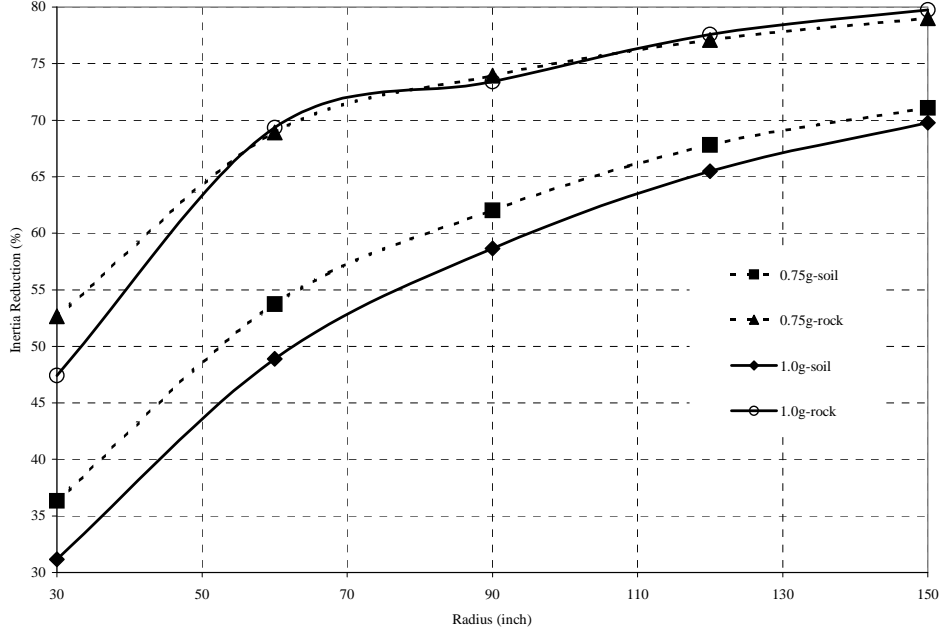


Figure 3-27 Comparison of Rock and Soil Inertia Reduction for PGA of 0.75g and 1.0g

3.4 FPS System for Large Displacement Assumption and Results

Based on the large displacement assumption, the normalized force N is perpendicular at the contact point of the articulated slider. The equilibrium equation in tangential direction becomes (see 0figure 3-3):

$$-F_f - W \sin \theta - M\ddot{U}_{gx} \cos \theta - M\ddot{U}_{gz} \sin \theta = MR\ddot{\theta} \quad (3-26)$$

where

F_f = friction force

W = weight of system

\ddot{U}_{gx} = ground motion in horizontal direction

\ddot{U}_{gz} = ground motion in vertical direction

R = radius of curvature of bearing

The equilibrium equation in radial direction becomes,

$$N - W \cos \theta + M\ddot{U}_{gx} \sin \theta - M\ddot{U}_{gz} \cos \theta = MR\dot{\theta}^2 \quad (3-27)$$

From equation (25) the normal force N is obtained as,

$$N = W \cos \theta - M\ddot{U}_{gx} \sin \theta + M\ddot{U}_{gz} \cos \theta + MR\dot{\theta}^2 \quad (3-28)$$

The friction force can be given as follows,

$$F_f = \mu_s NZ \quad (3-29)$$

Substituting equation (3-28) and equation (3-29) into equation (3-26) leads to equation (3-30),

$$\ddot{\theta} = \frac{-\mu_s Z}{R} (g \cos \theta - \ddot{U}_{gx} \sin \theta - \ddot{U}_{gz} \cos \theta + R\dot{\theta}^2) - \frac{1}{R} (g \sin \theta + \ddot{U}_{gx} \cos \theta + \ddot{U}_{gz} \sin \theta) \quad (3-30)$$

Since the tangential velocity at the steel-teflon interface of bearing becomes $R\dot{\theta}$, equation (3-4) (for parameter Z) becomes:

$$Y\dot{Z} + r|R\dot{\theta}|Z|Z|^{\eta-1} + \beta R\dot{\theta}|Z|^{\eta} - AR\dot{\theta} = 0 \quad (3-31)$$

Equation (3-30) and equation (3-31) are solved simultaneously by employing a Fortran code using the IVPAG routine in IMSL.

Figure (3-28) through figure (3-30) compare the average displacement response of FPS based on large and small displacement assumptions. The response deviation of 5% from large displacement assumption values is also shown for each radius of curvature on the graphs. It is noted that the displacement values from both methods for smaller PGA values (0.25g, 0.5g) are in good agreement. For larger PGA values (1.0g) with small radius of curvature there is a larger deviation from the small displacement values.

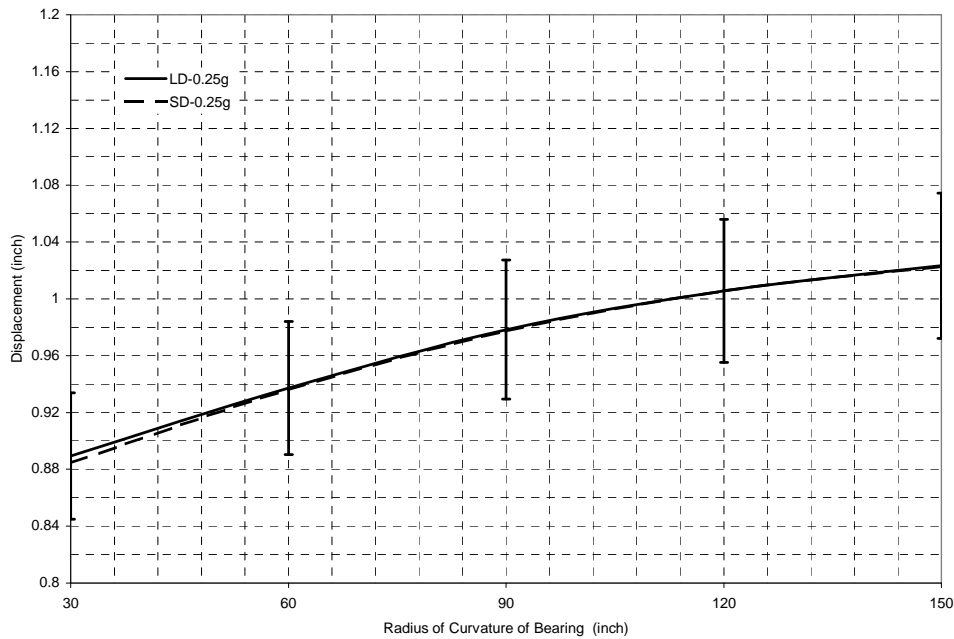


Figure 3-28 Comparison of Displacements Based on Small and Large Displacement Assumptions for PGA of 0.25g

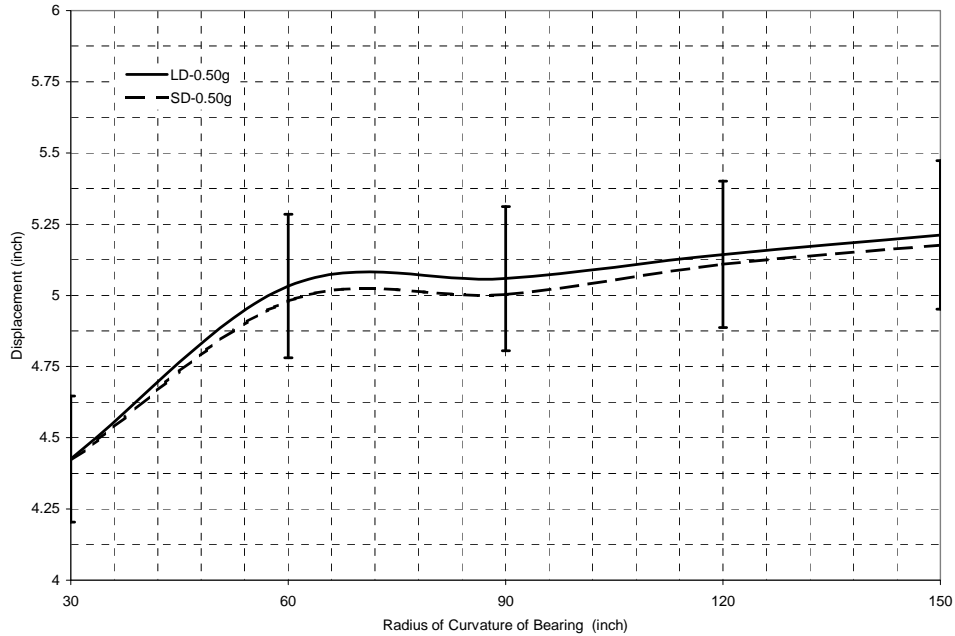


Figure 3-29 Comparison of Displacements Based on Small and Large Displacement Assumptions for PGA of 0.50g

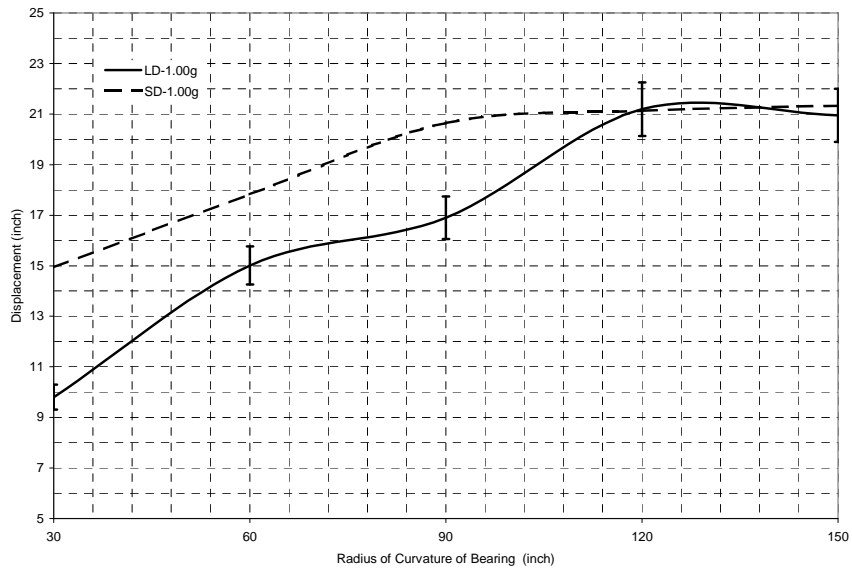


Figure 3-30 Comparison of Displacements Based on Small and Large Displacement Assumptions for PGA of 1.0g

Figure (3-31) through figure (3-33) compare the average inertia reduction response of FPS based on large and small displacement assumptions. Also shown for each radius of curvature is 5% deviation from large displacement assumption values. Inertia reduction responses for smaller PGA values (0.25g, 0.5g) are in good agreement using both assumptions. For larger PGA values (1.0g) with a small radius of curvature there is a larger deviation, however the small

displacement assumption is almost always conservative. It can be stated that using the small displacement assumption is in fairly good agreement with the large displacement assumption up to the PGA of 1.0g, which is stated as high performance level in IEEE 697.

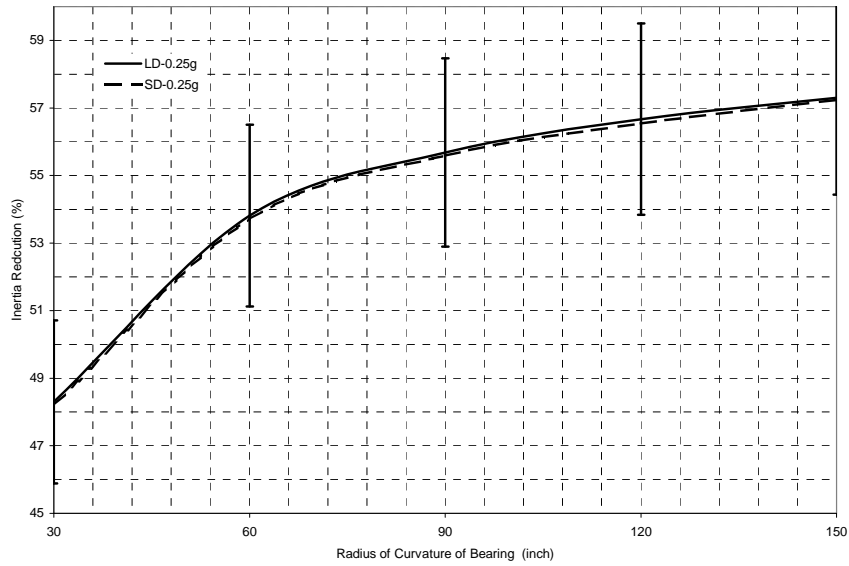


Figure 3-31 Comparison of Inertia Reductions Based on Small and Large Displacement Assumptions for PGA of 0.25g

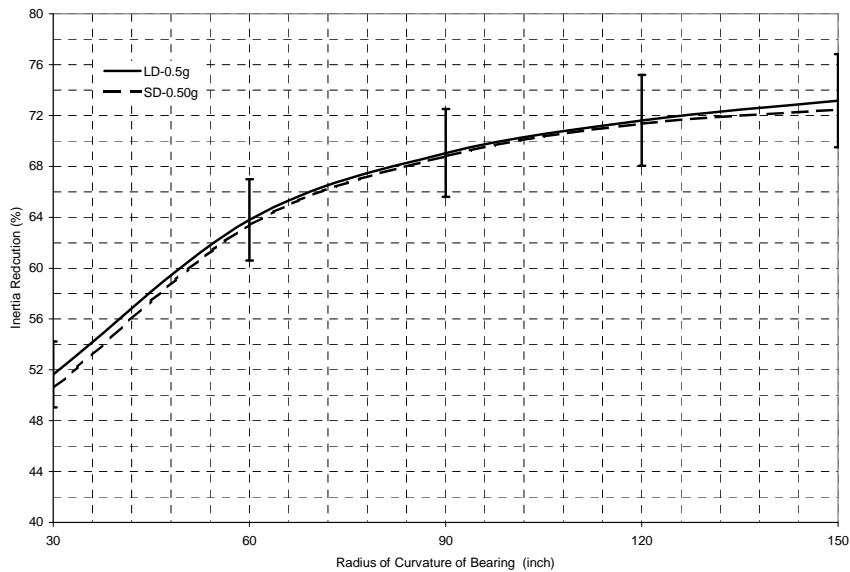


Figure 3-32 Comparison of Inertia Reductions Based on Small and Large Displacement Assumptions for PGA of 0.50g

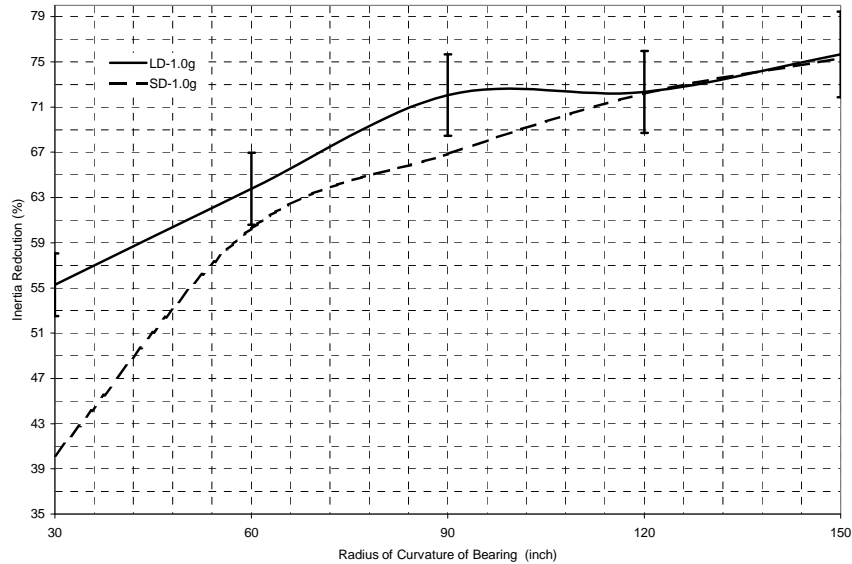


Figure 3-33 Comparison of Inertia Reductions Based on Small and Large Displacement Assumptions for PGA of 1.00g

3.5 Force Displacement Response of FPS Model

As discussed before, the design of FPS bearings combines the concepts of sliding and pendulum response. Therefore, for a horizontal load lower than the static friction force, the force-displacement response of a FPS bearing is rigid (sticking mode). The slope of this part of the curve is equal to stiffness of non-isolated structure. For higher loads, “yielding” or more exactly, sliding takes place and the stiffness of the structure is controlled by the isolation system stiffness. For a SDOF system, the post-yield stiffness is equal to the equivalent stiffness (or W/R). A typical load-displacement response for FPS bearings is shown in figure 3-34. This graph shows the overall energy dissipation behavior, which is very stable and can be represented with an ideal bi-linear response relationship. These characteristics have been verified through experimental work [Zayas, 1990]. The area enclosed by the hysteresis loops represents the energy dissipation capacity of the isolation device and is related to its frictional characteristics. Under the small displacement assumption, the loops take on a parallelogram shape. The vertical height of the parallelogram is twice the “yield” force or the force required to cause sliding (i.e., μW). Thus, using the length parameter D as defined in figure 3-34, the effective friction coefficient is equal to the enclosed area divided by $2DW$.

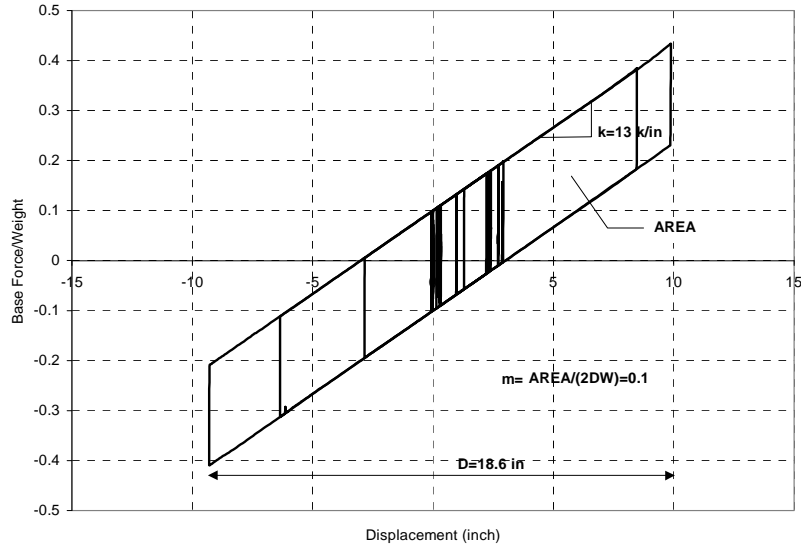


Figure 3-34 Typical Load-Displacement Hysteresis Loop for FPS Isolator

3.6 Finite Element of FPS Behavior

To study effect of changes in friction force on response of FPS system and its implication for response of secondary system (here bushings) a finite element was formulated and implemented into ADINA. The finite element developed for FPS consists of 2 nodes with 3 translational degrees of freedom in each node. The first node represents the sliding surface while the second node represents the articulated slider. There are small values of moment involved for keeping the static balance that are ignored here. Since the element is being implemented in ADINA as part of this study, it is required to add 3 rotational degrees of freedom to each node. However, all forces in these nodes and all the stiffness components related to them are equal to zero.

The global degrees of freedom are

$$U = \begin{bmatrix} u_{11} \\ u_{12} \\ u_{13} \\ u_{21} \\ u_{22} \\ u_{23} \end{bmatrix} \quad (3-32)$$

where the first subscript refers to the corresponding node and the second subscript shows the corresponding direction. The first two directions are horizontal and the 3rd direction is vertical. Two local coordinates are used to describe the position and behavior of the slider more easily. The first is

$$X = \begin{bmatrix} x_1 \\ x_2 \\ x_3 \end{bmatrix} = \begin{bmatrix} u_{21} - u_{11} \\ u_{22} - u_{12} \\ u_{23} - u_{13} \end{bmatrix} \quad (3-33)$$

that describes position of the slider relative to the sliding surface.

However, there is a need for another set of coordinates that can reflect the sliding behavior of the slider that occurs in a plane tangent to the surface at each point in time. These are the coordinates that should be used in the relations determining friction forces. After determining the forces, they are transformed into forces in global coordinates. The first of these coordinates, called v_1 is the vector in the tangent plane that has no x_2 component and is in the direction with positive x_1 component. The second vector is the tangent vector perpendicular to v_1 and the third vector is the normal vector with positive x_3 component. The direction of v_2 is chosen in a way to make this a right-hand coordinate system. The coordinates of these vectors in X coordinate system are as follows:

$$v_1 = \begin{pmatrix} 1/\sqrt{1 + \tan(\phi)^2 * \cos(\theta)^2} \\ 0 \\ \sqrt{1 - v_{11}^2} * \text{sign}(\cos(\theta)) \end{pmatrix} \quad (3-34)$$

$$v_3 = \begin{pmatrix} -\sin(\phi) * \cos(\theta) \\ -\sin(\phi) * \sin(\theta) \\ \cos(\theta) \end{pmatrix} \quad (3-35)$$

$$v_2 = v_3 \times v_1 \quad (3-36)$$

The angles Φ and θ in these equations are the angles between slider (node2) and vertical and x -axis in spherical coordinates.

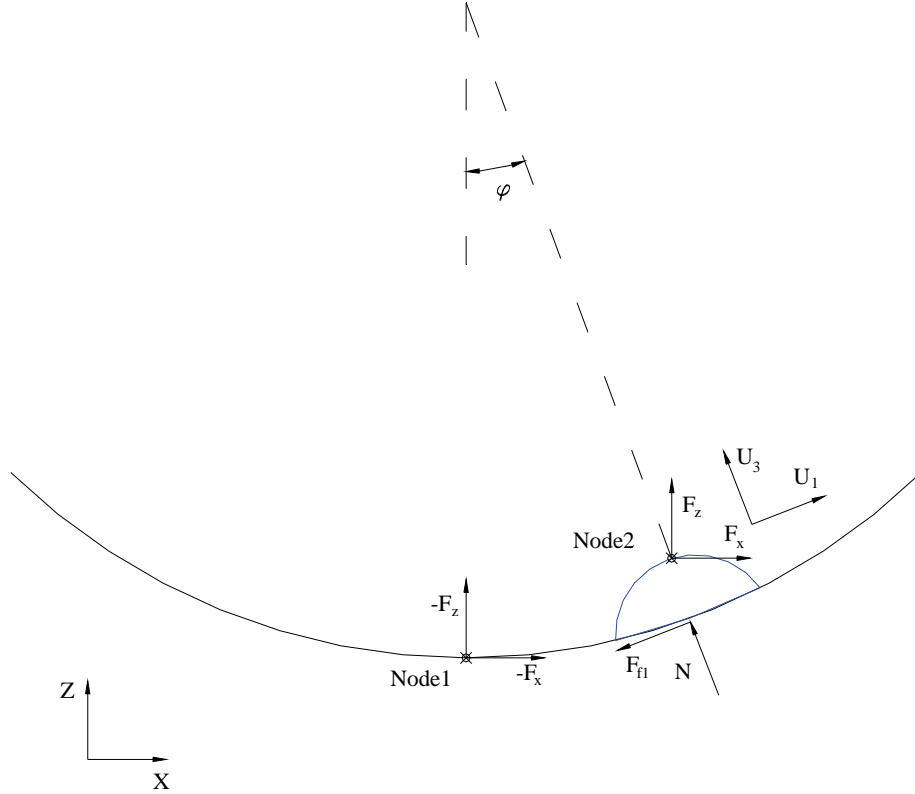


Figure 3-35 Diagrams of the Forces in FPS (only in-plane forces are shown).

To calculate the forces in the element in each time step based on the position of the nodes, the normal force should be first determined. To this end, a k_{normal} with high stiffness is considered to simulate the stiffness of the FPS surface in normal direction. A high damping close to the critical damping (damping ratio of 20%~90%) is also applied in this normal direction to prohibit excessive vibration in vertical direction causing unreal changes in normal force. Using this stiffness, the normal force at each time is determined based on the distance of slider from the surface (this is a nominal distance and as long as the stiffness is high enough and the tolerance is picked accordingly, it does not affect the results). Defining z_{surf} as the third component of the position of the point in the surface under slider in X coordinates, we have:

$$N = -k_{normal} * z_{normal,n+1} - c * vel_{normal} \quad (3-37)$$

Friction force at each moment is determined using the calculated normal force and the value of Z at the moment. Defining components of Z in v_1 and v_2 direction as Z_1 and Z_2 , the friction force applied by surface to the slider in these directions are equal to:

$$F_{f1} = -\mu NZ_1 \quad (3-38)$$

$$F_{f2} = -\mu NZ_2 \quad (3-39)$$

The external force at node 2 of FPS can be calculated as:

$$\begin{pmatrix} F_x \\ F_y \\ F_z \end{pmatrix} = -\begin{bmatrix} v_1 & v_2 & v_3 \end{bmatrix} \begin{pmatrix} F_{f1} \\ F_{f2} \\ N \end{pmatrix} \quad (3-40)$$

The stiffness matrix for the FPS element should satisfy the equation

$$K\Delta X = \Delta F \quad (3-41)$$

It is defined as a diagonal matrix as follows:

$$K = \begin{bmatrix} T & 0 & -T & 0 \\ 0 & 0 & 0 & 0 \\ -T & 0 & T & 0 \\ 0 & 0 & 0 & 0 \end{bmatrix} \quad (3-42)$$

$$T = \begin{bmatrix} \Delta F_{x1} / \Delta x_1 & 0 & 0 \\ 0 & \Delta F_{x2} / \Delta x_2 & 0 \\ 0 & 0 & \Delta F_{x3} / \Delta x_3 \end{bmatrix} \quad (3-43)$$

The details of these calculations are explained in the Appendix C.

3.7 Behavior of Fixed and Isolated Primary-Secondary Systems

The behavior of a transformer, isolated by FPS and modeled as a rigid mass, has been studied so far. There are also studies on effect of base isolation of structures on secondary systems. It was found that use of base isolation generally reduces the peak responses of secondary systems [Fan, 1990]. Laminating rubber bearings were found to be more effective in a wide range of frequencies compared to friction isolators (pure friction, and resilient friction). Using a simple model for friction that shows stick-slip behavior, it was observed that the frictional base isolation systems generate high frequencies in the structural responses. The resilient-friction isolation was observed to be more effective than pure friction isolation in most of the times. It was also found that use of isolation systems should be avoided in regions with low frequency energy content. These results are reaffirmed in another publication [Fan, 1992]. Another study showed effectiveness of base-isolation of primary system for reducing the secondary system response for all earthquakes, except those with very low frequency content. This study was performed using laminated rubber bearings [Kim, 1993].

To study the effects of FPS on secondary systems, a primary-secondary system was parametrically studied for both fixed and isolated cases. The more accurate friction model was used to model friction. The flexibility of primary system is considered in the model because of its effects on FPS and secondary system response. The primary system has three degrees of freedom, two horizontal and one vertical. The secondary system has two horizontal degrees of freedom and has the same vertical displacement as that of the primary system. All elements have linear elastic force-displacement behavior. The vertical degree of freedom is considered for the

primary system to make it possible to study effect of vertical excitation of the primary system, that can change normal force, and hence the friction force. Change in frequency content of this force can be expected, especially close to vertical frequency of the primary system. This may amplify the response of secondary systems having similar frequencies.

Figure 3-36 shows a 2-D diagram of the model considered. The model has the same characteristics in the other horizontal direction. The weight of primary system is equally divided between its top and bottom nodes. Primary system is taken to be much heavier than the secondary system. Since the focus of this study is on transformers and bushings, the physical characteristics of the model are chosen in a range close to actual transformer-bushing systems. Also, the words transformer and bushing might be used instead of primary system and secondary system in this section.

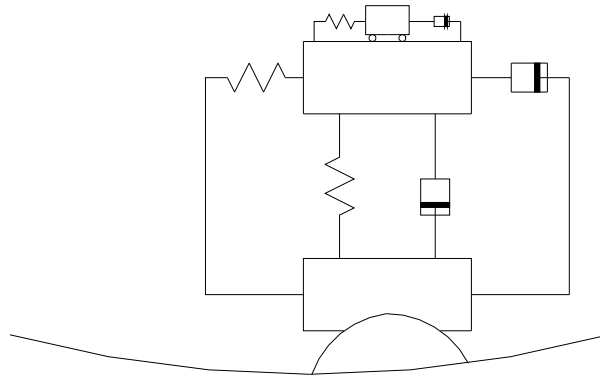


Figure 3-36 Primary-secondary Model.

Tables 3-3 and 3-4 show the physical characteristics of the primary and secondary systems used in the model. TT1 has the same characteristics as transformer type 25 MVA – 650 HV BIL discussed in Section 2. BUS1 has the same frequency as a 196 kV bushing fixed at the base [see section 2]. The structure of 230 kV bushings is also similar to 196 kV bushings [Gilani, 1999(a)]. BUS3 can represent the same bushing mounted on TT1 [Ersoy, 2002]. BUS2 represents a 550 kV bushing fixed at base [Gilani, 1999(b)]. TT4 and TT6 are included to study the effects of vertical frequency of transformer on different responses. However, it should be kept in mind that the vertical frequency of an actual transformer is considerably higher than its horizontal frequency, and cases like TT4 are not found in reality.

Table 3-3 Properties of the Primary Systems Studied

Primary	Horizontal frequency (Hz)	Vertical frequency (Hz)	Mass (kips)	Damping ratio
TT1	14.0	26.1	179	2%
TT2	8.0	16.0	773	2%
TT4	14.0	14.0	179	2%
TT6	14.0	21.0	179	2%

Table 3-4 Properties of the Secondary Systems Studied

Secondary	Frequency (Hz)	Mass (kips)	Damping ratio
BUS1	16.0	0.69	2%
BUS2	8.0	4.23	2%
BUS3	11.0	0.69	2%
BUS4	10.5	0.69	2%
BUS5	10.0	0.69	2%
BUS6	9.5	0.69	2%
BUS7	9.0	0.69	2%
BUS8	7.0	4.23	2%
BUS9	6.0	4.23	2%
BUS10	5.0	4.23	2%
BUS11	12.0	0.69	2%
BUS12	14.0	0.69	2%

Table 3-5 shows the data related to several analyses performed. The analyses are performed for El Centro earthquake with 1g PGA in two horizontal directions and a PGA of 0.8g in vertical direction according to IEEE [IEEE, 1998].

Table 3-5 Characteristics of the Primary-Secondary Systems Studied

Case	Primary	Secondary	Support
1	1	1	FPS, R = 60 in
2	1	3	FPS, R = 60 in
3	1	4	FPS, R = 60 in
4	1	5	FPS, R = 60 in
5	1	6	FPS, R = 60 in
6	1	7	FPS, R = 60 in
7	1	11	FPS, R = 60 in
8	1	12	FPS, R = 60 in
9	1	1	Fixed
10	1	3	Fixed
11	1	4	Fixed
12	1	5	Fixed
13	1	6	Fixed
14	1	7	Fixed
15	1	11	Fixed
16	1	12	Fixed
17	2	1	FPS, R = 60 in
18	2	2	FPS, R = 60 in
19	2	3	FPS, R = 60 in
20	2	4	FPS, R = 60 in
21	2	5	FPS, R = 60 in
22	2	6	FPS, R = 60 in
23	2	7	FPS, R = 60 in
24	2	8	FPS, R = 60 in
25	2	9	FPS, R = 60 in
26	2	10	FPS, R = 60 in
27	2	11	FPS, R = 60 in
28	2	1	Fixed
29	2	2	Fixed
30	2	3	Fixed
31	2	4	Fixed
32	2	5	Fixed
33	2	6	Fixed
34	2	7	Fixed
35	2	8	Fixed
36	2	9	Fixed
37	2	10	Fixed
38	2	11	Fixed
39	1	1	FPS, R = 30 in
40	1	3	FPS, R = 30 in
41	1	4	FPS, R = 30 in
42	1	5	FPS, R = 30 in
43	1	6	FPS, R = 30 in
44	1	7	FPS, R = 30 in
45	1	11	FPS, R = 30 in
46	1	12	FPS, R = 30 in
47	4	1	FPS, R = 60 in
48	4	3	FPS, R = 60 in
49	4	4	FPS, R = 60 in

Table 3-5 Characteristics of the Primary-Secondary Systems Studied (Continued)

Case	Primary	Secondary	Support
50	4	5	FPS, R = 60 in
51	4	6	FPS, R = 60 in
52	4	7	FPS, R = 60 in
53	4	11	FPS, R = 60 in
54	4	12	FPS, R = 60 in
55	4	1	Fixed
56	4	3	Fixed
57	4	4	Fixed
58	4	5	Fixed
59	4	6	Fixed
60	4	7	Fixed
61	4	11	Fixed
62	4	12	Fixed
63	6	1	FPS, R = 60 in
64	6	3	FPS, R = 60 in
65	6	4	FPS, R = 60 in
66	6	5	FPS, R = 60 in
67	6	6	FPS, R = 60 in
68	6	7	FPS, R = 60 in
69	6	11	FPS, R = 60 in
70	6	12	FPS, R = 60 in
71	6	1	Fixed
72	6	3	Fixed
73	6	4	Fixed
74	6	5	Fixed
75	6	6	Fixed
76	6	7	Fixed
77	6	11	Fixed
78	6	12	Fixed

Figure 3-37 shows the bushing relative displacement for different radii of FPS. The primary system TT1 is used in these analyses. As expected, the FPS with lower radius causes more displacement (and more force) in the bushing. For comparison, it should be said that a 230 kV bushing with a frequency in the range of 11~14 Hz depending on its support experiences failure in relative displacements between 0.3~0.35 in [Gilani, 1999(a)]. Lower frequencies belong to bushings with higher capacities and larger structures that will have higher allowable displacements. The results in this figure are all under 0.3 in, showing that use of FPS prevents any damage to the bushings.

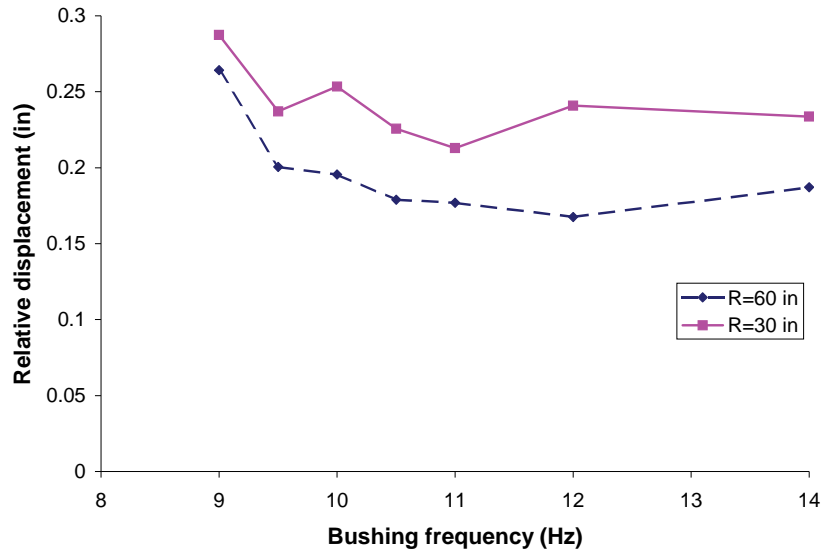


Figure 3-37 Bushing Response for TT1.

Figure 3-38 shows the effect of vertical frequency of transformer on the bushing response and compares this with the fixed-base response. The notations TT1, TT6, and TT4 refer to transformers with the same horizontal frequency. The vertical to horizontal frequency ratio for these transformers are 1.86, 1.5, and 1.0, respectively. The horizontal frequency of the transformer is assumed to be 14 Hz. As can be seen, the closer the vertical frequency is to the horizontal frequency, the higher the bushing response. This amplification can particularly be observed for the case when vertical frequency is equal to horizontal frequency. However, the FPS is still effective in reducing the bushing response compared to the fixed-base case.

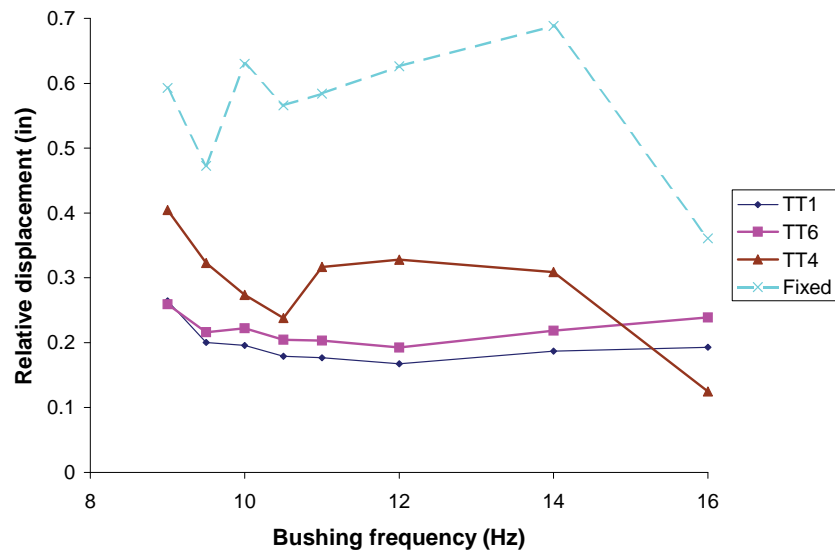


Figure 3-38 Effect of Vertical Frequency and Support Fixity on Bushing Response.

Figure 3-39 shows the bushing response for bushings mounted on another transformer with a horizontal frequency of 8 Hz. Again, the FPS is effective in reducing the bushing response, especially for lower frequencies. This is due to higher response of bushings with low frequencies in general. Base isolation is particularly effective when bushing has a frequency close to transformer, because FPS prevents the amplification of bushing response.

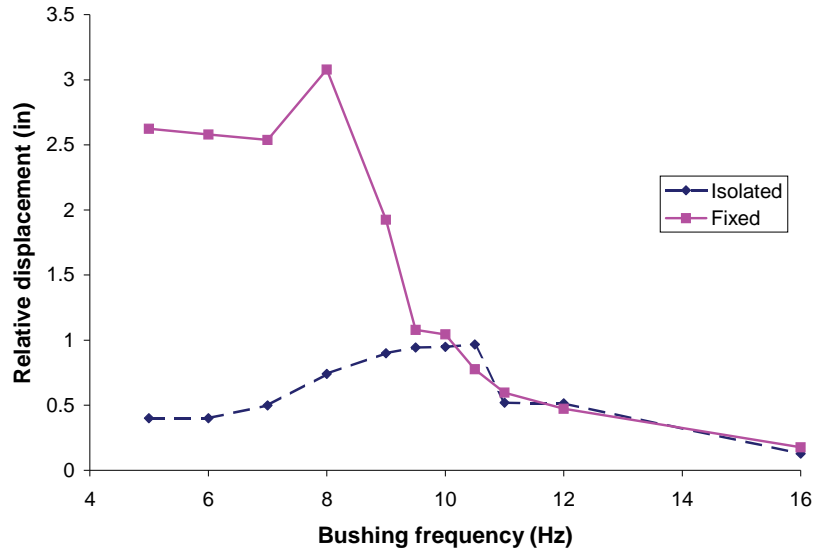


Figure 3-39 Bushing Response for TT2

Figure 3-40 compares the bushing response of isolated systems for two different transformers. TT1 has a horizontal frequency of 14 Hz while TT2 has a frequency of 8 Hz. As observed, the response for TT2 is usually higher than that of TT1. This can probably be attributed to the fact that its frequency is closer to the frequency range where the earthquakes have most of their energy. However, higher voltage transformers require higher voltage bushings. Higher voltages mean larger dimensions, lower frequencies, and more displacement capacities for both transformers and bushings. Therefore, transformers with lower frequencies often have bushings with higher displacement capacities as well. While bushings on TT1 are definitely safe, it cannot be directly determined from this graph whether bushings on TT2 will fail or not. This should be determined based on the specific frequency and allowable displacement of such bushings. However, it is very probable that the higher displacement capacity of such bushings will cover the increase in their response.

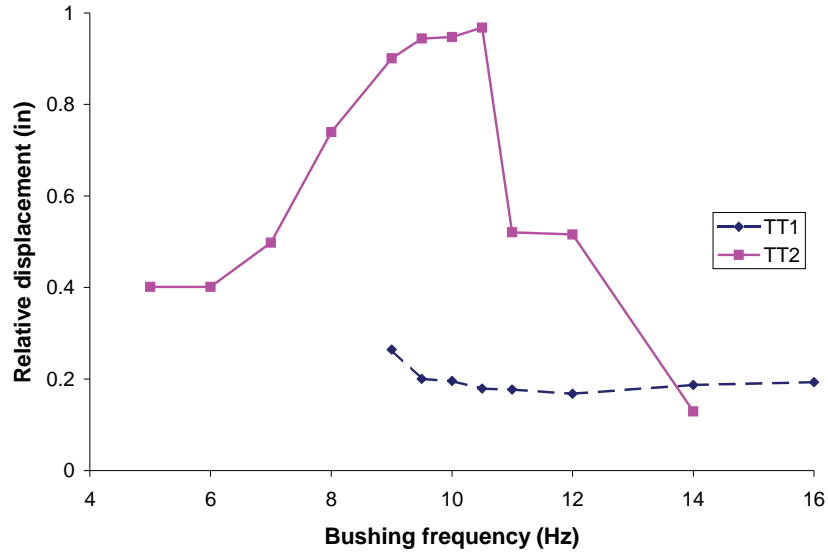


Figure 3-40 Effect of Transformer Frequency on Bushing Response.

Figure 3-41 compares the vertical force at support for different isolated and fixed systems. The frequency of bushing does not have much effect, because its weight is small compared to that of the transformer. It can be seen that closeness of vertical and horizontal frequency of transformer will result in increase in vertical force. For fixed TT4 and TT6, tension can be observed at times in the support. The isolated systems for these cases experience uplift, though it is very brief in the case of TT6.

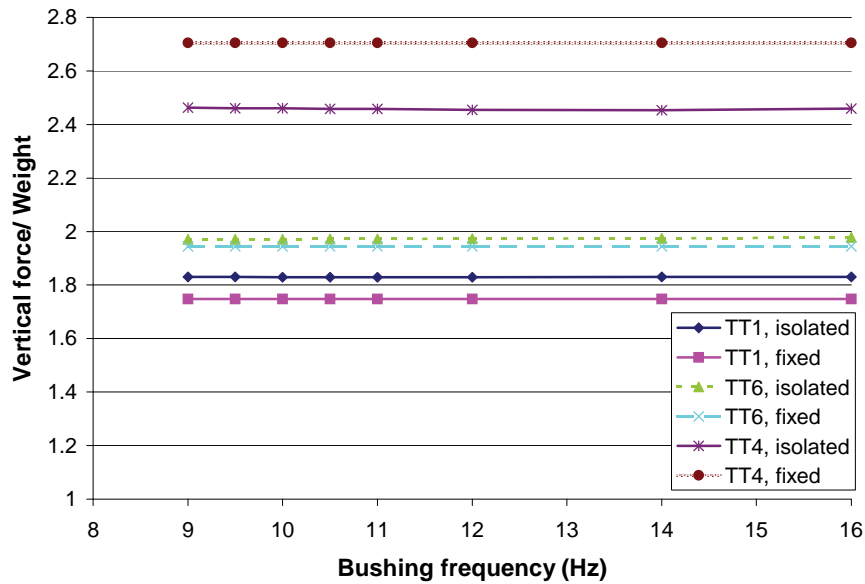


Figure 3-41 Vertical Force at Support.

Figures 3-42 and 3-43 compare the base shear force in the two horizontal directions. The effect of vertical frequency of transformer can be observed through the difference between response of TT1, TT6, and TT4 while the effect of isolation can be seen comparing the forces with those of fixed-base case. As can be seen, the isolation has been more effective in one direction (designated as x-direction). If the vertical and horizontal frequencies of the transformer are too close to each other, considerable increase in shear force is observed. However, the shear forces are still much less than those of fixed-base system in x-direction. In y-direction, FPS has been less effective in reducing base shear. For TT4, the shear force in y-direction in isolated system is higher than the fixed-base case due to the increase in normal force. However, it should be emphasized that the proximity of vertical and horizontal frequency of TT4 is unrealistic. The response of TT1 and TT6 that show efficacy of FPS are more representative of the behavior of actual isolated structures. It should be noted that the forces are presented in terms of the ratio of shear force over weight, not normal force. The normal forces are about twice higher than the weight, as mentioned previously.

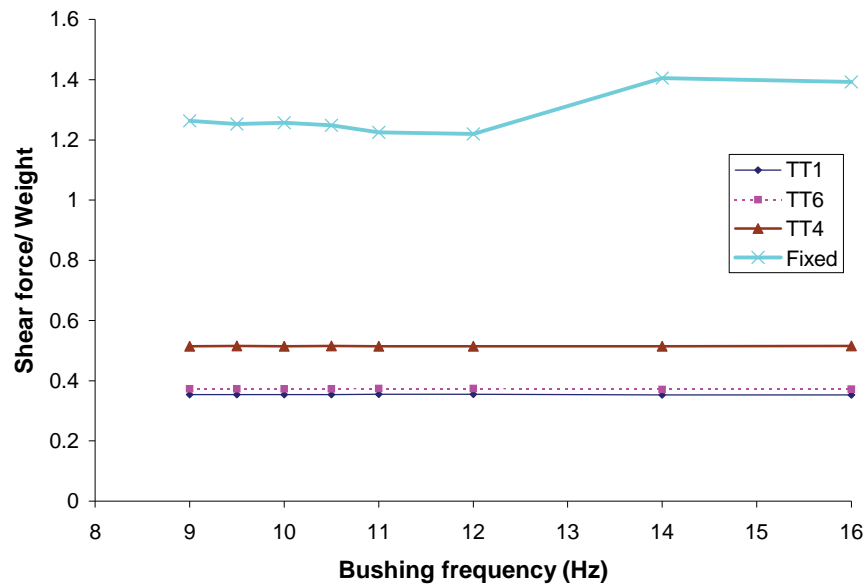


Figure 3-42 Effect of Vertical Frequency and Support Fixity on Shear Force in x-direction.

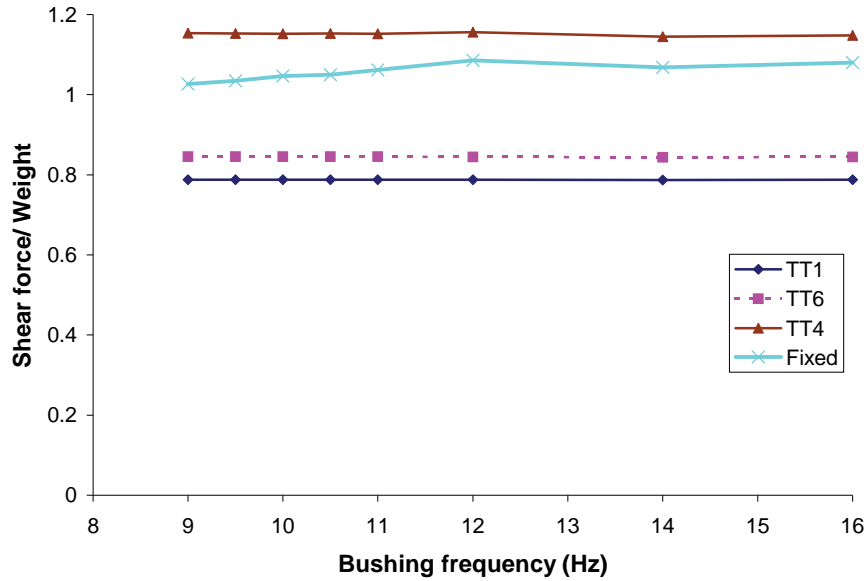


Figure 3-43 Effect of Vertical Frequency and Support Fixity on Shear Force in y-direction.

Figure 3-44 and figure3-45 show base shear forces for TT1 in both directions for two different FPS radii. The forces for R = 30 in are higher in both directions, but the difference is more in x-direction. In all these cases, the y-direction is the direction in which FPS slider moves the most. That is why FPS shows a higher resistance in this direction due to higher restoring forces and higher stiffness caused by the changed slope of the surface. The difference of response in y-direction between different radii is less, because they are closer to the response of a fixed-base system.

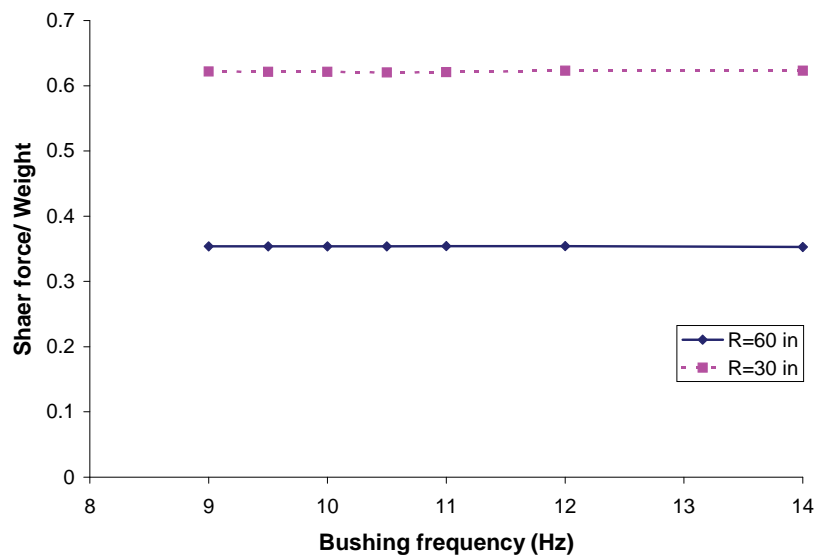


Figure 3-44 Shear Force in x-direction for TT1.

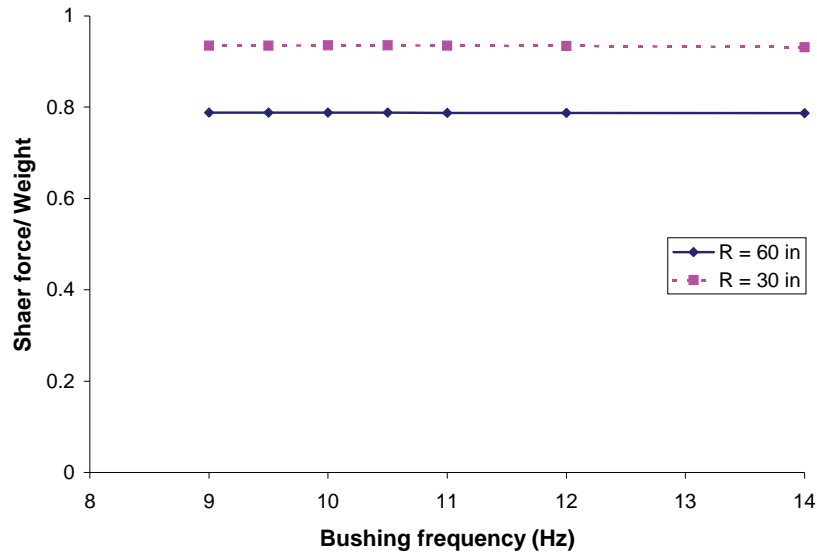


Figure 3-45 Shear Force in y-direction for TT1.

Figure 3-46 shows the same trends when comparing response of two different transformers. While response of TT2 that has a lower frequency is always more than TT1, the difference is more pronounced in x-direction compared to y-direction. Comparing this to Figure 3-47 that depicts fixed-base response of these two systems yields an interesting point. The most critical component of earthquake for a fixed-base structure might be different from an isolated structure. While the x-direction is much more critical in fixed-base cases, it is the y-component that has the most effect on response of the isolated structure. Such an observation can have different reasons. Richness of an earthquake in terms of frequencies close to natural frequency of a structure is the most important factor determining response of the structure. Therefore, having the same peak ground acceleration, the earthquake components with frequency content closer to natural frequency of the structure will have the most effect on it. However, in an isolated structure, proximity of the earthquake frequency content to natural frequency of the FPS is also an important factor. Moreover, the number and duration of times when the ground acceleration surpasses the sliding threshold of FPS is an important factor determining the amount of sliding and restoring force. Hence, it is possible that the earthquake component more effective on an isolated structure is different from the component more effective on the fixed structure.

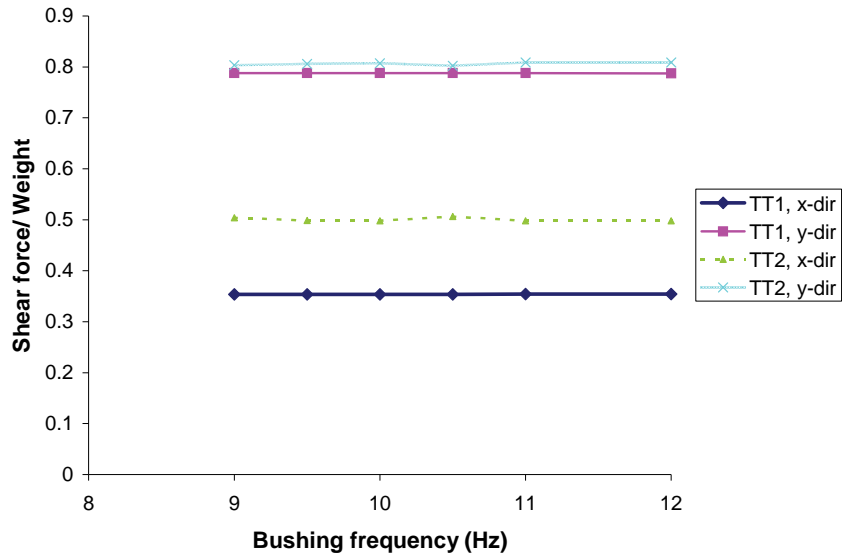


Figure 3-46 Effect of Transformer Frequency on Shear Force in Isolated Systems.

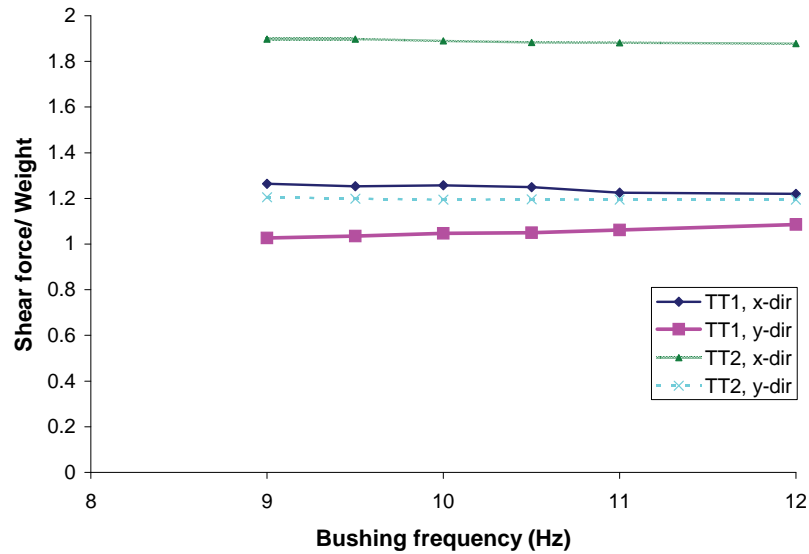


Figure 3-47 Effect of Transformer Frequency on Shear Force in Fixed-base Systems.

In summary, it can be said that these studies show effectiveness of FPS for reducing response of secondary system for all ranges of primary and secondary system frequencies. This is evident even when primary and secondary systems have the same frequencies. Efficiency of FPS in reducing the secondary system response, even for high frequencies, can probably be attributed to the more accurate model used for friction that does not generate artificial high frequencies in the response.

The isolation is also effective in reducing the shear force and response of primary system (since base shear is essentially equal to force in primary system). This however, does not necessarily mean that response of bushing will remain in allowable range for all cases. Such determination should be made based on these results, having the exact information about displacement capacity of a particular type of bushing. Closeness of the vertical and horizontal frequencies of a primary system can increase the secondary response and base shear. This effect, however, is limited for the practical values of frequencies of transformers. Also it should be noted that results of this work were intended for use for transformer-bushing systems and frequency range and mass proportions were chosen accordingly. The behavior trends might change if the structure of interest has primary or secondary systems of much lower frequencies such that they are close to frequency of the FPS.

SECTION 4

EXPERIMENTAL STUDY OF FRICTIONAL PENDULUM SYSTEM

As a part of this research project, in the summer of 1999, about 100 tests were conducted at the National Center for Research on Earthquake Engineering (NCREE) in Taiwan through a collaboration effort. The objective was to compare the response of fixed base transformer model supporting a bushing to those when the systems are isolated using FPS bearings. It represents the first effort in testing base isolated large-scale transformer bushing systems using an earthquake simulator. The testing schedule also included white noise tests to identify dynamic characteristics of the bushings and the transformer model. 1-D, 2-D and 3-D excitations were conducted employing several earthquake records with PGAs in the range of 0.125g to 0.375g. One type of bushing, namely 161 kV was used in the experimentation. Consistent with the practice employed by TaiPower, the bushing was attached perpendicular to the top of transformer model. The following sections discuss the test set-up and experimental results. Furthermore, comparisons between the analytical and experimental results are presented.

4.1 Earthquake Simulator

The earthquake simulator at the National Center for Research on Earthquake Engineering (NCREE) in Taiwan was used for the experiments described in this section. The NCREE earthquake simulator, also known as a shaking table, possesses 6 degrees of freedom to simulate earthquake motion in 3 axes. The size of the shaking table of the seismic simulator is 16' x 16' and its mass is 29.8 tons. Structural models with a maximum payload of 55.1 tons can be accommodated on the table. The table is driven by 12 hydraulic actuators (4 actuators for each axis). The reaction forces of the actuators are provided by the reaction mass of about 4400 tons. To further improve the quality of the testing environment, the reaction mass is isolated from the fixed foundation by 96 air springs and 80 dampers.

The total number of earthquake tests performed on the transformer model including both isolated and fixed conditions was 77. To this should be added many tests to identify the dynamic characteristics of the system. These were the first experimental tests on base isolated transformer models. Parallel to these tests, several hundred more tests were conducted to investigate the performance of other isolation devices. It is not within the scope of this report to present the results of those latter tests. Some of those can be found in a report by Murota et al. [Murota et al, 2005]

4.2 Instrumentation

The transformer model was equipped with LVDTs and accelerometers at three different levels; the load cells were placed at the bottom corners of the transformer model: Level 1, Level 2 and Level 3. The top of the bearing is referred to as Level 1. That of the load cell or bottom of the transformer is referenced as Level 2 and the top of the transformer is labeled as Level 3. The relative displacement of the bearing is obtained by subtracting the LVDT records at Level 2 from the shake table displacements.

The response of the 161 kV bushing was measured at four locations, namely bottom of the bushing, transformer level (or flange), middle of the bushing and at the top of the bushing.

A total of 70 channels were used to record response parameters. Accelerations were recorded on 34 of these channels. Load cell readings were taken on 12 channels and 18 channels were used for LVDT records. Six channels were used for shake table displacement and acceleration records.

4.3 Transformer Model and Bushing

Photographs of the transformer model and its instrumentation are shown in figure 4-1 and 4-2. The dimensions of the transformer model are 7'-10 1/2" x 7'-2 10/16" in plan. The height of the transformer is 8'-10 5/16". Four 18.64" radius FPS bearings were used to support the model for the isolated case.

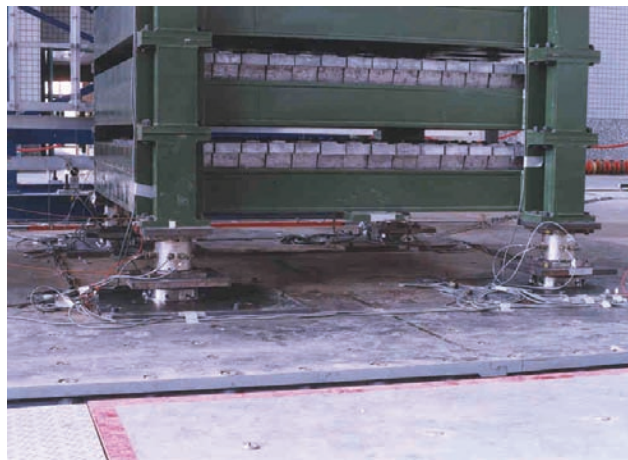


Figure 4-1 A View of the Transformer Model and Instrumentation



Figure 4-2 Transformer Model with the Bushing Mounted on the Top

The characteristics of the bushing (161 kV) are summarized in table 4-1. Those of the isolation system are shown in table 4-2.

Table 4-1 Characteristics of 161 kV Bushing

Type Form	VEU-140ZT
Insulation Class	161 kV
Rated Current	1200 A
BIL	750 kV
Approximated Weight	772 lbs
Total Length	11'-5 10/16"

Table 4-2 Characteristics of the Isolation System

Characteristics	Designed Value
Radius of Bearing	18.64 inch
Effective Stiffness	3.016 kips/inch
Equivalent Damping Ratio	0.14
Effective Period	1.38 s

4.4 Modal Analysis of Transformer Model and Bushing

The dynamic characteristics of the transformer model and the bushing were computed from the response of the model to random noise. They are presented in table 4-3.

Table 4-3 Dynamic Characteristics of the Transformer Model and the Bushing

	Frequency		
	x-direction	y-direction	Yaw-direction
Transformer Model	12.5	12.5	22.5
161 kV Bushing	12.0-12.5	12.0-12.5	24.0

The dynamic characteristics of the transformer model and the bushing were also obtained by FFT of the response of the testing frame and the bushing. Figure 4-3 shows the FFT of the testing frame. FFT of the bushing response and the bushing response with respect to the testing frame are shown in figure 4-4 and figure 4-5 respectively. As it can be seen, the same frequency responses are obtained from FFT analysis. The random noise analysis given in table 4-3 also shows the same values.

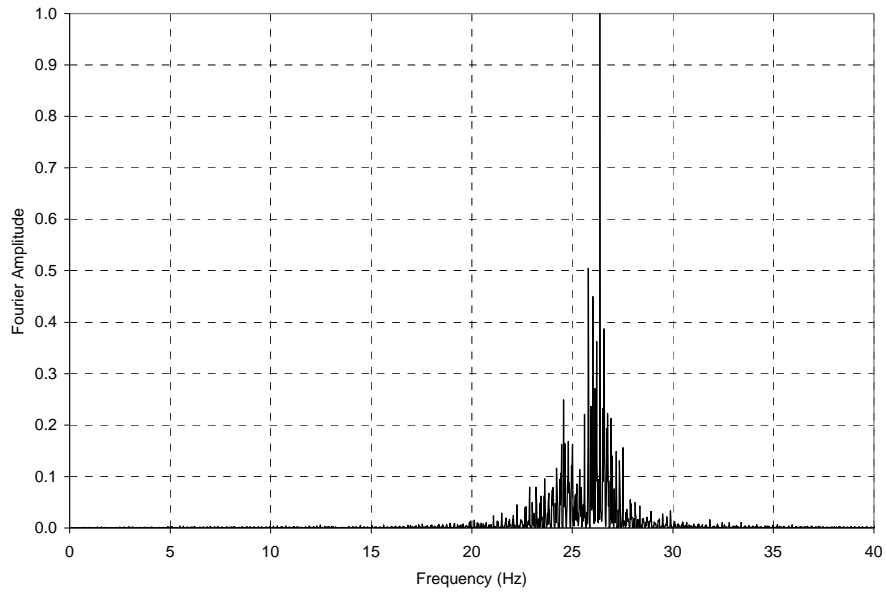


Figure 4-3 FFT of Testing Frame Response for 1-D Case of Sylmar Record with 0.375g in X direction

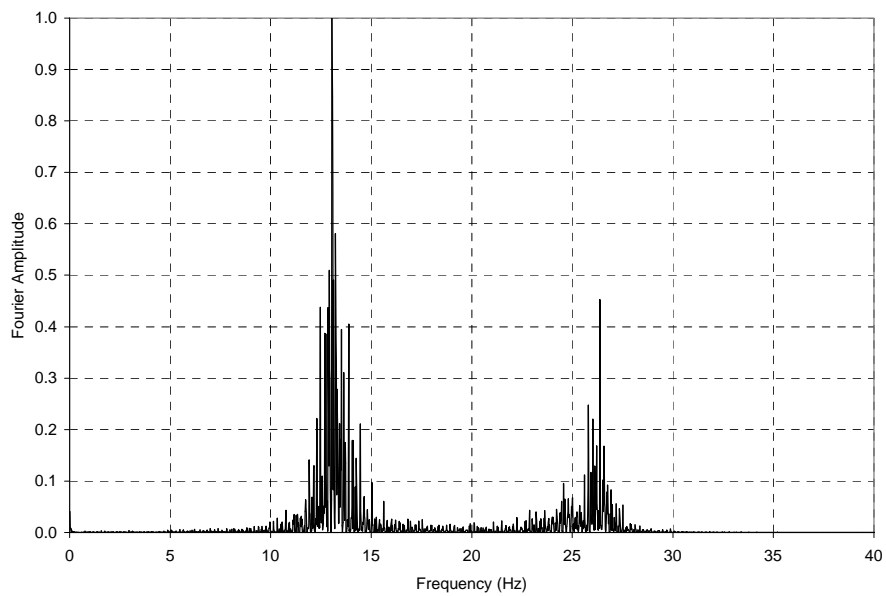


Figure 4-4 FFT of Bushing Response for 1-D Case of Sylmar Record with 0.375g in X Direction

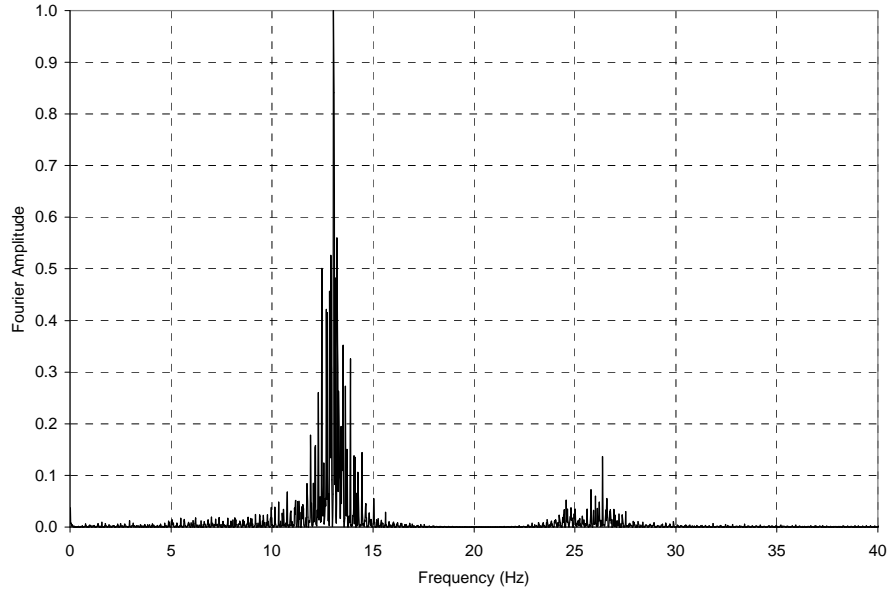


Figure 4-5 FFT of Bushing Response with Respect to Testing Frame for 1-D case of Sylmar Record with 0.375g in X Direction

4.5 Results

Several earthquake records were used in the tests, namely: CKS (Chiang Kai-Shek), Chi-I Ray-Li, El-Centro, Kobe-Takatori and Northridge-Sylmar. The test results for 1-D cases of the Sylmar record are tabulated in table 4-4 for isolated and non-isolated cases. And the results of the 2-D and 3-D cases of same record are tabulated in table 4-5. In these tables, A_2 and A_3 show the acceleration values (in g) at the bottom and the top of the transformer model, respectively. A_{b1} , A_{b2} , A_{b3} , A_{b4} represent the accelerations at different locations along the bushing. D_2 , and D_3 (in inches) are the relative displacement values of the transformer model at the top and bottom, respectively.

Some of the response acceleration maps for the 1-D cases indicate the effect of isolation system at different levels of the transformer model. (figure 4-6 through 4-8). In these figures the x-axis shows the acceleration values normalized with respect to PGA. Absolute maximum total acceleration values at different levels of transformer model and bushing, is divided by absolute maximum acceleration of the earthquake record (PGA of shake table). The y-axis shows different locations along the height of the test specimen ranging from the top of the shake table to the top of the bushing. As one can see from these figures, the acceleration responses for fixed base cases increase as the height above the base of the transformer increases. However, when base isolation (FPS) is introduced, the acceleration is reduced significantly at different levels throughout the height above the base.

Table 4-4 Responses for Northridge-Sylmar Record (Case 1 through Case 3)

Case No.	Input and Response	Fixed Base			Base Isolated		
		x	y	z	x	y	z
1	PGA _{Target}	0.125	-	-	0.125	-	-
	PGA _{Real}	0.147	-	-	0.138	-	-
	A ₂	0.160	-	-	0.078	-	-
	A ₃	0.246	-	-	0.117	-	-
	A _{B1}	0.272	-	-	0.166	-	-
	A _{B2}	0.251	-	-	0.128	-	-
	A _{B3}	0.513	-	-	0.142	-	-
	A _{B4}	0.919	-	-	0.232	-	-
	D ₂	0.034	-	-	0.306	-	-
	D ₃	0.050	-	-	0.310	-	-
2	PGA _{Target}	0.250	-	-	0.250	-	-
	PGA _{Real}	0.238	-	-	0.282	-	-
	A ₂	0.259	-	-	0.119	-	-
	A ₃	0.456	-	-	0.204	-	-
	A _{B1}	0.489	-	-	0.375	-	-
	A _{B2}	0.437	-	-	0.282	-	-
	A _{B3}	1.026	-	-	0.211	-	-
	A _{B4}	1.867	-	-	-	-	-
	D ₂	0.067	-	-	1.032	-	-
	D ₃	0.095	-	-	1.047	-	-
3	PGA _{Target}	0.375	-	-	0.375	-	-
	PGA _{Real}	0.378	-	-	0.379	-	-
	A ₂	0.419	-	-	0.166	-	-
	A ₃	0.666	-	-	0.332	-	-
	A _{B1}	0.826	-	-	0.572	-	-
	A _{B2}	0.602	-	-	0.420	-	-
	A _{B3}	1.424	-	-	0.256	-	-
	A _{B4}	2.749	-	-	0.623	-	-
	D ₂	0.089	-	-	1.824	-	-
	D ₃	0.120	-	-	1.840	-	-

Table 4-5 Responses for Northridge-Sylmar Record (Case 4 through Case 7)

Case No.	Input and Response	Fixed Base			Base Isolated		
		x	y	z	x	y	z
4	PGA _{Target}	0.250	0.125	-	0.250	0.125	-
	PGA _{Real}	0.231	0.109	-	0.264	0.146	-
	A ₂	0.251	0.108	-	0.123	0.116	-
	A ₃	0.428	0.116	-	0.188	0.201	-
	A _{B1}	0.482	0.481	-	0.398	0.448	-
	A _{B2}	0.427	0.284	-	0.272	0.373	-
	A _{B3}	0.966	0.618	-	0.226	0.274	-
	A _{B4}	1.793	1.310	-	0.433	0.631	-
	D ₂	0.061	0.066	-	0.832	0.849	-
	D ₃	0.114	0.130	-	0.886	0.856	-
5	PGA _{Target}	0.375	0.250	-	0.375	0.250	-
	PGA _{Real}	0.370	0.209	-	0.381	0.245	-
	A ₂	0.421	0.217	-	0.364	0.583	-
	A ₃	0.626	0.448	-	0.703	1.059	-
	A _{B1}	0.955	1.116	-	1.477	4.612	-
	A _{B2}	0.612	0.597	-	0.903	2.776	-
	A _{B3}	1.341	1.154	-	0.702	1.259	-
	A _{B4}	2.640	2.583	-	1.451	3.090	-
	D ₂	0.105	0.132	-	2.559	3.117	-
	D ₃	0.189	0.219	-	2.798	3.154	-
6	PGA _{Target}	0.250	0.125	0.125	0.250	0.125	0.125
	PGA _{Real}	0.236	0.116	0.119	0.268	0.153	0.124
	A ₂	0.257	0.128	-	0.137	0.127	-
	A ₃	0.432	0.254	0.154	0.202	0.201	0.173
	A _{B1}	0.521	0.416	0.161	0.408	0.423	0.175
	A _{B2}	0.413	0.267	0.178	0.305	0.344	0.173
	A _{B3}	1.061	0.543	0.188	0.248	0.271	0.163
	A _{B4}	2.010	1.105	0.161	0.453	0.659	0.176
	D ₂	0.057	0.072	-	0.821	0.889	-
	D ₃	0.115	0.131	-	0.875	0.880	-
7	PGA _{Target}	0.375	0.250	0.250	0.375	0.250	0.250
	PGA _{Real}	0.383	0.216	0.236	0.403	0.241	0.232
	A ₂	0.415	0.212	-	0.221	0.233	-
	A ₃	0.618	0.440	0.284	0.477	0.274	0.349
	A _{B1}	1.105	1.018	0.442	1.020	0.754	0.331
	A _{B2}	0.641	0.546	0.368	0.706	0.497	0.336
	A _{B3}	1.273	1.066	0.386	0.532	0.378	0.336
	A _{B4}	2.667	2.340	0.355	1.083	0.798	0.334
	D ₂	0.102	0.147	-	2.380	2.979	-
	D ₃	0.193	0.232	-	3.812	2.582	-

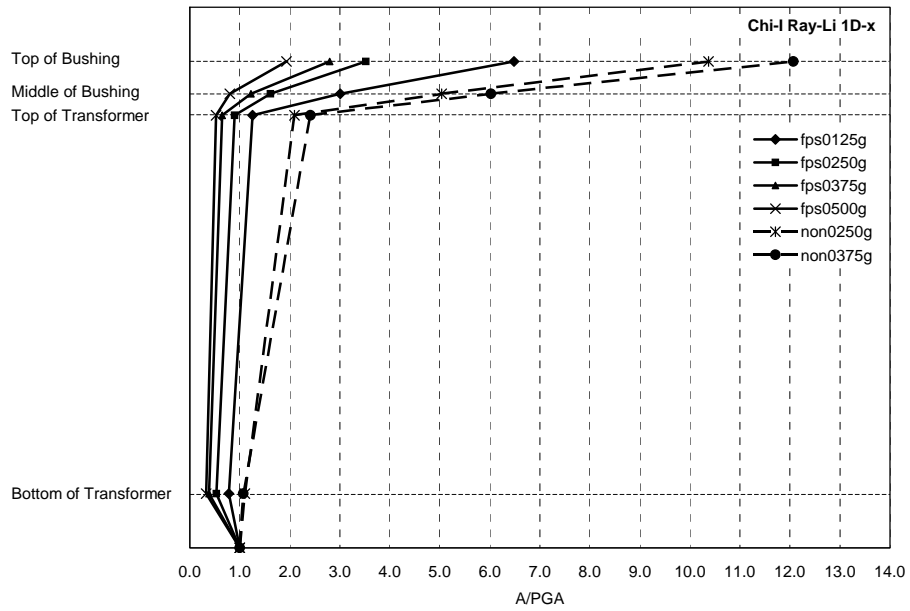


Figure 4-6 Acceleration Maps for Chi-I-Ray-Li Record for 1-D Case

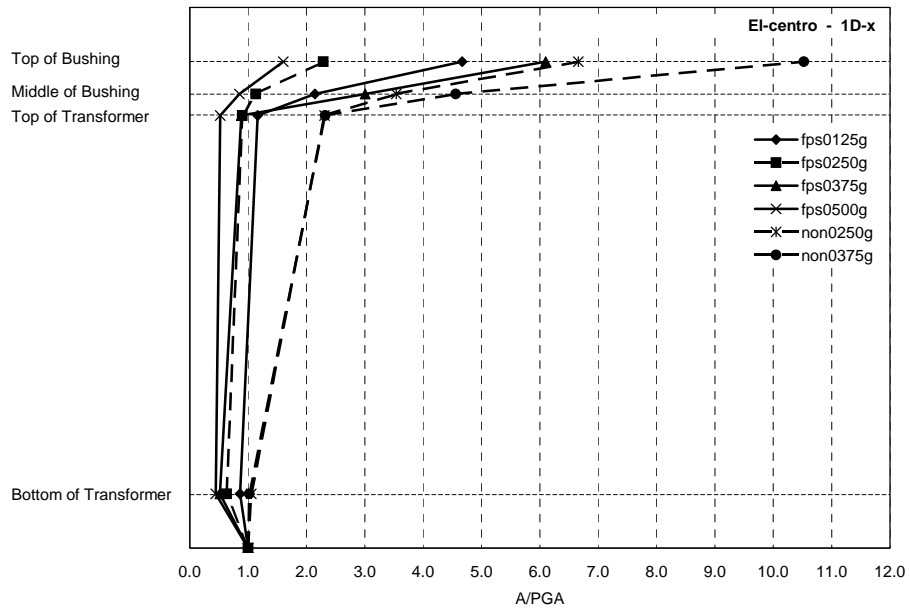


Figure 4-7 Acceleration Maps for El-Centro Record for 1-D Case

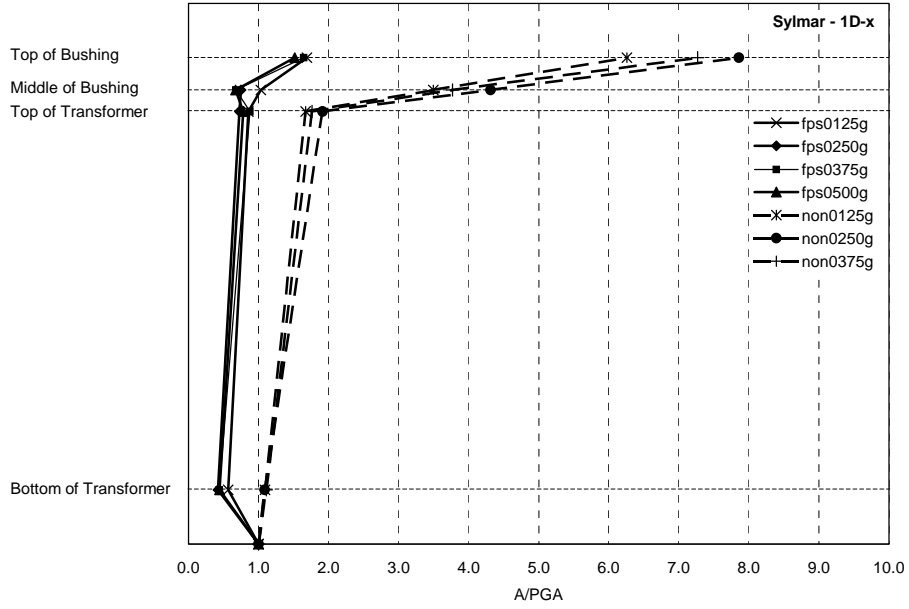


Figure 4-8 Acceleration Maps for Sylmar Record for 1-D Case

Typical response acceleration maps for 2-D cases indicating the effect of the isolation system for x and y directions at different levels of the transformer model are shown in figure 4-9 and figure 4-10 respectively.

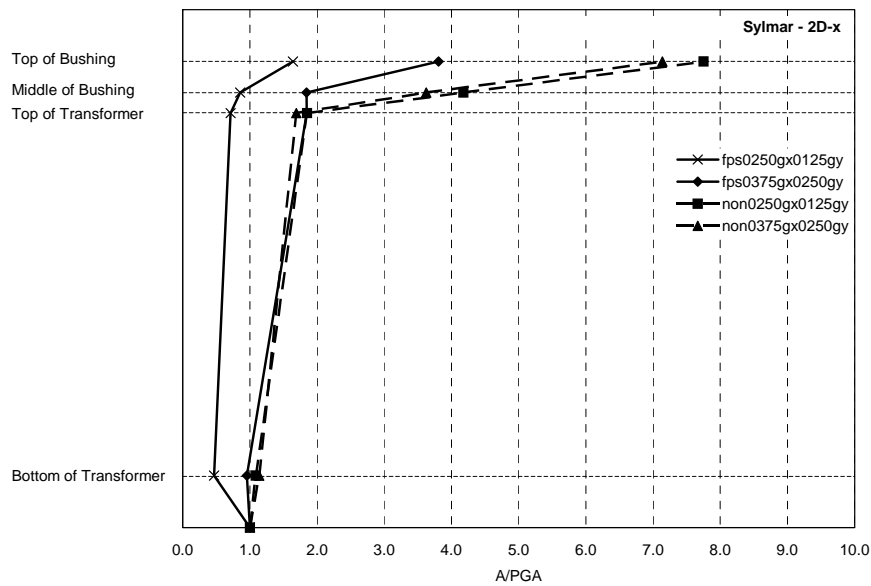


Figure 4-9 Acceleration Maps for Sylmar Record for 2-D Case in X Direction

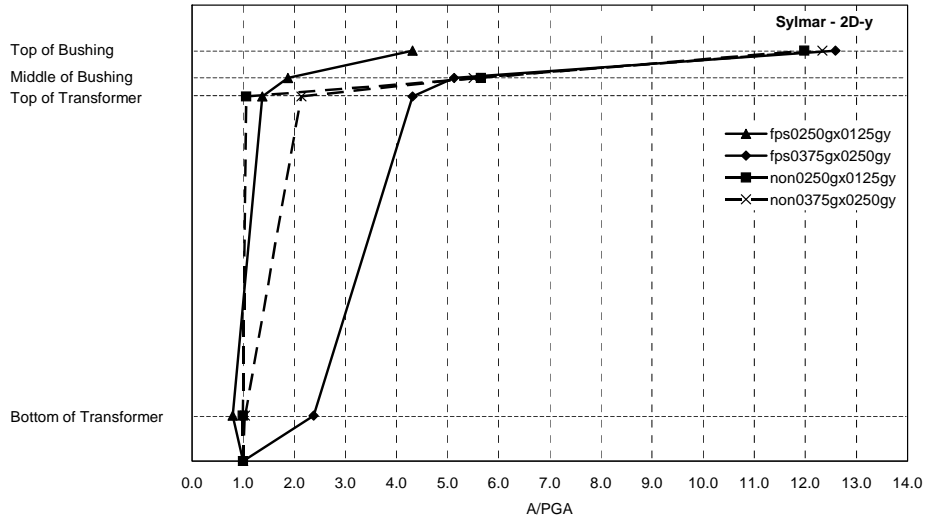


Figure 4-10 Acceleration Maps for Sylmar Record for 2-D Case in Y direction

Response acceleration maps for 3-D results indicating the effect of isolation system for orthogonal horizontal and vertical directions at different levels of the transformer model are shown in figure 4-11 through figure 4-13.

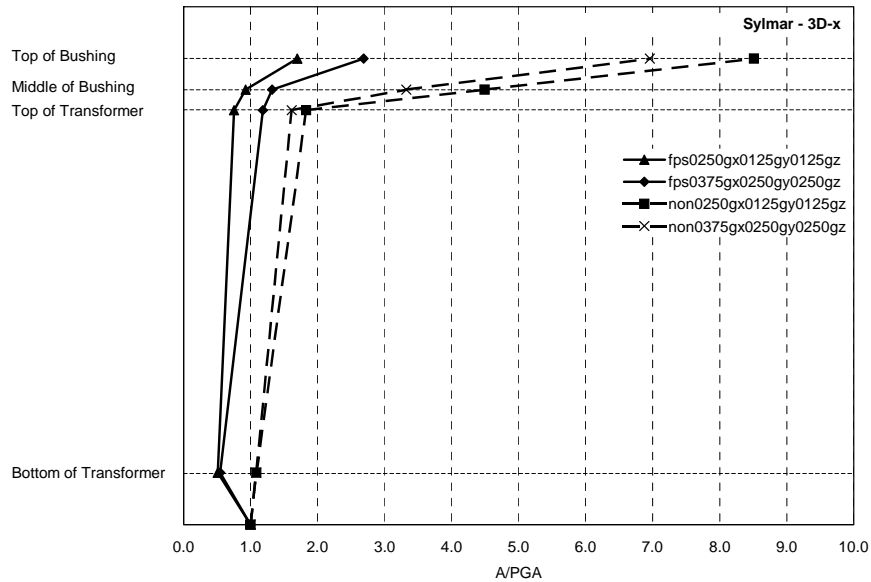


Figure 4-11 Acceleration Maps for Sylmar Record for 3-D Case in X-Direction

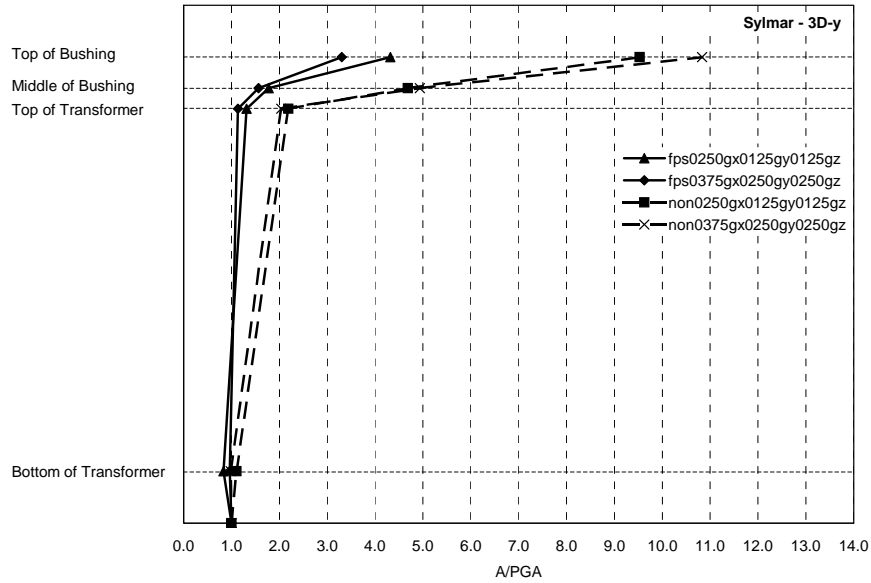


Figure 4-12 Acceleration Maps for Sylmar Record for 3-D Case in Y Direction

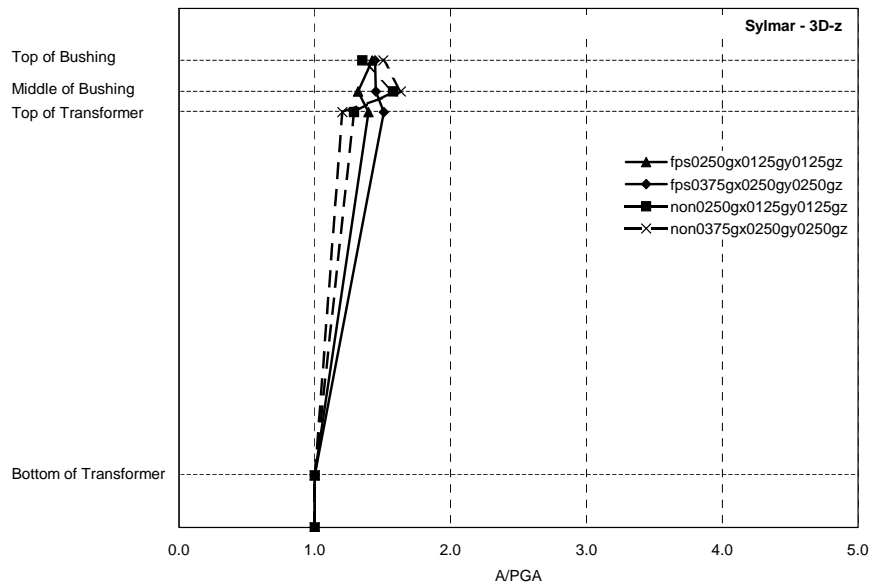


Figure 4-13 Acceleration Maps for Sylmar Record for 3-D Case in Z Direction

The level of acceleration reduction depends on the type of earthquake records used. That is, in addition to acceleration level and nature of the input (1-D vs. 2-D), the ground motion characteristics affect the level of acceleration reductions. Some of the observations from 1-D, 2-D and 3-D tests are discussed in the following paragraphs. Note that for flexible systems, accelerations are different at various levels (as seen in figure 4-6 through 4-13), and the effectiveness of the base-isolation is more apparent when one considers the entire system. For example, there is significantly more reduction in the bushing acceleration than that of the transformer. However, to simplify discussions and to be consistent with the discussions of the

results based on SDOF idealization; in the following sections inertia reduction is used. Inertia reduction here is with respect to the isolation level (base of the transformer). That is, similar to the SDOF discussions, inertia reduction is the percentage difference between $-M_b(\ddot{U}_b + \ddot{U}_g)$ and, $-M_b\ddot{U}_g$ where \ddot{U}_b is the acceleration at the isolation level.

For 1-D experiment in the x-direction and employing the Chi-I Ray-Li record, 47% and 62% inertia reductions were attained with PGA of 0.25g and 0.375g, respectively. However, the El-Centro record produced 37% and 49% inertia reductions at the same location with PGAs of 0.25g and 0.375g, respectively. The Kobe-Takatori record with PGA of 0.25g shows a 7% reduction in system acceleration. For the target acceleration of 0.125g using the Kobe-Takatori record, the system acceleration has increased due to low level of acceleration and response. This could be due to errors in experimental readings. The significant difference in the maximum displacements between the two cases of 0.125g and 0.25g PGA supports the fact that there might be an error in the case with 0.125g acceleration. Thus, similar to the analytical results, it is apparent that PGA has an effect on the level of inertia reductions. Furthermore, records with dominant frequency in the vicinity of the effective period of the isolation system show less inertia reduction. The 2-D and 3-D results are discussed in the following paragraph. Note that in these discussions, including the discussions of 1-D results, the PGA referred to is the target PGA. The actual or real input acceleration may have been different due to difficulty in matching exactly the intended PGA. The inertia reductions are calculated with respect to actual acceleration not the target acceleration.

For a 2-D case with Northridge-Sylmar record and targeted PGA of 0.25g in the x-direction and PGA of 0.125g in the y-direction, the inertia reductions are 54% and 21% in x and y directions, respectively (case 4, 0table 4-5). For the 3-D case using Northridge-Sylmar record with targeted 0.25g PGA in x-direction, 0.125g PGA in y-direction, and 0.125g in the vertical direction the inertia reduction in x-direction is 49% and it is 17% in the y-direction (case 6, table 4-5).

Similar to analytical results in Section 3, the coupling effect is also observed experimentally. That is, there is a difference between the components of the 2-D responses when compared to the 1-D results. For example, consider the 1-D case versus the 2-D case for the Northridge-Sylmar record. For the 1-D case the target PGA is 0.25g in the x-direction (case 2, table 4-4). For the 2-D case the target PGAs in the x-direction and y-direction are 0.25g and 0.125g, respectively (case 4, table 4-5). The acceleration reduction for the 1-D case is 58%, which is to be compared to x-direction of 2-D case. The acceleration reduction in the x-direction for the 2-D case, as discussed before, is 54%. This can be further compared to the 3-D case (case 6, table 4-5). For the 3-D case the target PGAs in x, y and vertical directions are 0.25g, 0.125g, and 0.125g, respectively. In this case the x-direction inertia reduction is equal to 49% and that for y-direction is 17%. Note that for the 2-D case the inertia reduction in the y-direction is equal to 21%. To summarize, in the x-direction the inertia reductions are 58%, 54% and 49% for 1-D, 2-D, and 3-D cases, respectively. In the y-direction they are 21%, and 17% for 2-D and 3-D cases, respectively.

To see the effect of higher PGAs, another three cases with Northridge-Sylmar record are compared. For the 1-D case the target PGA is 0.375g in x-direction (case 3, table 4-4). For the 2-

D case the target PGAs are 0.375g in x-direction, and 0.25g in y-direction (case 5, table 4-5), and for the 3-D case the target PGAs are 0.375g in x-direction, 0.25g in y-direction, and 0.25g in the vertical direction (case 7, table 4-5). The inertia reductions in the x-direction are 56%, 4%, and 45% for 1-D, 2-D and 3-D case, respectively. Inspection of the displacement results indicates that for the 2-D case the displacement capacity of the bearing has been reached, thus, resulting in higher system acceleration (lower inertia reduction) due to impact. The displacement capacity of the bearing is about 4 inches. As it can be seen from the above discussion, the vertical motion also has an effect on the response of FPS isolated structure. Note that due to the low displacement capacity of the bearings, it was not possible to conduct further tests with higher PGAs. Some previous studies show that the response acceleration of the bushing in the base isolated system sometimes larger than that of the fixed base system [Murota, 2001]. This is believed to be due to the fact that the higher vertical accelerations change the pressure. This causes change in coefficient of friction, eventually in friction force, and high frequency vibration of bushing occurs. More tests are required to draw more general conclusions.

Some of the experimental cases are simulated by the computer code developed in Section 3. The results are in good agreement with the experimental cases. Simulated cases are tabulated in table 4-6. Displacement and inertia reduction responses for the cases shown in figure 4-14 are obtained through analytical study.

Table 4-6 Simulated Experimental Cases

Case No.	PGA in x-direction	PGA in y-direction	PGA in z-direction
I	0.1376	-	-
II	0.2817	-	-
III	0.3793	-	-
IV	0.5164	-	-
V	0.2637	0.1462	-
VI	0.2676	0.1526	0.1526
VII	0.4031	0.2414	0.2316

Comparison of inertia reduction responses is shown in figure 4-14. Displacement responses also follow the same pattern.

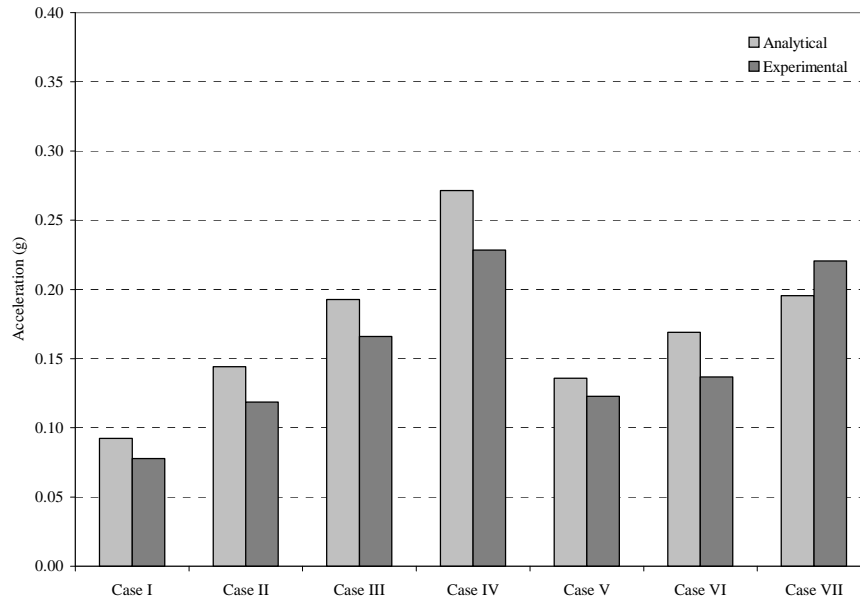


Figure 4-14 Comparison of Displacement Responses for Analytical and Experimental Studies

4.6 Force/Displacement Response of Transformer Model

The force/displacement responses of the transformer model are shown in the following figures. Figure 4-15 pertains to 1-D case for the Northridge-Sylmar record. It is seen that since the displacement limits are not reached for these two cases, the shape of hysteresis loop is very close to a typical hysteresis loop (See figure 3-34). In figure 4-16, the force/displacement response of a 2-D case is shown. As can be seen from the figure, the displacement capacity of the bearing is reached since there is an abrupt increase in the force. Recalling that the radius of curvature of the bearings used for the tests was very small (i.e., $R=18.64''$), simultaneous application of orthogonal horizontal accelerations with a PGA of 0.375g and 0.25g caused displacements as large as the displacement limit and impact occurred. However, figure 4-16 shows no impact although the same accelerations applied in horizontal orthogonal directions. Vertical ground motion reduces the displacements, which is consistent with the parametric study discussed earlier in that vertical motion can increase or reduce displacement responses.

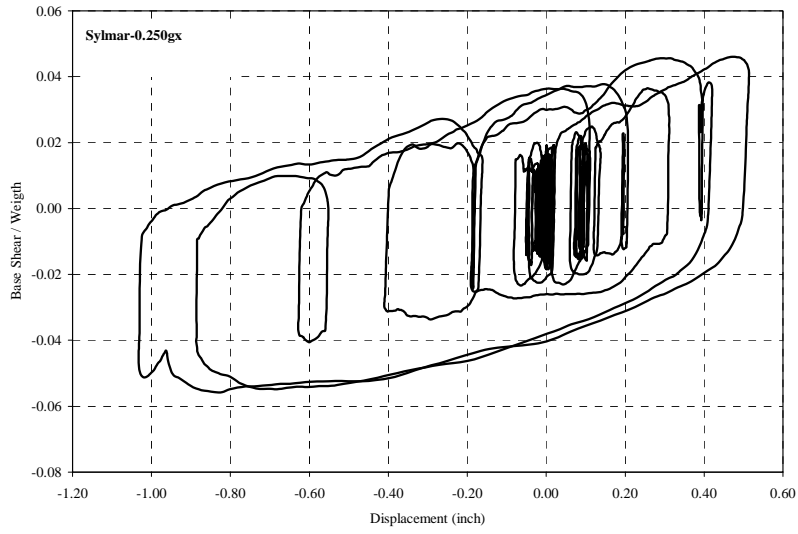


Figure 4-15 Hysteresis Loop of Northridge-Sylmar Record for PGA of 0.25g in X-Direction

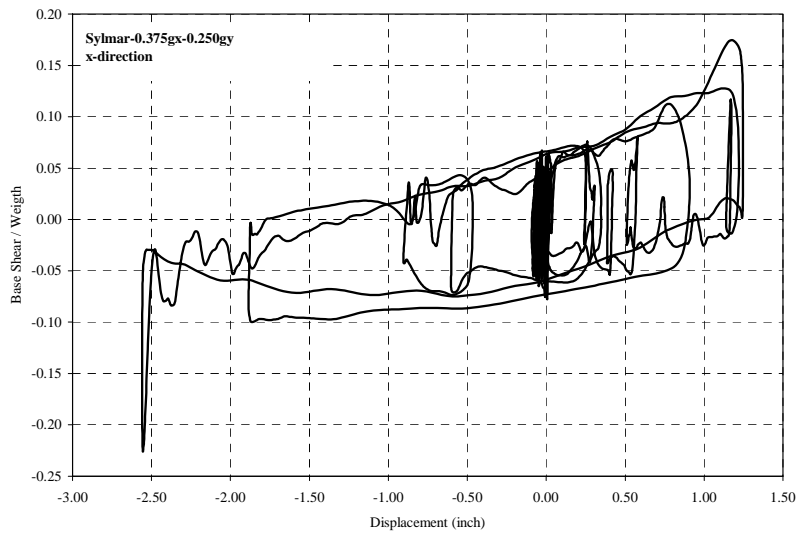


Figure 4-16 Hysteresis Loop of Northridge-Sylmar Record for PGA of 0.375g in X-Direction and 0.25g in Y-Direction

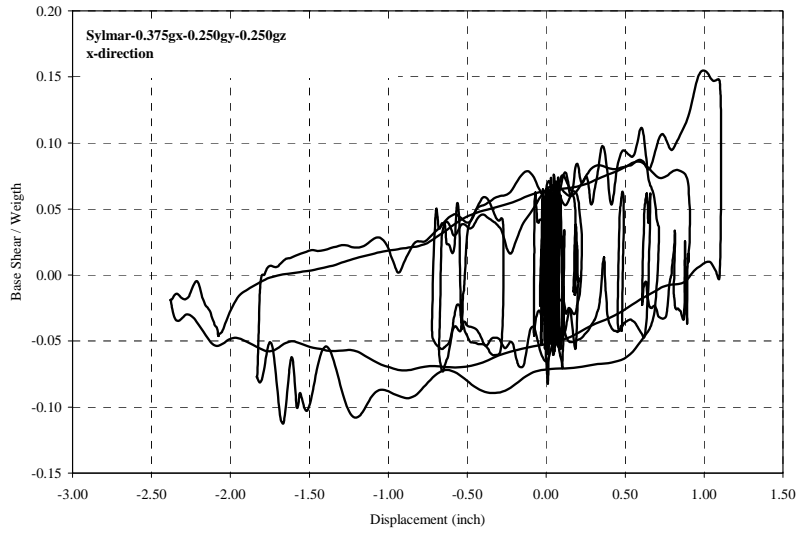


Figure 4-17 Hysteresis Loop of Northridge-Sylmar Record for PGA of 0.375g in X-Direction, 0.25g in Y-direction and 0.25g in Z-Direction

SECTION 5 SIMPLIFIED MODEL APPROACH

In Section 2 finite element study was performed to understand response of transformer bushing system. Then, base isolation (FPS) is identified as a practical technology for their seismic rehabilitation in Section 3. Section 4 presents the results of shake table experiments on transformer model and its bushing, with and without the base isolation. Both Section 3 and Section 4 support the effectiveness of FPS. However, an issue with the use of base isolation is the effect of possibly large displacements on the response of inter-connecting equipments, especially bushings. Therefore, a successful application of base isolation requires in-depth understanding of interaction of interconnecting system with transformer-bushing system.

In this chapter, the interaction of the substation equipment is discussed through a parameter study of a simplified model. Based on finite element analyses conducted in Section 2, bushing response is significantly affected by transformer dynamic response. Based on damage reports from previous earthquake, bushing failure is one of the most common failure types. Bushing damage is mostly caused by either failure of the gasket near the transformer top or interaction with other equipment components through cable conductors. A simple model is developed to investigate the effect of larger displacement for isolated case. A symbolic view of the modeled partial substation is shown in figure 5-1. The transformer bushing system is usually connected to lighter and less stiff substation equipment by means of a flexible conductor or a rigid conductor.

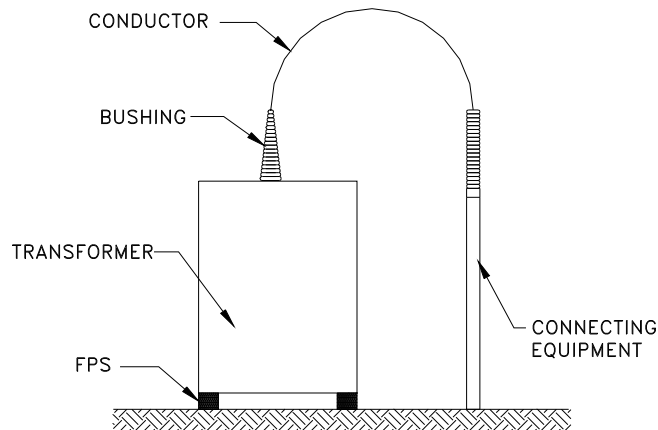


Figure 5-1 Typical Partial Substation

The proposed simplified model is shown in figure 5-2. In this model, FPS is simulated using a nonlinear spring with kinematic bilinear material properties [Zayas, 1989]. This is also known as the simple bilinear model. There are two stiffness values considered in the model: the elastic and yielding stiffness, with unloading and load reversal stages the same as the elastic stage. Material properties are given based on the FPS model phenomena that are explained in Section 3 of this report. Transformer and bushing flexibility is introduced by a linear spring. The stiffness of the spring is determined based on the finite element analysis for the transformer mounted bushing model. The frequency of the transformer is taken as 14 Hz in the parametric study, and that of

bushing is taken as 10 Hz. Typical interconnected substation electrical equipment components can be circuit switchers, insulator post of switches, bus supports and circuit breakers. Frequency values for these components are chosen as 1 Hz and 3 Hz for this study. The connection between transformer bushing systems and electrical equipment is simulated through a nonlinear link element having stiffness in tension only. Lumped mass elements are used for transformer and bushing.

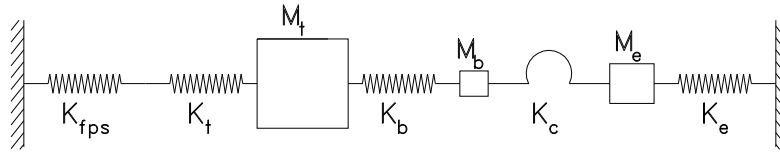


Figure 5-2 Simplified Model for Partial Substation

Rayleigh damping is introduced to the system, similar to 3-D finite element cases, except that the damping values are slightly different from 3-D analysis. As noticed from figure 5-3, the damping value is set to 2% for the frequencies of 2 Hz and 14 Hz. This frequency range gives a better approximation for 2% damping of the system. Two earthquake records are employed in this simple analysis. These two records (elcentro-s90w, taft-s69e) are selected as representative of soil and rock records based on the records used in FPS study, in which 10 soil and 10 rock records are used. The FPS results of these two records are closer to the average values of the rock and soil records. Two different stiffness values for the slack cable are chosen.

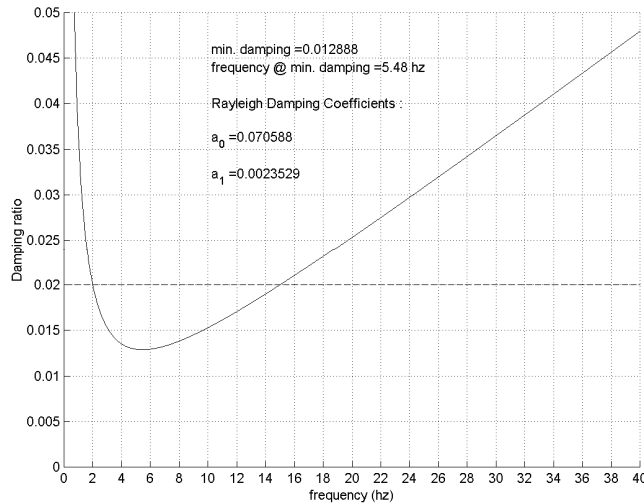


Figure 5-3 Rayleigh's Damping for Simple System

First, analysis is done on the 2-DOF system consisting of transformer mass, transformer stiffness, bushing mass, and bushing stiffness. Force in the bushing is an important parameter in bushing failure criteria so that bushing force in this simple model is matched to the force at the gasket level of bushing near the top of transformer in the FEA model. The force causing bushing failure at the gasket level (close to the transformer top) is about 2 kips.

In the first part of the parameter study, large slack is provided, i.e., no impact case. For all additional parameter studies, the slack configuration is based on the half circle assumption. For example, if straight line distance between the bushing and the connecting equipment item is x , then the total length of the slack cable is $\pi x/2$. And the amount of slack becomes $(\pi-2)x/2$. A simple model with base isolation and without impact is analyzed for two ground motions (one soil, and one rock record), two peak ground acceleration (0.5g, and 1.0g), and two radii of curvature (60", 120") of bearing. These results give the displacement response for the system in the case of no impact and they can be used with the FPS isolated system to eliminate the interaction of the transformer bushing system and the connecting equipment. Results from the base isolation section (Section 3) for SDOF systems (bushing has not been considered in that system), correlate well with this case.

In the second case, the effect of the interaction on the bushing and FPS is explored. From the first part of the parametric study the distances between the equipment are already obtained to prevent the interaction based on the half circle slack assumption. Two slack conditions are studied to assure the interaction; namely, no slack (cable is taut) and a slack equal to half of the maximum displacement of FPS. This part of the parameter study is done for two ground motions, two PGAs, three cases of support conditions (fixed case, and two radii of curvature of FPS bearing), two-cable stiffness, two slack conditions as explained before, and two connecting equipment frequencies. Also some sensitivity studies have been performed to elaborate on the effect of the stiffness of connecting equipment.

5.1 Simplified Model Analysis Results

The interaction between transformer bushing system and connecting equipment, depend on many parameters, like frequency of the transformer and the bushing, stiffness of the cable, the cable slack, stiffness of the connecting equipment, and base isolation parameters. This study is an attempt to incorporate all these variables into a viable, analytical model of the transformer and its attached components. When the amount of slack of the cable is greater than the total absolute displacement of the connected equipment, no interaction occurs. In case of insufficient slack, the interaction effect comes to bear and problem becomes nonlinear. The effect of interaction on the response of base isolation and bushing are the main concerns of this study.

The bushing spring force, transformer spring force, and effect of slack cable on the bushing and the isolation are monitored. The bushing spring force represents the shear at the base of the bushing near to the bushing flange. The transformer spring force shows the force at the base of a rigidly anchored transformer, while in the base isolated case, it shows the force at the isolation level. Displacement and inertia reduction responses for 3-DOF systems (FPS, transformer, and bushing) for different PGAs and two different earthquake records (El-Centro S90W, and Taft S69E) are obtained. The maximum responses for FPS are shown in table 5-1 and table 5-2.

Table 5-1 FPS Response for El-Centro S90W Record

Radius of Curvature of FPS (inch)	Bearing Displacement (inch)		Inertia Reduction (%)	
	PGA = 0.5g	PGA = 1.0g	PGA = 0.5g	PGA = 1.0g
60	7.30	26.68	56.2	43.9
120	9.28	40.59	67.0	56.4

Table 5-2 FPS Response for Taft S69E Record

Radius of Curvature of FPS (inch)	Bearing Displacement (inch)		Inertia Reduction (%)	
	PGA = 0.5g	PGA = 1.0g	PGA = 0.5g	PGA = 1.0g
60	3.70	9.25	67.4	74.7
120	3.29	12.06	74.3	80.5

The parameter study results are given in table 5-3, table 5-4, and table 5-5. Case 1 through case 8, case 25 through case 32, case 49 through case 56, and case 73 through case 80 are for the fixed support cases. For these cases two different slack types are employed, namely no slack (taut condition), and very large slack. When the cable is taut, there is interaction between the transformer bushing system and the interconnecting equipment. When very large slack is provided, there is no interaction between the systems (each system's response is independent from each other). In all the other cases FPS bearings are implemented as supports (with radii of curvature of 60 inch, and 120 inch). For FPS supported cases, two different slack conditions are provided: no slack (taut condition, slack type 1), and slack in the amount of half of the FPS displacement (slack type 2) shown in table 5-1 and table 5-2.

Table 5-3 Simple Model Case 1 through Case 32

Case No	Record Name	PGA	Bearing Type	Cable Area (inch ²)	Slack Type	fc (hz)
1	Elcentro-S90W	0.5g	Fixed	1	1	1
2	Elcentro-S90W	0.5g	Fixed	1	1	3
3	Elcentro-S90W	0.5g	Fixed	1	large	1
4	Elcentro-S90W	0.5g	Fixed	1	large	3
5	Elcentro-S90W	0.5g	Fixed	10	1	1
6	Elcentro-S90W	0.5g	Fixed	10	1	3
7	Elcentro-S90W	0.5g	Fixed	10	large	1
8	Elcentro-S90W	0.5g	Fixed	10	large	3
9	Elcentro-S90W	0.5g	FPS (R=60")	1	1	1
10	Elcentro-S90W	0.5g	FPS (R=60")	1	1	3
11	Elcentro-S90W	0.5g	FPS (R=60")	1	2	1
12	Elcentro-S90W	0.5g	FPS (R=60")	1	2	3
13	Elcentro-S90W	0.5g	FPS (R=60")	10	1	1
14	Elcentro-S90W	0.5g	FPS (R=60")	10	1	3
15	Elcentro-S90W	0.5g	FPS (R=60")	10	2	1
16	Elcentro-S90W	0.5g	FPS (R=60")	10	2	3
17	Elcentro-S90W	0.5g	FPS (R=120")	1	1	1
18	Elcentro-S90W	0.5g	FPS (R=120")	1	1	3
19	Elcentro-S90W	0.5g	FPS (R=120")	1	2	1
20	Elcentro-S90W	0.5g	FPS (R=120")	1	2	3
21	Elcentro-S90W	0.5g	FPS (R=120")	10	1	1
22	Elcentro-S90W	0.5g	FPS (R=120")	10	1	3
23	Elcentro-S90W	0.5g	FPS (R=120")	10	2	1
24	Elcentro-S90W	0.5g	FPS (R=120")	10	2	3
25	Elcentro-S90W	1.0g	Fixed	1	1	1
26	Elcentro-S90W	1.0g	Fixed	1	1	3
27	Elcentro-S90W	1.0g	Fixed	1	large	1
28	Elcentro-S90W	1.0g	Fixed	1	large	3
29	Elcentro-S90W	1.0g	Fixed	10	1	1
30	Elcentro-S90W	1.0g	Fixed	10	1	3
31	Elcentro-S90W	1.0g	Fixed	10	large	1
32	Elcentro-S90W	1.0g	Fixed	10	large	3

Table 5-4 Simple Model Case 33 through Case 64

Case No	Record Name	PGA	Bearing Type	Cable Area (inch ²)	Slack Type	fc (hz)
33	Elcentro-S90W	1.0g	FPS (R=60")	1	1	1
34	Elcentro-S90W	1.0g	FPS (R=60")	1	1	3
35	Elcentro-S90W	1.0g	FPS (R=60")	1	2	1
36	Elcentro-S90W	1.0g	FPS (R=60")	1	2	3
37	Elcentro-S90W	1.0g	FPS (R=60")	10	1	1
38	Elcentro-S90W	1.0g	FPS (R=60")	10	1	3
39	Elcentro-S90W	1.0g	FPS (R=60")	10	2	1
40	Elcentro-S90W	1.0g	FPS (R=60")	10	2	3
41	Elcentro-S90W	1.0g	FPS (R=120")	1	1	1
42	Elcentro-S90W	1.0g	FPS (R=120")	1	1	3
43	Elcentro-S90W	1.0g	FPS (R=120")	1	2	1
44	Elcentro-S90W	1.0g	FPS (R=120")	1	2	3
45	Elcentro-S90W	1.0g	FPS (R=120")	10	1	1
46	Elcentro-S90W	1.0g	FPS (R=120")	10	1	3
47	Elcentro-S90W	1.0g	FPS (R=120")	10	2	1
48	Elcentro-S90W	1.0g	FPS (R=120")	10	2	3
49	Taft-N69E	0.5g	Fixed	1	1	1
50	Taft-N69E	0.5g	Fixed	1	1	3
51	Taft-N69E	0.5g	Fixed	1	large	1
52	Taft-N69E	0.5g	Fixed	1	large	3
53	Taft-N69E	0.5g	Fixed	10	1	1
54	Taft-N69E	0.5g	Fixed	10	1	3
55	Taft-N69E	0.5g	Fixed	10	large	1
56	Taft-N69E	0.5g	Fixed	10	large	3
57	Taft-N69E	0.5g	FPS (R=60")	1	1	1
58	Taft-N69E	0.5g	FPS (R=60")	1	1	3
59	Taft-N69E	0.5g	FPS (R=60")	1	2	1
60	Taft-N69E	0.5g	FPS (R=60")	1	2	3
61	Taft-N69E	0.5g	FPS (R=60")	10	1	1
62	Taft-N69E	0.5g	FPS (R=60")	10	1	3
63	Taft-N69E	0.5g	FPS (R=60")	10	2	1
64	Taft-N69E	0.5g	FPS (R=60")	10	2	3

Table 5-5 Simple Model Case 65 through Case 96

Case No	Record Name	PGA	Bearing Type	Cable Area (inch ²)	Slack Type	fc (hz)
65	Taft-N69E	0.5g	FPS (R=120")	1	1	1
66	Taft-N69E	0.5g	FPS (R=120")	1	1	3
67	Taft-N69E	0.5g	FPS (R=120")	1	2	1
68	Taft-N69E	0.5g	FPS (R=120")	1	2	3
69	Taft-N69E	0.5g	FPS (R=120")	10	1	1
70	Taft-N69E	0.5g	FPS (R=120")	10	1	3
71	Taft-N69E	0.5g	FPS (R=120")	10	2	1
72	Taft-N69E	0.5g	FPS (R=120")	10	2	3
73	Taft-N69E	1.0g	Fixed	1	1	1
74	Taft-N69E	1.0g	Fixed	1	1	3
75	Taft-N69E	1.0g	Fixed	1	large	1
76	Taft-N69E	1.0g	Fixed	1	large	3
77	Taft-N69E	1.0g	Fixed	10	1	1
78	Taft-N69E	1.0g	Fixed	10	1	3
79	Taft-N69E	1.0g	Fixed	10	large	1
80	Taft-N69E	1.0g	Fixed	10	large	3
81	Taft-N69E	1.0g	FPS (R=60")	1	1	1
82	Taft-N69E	1.0g	FPS (R=60")	1	1	3
83	Taft-N69E	1.0g	FPS (R=60")	1	2	1
84	Taft-N69E	1.0g	FPS (R=60")	1	2	3
85	Taft-N69E	1.0g	FPS (R=60")	10	1	1
86	Taft-N69E	1.0g	FPS (R=60")	10	1	3
87	Taft-N69E	1.0g	FPS (R=60")	10	2	1
88	Taft-N69E	1.0g	FPS (R=60")	10	2	3
89	Taft-N69E	1.0g	FPS (R=120")	1	1	1
90	Taft-N69E	1.0g	FPS (R=120")	1	1	3
91	Taft-N69E	1.0g	FPS (R=120")	1	2	1
92	Taft-N69E	1.0g	FPS (R=120")	1	2	3
93	Taft-N69E	1.0g	FPS (R=120")	10	1	1
94	Taft-N69E	1.0g	FPS (R=120")	10	1	3
95	Taft-N69E	1.0g	FPS (R=120")	10	2	1
96	Taft-N69E	1.0g	FPS (R=120")	10	2	3

The most important observation for the simplified model approach is that the bushing forces are always larger than the capacity of the bushings for both records of PGA of 0.5g and 1.0g when there is impact. As expected, the impact forces in the bushing for PGA of 0.5g cases are lower than the ones for PGA of 1.0g. Case 1 is one of the fixed cases with no slack condition (other parameters for this case are shown in table 5-3). Figure 5-4 and figure 5-5 show the displacement and forces for this case. As seen from figure 5-4, the displacement value of the support is zero and the force in the bushing is 20 kips (0figure 5-5) which causes the bushing to fail. When the large slack is provided for the fixed base cases (case 3, case 4, case 7, case 8, case 27, case 28, case 31, case 32, case 51, case 52, case 55, case 56, case 75, case 76, case 79, case 80), the bushing forces are smaller and are safe. However, as was noted before, bushings could fail because of the interaction of transformer with bushing (amplification of ground motion due to transformer body). This depends on the characteristics of the ground motion used for the analysis.

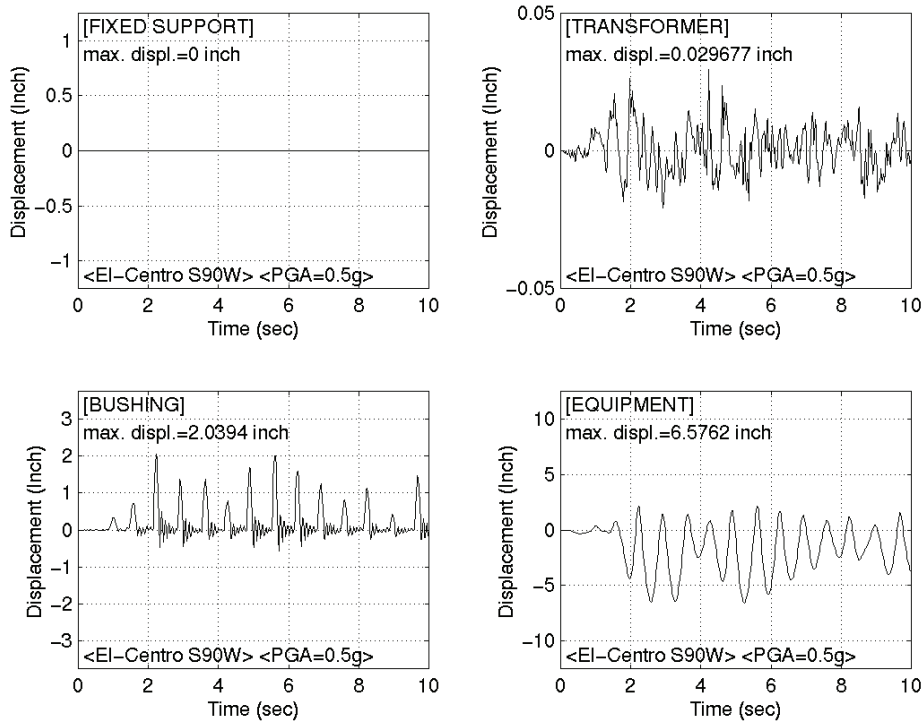


Figure 5-4 Displacement Responses of Case 1

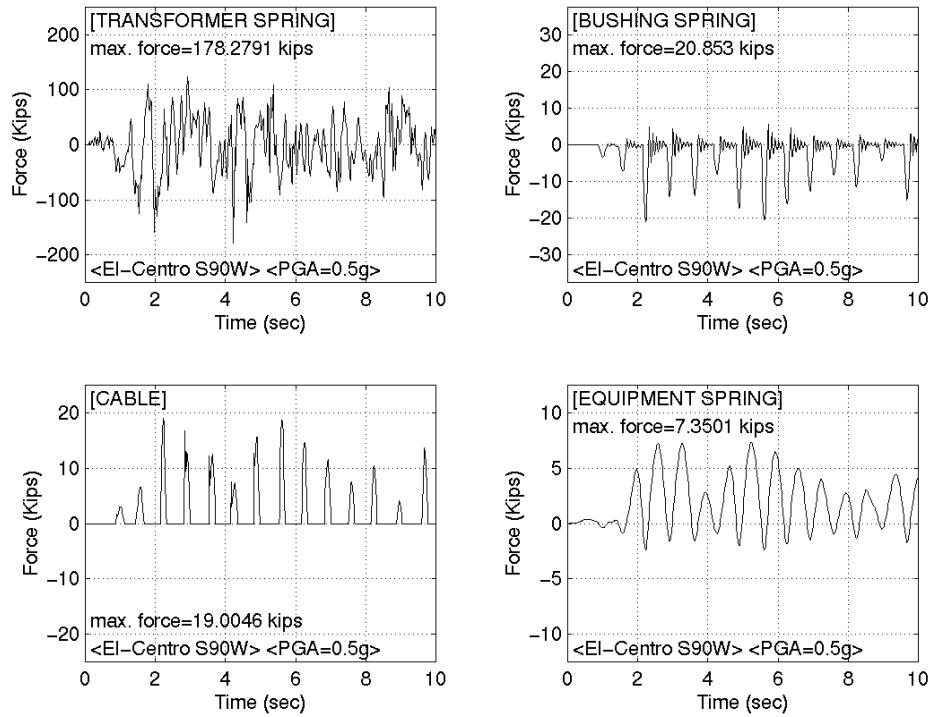


Figure 5-5 Force Responses for Case 1

The impact force of the bushing is larger for the base isolated cases of no slack than the fixed cases with no slack. Case 12 is one of the sample cases with FPS isolated support, shown in this section. Figure 5-6 and figure 5-7 show the displacement and forces for this case. If there is no interaction the transformer bushing system displaces the same amount as the FPS support however when the interaction happens (cable is taut), impact occurs in the bushing. As noted from 0 5-7, the bushing force becomes about 15 kips and causes failure of the bushing (force causing failure in the bushing is 2 kips). Similar charts have been developed for all other cases, however for the sake of space they are not provided as figures. Instead, the maximum responses of the other cases are tabulated in table 5-6 through table 5-8.

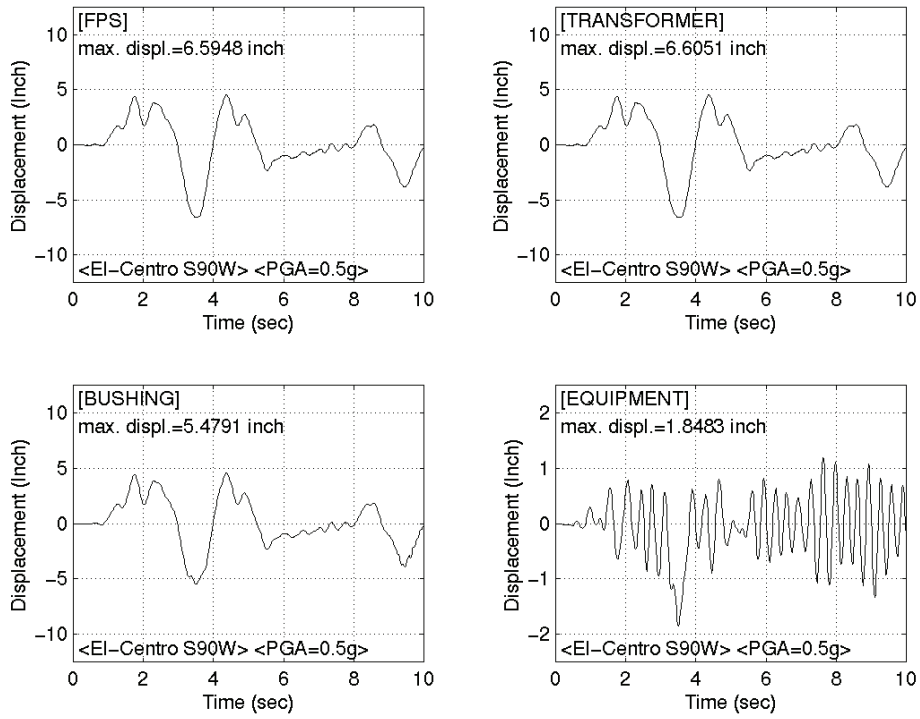


Figure 5-6 Displacement Responses of Case 12

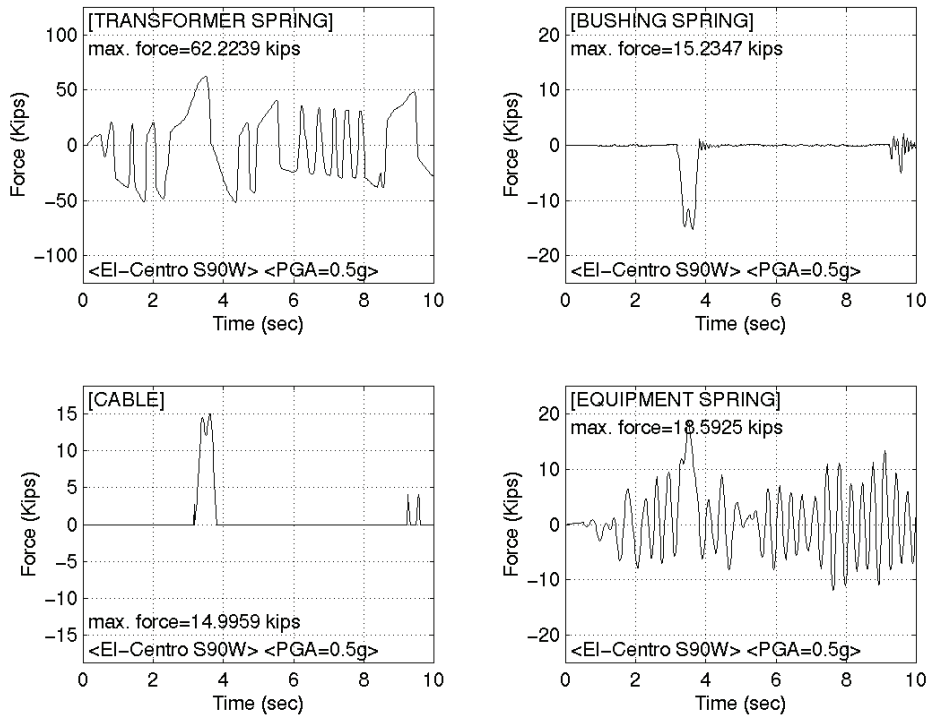


Figure 5-7 Force Responses of Case 12

The effect of interaction on the response of base isolation is one of the main concerns of this study. It is observed that the interaction does not have significant effect on base isolation response. Inertia reductions are affected by $\pm 15\%$ compared to the first part of the parameter study (large slack is provided, no impact cases). The effect of the cable stiffness on the response for a practical range of cable area is compared (case 1 vs. case 5, case 2 vs. case 6, case 9 vs. case 13, case 10 vs. case 14, case 11 vs. case 15, case 12 vs. case 16, etc.). It is seen that effect of the cable stiffness on the bushing response force is insignificant for the practical range of cable stiffness used in this parameter study.

Table 5-6 Simplified Analysis Responses for Case 1 through Case 32

Case No	Displacements				Spring Forces			
	Support	Transformer	Bushing	Connecting Equipment	Transformer	Bushing	Cable	Connecting Equipment
1	0.00	0.03	2.04	6.58	178.28	20.85	19.00	7.35
2	0.00	0.03	0.73	0.94	172.39	7.26	6.05	9.45
3	0.00	0.03	0.12	5.28	171.37	1.14	0.00	5.90
4	0.00	0.03	0.12	1.48	171.37	1.14	0.00	14.87
5	0.00	0.03	2.05	6.47	177.50	20.96	29.59	7.23
6	0.00	0.03	0.75	0.93	172.52	7.44	6.19	9.40
7	0.00	0.03	0.12	5.28	171.37	1.14	0.00	5.90
8	0.00	0.03	0.12	1.48	171.37	1.14	0.00	14.87
9	6.47	6.48	6.63	8.26	61.58	19.15	17.94	9.24
10	5.13	5.14	4.43	3.23	54.92	30.18	29.32	32.47
11	6.72	6.73	6.93	7.37	62.81	17.99	17.57	8.23
12	6.59	6.61	5.48	1.85	62.22	15.23	15.00	18.59
13	6.47	6.48	6.63	8.25	61.58	19.31	42.31	9.22
14	5.11	5.12	4.43	3.26	54.79	30.75	29.85	32.77
15	6.71	6.72	6.95	7.35	62.79	18.27	45.72	8.22
16	6.59	6.60	5.45	1.87	62.18	15.47	15.22	18.78
17	8.21	8.22	8.21	9.25	50.15	23.19	21.82	10.34
18	6.14	6.15	5.55	3.66	44.97	34.89	34.15	36.83
19	8.53	8.54	8.74	8.43	50.93	23.20	21.37	9.42
20	8.30	8.31	6.31	2.36	50.38	25.77	25.15	23.72
21	8.21	8.22	8.20	9.23	50.14	23.29	21.87	10.32
22	6.09	6.10	5.55	3.69	44.82	35.42	34.66	37.08
23	8.53	8.54	8.74	8.41	50.92	23.48	21.56	9.40
24	8.29	8.30	6.28	2.38	50.34	26.20	25.55	23.95
25	0.00	0.06	4.08	13.15	356.56	41.71	38.01	14.70
26	0.00	0.06	1.47	1.88	344.78	14.53	12.10	18.90
27	0.00	0.06	0.25	10.56	342.74	2.28	0.00	11.81
28	0.00	0.06	0.25	2.96	342.74	2.28	0.00	29.73
29	0.00	0.06	4.10	12.94	354.99	41.92	59.18	14.47
30	0.00	0.06	1.50	1.87	345.03	14.89	12.38	18.80
31	0.00	0.06	0.25	10.56	342.74	2.28	0.00	11.81
32	0.00	0.06	0.25	2.96	342.74	2.28	0.00	29.73

Table 5-7 Simplified Analysis Responses for Case 33 through Case 64

Case No	Displacements				Spring Forces			
	Support	Transformer	Bushing	Connecting Equipment	Transformer	Bushing	Cable	Connecting Equipment
33	23.90	23.92	22.53	23.40	148.75	48.81	46.61	26.16
34	26.17	26.19	26.19	9.80	160.10	91.82	90.50	98.61
35	25.08	25.10	25.52	19.44	154.63	44.26	40.85	21.72
36	24.16	24.19	24.24	5.46	150.05	49.18	49.36	54.88
37	23.89	23.91	22.80	23.35	148.69	49.31	46.96	26.10
38	26.18	26.21	26.21	9.90	160.17	93.03	91.58	99.62
39	25.07	25.10	25.54	19.41	154.60	44.69	116.89	21.69
40	24.20	24.23	24.28	5.51	150.20	49.76	49.98	55.48
41	35.47	35.49	35.50	35.52	118.30	71.03	67.77	89.70
42	34.16	34.18	34.21	13.53	115.02	137.12	135.29	136.06
43	38.36	38.38	38.61	24.67	125.52	62.82	58.67	27.57
44	36.70	36.72	29.56	9.14	121.38	95.84	93.53	81.94
45	35.43	35.45	35.60	35.66	118.19	70.87	67.50	89.86
46	34.24	34.26	34.29	13.65	115.22	139.09	137.11	137.36
47	38.35	38.38	38.60	24.64	125.51	63.65	59.32	27.54
48	36.66	36.68	29.45	9.24	121.26	96.89	94.54	82.95
49	0.00	0.03	1.44	5.23	156.15	14.70	13.38	5.85
50	0.00	0.03	0.79	1.15	156.14	8.01	8.66	11.55
51	0.00	0.03	0.09	5.45	156.61	0.70	0.00	6.10
52	0.00	0.03	0.09	2.38	156.61	0.70	0.00	23.90
53	0.00	0.03	1.48	5.30	156.00	15.02	19.21	5.93
54	0.00	0.03	0.80	1.15	156.16	8.07	27.04	11.52
55	0.00	0.03	0.09	5.45	156.61	0.70	0.00	6.10
56	0.00	0.03	0.09	2.38	156.61	0.70	0.00	23.90
57	4.36	4.37	4.42	4.88	51.07	13.77	12.67	5.45
58	4.39	4.40	4.45	1.54	51.12	15.39	14.01	15.53
59	4.03	4.04	4.09	5.51	49.41	14.35	13.04	6.16
60	3.80	3.81	3.82	2.04	48.24	7.69	6.87	20.51
61	4.36	4.37	4.35	4.88	51.04	13.95	12.80	5.45
62	4.40	4.40	4.45	1.55	51.16	15.74	14.28	15.57
63	4.01	4.02	4.06	5.48	49.32	14.60	13.20	6.12
64	3.80	3.81	3.82	2.03	48.25	7.93	7.05	20.46

Table 5-8 Simplified Analysis Responses for Case 65 through Case 96

Case No	Displacements				Spring Forces			
	Support	Transformer	Bushing	Connecting Equipment	Transformer	Bushing	Cable	Connecting Equipment
65	4.24	4.24	4.28	4.94	40.20	15.10	13.88	5.53
66	4.49	4.50	4.51	1.22	40.85	12.50	11.76	12.31
67	3.94	3.94	3.98	5.67	39.46	14.57	13.21	6.34
68	3.61	3.62	3.65	1.79	38.64	8.76	8.02	18.04
69	4.24	4.25	4.30	4.97	40.21	15.29	14.01	5.96
70	4.51	4.52	4.53	1.23	40.91	12.82	17.87	12.40
71	3.92	3.92	3.95	5.65	39.41	14.83	13.39	6.32
72	3.62	3.62	3.65	1.79	38.65	8.97	11.26	18.00
73	0.00	0.05	2.88	10.46	312.30	29.41	26.77	11.69
74	0.00	0.05	1.58	2.30	312.27	16.02	17.33	23.11
75	0.00	0.05	0.18	10.91	313.23	1.39	0.00	12.19
76	0.00	0.05	0.18	4.75	313.23	1.39	0.00	47.79
77	0.00	0.05	2.96	10.61	312.00	30.03	38.42	11.86
78	0.00	0.05	1.59	2.29	312.31	16.14	54.08	23.04
79	0.00	0.05	0.18	10.91	313.23	1.39	0.00	12.19
80	0.00	0.05	0.18	4.75	313.23	1.39	0.00	47.79
81	9.74	9.75	9.85	12.41	77.94	33.27	30.93	13.87
82	11.13	11.15	11.21	4.60	84.92	46.68	45.46	46.32
83	9.54	9.56	9.73	13.52	76.96	36.72	33.49	15.11
84	9.25	9.26	9.29	3.28	75.49	26.13	24.30	32.97
85	9.80	9.82	9.92	12.44	78.27	33.92	55.27	13.90
86	11.20	11.21	11.27	4.67	85.24	47.81	46.53	46.97
87	9.52	9.54	9.71	13.37	76.87	36.87	49.79	14.95
88	9.25	9.26	9.29	3.31	75.49	26.61	24.72	33.25
89	11.21	11.22	11.23	10.00	57.64	28.20	25.91	11.18
90	11.53	11.53	11.50	2.68	58.44	25.55	23.86	26.91
91	11.85	11.86	11.92	16.12	59.26	33.07	32.26	18.01
92	12.06	12.07	12.09	3.77	59.78	17.23	16.75	37.90
93	11.16	11.17	11.18	10.04	57.53	28.55	26.17	11.22
94	11.52	11.53	11.49	2.69	58.42	26.10	44.31	27.04
95	11.83	11.84	11.89	16.08	59.21	33.39	30.06	17.97
96	12.06	12.07	12.09	3.76	59.78	17.53	16.17	37.81

Figure 5-8 shows the displacement response of the bushing and the connecting equipment of a representative fixed case (case 25). Figure 5-9 shows the displacement response of the bushing and the interconnecting equipment of a representative base isolated case (case 41). The amount of slack for both of these cases is zero. The support displacements for case 25 and case 41 are 0” and 35”, respectively. It is noticed in figure 5-8 that the vibrations of the bushing and the interconnecting equipment are mostly out of phase. Other fixed base cases support this observation. However, for the base isolated case (case 41), the bushing and the interconnecting equipment move mostly in the same direction. Time histories of gap opening, (displacement difference of the connecting equipment and bushing) of these two cases (case 25, case 41) are shown in figure 5-10. When the relative displacement value becomes positive, the interaction occurs between the bushing and the connecting equipment. It should be pointed out that even for the fixed transformer case there is a need to provide a good amount of slack because of the out of phase vibrations of the bushing and the interconnecting equipment. The maximum absolute relative displacements are 13 inch and 27 inch for fixed base case and base isolated case, respectively. On the other hand, support displacements are 0” and 41” for fixed base case and base isolated case, respectively. The feasibility of the base isolation is more obvious when the relative displacement between the bushing and the interconnecting equipment is compared to the support displacements of the two cases.

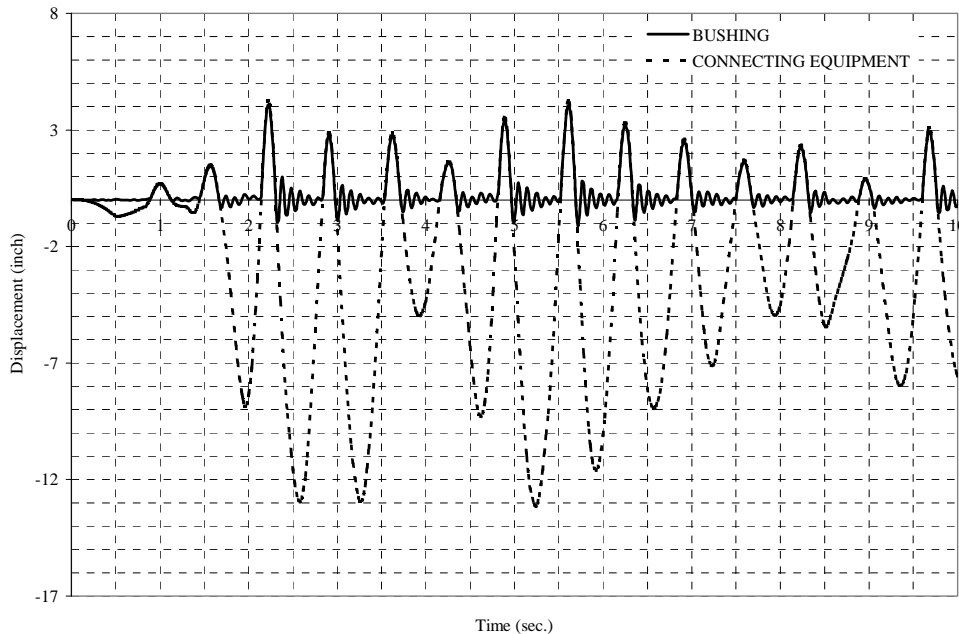


Figure 5-8 Displacement Response of Bushing and Connecting Equipment for Case 25

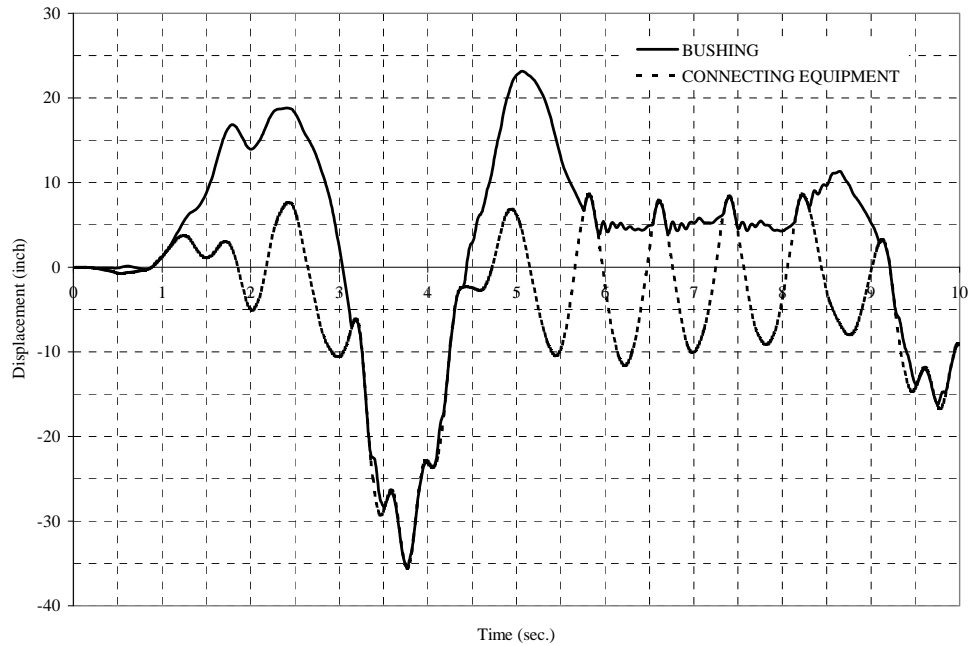


Figure 5-9 Displacement Response of Bushing and Connecting Equipment for Case 41

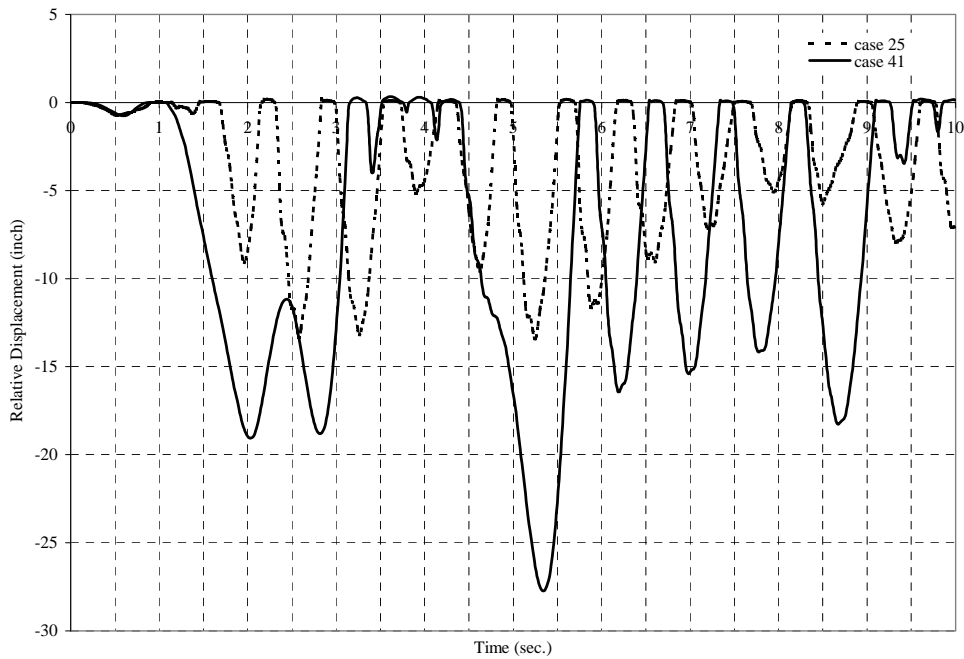


Figure 5-10 Relative Displacement of Bushing and Connecting Equipment for Case 25 and Case 41

For the cases studied, mass and stiffness parameters of the interconnecting equipment are taken from one of the sample equipment. Frequencies of the interconnecting equipment taken in these analyses are 1 Hz and 3 Hz. However mass and stiffness parameters of the interconnecting equipment can vary from equipment to equipment. The response effect of equipment items with

different stiffness and mass properties having the same frequency are different. For example, consider two interconnecting equipment items with 1 Hz frequency. Assume one of them has stiffness, k and mass m and the other one has stiffness $1000k$ and mass $1000m$. Even though they have the same frequency their displacement response will be same but force response will be different.

To study this effect, eight more cases are included. Two new cases are developed corresponding to cases 11, 12, 19, and 20. For the first one, interconnecting equipment stiffness and mass are taken as $1/1000k$ and $1/1000m$. For the other newly developed case, stiffness and mass are taken as $1000k$ and $1000m$. Figure 5-11 and figure 5-12 show this effect for case 12 with stiffness and mass of $1000k$ and $1000m$ and with stiffness and mass of $1/1000k$ and $1/1000m$. Recalling that the force response with stiffness (k) and mass (m) values of this case (case 12) is given in figure 5-7, comparison can be made between case 12 and derivatives of case 12 ($1000k$ and $1000m$, $1/1000k$ and $1/1000m$). Figure 5-11 and figure 5-12 show that the stiffness of the connecting equipment has a significant effect on the bushing response. Stiffer interconnecting equipment develops significantly more forces on the bushing.

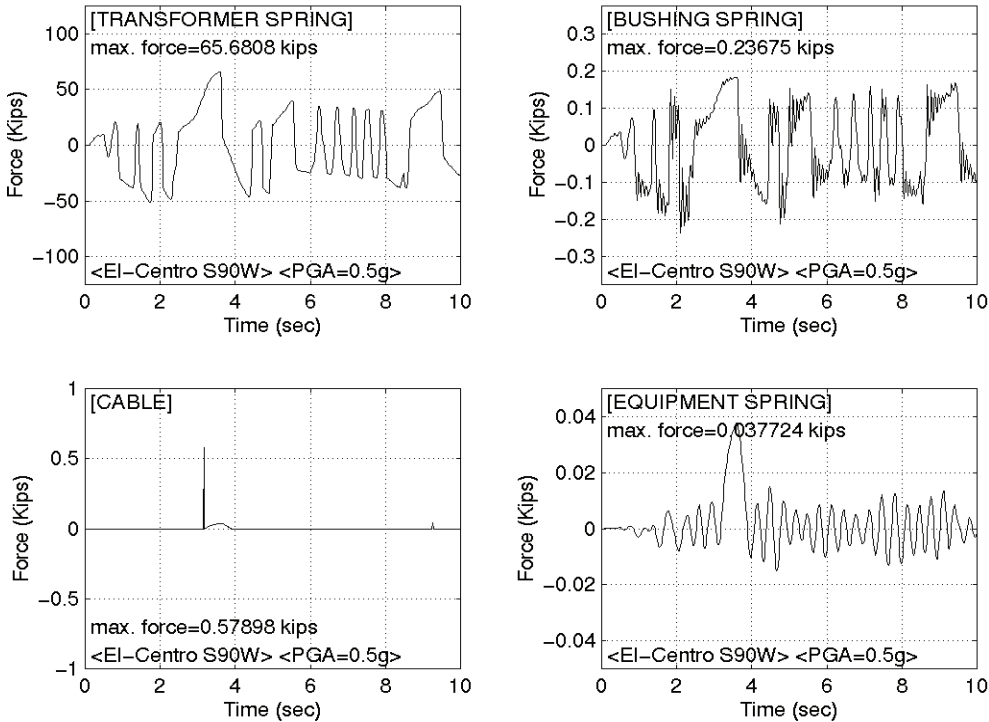


Figure 5-11 Force Response of Case 12 with $1/1000k$ and $1/1000m$

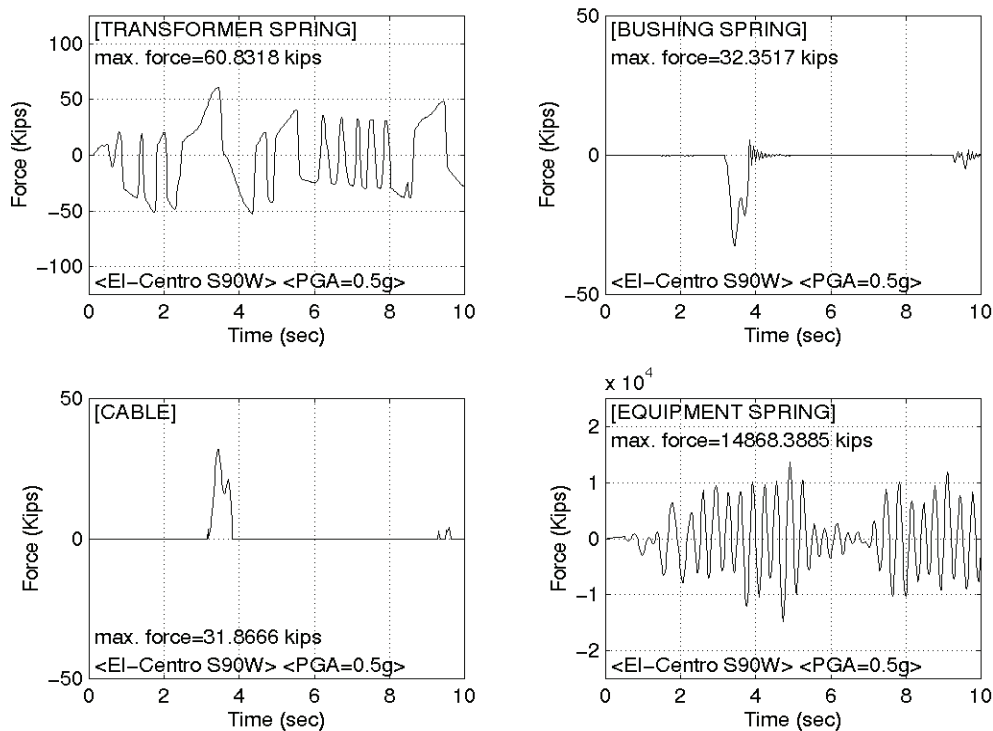


Figure 5-12 Force Response of Case 12 with 1000 k and 1000 m

5.2 Simplified Model for Interaction Study

The same model as in previous section is used with the difference that the mass of transformer is divided between its bottom and top nodes (the nodes at the end of the FPS and transformer elements, respectively). This is because the stiffness of FPS is determined by the whole weight of the transformer, while the effective mass of the transformer in dynamic behavior is only a part of its whole mass. Since the absolute displacement of the whole transformer is almost the same due to predominance of the FPS displacement, equal distribution of the transformer mass between its top and bottom nodes is justified. This model is shown in figure 5-13

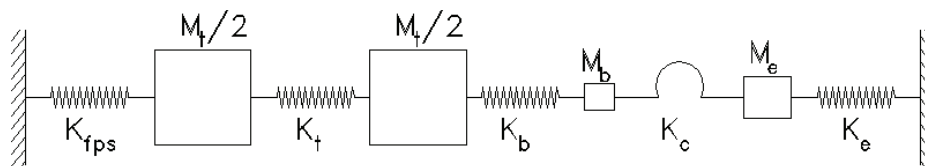


Figure 5-13 Simplified Model Used in This Study.

A wider range of frequencies is considered to see how sensitive the interactions are to the frequency of different components. In order to study the effect of the relative frequency of the interconnecting equipment to that of the FPS, a frequency ratio of

$$FR = \frac{\text{Interconnecting frequency}}{\text{FPS frequency}} \quad (5-1)$$

is defined. The FPS frequency is used for this comparison instead of that of the transformer or bushing because the previous studies show that FPS displacement dominates the overall system response and that transformer and bushing have a displacement very close to it. To vary this ratio, the frequency of interconnecting equipment is changed. Since its mass is kept constant, this means that its stiffness is changed. However, in order to see what behavior a system with the same FR (as define by equation 5-1) and a different interconnecting mass will have, the analyses are done for two different masses. The radius of R = 40 inch is used for FPS, which means a period of 2.0 seconds for the isolation. A weight of 200 kips and a frequency of 11 Hz for transformer and a weight of 5 kips with 10 Hz frequency for bushing are assumed. The strong horizontal component of the 1940 El Centro earthquake with a peak acceleration of 1.0g is applied to the model. Table 5-9 shows the interconnecting equipment characteristics for the cases studied.

Table 5-9 Interconnecting Equipment Characteristics for Studies on Effects of Frequency Ratio on Interaction

Case	Interconnecting Equipment Mass (kips)	FR
1	5	0.4
2	5	0.6
3	5	0.8
4	5	1.0
5	5	1.1
6	5	1.2
7	5	1.5
8	5	2.0
9	5	3.0
10	5	4.0
11	5	6.0
12	5	8.5
13	5	10.0
14	5	12.0
15	5	15.0
16	10	4.0
17	10	6.0
18	10	8.5
19	10	10.0
20	10	12.0
21	10	15.0

Figures 5-14 to 5-16 show the displacements of FPS and interconnecting equipment and relative displacement of the bushing for different ratios of FR. As can be seen, the response of FPS doesn't change for lower values of FR and then starts to increase. As mentioned before, this is because of the constancy of the interconnecting equipment mass. This results in unrealistically high stiffness for high values of FR, and low stiffness for very low FR values. The bushing response shows the change of bushing response for different FR values and it is minimum around $FR = 1$ with the minimum value of 0.32 in that is equal to the failure displacement of the 196 kV bushing (0.3~0.35 in) [Gilani, 1999(a)]. If there were enough slack to prevent interaction, the relative displacement of bushing would be slightly less than 0.05 in, which is acceptable. This shows that interaction has very adverse effects, even in frequency ratios that would result in little or no interaction in linear systems. The interconnecting equipment displacement is a reflection of its stiffness that is dependant upon FR and is unrealistically high in low frequencies because of its very small stiffness.

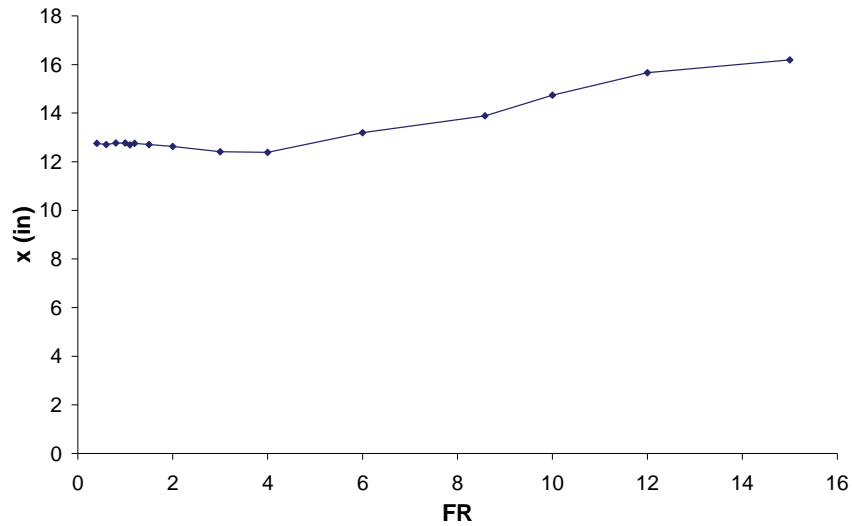


Figure 5-14 FPS Displacement Versus Frequency Ratio.

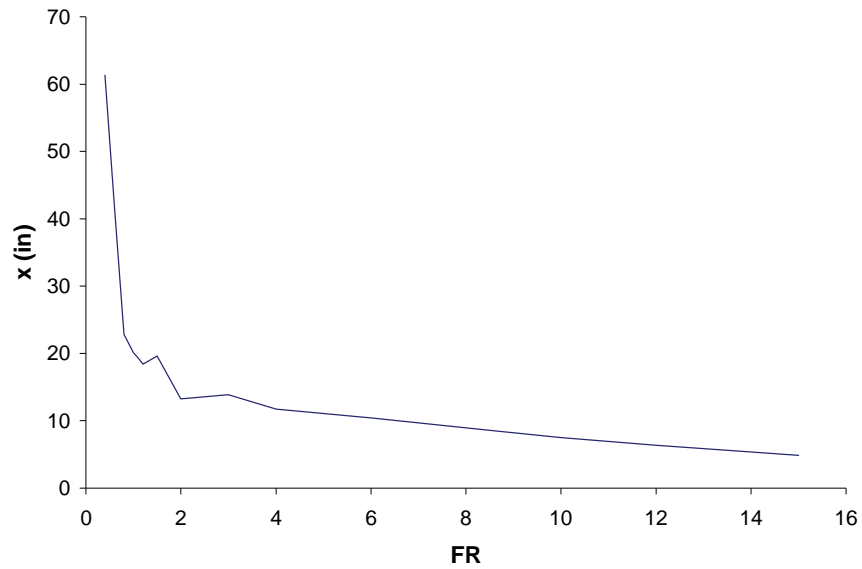


Figure 5-15 Displacement of Interconnecting Equipment Versus Frequency Ratio.

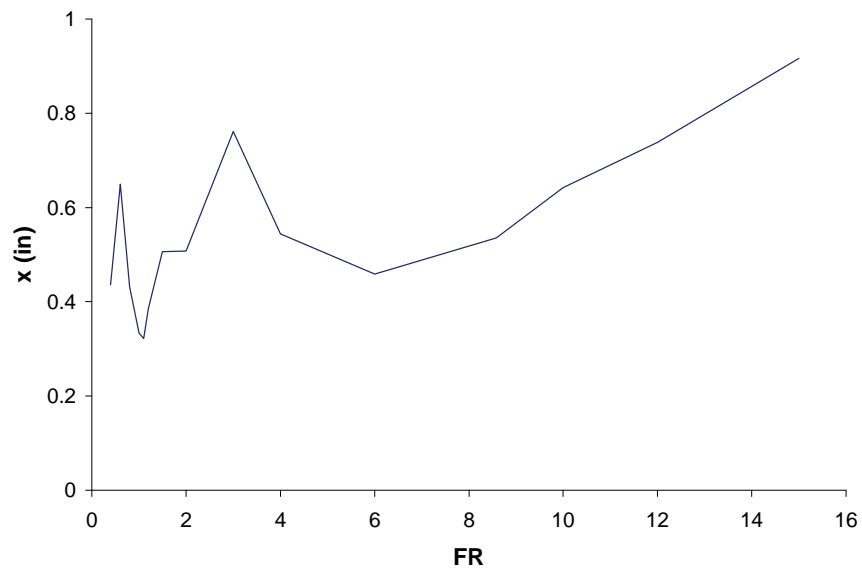


Figure 5-16 Relative Displacement of Bushing Versus Frequency Ratio.

Figures 5-17 and 5-18 show the effect of the interconnecting mass on FPS and bushing response. The abbreviation INC in these figures and throughout this text refers to the interconnecting equipment. As observed, the interaction has more effect on FPS and bushing response when the interconnecting equipment has a higher mass.

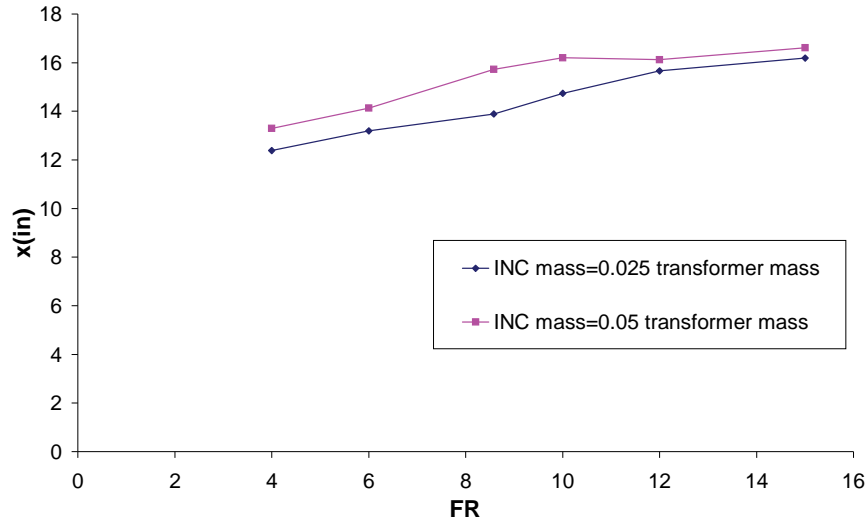


Figure 5-17 Effect of Interconnecting Equipment Mass on FPS Displacement.

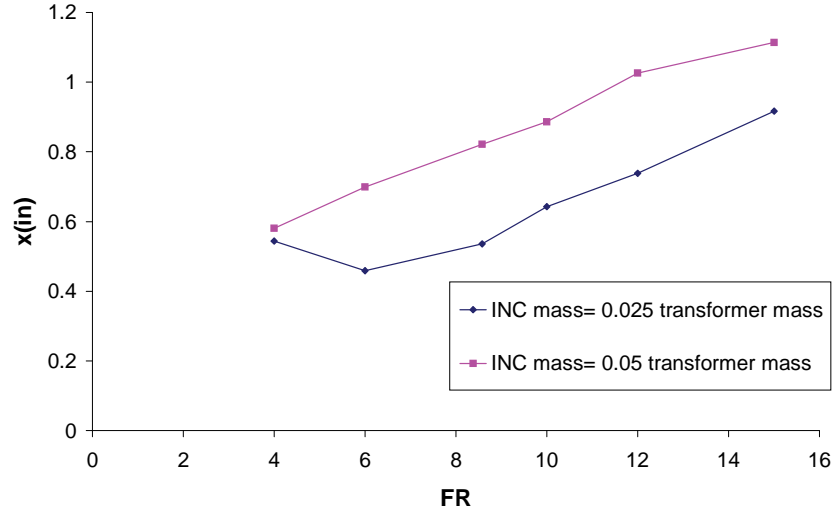


Figure 5-18 Effect of Interconnecting Equipment Mass on Relative Displacement of Bushing.

To study the impact of the amount of slack on interaction effects, another set of studies is done. The slack ratio defined as :

$$\text{Slack Ratio} = \frac{\text{Provided slack}}{\text{Slack required to prevent interaction}} \quad (5-2)$$

is employed to quantify the relative amount of slack. Table 5-10 shows the properties of the interconnecting equipment considered. Their frequencies are in a range of 1 to 4 Hz. TT1 and BUSH3 as mentioned are selected as the transformer and bushing elements. An FPS with R = 60 in (T = 2.48 s) is used for isolation. Table 5-11 shows the details of the cases considered.

Table 5-10 Interconnecting Equipment Characteristics for Studies on Effect of Slack Ratio on Interaction

Interconnecting Equipment	Frequency (Hz)	Mass (kips)	Stiffness (kips/in)
INC1	1	6.9	0.70
INC2	2	6.9	2.82
INC3	3	6.9	6.34
INC4	4	6.9	11.28
INC5	1	110.39	11.28
INC6	2	27.6	11.28
INC7	3	12.27	11.28

Table 5-11 The Cases Studied on Interaction of Isolated Transformer-Bushing and Interconnecting Equipment

Case	Interconnecting Equipment	Slack ratio
1	INC1	0%
2	INC1	100%
3	INC2	0%
4	INC2	100%
5	INC3	0%
6	INC3	10%
7	INC3	20%
8	INC3	30%
9	INC3	40%
10	INC3	50%
11	INC3	60%
12	INC3	70%
13	INC3	80%
14	INC3	90%
15	INC3	100%
16	INC4	0%
17	INC4	10%
18	INC4	20%
19	INC4	30%
20	INC4	40%
21	INC4	50%
22	INC4	60%
23	INC4	70%
24	INC4	80%
25	INC4	90%
26	INC4	100%
27	INC5	0%
28	INC5	100%
29	INC6	0%
30	INC6	100%
31	INC7	0%
32	INC7	100%

Table 5-12 presents a summary of the maximum responses for different cases. Positive or negative displacement in the cable refers to sign of the change in distance between two ends of the cable. These results are analyzed and interpreted in what follows in this section.

Table 5-12 Maximum Results of Interaction of Isolated Transformer-Bushing and Interconnecting Equipment

Case	FPS disp. (in)	Transformer rel. disp. (in)	Bushing rel. disp. (in)	Cable Positive disp. (in)	Cable Negative disp. (in)	INC disp. (in)	Support Reaction (kips)	Cable Force (kips)
1	20.2245	0.01128	4.0300	0.51214	20.9221	15.059	30.0448	102.4
2	16.6104	0.00910	0.0421	23.1742	32.9504	19.633	26.1955	0
3	20.0731	0.01228	3.2601	0.39096	23.6968	6.7474	29.8834	78.2
4	16.6104	0.00910	0.0421	12.2273	21.1082	6.1061	26.1955	0
5	19.0661	0.01341	3.9301	0.26034	20.3512	4.9766	28.8109	52.1
6	18.8475	0.01127	3.4058	1.40077	20.1751	4.2425	28.5782	51.2
7	18.9372	0.01082	3.1309	2.5451	20.4563	4.0805	28.6736	51.1
8	18.984	0.01162	3.1766	3.75319	20.818	4.1000	28.7235	63.8
9	19.3753	0.01041	2.9281	4.90446	20.8794	3.7259	29.1402	65.1
10	18.9364	0.00830	2.5742	6.06171	19.6243	3.3038	28.6728	67.6
11	18.8232	0.00882	2.2288	7.1513	18.9974	2.9528	28.5522	56.5
12	18.2283	0.01114	1.7570	8.25529	18.2711	3.1461	27.9187	48.4
13	17.5538	0.01061	1.5311	9.35923	18.7403	3.8158	27.2002	40.2
14	17.0109	0.00908	0.9077	10.4433	18.2871	3.2158	26.6221	28.0
15	16.6104	0.00910	0.0421	11.4479	17.6464	2.6602	26.1955	0
16	17.7541	0.01340	5.1598	0.35217	18.3789	4.0241	27.4137	70.4
17	17.2213	0.01262	4.7445	1.35111	17.8197	3.6984	26.8462	64.3
18	17.2329	0.01266	3.8012	2.31585	17.861	2.8808	26.8585	51.4
19	17.6664	0.01138	3.2796	3.33503	18.4742	2.4601	27.3202	49.3
20	18.1494	0.01029	2.7989	4.3724	19.0852	2.2138	27.8346	50.9
21	18.5737	0.00882	2.3890	5.37586	19.3991	2.0956	28.2865	45.7
22	18.522	0.00882	2.0169	6.40017	19.104	2.0956	28.2315	44.7
23	18.2543	0.00980	1.5359	7.39779	18.7094	2.0956	27.9463	38.3
24	17.9605	0.00978	1.1381	8.36973	18.6216	2.0956	27.6335	26.8
25	17.3962	0.00902	0.7821	9.3572	18.4387	2.0956	27.0324	18.4
26	16.6104	0.00910	0.0421	10.2947	17.7833	2.0956	26.1955	0
27	25.8523	0.03148	10.8418	0.77531	41.2927	17.301	36.0386	155.1
28	16.6104	0.00910	0.0421	23.1742	32.9504	19.633	26.1955	0
29	20.1582	0.02241	8.4990	0.56748	26.3809	8.3451	29.9741	113.5
30	16.6104	0.00910	0.0421	12.2273	21.1082	6.1061	26.1955	0
31	17.7752	0.01577	5.4031	0.36604	18.6194	3.9436	27.4361	73.2
32	16.6104	0.00910	0.0421	11.4479	17.6464	2.6602	26.1955	0

Figure 5-19 shows a time history of the displacement of FPS and interconnecting equipment and relative displacement of bushing when no slack is provided (Case 1). As observed in this figure, the heavy weight of transformer carried on FPS tends to dominate the responses. Hence, when FPS has negative displacement (moving away from interconnecting equipment) it pulls the interconnecting equipment with it. This will put bushing under an enormous force due to pulling by FPS and resistance by the interconnecting equipment. Therefore, it is observed that bushing experiences large peaks in its response when FPS has negative displacement. In other times, bushing has much smaller response that is free from influence of the interconnecting equipment.

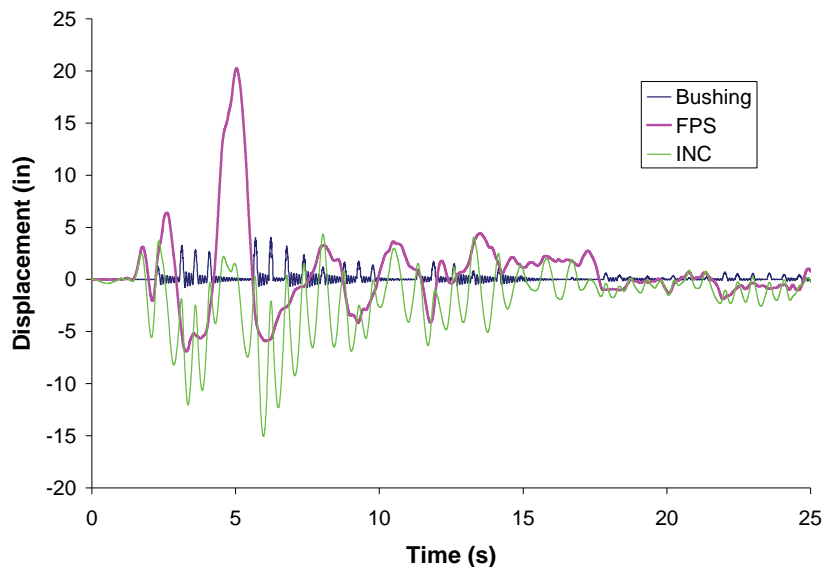


Figure 5-19 Time History Responses In Simplified Model, Case 1.

Figures 5-20 and 5-21 compare the relative displacement in the cable and displacement of FPS in the presence or absence of sufficient slack.

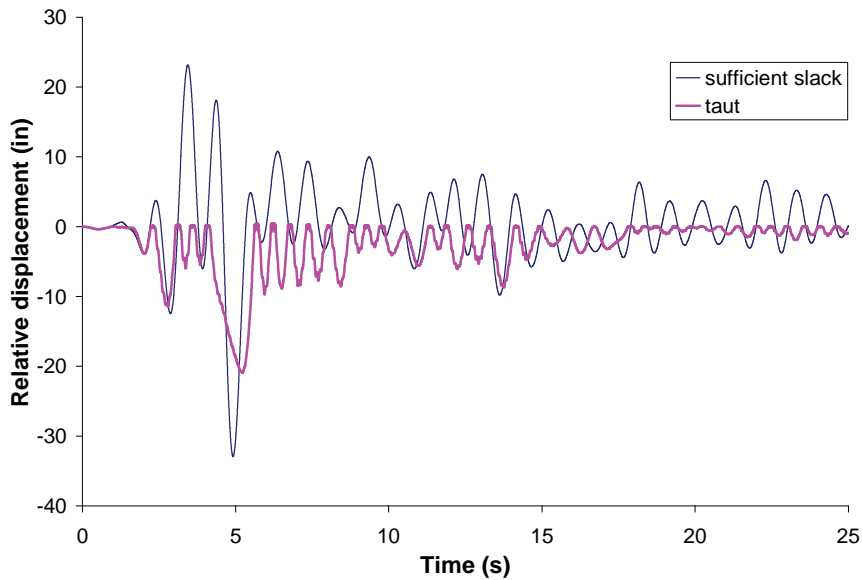


Figure 5-20 Relative Displacement of The Cable in Simplified Model, Case 1.

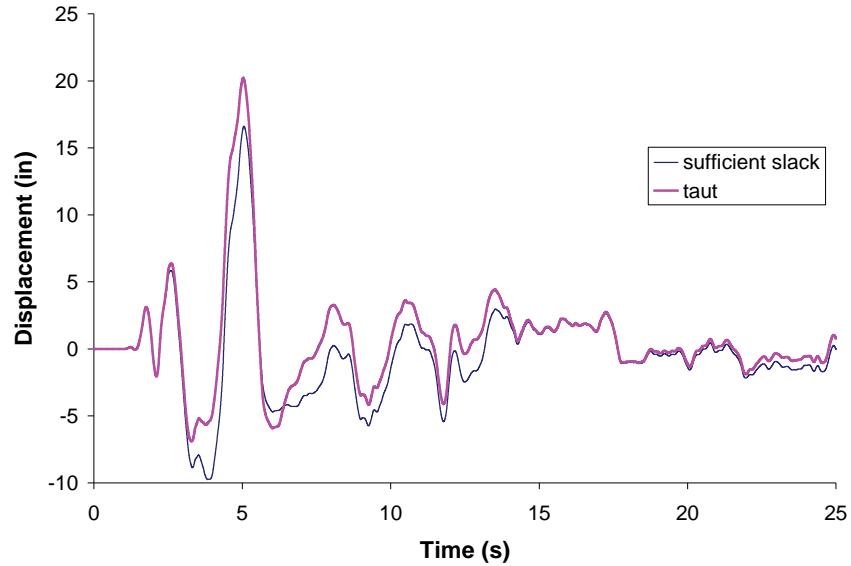


Figure 5-21 FPS Displacement in Simplified Model, Case 1.

To see how much partial slackness of the cable can help reduce the adverse interaction effects, the analyses for INC3 and INC4 are done for different slack percentages compared to the slack required to prevent interaction. The slack ratio in these analyses is the inverse of the factor β used in other studies [Hong, 2001]. Those results are presented for values of β as high as 2 that are equivalent to slack ratios of 50%~100% in our graphs. For $\beta < 1$, there will be no interaction in our model.

Figure 5-22 shows the relative displacement of bushing. As obviously observed, even small tautness of the cable will amplify the response of bushing considerably. For slack ratio of 90%, interaction with INC3 causes a relative displacement of 0.91 in the bushing that is more than 21 times that of the sufficient slack case. This ratio is 18 when interaction is with INC4. These values are much higher than the allowable displacement in the bushing that is of order of 0.3 in for a 230 kV bushing [Gilani, 1999(a)]. This suggests that any interaction should be prevented to ensure that bushing does not undergo excessive displacements and sustain large forces. Even the slightest interaction has the potential of damaging the bushing. As expected, it is seen that as the slack is reduced, the bushing response is increased.

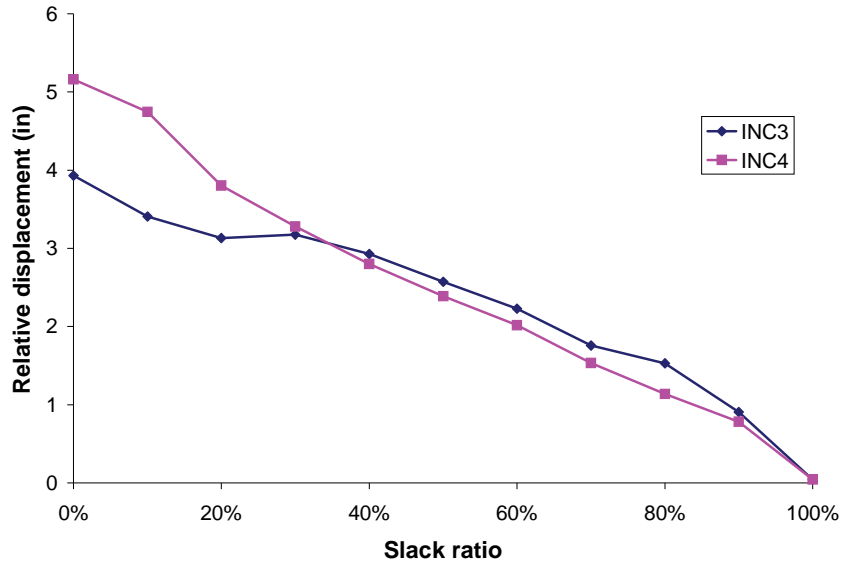


Figure 5-22 Relative Displacement of Bushing Versus Slack Ratio.

Figure 5-23 shows the interconnecting equipment displacements. Here too, the decrease in slack usually has the effect of amplifying the interconnecting equipment response. However, the amplifications are much more modest compared to those of bushing. The amplification for INC3 and INC 4 are about 1.9 for completely taut cable.

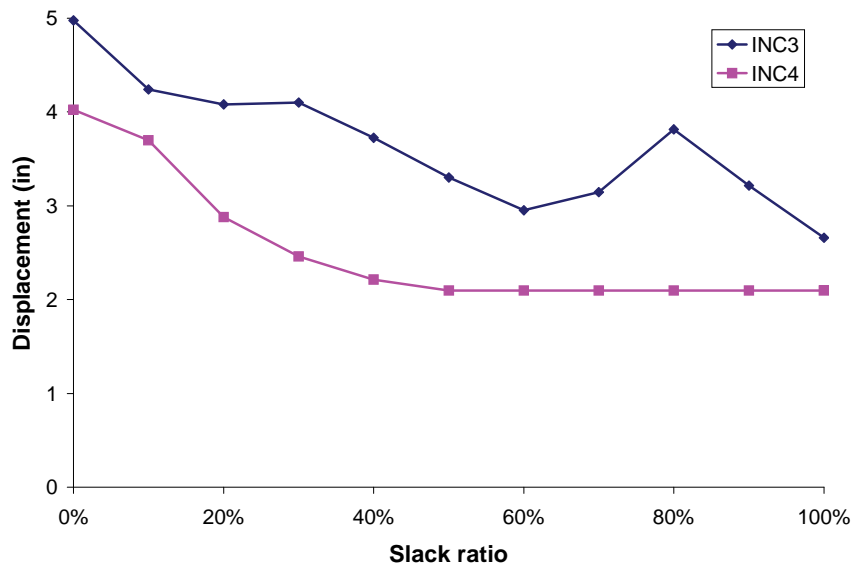


Figure 5-23 Interconnecting Equipment Displacement Versus Slack Ratio.

Figure 5-24 shows the cable force as a percentage of the transformer weight. This force has a general rising tendency with a decrease in slack. However, this tendency is not always true and

sometimes less slack might actually mean slight decrease in cable force due to nonlinear nature of interaction.

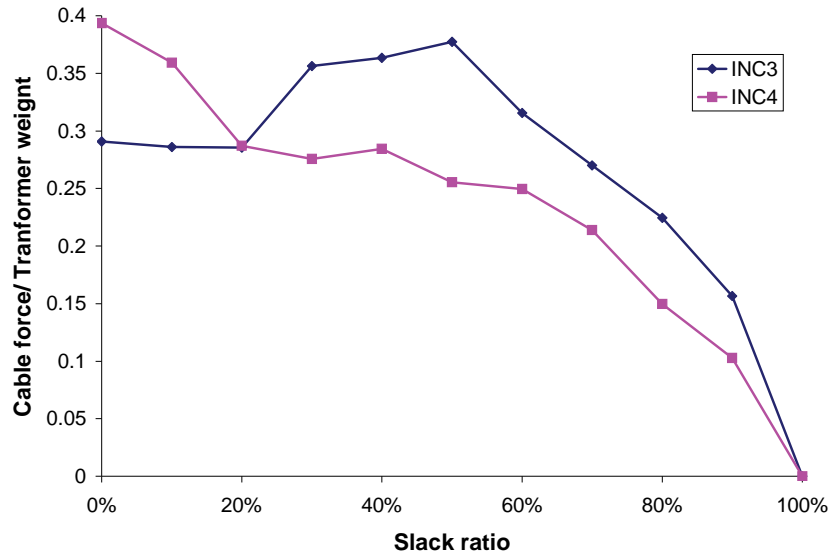


Figure 5-24 Cable Force Versus Slack Ratio.

Figure 5-25 shows FPS displacements. It can be seen that although the interaction effect generally increases with a decrease in slack, this relation does not hold very tightly. It should be mentioned here that interaction tends to increase the displacement of FPS toward the interconnecting equipment. Therefore, if the maximum displacement of FPS were in the direction away from the interconnecting equipment, a decrease in this displacement would be observed in the presence of interaction.

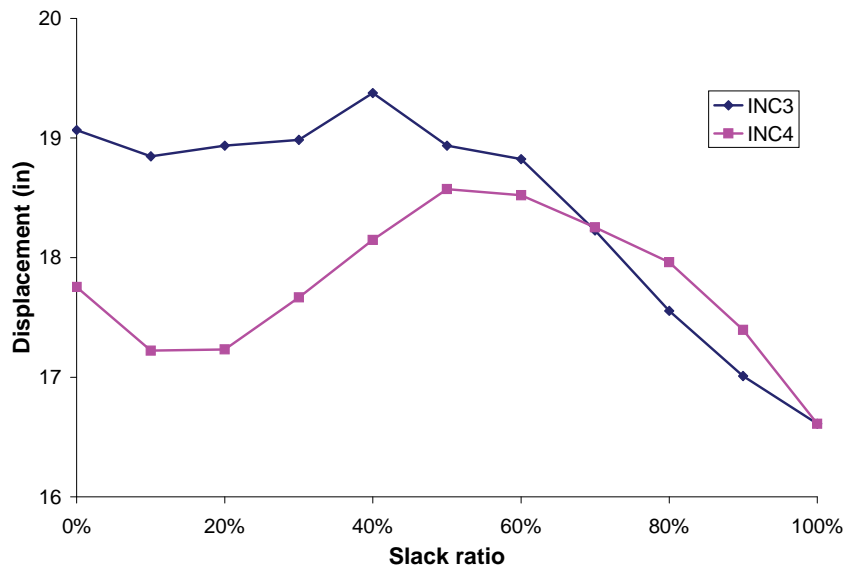


Figure 5-25 FPS Displacement Versus Slack Ratio.

Finally, figure 5 shows the transformer force. Transformer response is not affected by the interaction dramatically and despite the increase in its forces, these forces remain very low. Even for certain slack ratios, interaction might reduce the transformer response.

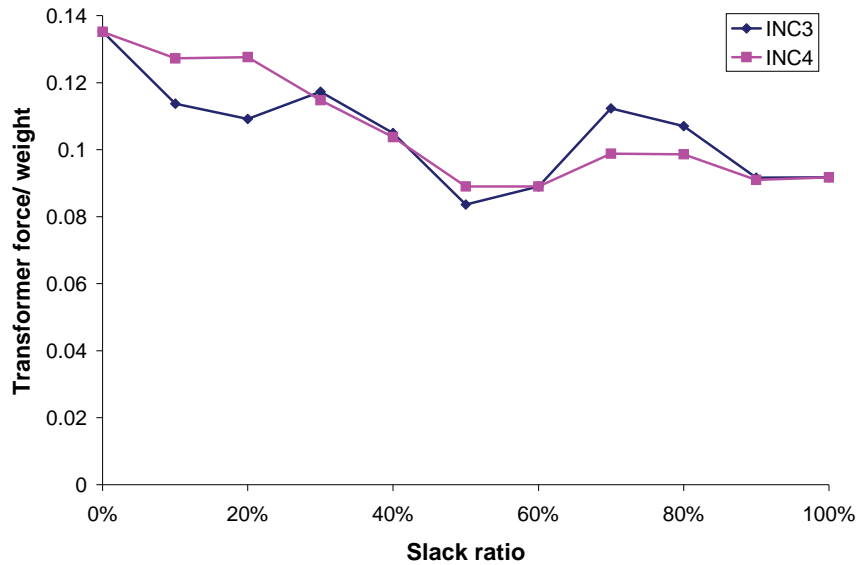


Figure 5-26 Transformer Force Versus Slack Ratio.

It should be noted that these are based on limited data, which does not allow conclusive observation on the effect of frequency. For more conclusive interpretations, the results mentioned at the beginning of this section should be used. Figures 5.27 through 4.31 show the effect of interconnecting equipment stiffness and mass, using taut cable connection. For the line with fixed stiffness, decrease in frequency means increase in mass of the interconnecting equipment. For the line with constant mass, this translates into reduction in stiffness. Hence, for any frequency (Except 4 Hz), the point on the line with fixed mass has lower mass and stiffness compared to the other line. Figure 5.27 shows the interaction effects on bushing relative displacement. The response of bushing without interaction is not shown since it is of two lower orders of magnitude. It can be seen that increase in mass and stiffness of interconnecting equipment can exacerbate the bushing response amplification. However the changes are more pronounced when mass is changing rather than stiffness, suggesting that mass has a more prominent role.

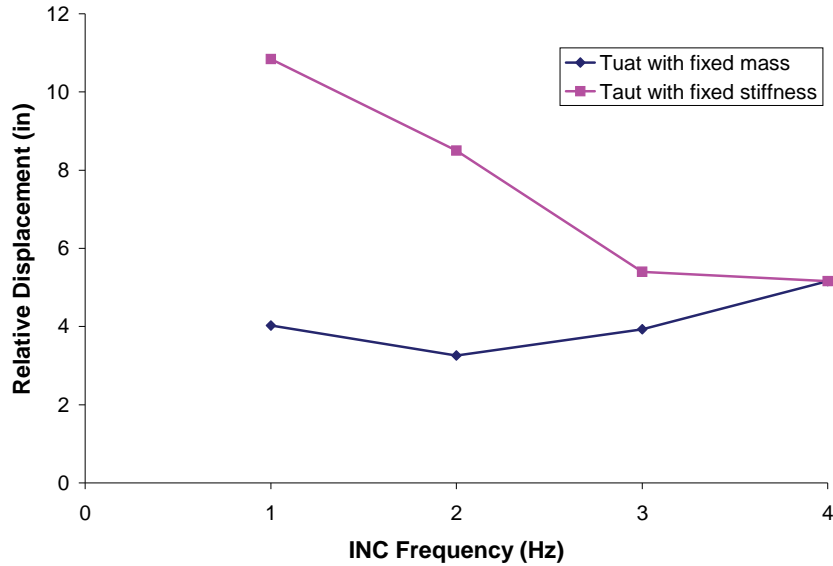


Figure 5-27 Bushing Relative Displacement Versus INC Frequency.

Figure 5-28 shows the interconnecting equipment displacement. Presence of interaction might increase or decrease this response. Hence, while interaction can easily increase the bushing response by 2 orders of magnitude, its effect on interconnecting equipment is more limited and can even be positive in some cases.

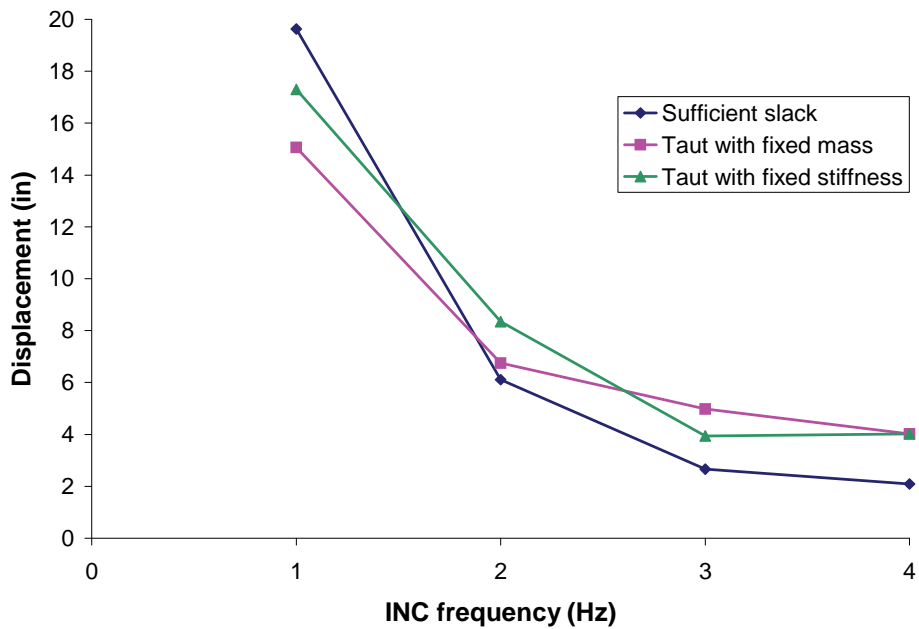


Figure 5-28 Interconnecting Equipment Displacement Versus INC Frequency.

Figure 5-29 shows relative displacement in transformer. Interaction always has adverse effect on transformer response. This effect is limited when the INC mass is constant, but is increased considerably with an increase in INC mass.

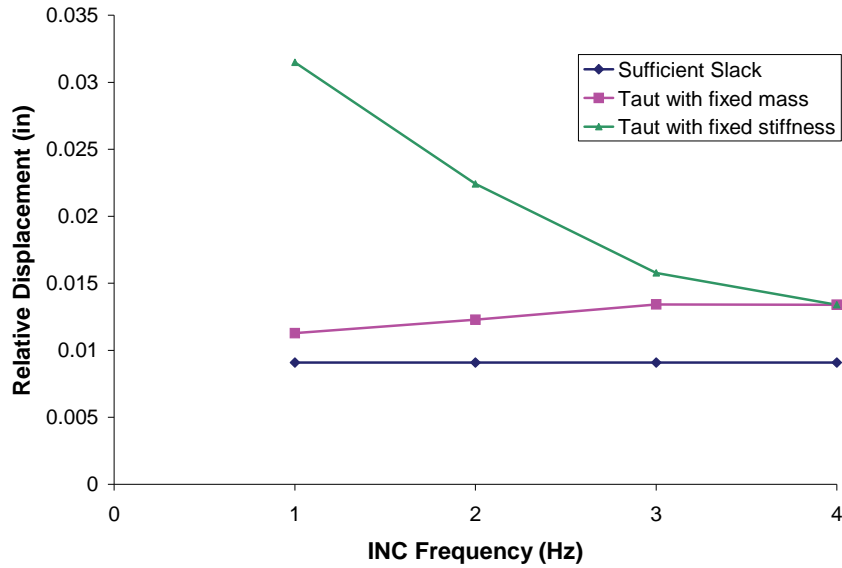


Figure 5-29 Transformer Relative Displacement Versus INC Frequency.

Figure 5-30 shows FPS displacement. As mentioned before, interaction tends to pull FPS toward the INC. Hence, it is possible that FPS response is reduced by interaction depending in position of interconnecting equipment relative to FPS and the earthquake record used. Here cases with lower frequencies show a slightly stronger effect on FPS response.

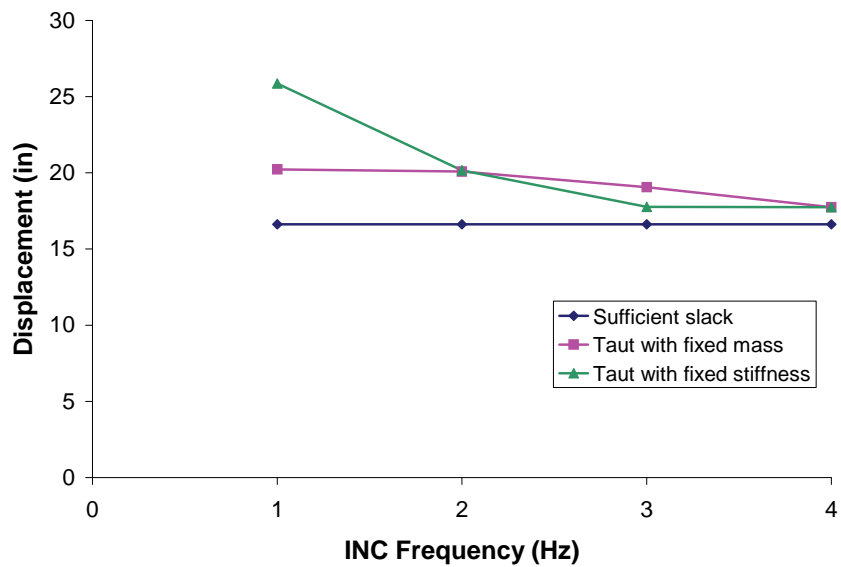


Figure 5-30 FPS Displacement Versus INC Frequency.

Finally, figure 5-31 shows cable force in presence of interaction. In general, this force tends to increase with a decrease in INC frequency, probably because they would have higher displacements if left alone.

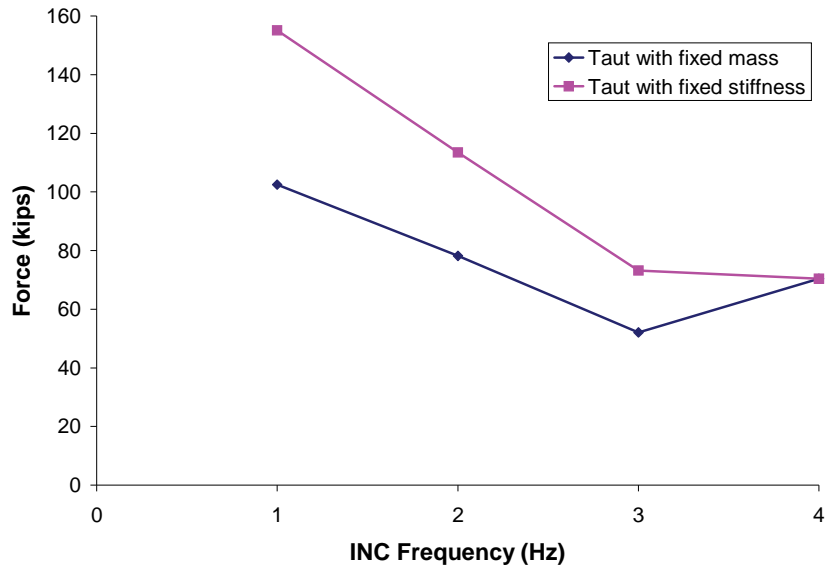


Figure 5-31 Cable Force Versus INC Frequency.

Summing up the analyses results, interaction has the most severe affect on bushing response. The amplifications due to interaction are so high, even for small tautness, that any occurrence of them means failure of bushing. If the FPS is to be used for seismic isolation of transformer, enough slack should be provided in the connecting cable to prevent any interaction between transformer-bushing and interconnecting equipment. One way to be sure that this interaction does not happen is to provide the slack equal to sum of the maximum absolute value of displacement of FPS and the interconnecting equipment (see section 5.1). Although this might be too conservative in some cases, the adverse effect of the slightest interaction justifies such conservatism. The relative displacements of bushing and transformer are negligible compared to that of FPS.

Another observation worth consideration is the existence of differences in trends observed in interaction of fixed equipment, and those observed when there is isolation. For instance, the interaction tends to amplify the response of both of the equipment connected by a cable, particularly that of the higher frequency equipment when both are fixed [Hong, 2001]. However, FPS being the low frequency and interconnecting equipment being the high frequency component in this study, a different trend is observed. The response of the engaged interconnecting equipment may be below its stand-alone response. On the other hand, the FPS is pulled more toward the interconnecting equipment, whether this means a decrease or increase in its maximum response.

5.3 FPS Graphs to Select FPS Radius and Cable Slack

For the same bearing material, the radius of FPS bearing is the only parameter that can be changed to get a different isolation behavior. Changes in this radius will change the natural frequency, FPS displacement, and inertial forces applied to the structure. To be able to choose the proper radius, numerous analyses are performed for different FPS radii and earthquake excitations and effects of radius and peak ground excitation on displacement and inertia response are determined. The results can be used to select the proper radius to get the desired inertia reduction for the specified soil condition and peak ground acceleration. Once the radius is chosen, the maximum displacement of FPS can also be determined. Consequently, one can determine the amount of slack that should be provided in the connecting cable to prevent interaction between transformer-bushing and interconnecting equipment. Table 5-13 lists the earthquakes used to develop these graphs. These earthquakes are obtained from the PEER strong motion database [PEER, 2002].

Table 5-13 Earthquake Records Used

Case	Earthquake	Station	Ground
1	San Fernando 1971/02/09 14:00	126 Lake Hughes #4	Rock
2	Loma Prieta 1989/10/18 00:05	1161 APEEL 9 - Crystal Springs	Rock
3	Kern County 1952/07/21 11:53	1095 Taft Lincoln School	Rock
4	Kobe 1995/01/16 20:46	0 KJMA	Rock
5	Parkfield 1966/06/28 04:26	1438 Temblor pre-1969	Rock
6	Imperial Valley 1940/05/19 04:37	117 El Centro Array #9	Soil
7	Kern County 1952/07/21 11:53	135 LA - Hollywood Stor FF	Soil
8	Northridge 1994/01/17 12:31	75 Sylmar - Converter Sta East	Soil
9	Parkfield 1966/06/28 04:26	1014 Cholame #5	Soil
10	Mt. Lewis 1986/03/31 11:55	57191 Halls Valley	Soil

Figures 5-32 and 5-33 show the average displacement response and inertia reduction for FPS bearings under a horizontal excitation with a vertical excitation whose peak is set equal to 80% of the horizontal peak according to IEEE [IEEE, 1998]. As can be seen, with increase in radius, the change in displacement will decrease since the surface tends towards a flat surface. The displacements and their differences are higher in higher PGAs as expected, since friction happens more frequently in higher PGAs. Inertia reduction is higher for high radii, and a change in radius usually has more effect on inertia reduction compared to displacement. While the inertia reduction increases with increasing PGA, it tends to flatten in PGAs higher than about 0.5g. In case of R = 30 in, this inertia reduction starts decreasing after a certain PGA. This is because large displacements mean that the slider is in a rather steep position meaning it is under a large re-centering force. Choice of the radius should be based on a balance between displacement, inertia reduction, and bearing cost. The cost increases with increasing radius; therefore, the bearing with lowest radius that satisfies the structural requirements should be chosen. Based on the graphs, a radius of 30~60 inch seems proper. Higher radii will provide little benefit in terms of higher inertia reductions, have higher displacements, and have much higher costs. Also, looking at benefits for different PGAs, it can be said that for structures in places with PGA < 0.2g, cost is the only important factor and R = 30 in is suggested. For 0.2g < PGA < 0.6g,

cost and inertia reduction are the factors to be balanced. For $PGA > 0.6g$, all the factors should be considered.

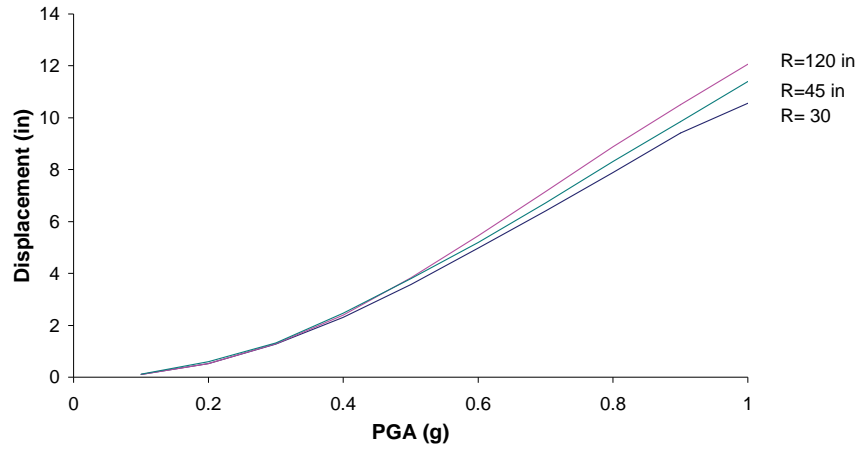


Figure 5-32 Average FPS Displacement Versus FPS Radius.

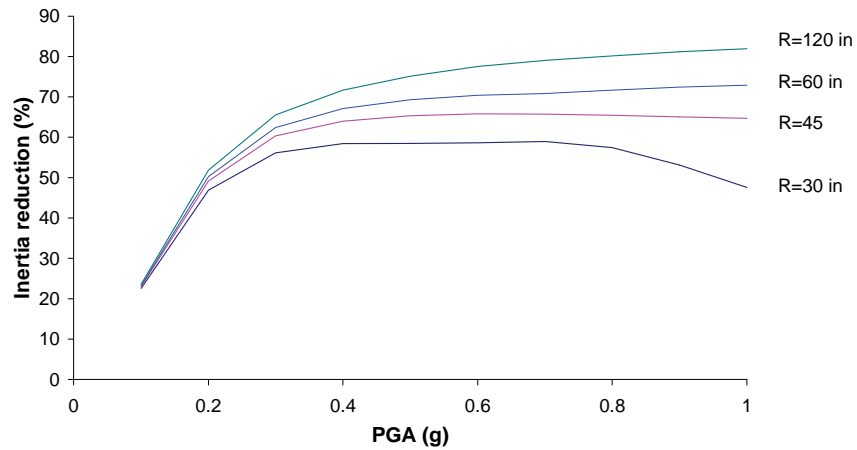


Figure 5-33 Average Inertia Reduction Versus FPS Radius.

Figures 5-34 through 5-37 show the same results for rock and soil earthquake records. It can be seen that for rock records, the displacement for $R = 45$ is slightly higher and the other radii have very close displacements. This suggests that for the records on rock, the radius of FPS does not have much effect on the displacement responses. Hence, displacement is not among the factors used to determine the desired radius. The inertia reductions are, however, much different from one radius to another. Therefore, the inertia reduction plays a more prominent role in selecting the proper radius. The decrease in efficiency of FPS in higher PGAs is more pronounced for rock records compared to the average. This is especially more obvious for $PGA > 0.7g$ and for $R = 30$

in. In soil records, the displacement for $R = 30$ in is visibly less than the others. The rest of radii have almost the same displacement response. The inertia reductions for soil are less affected by radius compared to rock records. Also, the decrease in efficiency in higher PGAs is not observed in soil records. In general, it can be said that it is easier justified for rock ground conditions to pick higher FPS radii compared to soil conditions due to the higher gain in terms of inertia reduction. For the practical range of radii considered, it can be said that in all cases displacement is of lower prominence. $R = 45$ in seems to be the choice that combines most of the benefits in general. $R = 60$ in may be preferred if the gain in terms of inertia reduction can balance the increased FPS cost. $R = 30$ in may be chosen in cases where the normal structural design can sustain the increased inertial forces with little or no reinforcement.

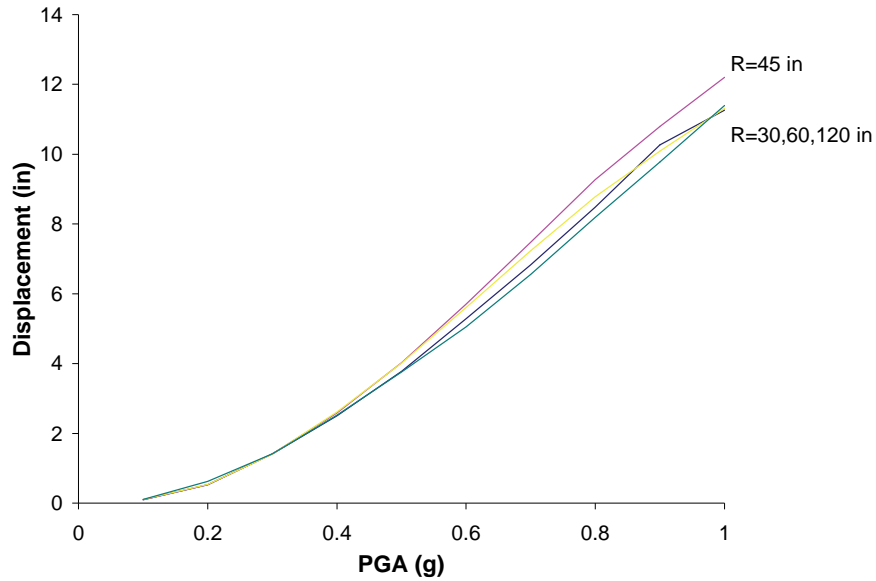


Figure 5-34 Average FPS Displacements Versus FPS Radius for Rock.

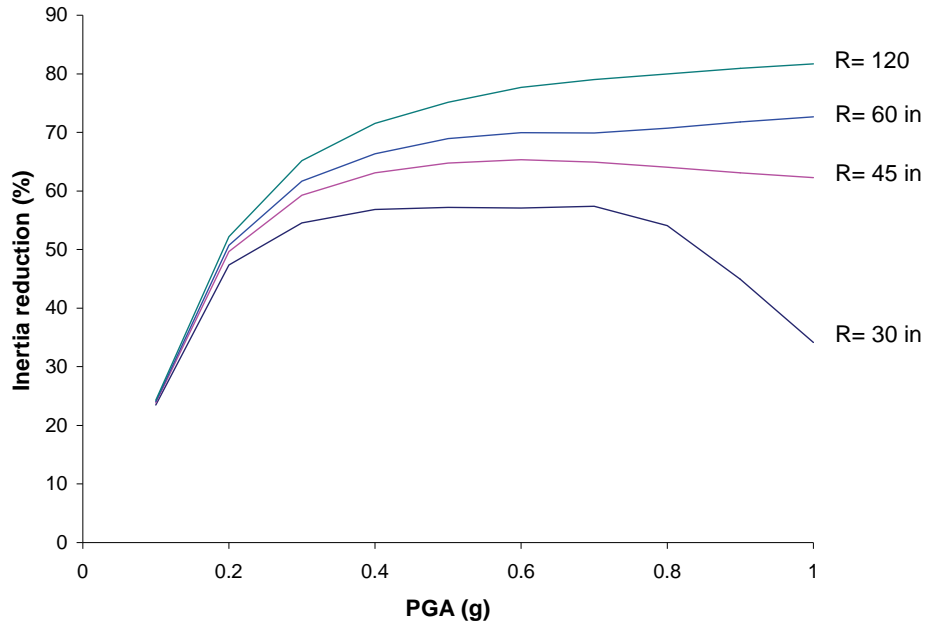


Figure 5-35 Average Inertia Reduction Versus FPS Radius for Rock.

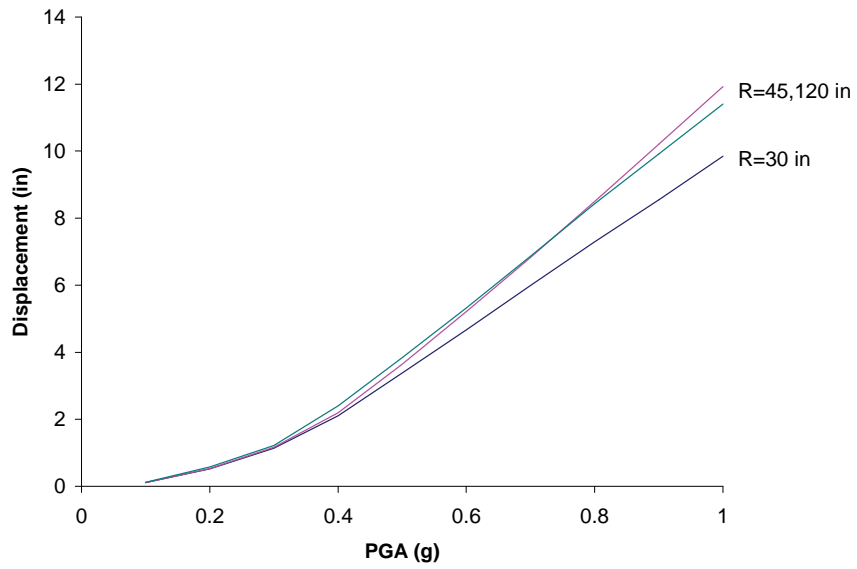


Figure 5-36 Average FPS Displacement Versus FPS Radius for Soil.

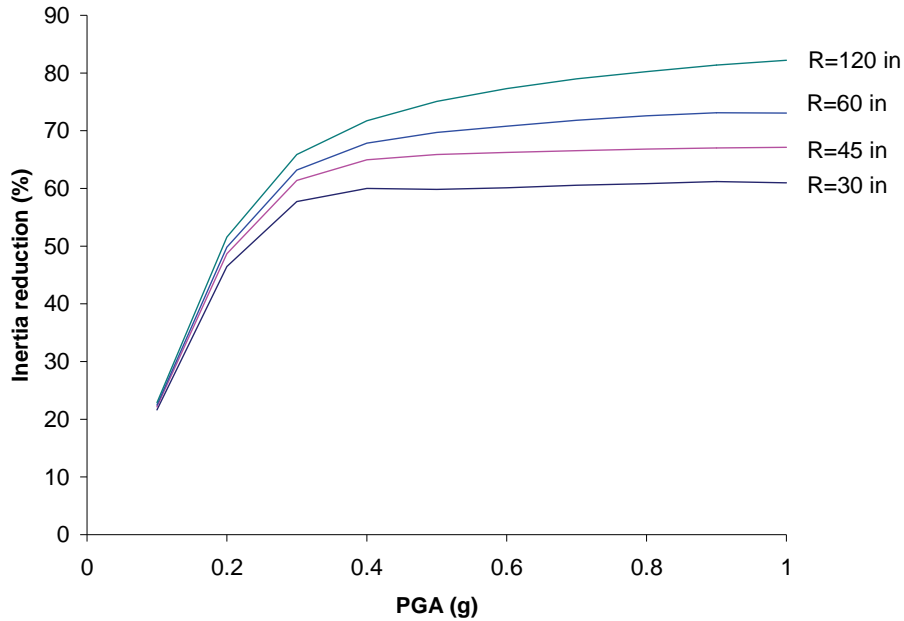


Figure 5-37 Average Inertia Reduction Versus FPS Radius for Soil.

The displacement from these graphs can be used to determine the slack provided in the connection from bushing to the interconnecting equipment. This value should be added to the peak displacement response of the interconnecting equipment. Although not considered in this study, it is recommended based on other studies that the cable connects the top of bushing to the point with the same elevation in the interconnecting equipment [Hong, 2001].

5.4 Practical Aspects and Design Recommendations

Unanchored transformers should be avoided in earthquake prone regions. Tilting of an unanchored transformer is very likely in moderate and high seismic prone regions. As an example, consider TT3 from Section 2 of this report. The weight of the transformer is 512 kips and the dimensions of the transformer are B=100 inch, L=280 inch, H=180 inch (see figure 5-38).

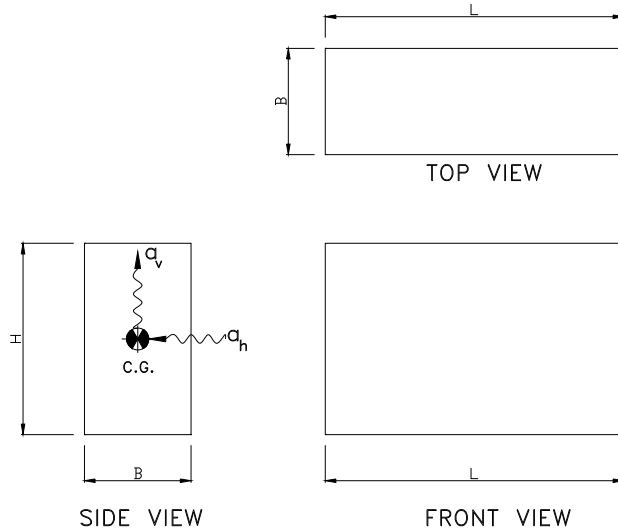


Figure 5-38 Outline View of TT3

Based on the IEEE requirement, 0.5g of horizontal acceleration and 0.4g of vertical acceleration are applied to the transformer center of gravity. Assuming the center of gravity of the transformer is located $H/2$ above the bottom of transformer, the overturning moment at the heel of transformer in critical direction (narrow side), M_o becomes:

$$M_o = \left(\frac{W}{g}\right)a_h\left(\frac{H}{2}\right) = \left(\frac{512}{g}\right)0.5g\left(\frac{180}{2} \times \frac{1}{12}\right) = 1920 \text{ kips.ft}$$

And the resisting moment, M_R becomes:

$$M_R = \left(\frac{W}{g}\right)(1g - a_v)\left(\frac{B}{2}\right) = \left(\frac{512}{g}\right)(1g - 0.4g)\left(\frac{100}{2} \times \frac{1}{12}\right) = 1280 \text{ kips.ft}$$

Since resisting moment is less than overturning moment, tipping of the transformer is possible. Therefore anchorage of the transformer is required. Vertical tipping reaction, V , can be calculated as:

$$V = \frac{M_o - M_R}{B} = \frac{1920 - 1280}{100/12} = 76.8 \text{ kips}$$

Assuming the transformer top is in contact with the concrete foundation and the coefficient of friction of concrete metal interface is 0.25. The lateral force at the bottom of transformer, F_h , becomes:

$$F_h = \left(\frac{W}{g}\right) \times a_{gh} - \mu_s W = W(0.5 - 0.25) = 128 \text{ kips}$$

And the resultant force at the base of the transformer is:

$$F_R = \sqrt{F_h^2 + V^2} = \sqrt{128^2 + 76.8^2} = 149 \text{ kips}$$

If welding with 1/2" leg is preferred for anchorage, and the allowable stress of the weld is assumed as 30 ksi, total length of the weld, W_L , along the narrow sides (both sides) of the transformer becomes:

$$W_L = \frac{F_R}{30 * \frac{(1/2)''}{\sqrt{2}}} = 21.07 \text{ inch}$$

Therefore, providing a 21-inch long weld is enough for fixing this transformer.

The same calculations are performed for high seismic performance level (1.0 g in horizontal, and 0.8g in vertical direction). The resultant force at the base of the transformer, F_R , and the required weld, W_L , become 561.5 kips and 73 inch respectively.

It is clear that anchorage forces required increase dramatically for high seismic performance level. The maximum dynamic amplification factor at the midlevel of this transformer is found to be 1.624 in Section 2 of this report. Then, the required weld for this transformer type for high performance level becomes total of 153-inch long for two of the critical sides. Welding can be done in many ways, for example: some structural shape (angel, channel, etc.) with horizontal and vertical shear studs welded on it is embedded inside the concrete foundation pad parallel to shorter sides of the transformer and transformer bottom plates welded to these plates (fillet weld, etc.).

Proper anchorage should be implemented for existing transformers in the moderate or high earthquake prone regions by use of welds and anchor bolts. Embedment of structural shapes in the concrete foundation for anchorage purposes is challenging so that some structural shapes could be anchored to the foundation through some anchor bolts. This structural shape can be welded to the transformer tank. New transformer tank designs should consider the anchorage of the transformer tank to the concrete pad below.

Advantages of using FPS for transformers have been mentioned before in previous chapters. It should also be mentioned that application of FPS has advantages in functionality and maintenance needs of transformers, compared to anchorage. They can be used when enough clearances are insured to provide slack for the connections. The minimum required clearances with the assumption of half circle connection between equipment item and the bushing, based on the average results of FPS study are given for moderate and high seismic performance level regions in table 5-14 and table 5-15 respectively. The use of base isolation reduces the lateral force, foundation forces at the base of the transformer and even the bushing forces are reduced. However, simplified analysis results show that base isolated systems without proper amount of slack will cause high impact forces on the bushing. Therefore, FPS should not be used without providing proper amount of slack.

Table 5-14 Required Slack for FPS Displacements (Moderate Seismic Performance Level)

Radius of Curvature of FPS (inch)	Bearing Displacement (inch)	Minimum Required Distance Between Equipment Items (inch)
30	4.4	7.7
60	5.0	8.8
90	5.0	8.8
120	5.1	8.9
150	5.2	9.1

Table 5-15 Required Slack for FPS Displacements (High Seismic Performance Level)

Radius of Curvature of FPS (inch)	Bearing Displacement (inch)	Minimum Required Distance Between Equipment Items (inch)
30	14.9	26.1
60	17.9	31.4
90	20.6	36.1
120	21.1	37.0
150	21.3	37.3

The values given in table 5-14 and table 5-15 depend on the average values of the FPS displacements. It should be kept in mind that the displacement of the interconnecting equipment should also be taken into account. Average FPS displacement based on PGA and radius of curvature is discussed in Section 3 of this report. Displacement of interconnecting equipment (circuit breaker, disconnect switches, etc.) is obtained either through finite element modeling or from the IEEE response spectra. Absolute sum of these displacements provide the amount of required slack.

SECTION 6

EVALUATING THE APPLICATION OF BASE-ISOLATION: A CASE STUDY

This section is devoted to a case study analysis to discuss the effectiveness and viability of Friction Pendulum System (FPS) as a mitigation measure for power transformers. As discussed, FPS is capable of reducing the inertia forces significantly, alleviating many problems associated with seismic performance of transformers and bushings. Lower loads means not only better seismic response for transformer and bushings, but also lower forces need to be transferred to the foundation resulting in more economical foundation and connections. Furthermore, shaking of transformer internal components will be minimized, thus, preventing possible adverse affect of ground motions on transformer electromagnetic performance and its longevity.

6.1 Transformers and Bushings Characteristics

In collaboration with Bonneville Power Administration (BPA) three actual transformers are being considered to better quantify the advantages and issues discussed vis-à-vis application of base-isolation.

The weight of the larger transformer, which is the subject of this section, is 512.6 Kips and is used in all cases. For the sake of thoroughness a range of frequencies are used for both the transformer and the bushings (230kV and 500 kV). These values are used based on existing literature [Gilani et. al. 1999], [Gilani et. al. 1998] and prior experience with dynamic frequency analysis of transformer-bushing systems presented in previous sections. These are shown in table 6-1, which constitute 18 different cases. Consistent with IEEE 693 2% damping is assumed.

The main objective in this section is to compare time histories of various parameters and response maxima for various cases under fixed base condition, which have recently been completed for BPA, to the base-isolated case. Elevations of the larger transformer are shown in figure 6-1, which is a single-phase auto-transformer with 433.3 MVA capacity.

6.2 Modeling

For the fixed base case, the simplified model (of previous section) consists of two masses and two springs representing transformer-bushing system, as shown in figure 6-2a. Masses and stiffness are selected such that they represent the range of dynamic characteristics shown in table 6-1.

For the base isolated case, an elasto-plastic bilinear spring with kinematic hardening is added to represent the FPS bearings (figure 6-2b). It is well established that bilinear hysteresis model with kinematic hardening represents the response of FPS bearings with good accuracy. Parameters defining FPS bilinear hysteretic model are shown in figure 6-3. As it can be seen properties of the bi-linear spring depends entirely on the characteristics of the FPS, and is independent of the

system supported. This model is simulated in the analyses through material property of the spring element representing the FPS isolator.

Based on the FPS responses presented in previous sections, it is decided to use bearings with radius and friction coefficient equal to 88 inch and 7%, respectively.

Table 6-1 Properties of the Transformers and the Bushings

Case Number	Transformer Frequency f_t (Hz)	Transformer Weight (kips)	Bushing Frequency f_b (Hz)	Bushing Weight (lb)
1	5	512.6	3	500
2	5	512.6	6	500
3	5	512.6	8	3740
4	5	512.6	12	770
5	5	512.6	15	1050
6	5	512.6	18	920
7	12	512.6	3	500
8	12	512.6	6	500
9	12	512.6	8	3740
10	12	512.6	12	770
11	12	512.6	15	1050
12	12	512.6	18	920
13	15	512.6	3	500
14	15	512.6	6	500
15	15	512.6	8	3740
16	15	512.6	12	770
17	15	512.6	15	1050
18	15	512.6	18	920

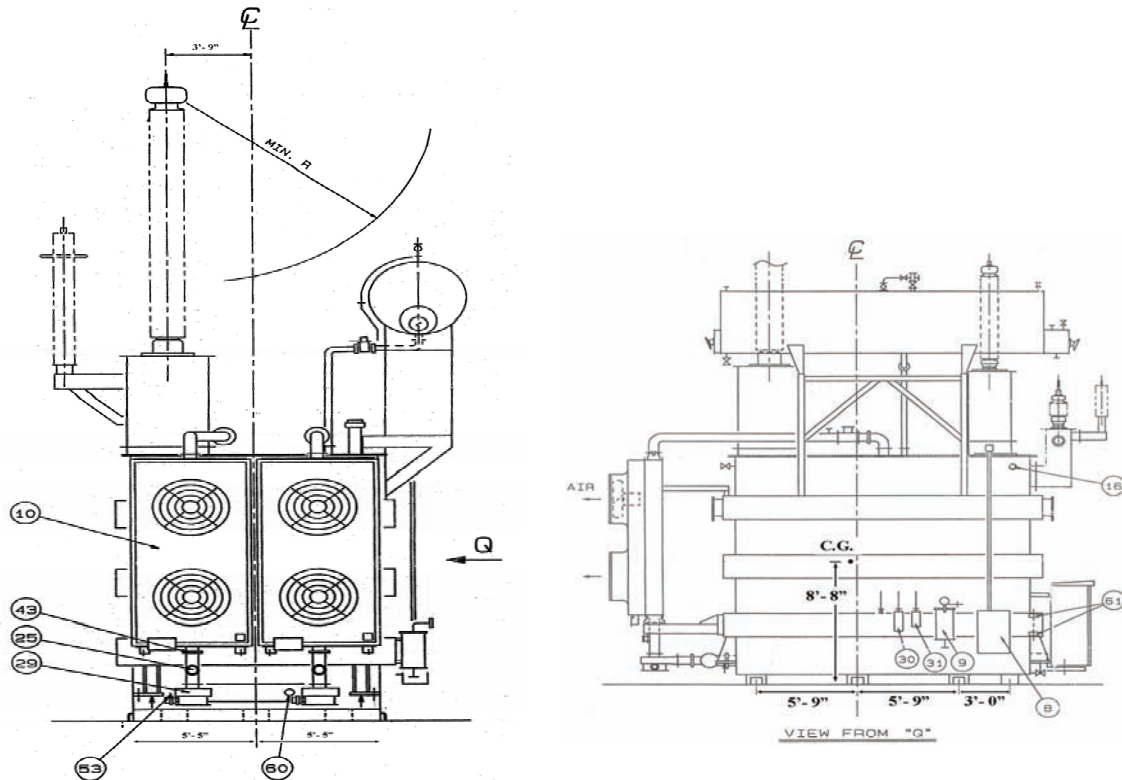


Figure 6-1 Front and Side Elevation of a 433.3 MVA Substation Transformer (not to scale).

For a FPS with a radius equal to 88 inch the frequency is equal to 0.33 Hz (3-sec period).

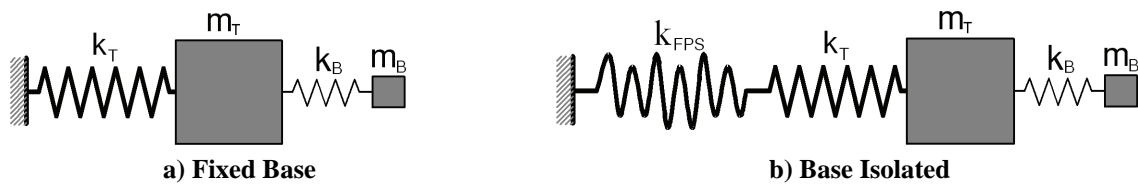


Figure 6-2 Simplified 2-DOF Model

6.3 Seismic Forces Based on IEEE

The transformer is located in a high seismic region and has to be qualified for high performance level based on IEEE 693. For limit state condition, this means that it has to be designed to withstand earthquakes with peak ground acceleration of 1.0g in horizontal directions and 0.8g in the vertical direction. Although in previous sections finite element results indicate dynamic amplification in the transformer, IEEE 693 assumes a rigid body response, thus, the PGAs can be used in determining the inertia forces in the transformer.

W: weight of structure
 R: radius of FPS
 m: dynamic friction
 k_{FPS} : hardening stiffness

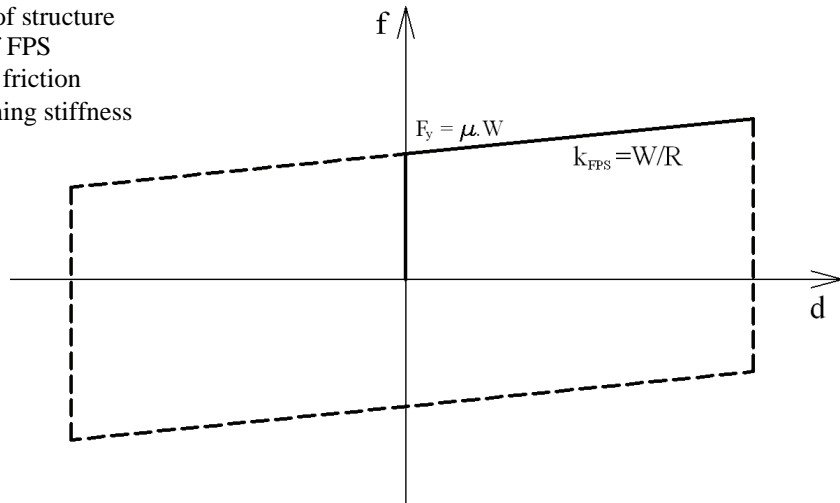


Figure 6-3. Modeling the FPS as a Bi-linear Hysteretic Element with Kinematic Hardening

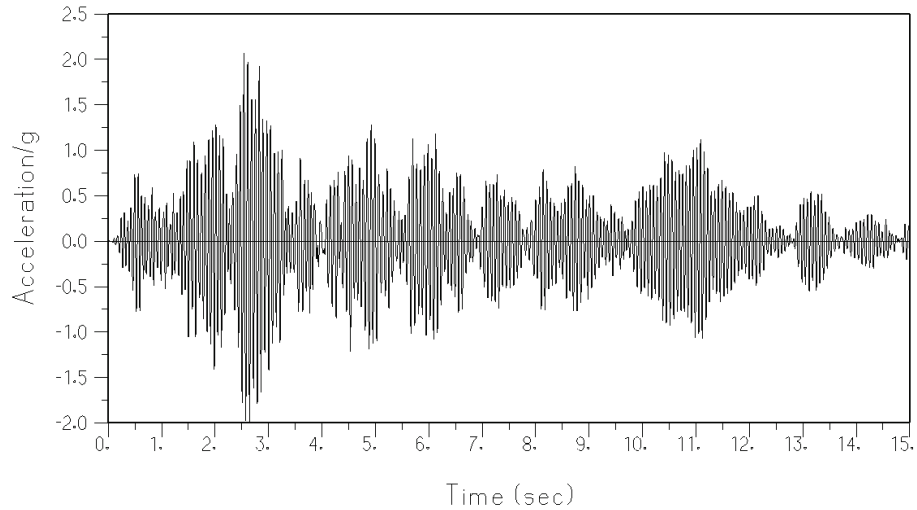
6.4 Results of Time History Analyses

One of the most important factors affecting the earthquake characteristics is geotechnical site conditions. Geotechnical conditions are usually categorized into four groups namely: bed rock and hard rock; sedimentary and conglomerated rock; soil and glacial till; and alluvium and unconsolidated deposits. In this study, records from the first two sites are combined to represent “Rock” sites, and records from the other two are combined into another group representing “Soil” sites. Based on previous analyses and comparison of responses to various records to averages (as discussed in Section 3), it is determined that San Fernando and El Centro records are good representative of rock and soil sites, respectively. Therefore these records were selected as ground motion inputs for the analyses presented in the following sections. The records are scaled to 1.0g peak ground acceleration.

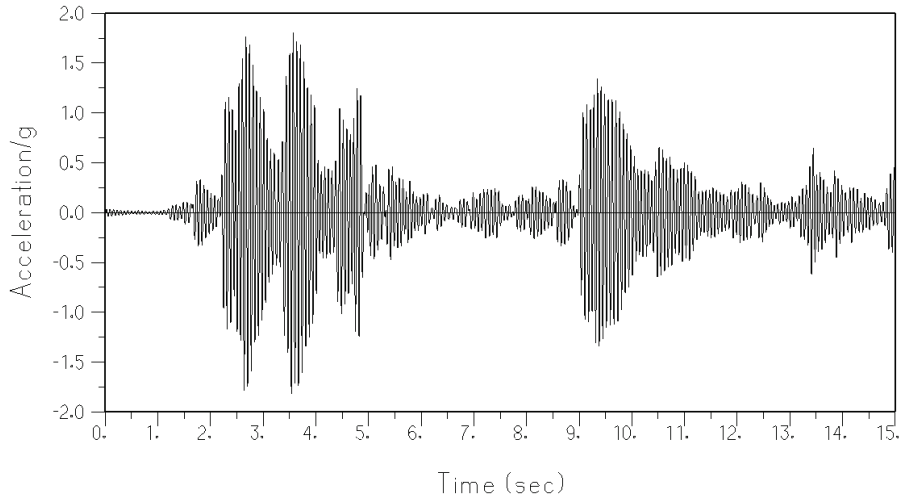
6.4.1 Transformer Responses

6.4.1.1 Fixed Base Case

The model shown in figure 6-2a is used for fixed base analyses. Figure 6-4 shows acceleration time-histories for Case 15 from table 6-1.



a) Response to San Fernando record



b) Response to El Centro record

**Figure 6-4 Time History of Transformer Acceleration
(Case 15-fixed base)**

The maximum accelerations of the transformers for all cases and for both rock and soil site conditions are plotted in figures 6-5 and 6-6.

As it can be seen from these figures there is significant dynamic amplification of the response of the transformer. The peak dynamic amplification factor (DAF) is 3.8 for a transformer with 12 Hz frequency subjected to San Fernando earthquake record, and the minimum is 1.7 for a 5 Hz transformer subjected to the same record. This demonstrates the need for reconsideration to IEEE 693 assumption of rigid body response in transformers (i.e., DAF of 1.), and as shown in the next section further highlights the effectiveness of new technologies such as base-isolation in minimizing the dynamic response.

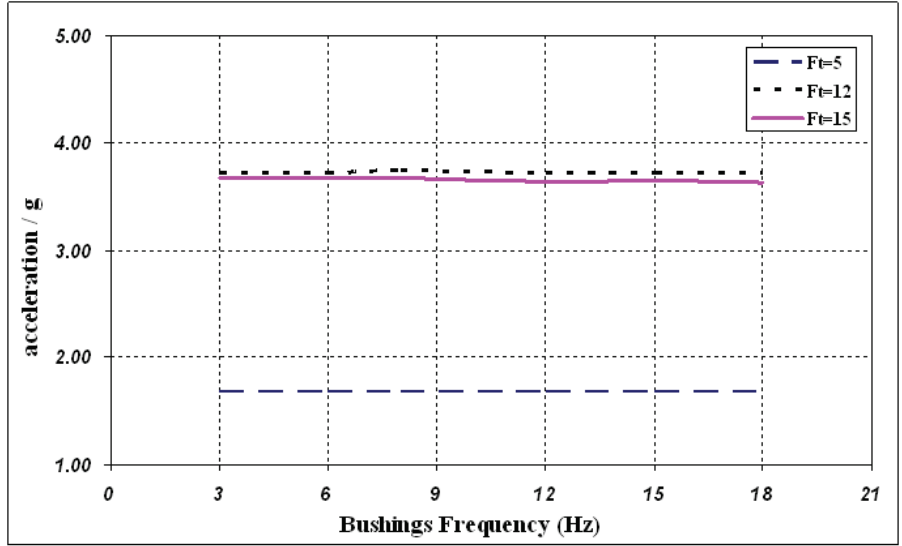


Figure 6-5 Maximum Acceleration Responses of Transformers (San Fernando - fixed base)

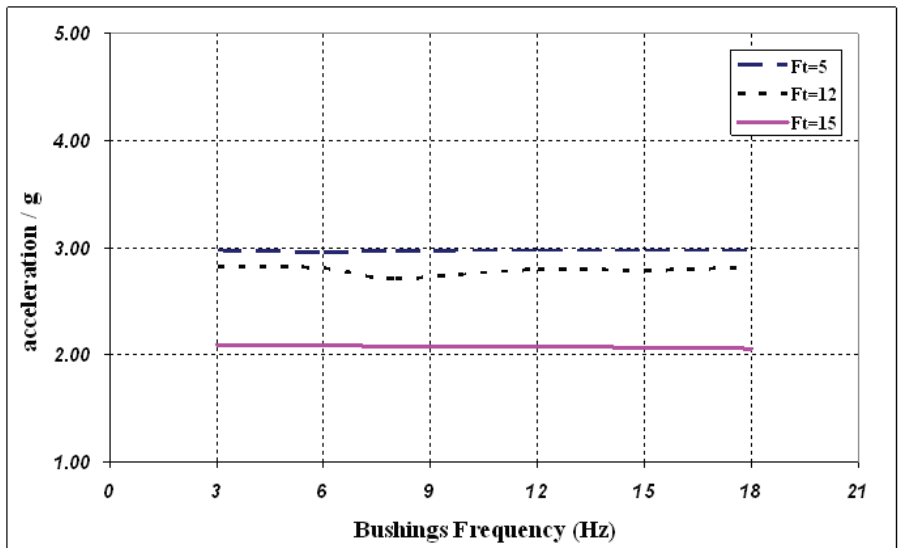


Figure 6-6 Maximum Acceleration Responses of Transformers (El Centro - fixed base)

6.4.1.2. Base Isolated

The model shown on figure 6-2b is used for base isolated analyses. Figure 6-7 shows the force-displacement hysteresis loops for Case 15 subjected to the San Fernando record. The area bounded by the graph in every cycle represents the amount of energy dissipated. This is one of the response characteristic of base-isolation that reduces the inertia forces transmitted to the system.

Acceleration time histories are shown in figure 6-8 for the same case and subjected to both earthquake inputs. Both have similar amplitude but due to single shock nature of San Fernando record the response is limited to a narrow time-period while response to El Centro record has multiple peaks of comparable amplitude.

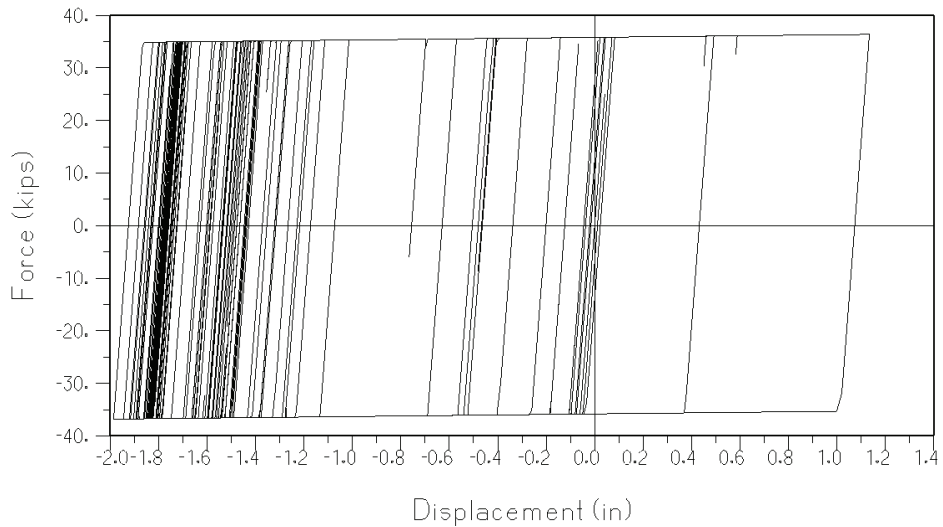
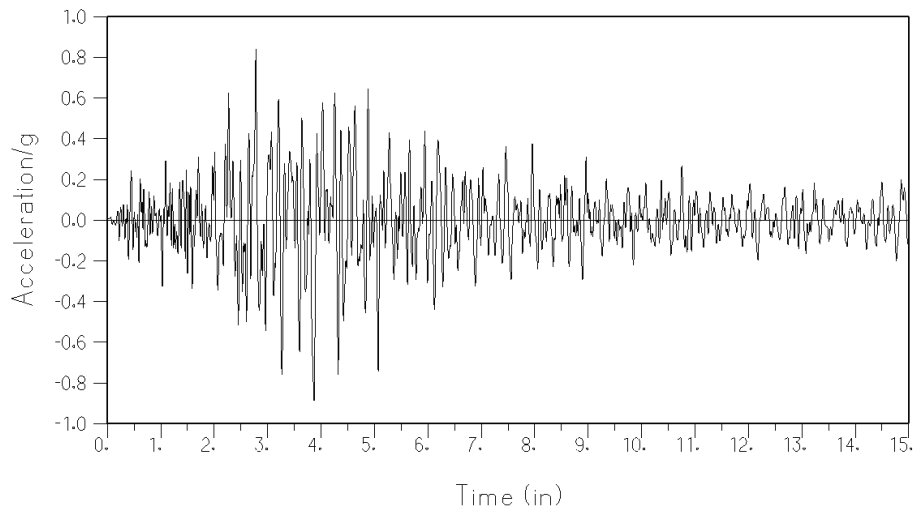
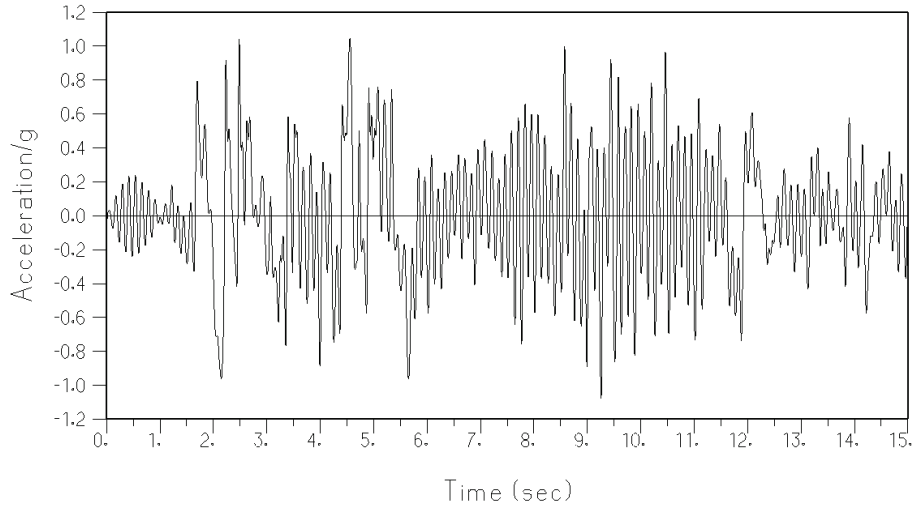


Figure 6-7 Hysteresis Behavior of the FPS During the Application of San Fernando Record



a) Response to San Fernando record



b) Response to El Centro record

Figure 6-8 Time History of Transformer Acceleration (Case 15-base isolated)

In figures 6-9 to 6-11 the responses of the transformers with FPS base isolators have been compared with the cases when base is fixed. These graphs show the ratio of acceleration responses of transformers in base isolated systems to the acceleration in fixed base systems. As it can be seen, the inertia reductions in all cases are more than 85%. Hence, by using a base-isolator system the seismic forces in transformers can be reduced substantially.

An important characteristic of FPS isolated transformers is that their responses are insensitive to their own natural frequencies. As mentioned before the frequency of the isolated-transformer will only depend on the radius of the bearings, which is selected in such manner that the period is lengthened (frequency is reduced). This will ensure that the response frequency is outside high energy zone of the earthquake. As it can be seen, in all cases the inertia reduction for San Fernando record is more than El Centro, which demonstrates that FPS is more effective for structures located on rock sites (where spread in system frequency and dominant ground motion frequencies is higher).

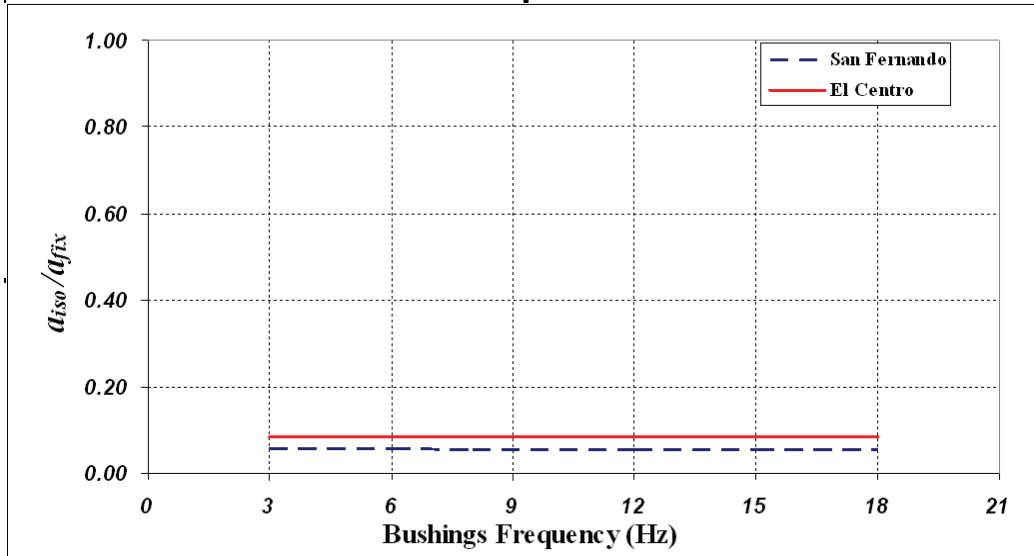


Figure 6-9 Reduction in Transformer Accelerations ($f_t=5$ Hz)

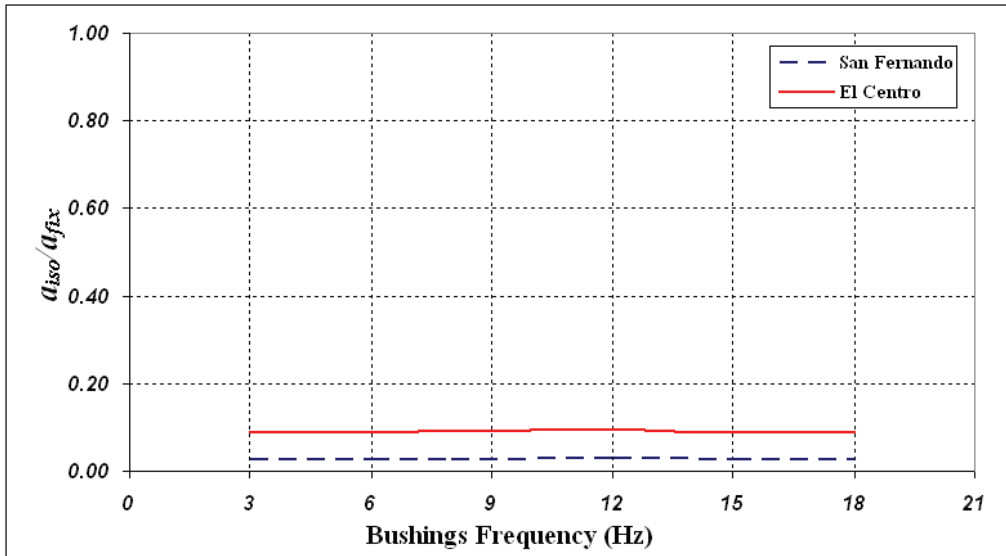


Figure 6-10 Reduction in Transformer Accelerations ($f_t=12$ Hz)

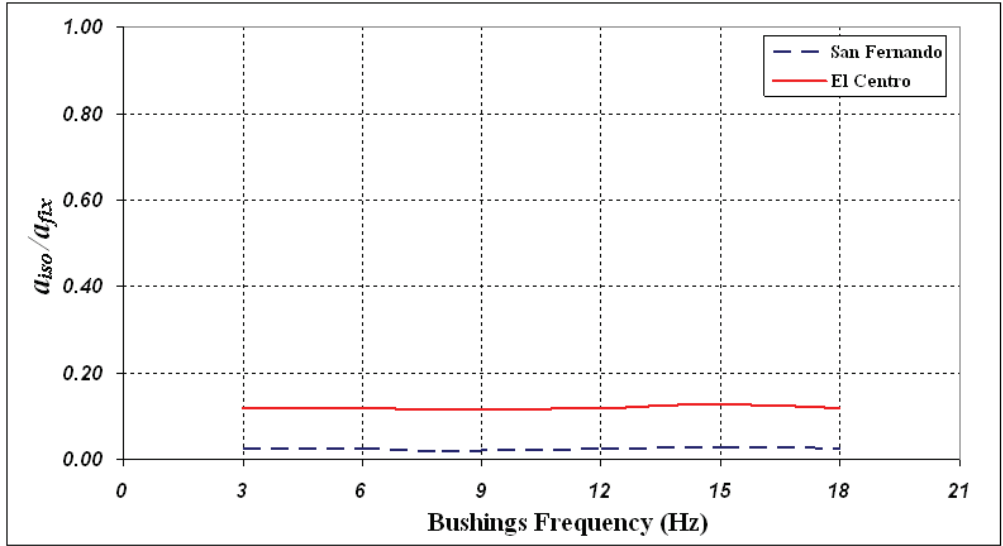


Figure 6-11 Reduction in Transformer Accelerations (f_t=15 Hz)

6.4.2 Bushings Responses

6.4.2.1 Fixed Base

In this section responses of bushings for a range of bushing and transformer frequencies when the supporting transformer is fixed are presented. Figures 6-12 and 6-13 show the acceleration responses for the two site conditions. As it can be seen, the acceleration response of bushings is very high and quite sensitive to the transformer’s natural frequency. Furthermore, the response of bushings mounted on transformers with higher frequencies is higher when the system is located on rock.

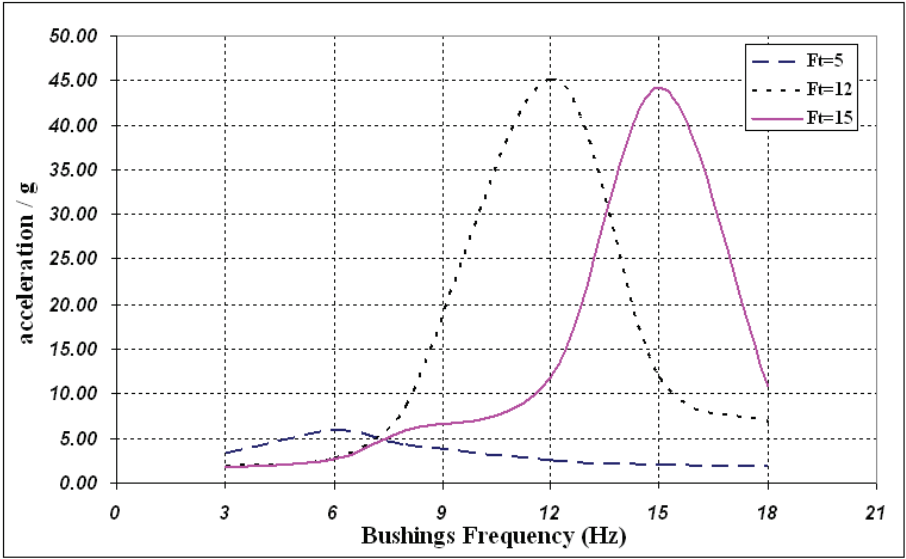


Figure 6-12 Maximum Acceleration Responses of Bushings (San Fernando - fixed base)

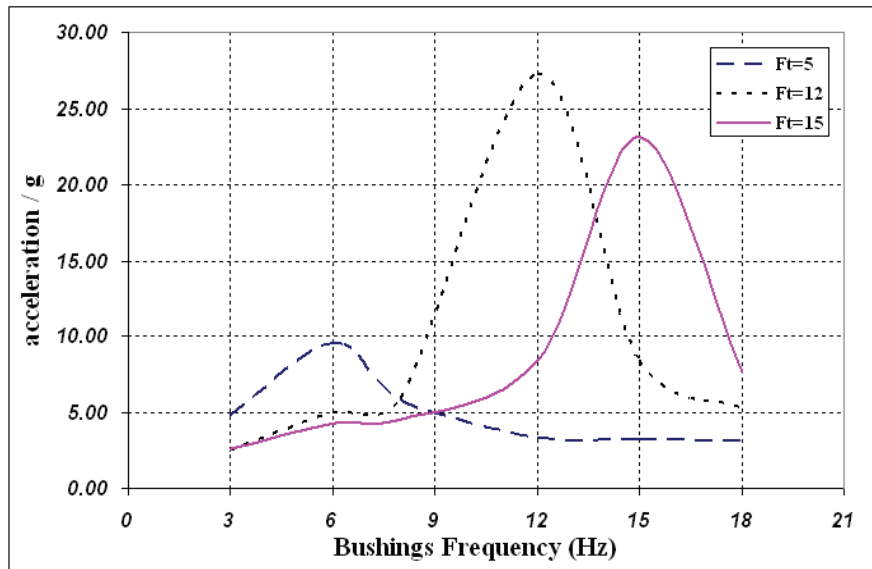
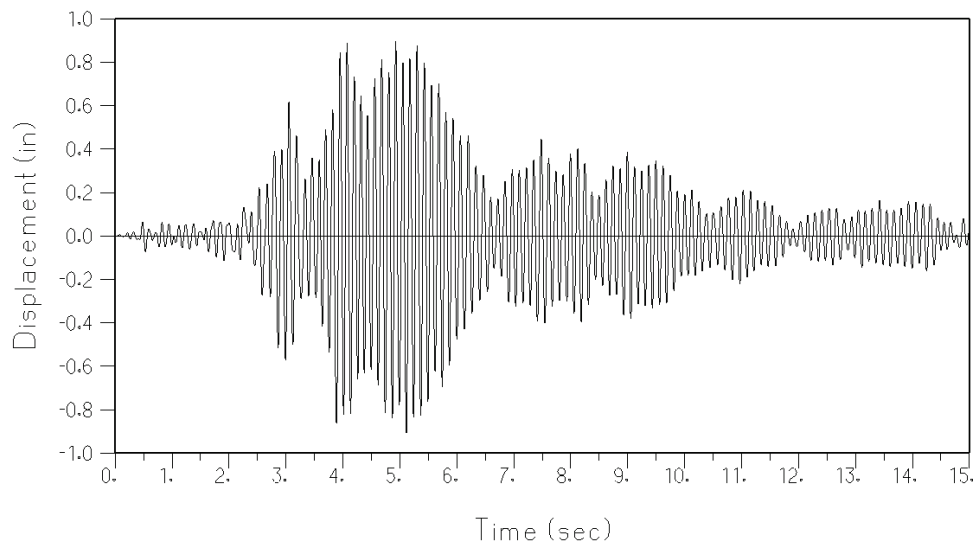
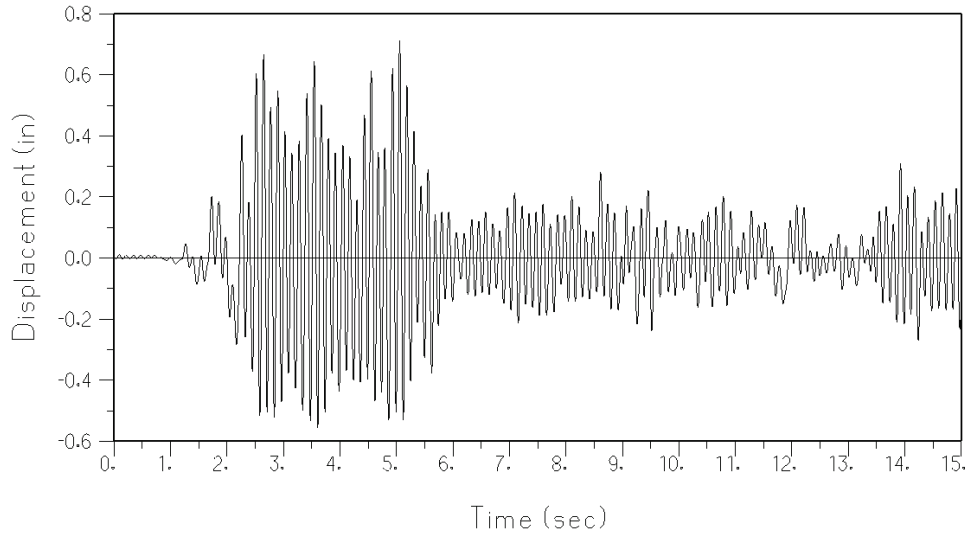


Figure 6-13 Maximum Acceleration Responses of Bushings (El Centro - fixed base)

Since bushings are connected by cables to other equipment in power substations, another important parameter is their displacement responses. Therefore, assessment of bushings displacement during earthquake ground motion is of critical importance to response of interconnecting equipment. The time histories of bushing displacement for Case 15 are shown in figure 6-14.



a) Response to San Fernando record



b) Response to El Centro record

**Figure 6-14 Time History of Bushing Displacement
(Case 15 – fixed base)**

The maximum displacement responses of all bushings supported on transformers with fixed based are shown in figures 6-15 and 6-16.

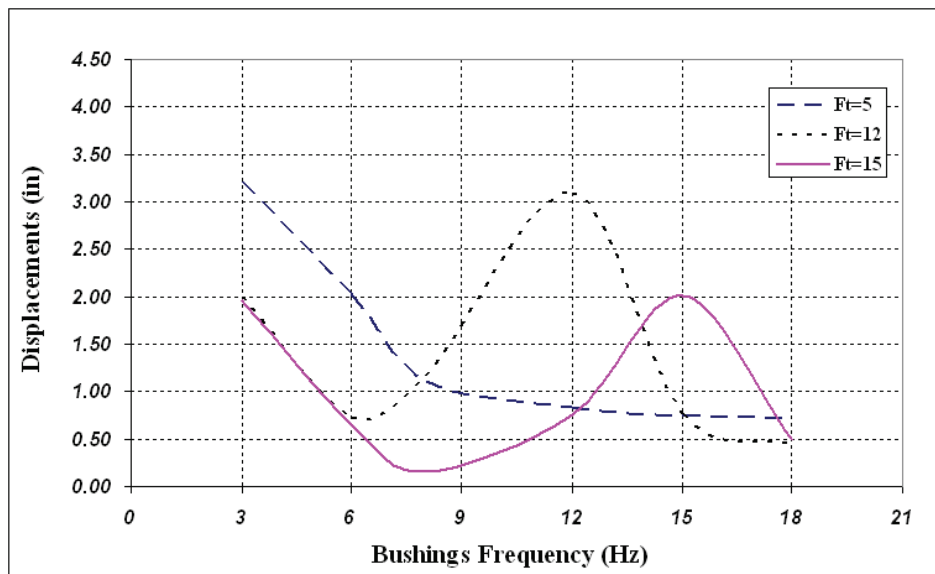


**Figure 6-15 Maximum Displacements of Bushings
(San Fernando - fixed base)**

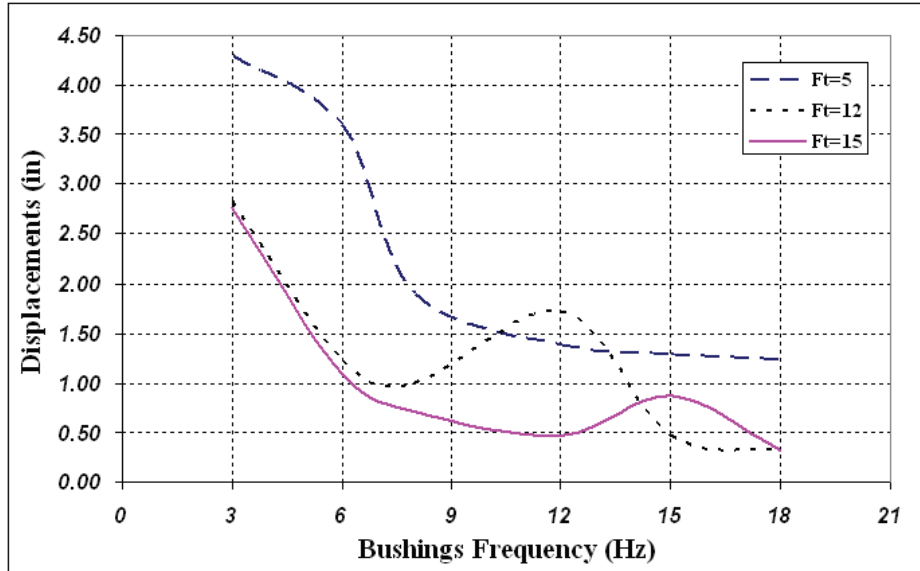


Figure 6-16 Maximum Displacements of Bushings (El Centro - fixed base)

6.4.2.2 Base Isolated

The effect of isolating the transformer with FPS bearings on the response of the bushings is discussed in this section. Figures 6-17 through 6-19 show the bushing acceleration responses for various cases. As it can be seen, the inertia reduction ranges from 50% to more than 95%. The maximum inertia reduction happens when the transformer frequency is very close to the bushings frequency. In these cases, use of FPS results in shifting of the transformer frequency, thus, preventing resonance response. As it was pointed out in previous sections in many practical situations frequencies of transformers and bushings are in a narrow range with the possibility of resonance condition.

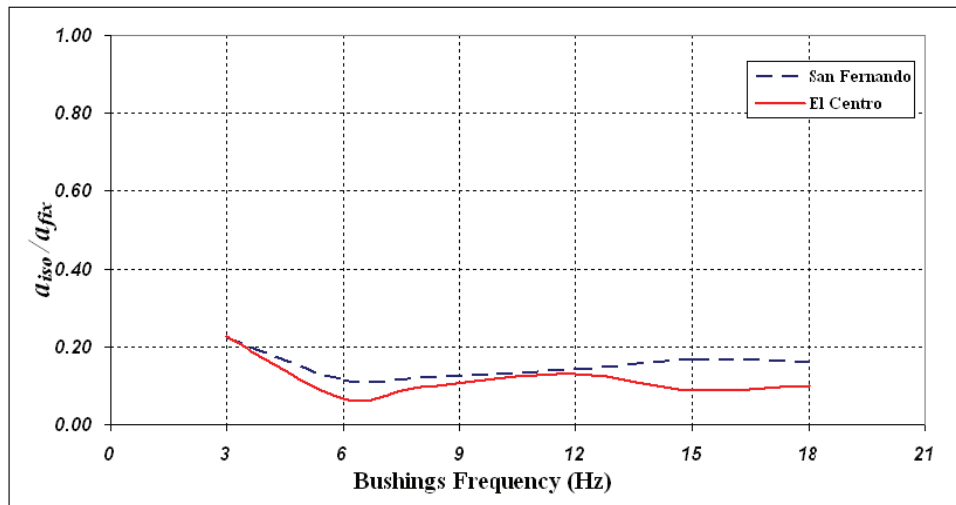


Figure 6-17 Reduction in Bushings Acceleration (Ft=5 Hz)

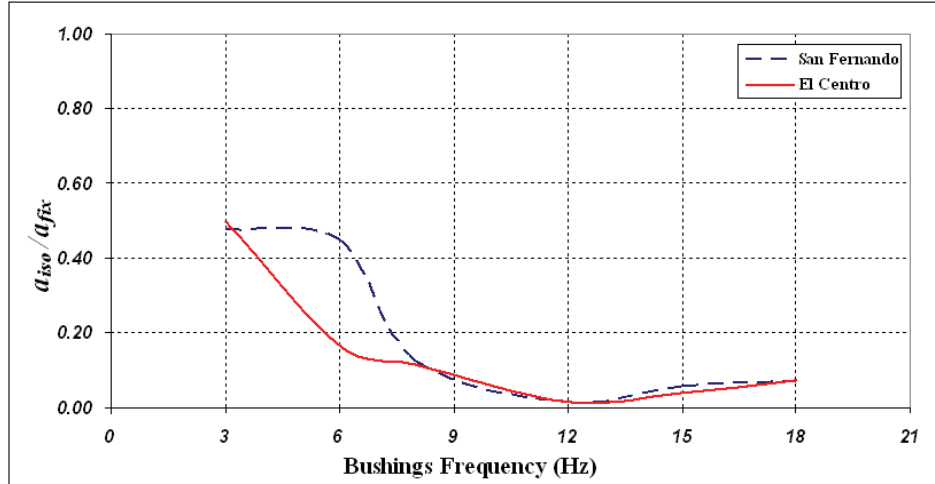


Figure 6-18 Reduction in Bushings Acceleration (Ft=12 Hz)

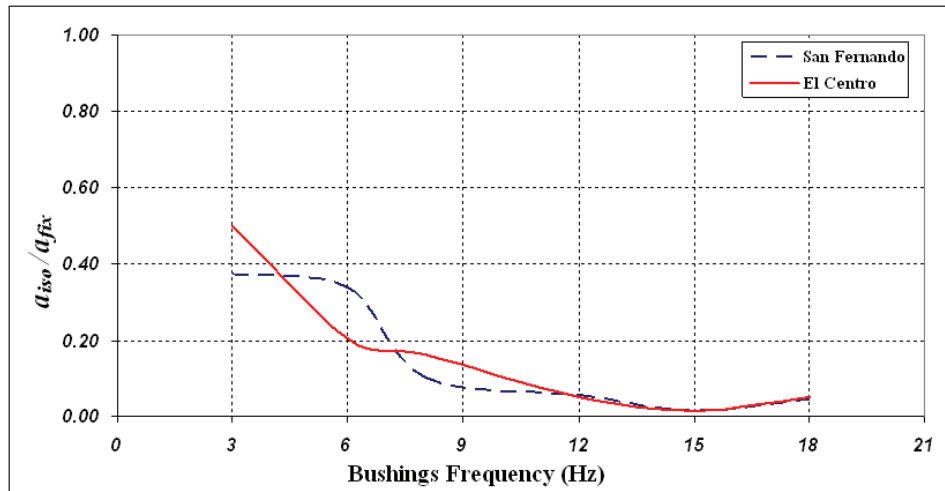


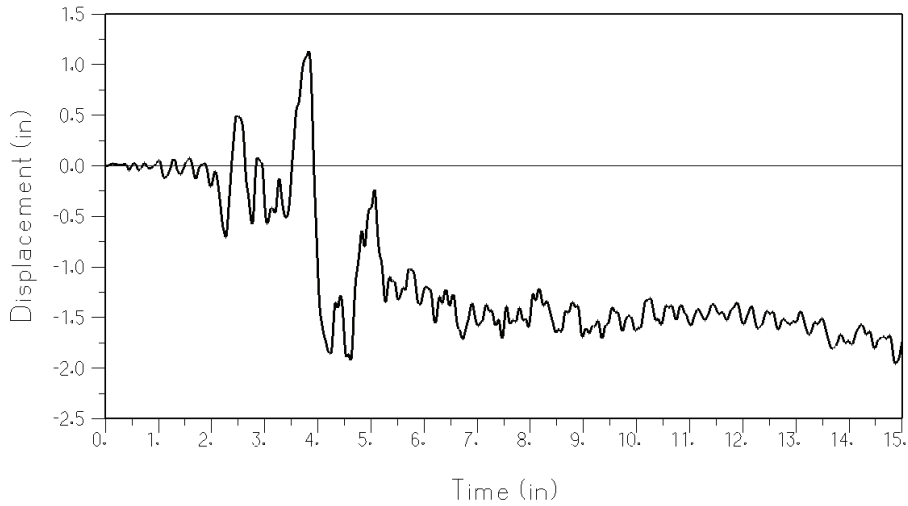
Figure 6-19 Reduction in Bushings Acceleration (Ft=15 Hz)

6.5 Additional Slack Required

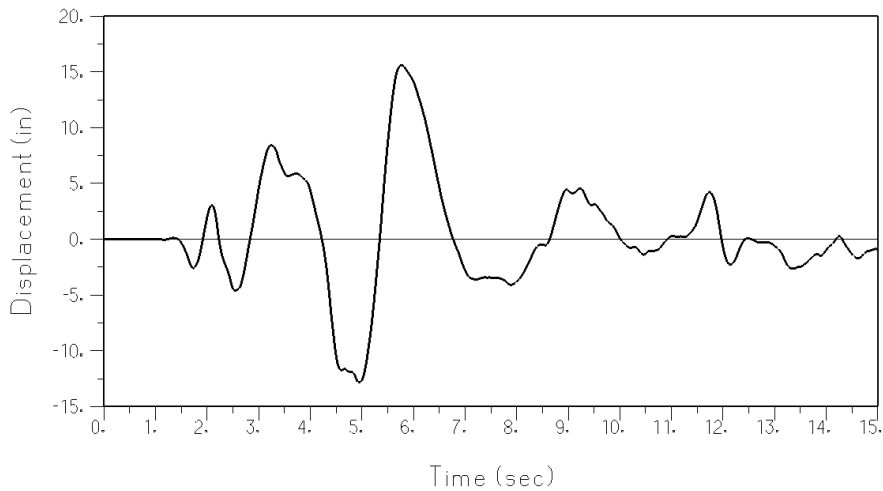
Obviously application of base-isolation will result in an increase in displacement demand as the system frequency is sifted to region of lower acceleration but higher displacement demand. If increased displacement demand is higher than the slack provided (i.e., the cable is taut) then significantly higher forces will be exerted on the bushing through the interconnected electrical equipment. Thus, an important aspect of this study on an actual substation design is to determine if such displacement increase can be easily accommodated without any impact on electrical performance.

Consistent with fixed-based case, bushing displacement time histories for Case 15 are presented for base isolated case in figure 6-20. Bushing displacement when the system is subjected to El Centro (soil) record is significantly higher than when it is subjected to San Fernando (rock)

record by an order of magnitude. The maximum displacement responses of bushings to El Centro record for different base conditions are shown in figure 6-21 and 6-22. The maximum displacement increase as a result of application of base-isolation is about 12.6” (16.9” – 4.3”). That is, additional slack over fixed-base case needs to be provided at 230kV and 550 kV bushing connections to the bus bars.



a) Response to San Fernando record



b) Response to El Centro record

**Figure 6-20 Time History of Bushing Displacement
(Case 15-base isolated)**

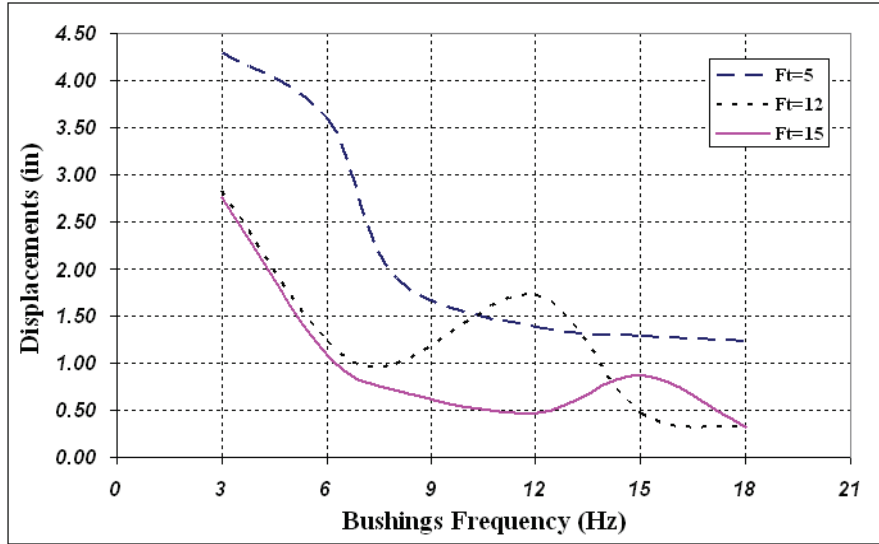


**Figure 6-21 Maximum Bushings Displacements
(El Centro -fixed base)**

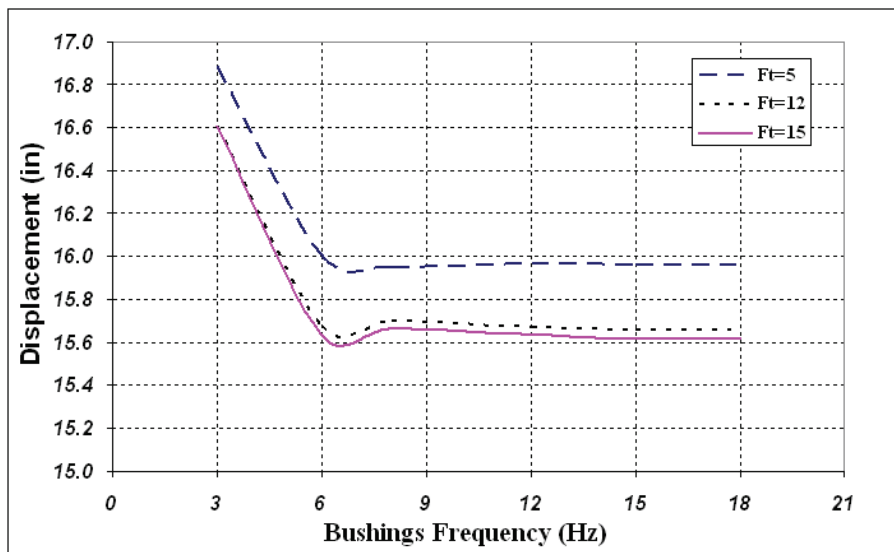


**Figure 6-22 Maximum Bushings Displacements
(El Centro-base isolated)**

Figure 6-23 shows bushing connection to the bus. Based on the above calculation the connection must accommodate 12.6” of slack, which can easily be accommodated as detailed measurement of the geometry indicates that it poses more than 20” of slack. It should be noted that analysis of this cable was performed with various inputs (soil vs. rock and base-isolated vs. fixed) to further assess impact of cable vibration. The model was similar to the model shown in figure 6-2b but it included the cable and an additional SDOF to represent the bus support (insulator and pedestal). The cable was modeled using nonlinear beam elements with large deformation. It was

determined that base-isolation does not have any adverse affect on cable vibration and reaction forces.

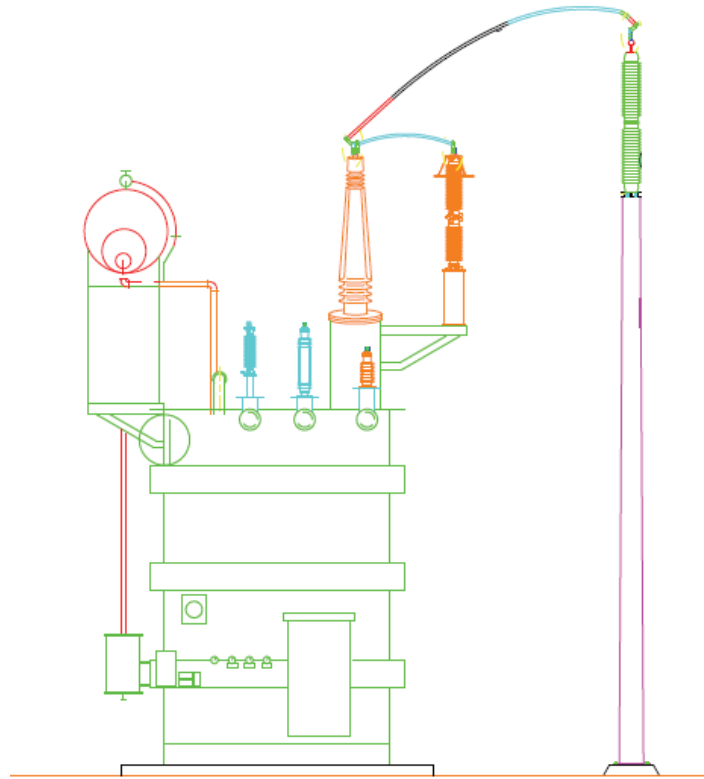


Figure 6-23 230kV Bushing to Bus Connection.

Figure 6-24 shows the 500kV bushing connection to the bus. This connection does not have adequate slack and analyses shows that large forces will be developed without additional slack, especially when the transformer is isolated. However, it is possible to provide 2-ft of slack without any electrical implication by increasing cable length on an upward curvature. Again analyses of the cable (with added length) under various inputs did not demonstrate any adverse affects when base-isolation is employed.

The electrical control cables and tank grounding connections at the base of the transformer will also require special provisions to account for the transformer base motion. Techniques used in building base isolation and/or Plug-Plug flexible cable system can be used to allow for base movement. This will ensure zero down time during an event.

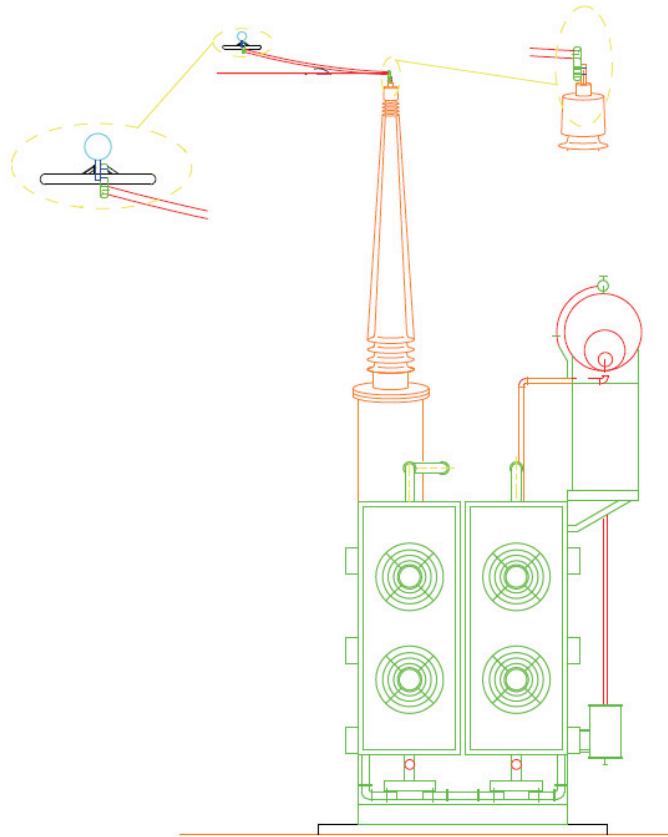


Figure 6-24 500kV Bushing to Bus Connection.

6.6 Check for Uplift

A critical issue with the use of base-isolators, as discussed before, is the possibility of rocking and uplift, which can potentially limit or compromise effectiveness of the isolators.

Figure 6-25 can be used to check the mode of response for the isolated case. Coefficient of friction for the bearing is 0.08, however, as discussed the base-shear consists of the sum of friction and self-centering component of the transformer weight. In other word, the equivalent coefficient of friction¹, μ_{eqvl} , to be used in figure 6-25 is related to inertia reduction (IR) as follow:

$$\mu_{eqvl} = 1 - IR = 1 - 0.86 = 0.14$$

For the response to be governed by sliding mode (i.e., no rocking and uplift), this value must be smaller than width to height (or B/H) ratio for the transformer. Considering figure 6-1, the worse

¹ Maximum of this value or static coefficient of friction must be used. Clearly, this will control.

case (or smaller) value for B/H is 0.62 (or 5'-5" / 8'-8"). Thus, the base-isolated system will have an adequate margin of safety against undesirable rocking (and uplift) mode of response.

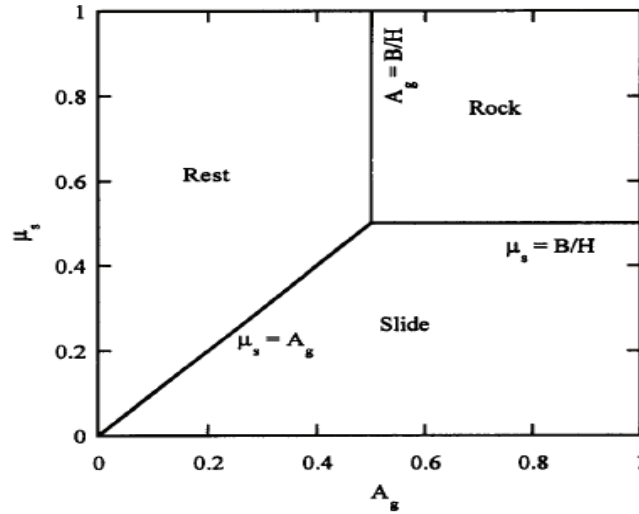


Figure 6-25 Boundaries of Rest, Slide and Rock Modes for Height/Width Ratio of 2 [Shenton 1996]

6.7 Foundation Seismic Forces

Based on IEEE 693, pad-type foundations are designed for a lower force than what is developed in the transformer. For this case study the value of foundation force will be about 45% of transformer weight, which is much smaller than forces that will be developed in the transformer even under rigid body assumption. It can be argued that this is consistent with IEEE 693 Required Response Spectrum (RRS) approach, where 50% spectral values are used in conjunction with allowable stress method.

However, due to nonlinear nature of isolation, a more appropriate comparison between the two cases of fixed and isolated transformer will require the use of actual transformer seismic forces in the design of the foundation. In such situation, it will be shown in Section 8 that the difference between the two cases is significant further demonstrating the beneficial value of base-isolation to mitigate seismic risk and ensure minimum or no damage to critical power system infrastructure during an event.

SECTION 7

INTERNAL COMPONENTS OF HIGH-POWER CORE-FORM ELECTRICAL TRANSFORMERS

Transformers are critical devices, which change or transform voltage levels between two circuits. Current values are also changed in the process. However, the power transferred between the circuits is unchanged, except for a typically small loss. This operation is based on principle of induction discovered by Faraday and works only in presence of alternating or transient current. The induced voltage is proportional to the number of turns linked by the changing flux [Del Vecchio, 2002].

The efficiency of transferring electrical power over long distances increases as the voltage levels rise. This can be seen for the transfer of the electrical power $P = V.I$ noting that:

$$Loss = \frac{\rho LP^2}{AV^2} \quad (7-1)$$

$$Voltagedrop = \frac{\rho LP}{AV} \quad (7-2)$$

In these relations, A is the area of the conductor, L is its length, ρ is electrical resistivity, and V and I are the electric potential and current. Since P , L , ρ are given, the loss and voltage drop can be made as small as desired by increasing the voltage V . However, there are other limits to this increase in voltage, such as the availability of adequate and safe insulation structures and the increase of corona losses. Also, a balance should be achieved between the extra cost of material due to increase in A and the gained loss reduction.

In practice, voltages in the range of 100-500 kV and more recently as high as 765 kV are used for long distance power transmission. These voltages are, however, incompatible with much lower voltages safe for households use. In addition, due to reasons of cost and efficiency generators are designed to produce electrical power at voltage levels of 10 to 40 kV. Hence, there is a need for power transformers to boost the voltage at the generation end and to decrease it at the receiving end. The task of decreasing the voltage is usually done in more than one step.

There is often a need for adjustments in voltage to compensate for the voltage loss in the lines and other equipment. These voltage drops depend on the current level and vary throughout the day. This is accomplished by equipping transformers with tap changers, that are devices adding or subtracting turns from a winding, thus altering its voltage. Load or no-load tap changers are used to perform this task under load conditions or with the power disconnected from transformer, respectively.

Transformers are fairly passive devices containing very few moving parts. These include tap changers and cooling fans, which are needed on most units and sometimes pumps that are used on oil-filled transformers to improve cooling. Transformers are expected to have a long life of 25-50 years with little need for maintenance. There are a few routine maintenances. The oil quality must be checked periodically and filtered or replaced if necessary in the oil-filled transformers to protect them against electrical breakdown. Other key transformer parameters

such as oil and winding temperatures, voltages, currents, and oil quality as reflected in gas evolution are monitored continuously in many power systems [Del Vecchio, 2002].

7.1 Components of the Internal Structure

7.1.1 Core

The core is made of thin layers or laminations of dielectric steel especially developed for its good magnetic properties. The magnetic properties are best in the rolling direction. Therefore, in a good core design this is the direction the flux should naturally want to take. The lamination can be wrapped around the cores or stacked. Wrapped or wound cores have few, if any, joints so they have the ability to carry the flux nearly uninterrupted by gaps. However, the stacked cores have gaps at the corners where the core steel changes direction. These results in poorer magnetic characteristics compared to wound cores. Stacked cores are much more common in larger power transformers. The laminations for both types of cores are coated with an insulating coating to prevent development of large eddy current paths, which could lead to high losses.

In stacked cores for core-form transformers; the coils are circular cylinders that surround the core. Hence the preferred cross section shape of circle is chosen for the core since this will maximize the flux carrying area. In practice, the core is built in steps that approximate a circular cross section. The space between the core and the innermost coil is needed to provide insulation clearance for the voltage difference between the winding and the core, which is at ground potential and is also used for structural elements [Del Vecchio, 2002].

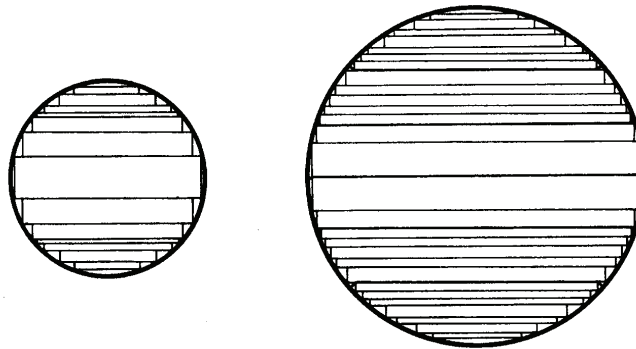


Figure 7-1 Core Sections, 7-Step Taped (left); and 14-Step Banded (right) [Del Vecchio, 2002].

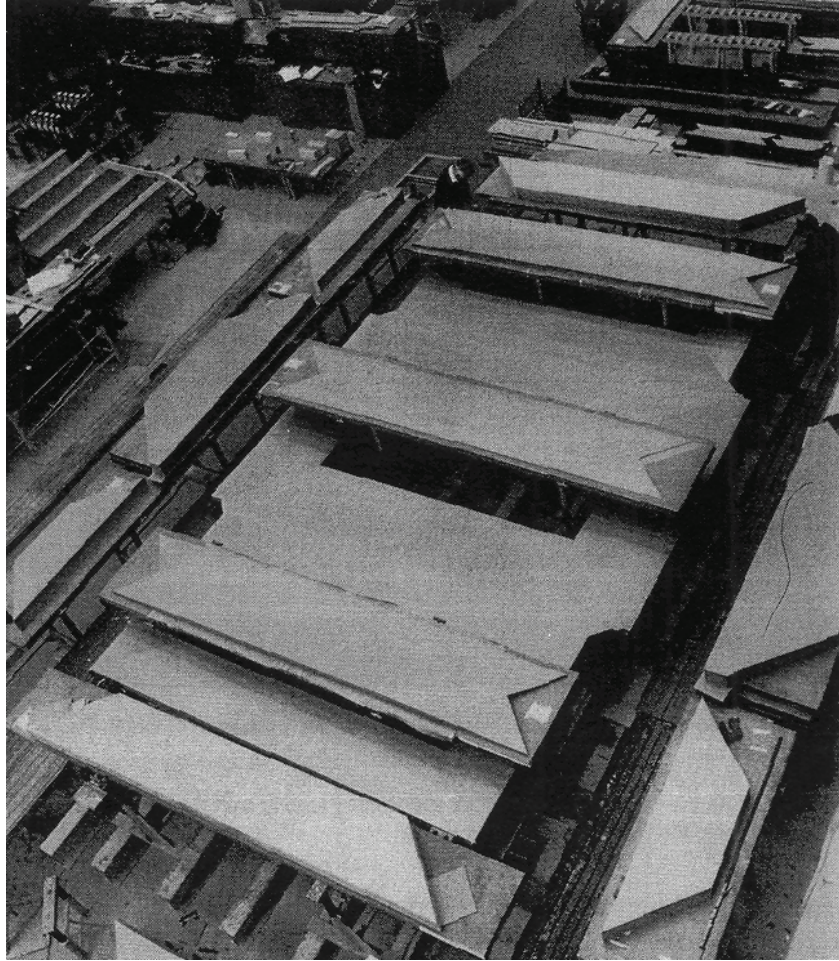


Figure 7-2 Four-limb Core in Course of Building (GEC Alsthom) [Del Vecchio, 2002].

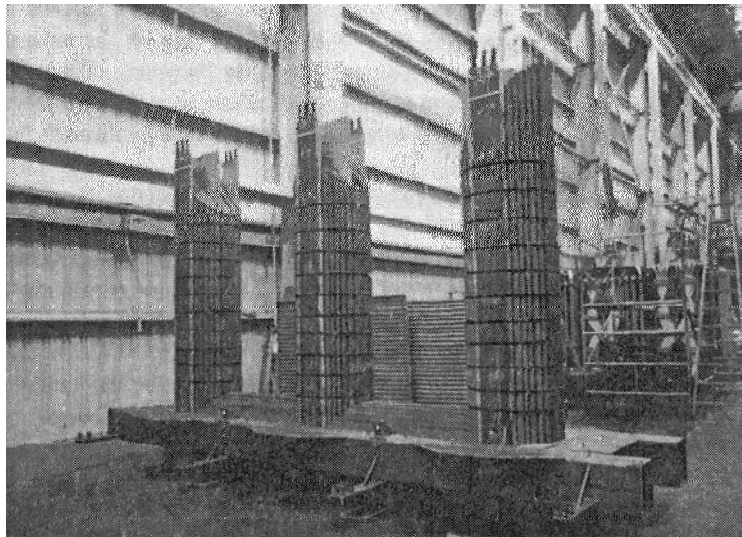


Figure 7-3 Three-phase Stepped Core for a Core-form Transformer without the Top Yoke [Heathcote, 1998].

7.1.2 Transformer Cooling

Electric resistance, changing flux in the electrical steel, and stray time-varying flux in metallic tank walls and other metallic structures result in losses inside a transformer. These losses lead to temperature rises that must be controlled by cooling. The primary cooling media for transformers are oil and air. In oil cooled transformers, the coils and core are immersed in an oil-filled tank. Radiators or other types of heat exchangers are usually used to circulate the oil so that the ultimate cooling medium is the surrounding air or possibly water for some types of heat exchangers.

The cooling medium in contact with coils and core must provide adequate dielectric strength to prevent electrical breakdown or discharge between components at different electric potentials. Oil immersion is more common in higher voltage transformers because of its higher breakdown strength compared to air. One can often rely on natural convection of oil through the windings driven by buoyancy effects, to provide adequate cooling so that pumping is not necessary. Air is a more efficient means of cooling when it is blown by fans through windings for air-cooled units. Oil is the preferred medium for units not restricted by limitations like weight, mobility and fire hazard for indoor transformers. There are other cooling media for special case like reduction of fire hazard such as hexafluoride gas or silicone oil.

7.1.3 Windings

There are two main methods of winding the coils for core-form power transformers. Both are cylindrical coils, having an overall rectangular cross section. In a disk coil, the turns are arranged in horizontal layers called disks, which are wound alternately out-in, in-out. The winding is usually continuous and the last inner or outer turn gradually transitions between the adjacent layers. If the disks have only one turn, the winding is called a helical winding. The total number of turns usually dictates whether the winding is a disk or helical winding. The turns within a disk are usually touching and a double layer of insulation separates the metallic conductors. There is open space between the disks except for structural separators called key spacers. This allows room for cooling fluid to flow between the disks, in addition to providing clearance for bearing the voltage difference between them [Del Vecchio, 2002].

In a layer coil, the coils are wound in vertical layers, top-bottom, bottom-top, etc. The turns are typically wound in contact with each other in layers that are separated by means of spacers so that cooling fluid can flow between them. These coils are also usually continuous with the last bottom or top turn transitioning between the layers.

Both types of windings are used in practice and one or the other can be more efficient in certain applications. Generally, they can both be designed to function well in terms of ease of cooling, ability to withstand high voltage surges, and mechanical strength under short-circuit conditions.

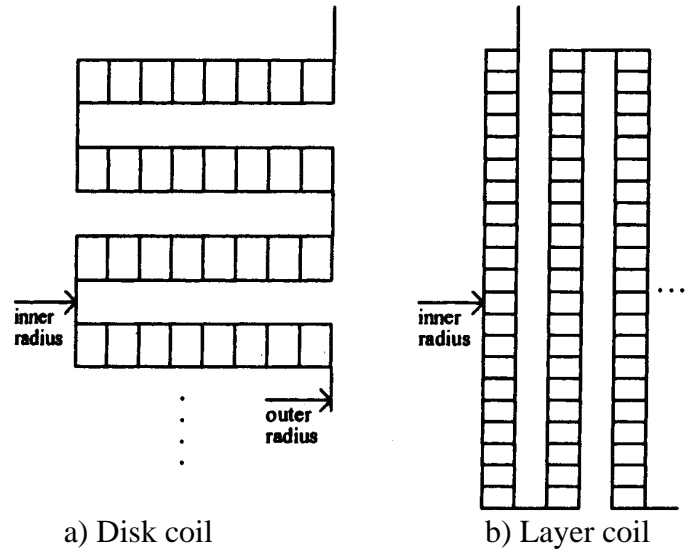


Figure 7-4 Two Major Types of Coil Construction for Core-form Power Transformers [Heathcote, 1998].

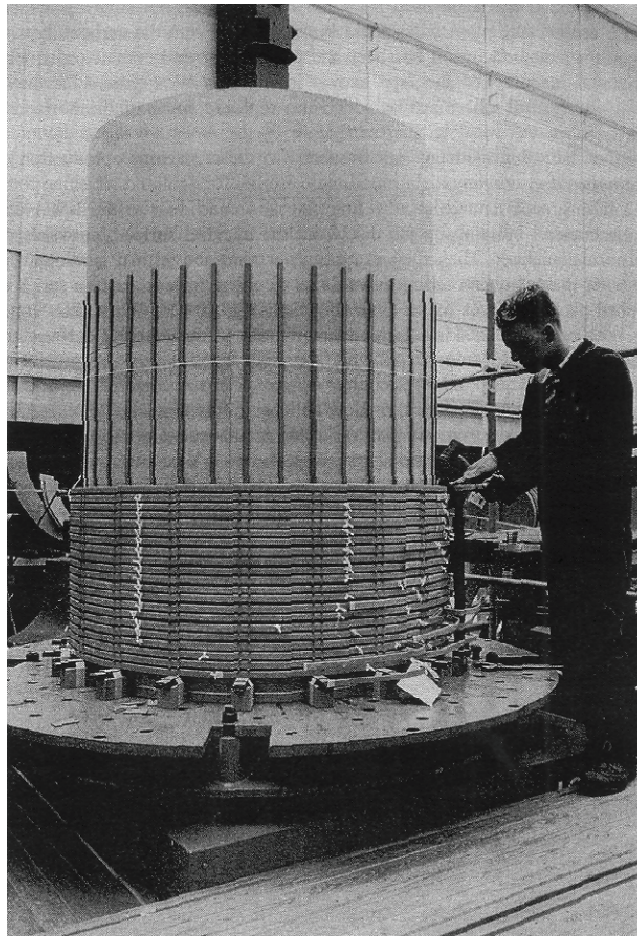


Figure 7-5 Winding in Progress [Heathcote, 1998].

When the coils are wound with more than one wire or cable in parallel, transposition or cross-overs must be inserted which interchange the positions of cables at various positions along the winding. This will cancel loop voltages induced by stray flux that would otherwise drive currents around the loops formed when the parallel turns are joined at either end of the winding, and hence create extra losses.

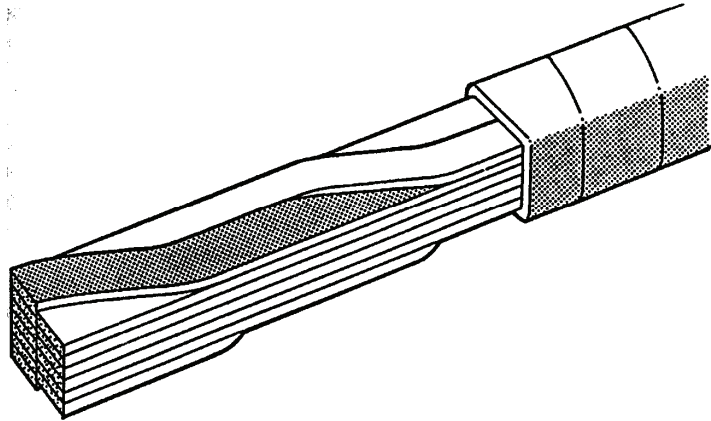


Figure 7-6 Continuously Transposed Conductor [Heathcote, 1998].

The stray flux also causes localized eddy currents in the conducting wire whose magnitude depends on dimensions of the wire cross-section. Subdividing the wire into strands of smaller cross-sectional dimensions can reduce these eddy currents and their associated losses. However, these strands are then in parallel and must therefore be transposed to reduce the loop voltages and currents. This is done during the winding process when the parallel strands are wound individually. Wire of this type, called magnet wire, consists of strands covered with an insulating paper wrap. The transposition can also be built into the wire to make what is called the continuously transposed wire, generally consisting of a bundle of 5-83 strands, each covered with a thin enamel coating. Strands are transposed one at a time along the cable so that all the strands are eventually transposed approximately every 10-12 inches along the length of the cable. The overall bundle is then sheathed in paper wrap [Del Vecchio, 2002].

7.1.4 Insulating Structure

Transformer windings and leads operate at high voltages relative to the core, tank, and structural elements. Also, different windings and even different parts of the same winding have different voltages. This requires providing some form of insulation between these various parts to prevent voltage breakdown or corona discharges. The surrounding oil or air that provides cooling has some insulating value. This oil has a special composition and must be purified to remove small particles and moisture. The type of oil most commonly used is called transformer oil. Further insulation is provided by paper covering over the wire or cables. This paper has a high insulation value when saturated with oil. Other types of wire covering are sometimes used for specialty applications. Pressboard is another insulation structure that is generally available in sheet form, often made in cylindrical shape. This is a material of cellulose fibers compacted together into a

fairly dense and rigid matrix. Key spacers, blocking material, pressure rings, and lead support structures are also commonly made of pressboard.

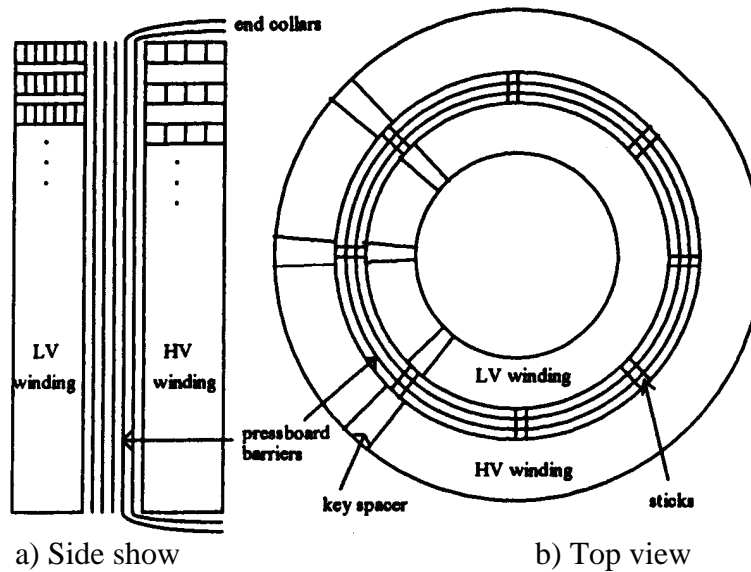


Figure 7-7 Major Insulation Structure Consisting of Multiple Barriers Between Windings. Not all the key spacers or sticks are shown [Del Vecchio, 2002].

Although normal operating voltages are quite high, 10-500 kV, the transformer must be designed to withstand even higher voltages that can occur if lightning strikes the electrical system or when power is suddenly switched on or off in some part of the system. However infrequently these happen, unless the insulation is designed to withstand them they could permanently damage the insulation, disabling the unit. These events usually have short durations. There is a time dependency on how insulation breaks down. A combination of oil and pressboard barriers can bear higher voltages for shorter periods of time. Therefore, a high-voltage short-duration impulse is no more likely to cause breakdown than a long-duration low-voltage pulse. This means that the same insulation that is used to withstand normal operating voltages that are continuously present can also withstand the high voltages briefly present when lightning strikes or during switching operation. Lightning or surge arrestors are used to limit these abnormal voltages to insure that they do not exceed the breakdown limits determined by their expected duration. These arrestors thus guarantee that the voltages will not go above a certain value so that breakdown will not occur, provided their durations remain within the expected range.

Due to the different dielectric constants of oil or air and paper, the electric stresses are unequally divided between them. Because the oil dielectric constant is half of that of paper, and that of air is even a smaller fraction of paper's, the electric stresses are generally higher in oil or air than in the paper insulation. Unfortunately, oil or air has a lower breakdown stress than paper. For oil, it has been found that subdividing the oil gaps by mean of thin insulating barriers, usually made of pressboard, can raise the breakdown stress in oil. Thus, large oil gaps between the windings are usually subdivided by multiple pressboard barriers, referred to as the major insulating structure.

Long vertical narrow sticks glued around the circumference of the cylindrical pressboard barriers maintain these oil gap thicknesses. The barriers are often extended by means of end collars curving around the ends of the winding to provide subdivided oil gaps at either end of the winding and strengthen these end oil gaps against voltage breakdown

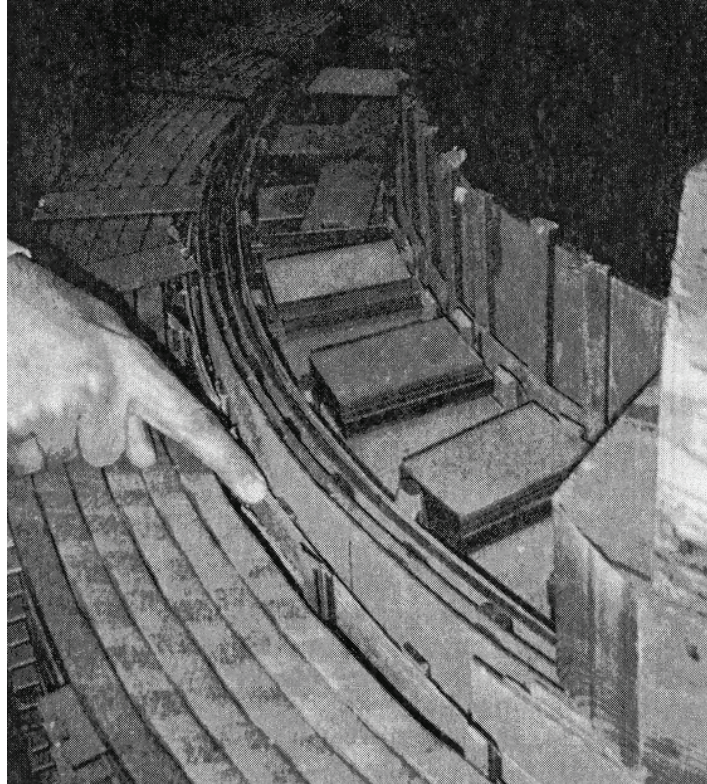


Figure 7-8 Top View of Two Windings Showing the Major Insulation Structure, Key Spacers, and Sticks [Del Vecchio, 2002].

The minor insulation structure consists of the smaller oil gaps separating the disks and maintained by key spacers. Key spacers are narrow insulators, usually made of pressboard, that are spaced radially around the disk's circumference. Usually these oil gaps are small enough that subdivision is not required. Also the turn-to-turn insulation, usually made of paper, can be considered as part of the minor insulation structure.

The leads which connect the windings to bushings or tap changers or to other windings are also at high voltage and pass close to tank wall or structural supports which are grounded and must be properly insulated. They may also pass close to other leads at different voltages. Additional insulation may be required at bends in the leads, particularly if they are sharp, since high voltages can be developed in these areas.

In addition to voltage breakdown in oil that can be resisted by means of barrier subdivisions, there is another breakdown process, which has to be guarded against. This is breakdown due to creep that occurs along the surface of the insulation. It requires sufficiently high electric stresses directed along the surface present over sufficiently long uninterrupted paths. Thus, the barriers

themselves, sticks, key spacers, and lead supports can be a source of this breakdown. It is desired to position these insulation structures so that their surfaces conform to voltage equipotential surfaces to which the electrical field is perpendicular, thus eliminating any electric field directed along the surfaces. This, however, is not always possible and a compromise must be made.

The major and minor insulation designs, such as overall winding to winding and the number of barriers as well as disk to disk separation and paper covering thickness, are often determined by design rules based on extensive experiments. However, it is often desirable in cases of newer or unusual designs to do a field analysis using a finite element program or other numerical procedure. This can be especially helpful when potential of creep breakdown exists. However, it should be added that the breakdown process is not completely understood and deciding what level of electrical stress is acceptable usually involves some judgment [Del Vecchio, 2002].

7.1.5 Structural Elements

Under normal operating conditions, the transformer windings are under quite modest electromagnetic forces. However, the winding currents can increase 10-30 fold in a short-circuit fault, resulting in forces of 100-900 times normal since the forces increase proportional to the square of electric currents. The windings and supporting structure must be designed to withstand these fault current forces without any permanent distortion or damage. The current protection devices that are usually installed will interrupt the fault currents after a few cycles. Fault currents can be caused by rare events like a falling tree on transmission lines that provides a direct current path to ground, or by animals or birds bridging across two lines belonging to different phases. However, the probability of such accidents over a long life of up to 50 years is credible enough to justify design for such forces.

The coils are usually supported by thick boards of pressboard or other material covering the winding ends, which are called pressure rings. They have a center opening that allows the core to pass through. The rings are in the range of 1-4 inches for large power transformers. Since all the windings are not of the same height, some blocking made of pressboard or wood is required between the top of the windings and the rings. In order to provide some clearance between the high winding voltages and the grounded core and clamp, additional blocking is usually provided between the ring and the top yoke and clamping structure [Del Vecchio, 2002].

Vertical tie-plates that pass along the sides of the core join the top and bottom clamps. These tie plates have threaded ends that are used to pull the top and bottom clamps together by means of tightening bolts, compressing the windings. These compressive forces are transmitted along the windings via the key spacers strong enough in compression to accommodate these forces. The clamps and tie plates are made of steel. Axial forces that tend to elongate the windings when a fault occurs will have to pull the tie plates in tension. Also since the coils and core are lifted as a unit through lifting hooks attached to the clamps, the tie-plates must be strong enough to carry the gravitational load. The tie plates are usually about 1 cm (3/8 in) thick. They are of varying width depending on the expected short circuit forces and transformer weight, and are often subdivided in width to reduce eddy current losses [Del Vecchio, 2002].

The radial fault forces are countered inwardly by means of the sticks separating the oil barriers, and through additional support next to the core. The windings themselves, particularly the innermost one, provide additional resistance to inward radial forces. The radial force applied to the outermost winding is usually outward and puts the wires or cables in tension. Since there is no supporting structure on the outside to counter these forces, the material itself must be strong enough to resist these tensile forces. A measure of the material's strength is its proof stress that is the stress required to produce a permanent elongation of 0.2% (sometimes 0.1%). Copper of specified proof stress can be ordered from the wire or cable company.

There are also extra loads acting upon leads during a fault that are produced by the stray flux from the coils or from the nearby lead interacting with the lead's current. Therefore, braces made of wood or pressboards that extend from the clamps are used to support the leads. This lead support structure can be quite complicated, especially if there are many leads and interconnections and is usually custom made for each unit.

The assembled coil, core, clamps, and lead structure are placed in a transformer tank. The tank serves many functions including containment of the oil for an oil-filled unit, protection of the coils and other transformer structures and also protecting personnel from the high voltages present. It keeps stray flux from getting outside the tank if it is made of soft (magnetic) steel. The tank is also usually made airtight to prevent air from entering and oxidizing the oil.

There are also numerous attachments to the tank such as bushings for getting the electrical power into and out of the unit, and transferring sensor information to remote processors and receiving control signals, and radiators with or without fans to provide cooling. There is a separate tank compartment on certain units for tap changing equipment. Also attached to some of the tanks over the top of the radiators are conservators. They are large, usually cylindrical, structures that contain oil in communication with the main tank oil. A conservator also has an air space, which is separated from the oil by a sealed diaphragm. Thus, the flexible diaphragm accommodates the changes in the tank oil volume due to temperature changes, while maintaining a sealed oil environment [Del Vecchio, 2002].

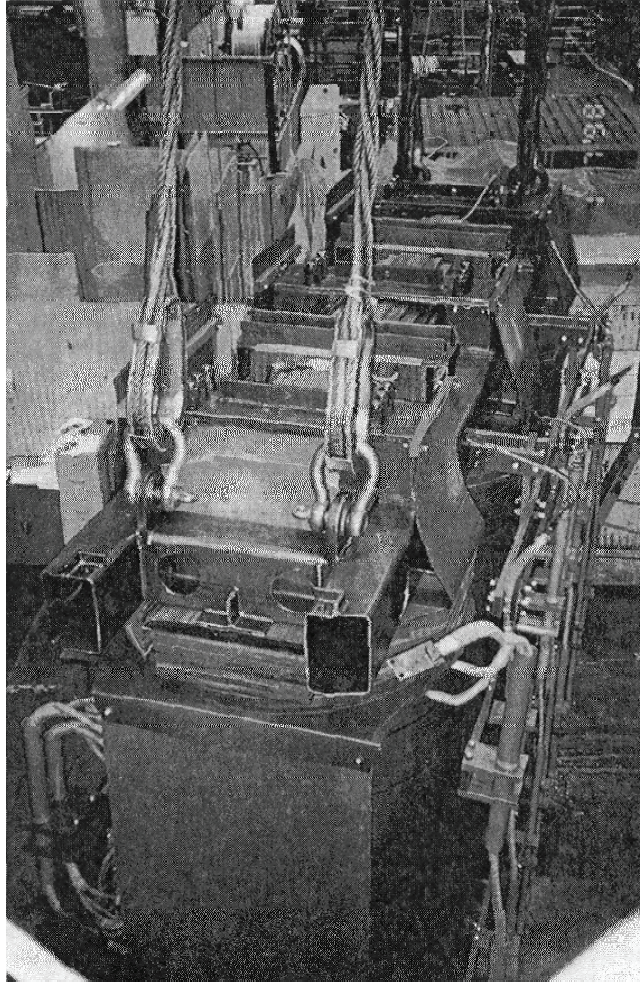


Figure 7-9 Top View of Clamping Structure for a 3-phase Transformer [Del Vecchio, 2002].

7.2 Mechanical Design of Internal Components

Transformers undergo large forces during fault conditions and must be designed to withstand them. These fault currents must be calculated for the standard fault types such as single line to ground, double line to ground, line to line, and all three lines to ground. The data in this section on mechanical design of internal components are based on Del Vecchio [Del Vecchio, 2002] unless otherwise mentioned.

The force density (force/unit volume), f , generated in the windings by the magnetic induction, B , is determined by Lorentz force law:

$$f = J \times B \quad (7-3)$$

where J is the current density and SI units are used. An electrical finite element analysis is performed to determine the values of magnetic induction, and hence f , inside the transformer. These force densities are used to determine differences in forces and stresses. To allow for a transient overshoot, the currents are multiplied by an asymmetry factor. This procedure can still

be considered static since it does not take the effects dynamic effects of the sudden application of load such as excitations into account. Where these dynamic effects are important, the results of a few studies on these dynamic effects are used to adopt an appropriate enhancement factor [Del Vecchio, 2002].

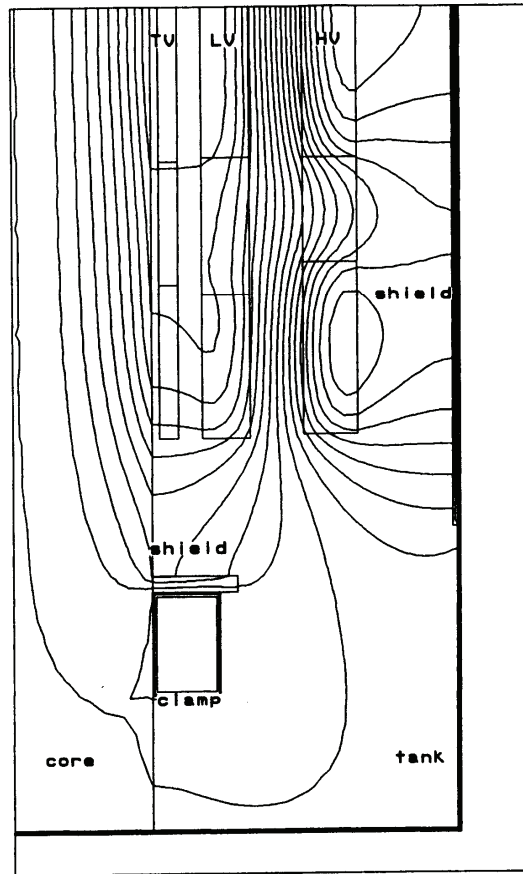


Figure 7-10 Plot of Transformer Leakage Flux. Only the bottom half is shown and the figure is assumed to be cylindrically symmetrical about the core center line. [Del Vecchio, 2002].

7.2.1 Force Calculations

As mentioned, the force density throughout the winding is determined through use of finite element analysis. For radial pressure, the radial stresses at each level are integrated to give the pressure at that level and the worst case is used for stress analysis. It should be noted that vector integration of all these force densities results in a total force of zero. Likewise, the axial force density at each level is integrated and the worst case is used for stress analysis. The axial forces are also summed, starting at the bottom of the coil and their sum is a net upward or downward force that is countered by an equal and opposite force by the pressure ring. Depending on the direction of the force, the ring exerting this force will be the top or bottom ring. The gravitational forces are ignored compared to electromagnetic forces. Starting from bottom or top accordingly, sum of the forces is maximum at a point. This force is called the maximum compressive force

and is a worst-case force used in the stress analysis. The sum of axial loads in all the windings should be zero [Del Vecchio, 2002].

The pressure rings are sized based on the net upward or downward axial force due to all the windings, called the total end thrust. If the windings are symmetric about a horizontal center plane, the total axial force on each winding is almost zero and no end thrust is present. However, when one or more windings are even slightly offset vertically from the others, net axial forces develop on each winding that push some windings up and some down. To take into account possible misalignment in the transformer's construction, it is a good practice to include some offset, say $\frac{1}{4}$ to $\frac{1}{2}$ in, in the calculations [Del Vecchio, 2002].

7.2.2 Stress Analysis

Stresses should be calculated from the resulting forces. Due to the complexity of the structure of windings and the dissimilar materials used and the many openings for the cooling oil, suitable approximations should be made to simplify the complicated stress analysis.

In practice, the windings on different levels of the winding are connected to each other to maintain electrical continuity. However, the coil is assumed to have distinct horizontal sections that are closed on themselves forming rings [Del Vecchio, 2002].

Another approximation is made for the cables that comprise the windings. While magnet wires consist of a single strand of copper surrounded by paper covering and are treated almost without approximation, transposed cables consist of multiple enamel coated copper strands arranged in a nearly rectangular pattern. There is some rigidity in the collection of strands because of transpositions. In addition, bonded cable is often used in which all strands are bonded together by means of epoxy coating over the enamel that is subjected to a heat treatment. The cable can be treated as a rigid structure in this case, though there are questions on how to assess its material properties. Without bonding, the cable is assumed to have a radial thickness equivalent to 2 radial strands for radial force considerations. If there is bonding, a radial thickness equivalent to 80% of the actual radial thickness is assumed [Del Vecchio, 2002].

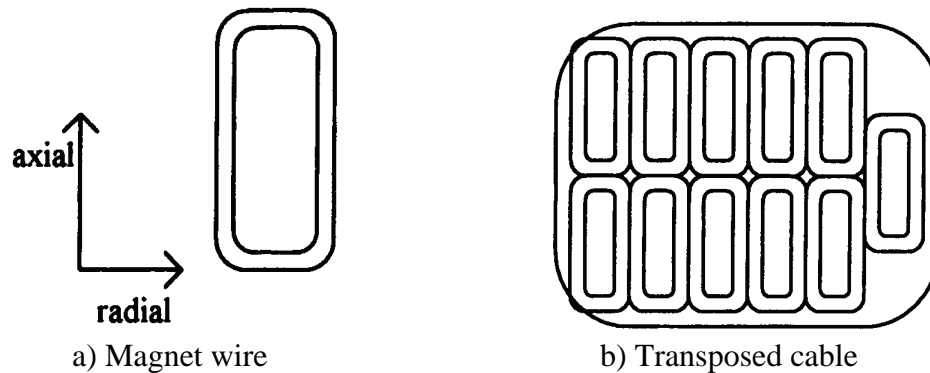


Figure 7-11 Types of Wire or Cable Used in Transformer Coils [Del Vecchio, 2002].

7.2.2.1 Compressive Stress in Key Spacers

The maximum axial compressive force F_c is used for the purpose of obtaining the key spacer compressive stress σ_{ks} , according to:

$$\sigma_{ks} = \frac{F_c}{N_{ks} W_{ks} B} \quad (7-4)$$

where N_{ks} is the number of key spacers around the section, W_{ks} is the width of a key spacer, and B is the radial build of the coil. Key spacers with maximum compressive stresses as high as 310 MPA (45,000 psi) are used [Del Vecchio, 2002].

7.2.2.2 Axial Bending Stress per Strand

The maximum axial force F_a over the vertical subdivisions is calculated for each coil. The number of strands in the entire coil, N_s , is given by [Del Vecchio, 2002]

$$N_s = N_t N_h N_w N_{st} \quad (7-5)$$

where N_t is the number of turns/leg, N_h is the number of cables/turn high (radially), N_w is the number of cables/turn wide (axially), and N_{st} is the number of strands/cable. For the coils consisting of two separate center fed windings stacked axially with each of them having electrical turns, the winding is divided into N_p sections for this analysis, and the maximum force/unit length on a single strand, q_{st} , is given by:

$$q_{st} = \frac{N_p F_a}{N_s \pi D_m} \quad (7-6)$$

where D_m is the average diameter of the coil.

This problem can be analyzed analogous to a uniformly loaded rectangular beam with built-in ends. The moment is calculated as [Del Vecchio, 2002].

$$M(x) = \frac{q}{2} \left[x(L-x) - \frac{L^2}{6} \right] \quad (7-7)$$

and the maximum stress will be :

$$\sigma_{x,\max} = \frac{q}{2t} \left(\frac{L}{h} \right)^2 \quad (7-8)$$

Introducing the actual load into to this equation, the maximum axial bending stress can be calculated as :

$$\sigma_{x,\max} = \frac{N_p F_a}{2N_s \pi D_m t} \left(\frac{L}{h} \right)^2 \quad (7-9)$$

The span length, L , can be calculated as:

$$L = \frac{\pi D_m}{N_{ks}} - W_{ks} \quad (7-10)$$

The strand height h and thickness t apply to a single strand, whether in a cable having many strands or as a single strand in a magnet wire. For bonded cables, the maximum axial bending stress is divided by 3 to take into account the greater rigidity of bonded cable [Del Vecchio, 2002].

7.2.2.3 Tilting Strength

If large enough, the axial compressive force that is applied to the key spacers can cause tilting in the individual strands of the conductors that are pressed between the key spacers. Considering a small section in the azimuthal direction of length Δl , the pressure exerts a torque, τ_c , given by [Del Vecchio, 2002]:

$$\tau_c = P_c (t \Delta l) h \sin \theta \quad (7-11)$$

where t is the radial thickness of the strand and where $t \Delta l$ is the area on which the pressure P_c acts. The axial height of the strand is h and θ is the tilting angle from the vertical, assumed to be small. Due to tilting, the material of the ring will stretch above its axial center and compress below it. This produces stresses in the ring that cause the opposing torque. y being the distance above the axial center of the strand, it follows that:

$$\sigma = E \varepsilon = \frac{E y \tan \theta}{R} \quad (7-12)$$

$$F_r = \sigma (t \Delta y) \Delta \varphi = \sigma (t \Delta y) \frac{\Delta l}{R} \quad (7-13)$$

where E is the Young's modulus, and F_r is an inward force.

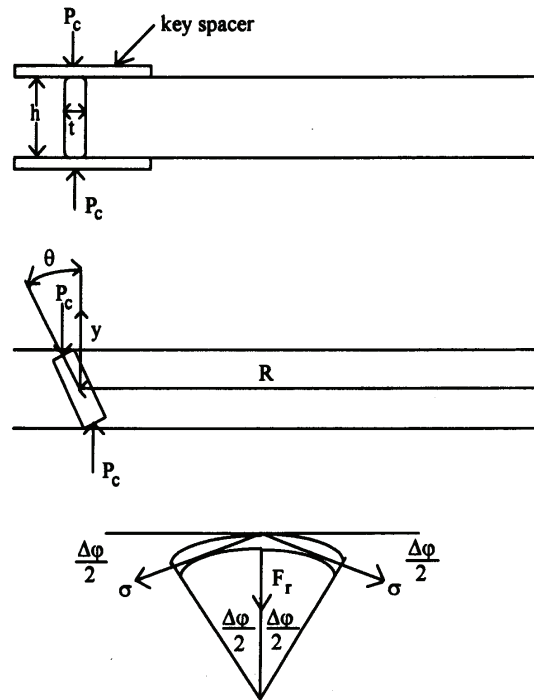


Figure 7-12 Geometry of Strand Tilting Due to Axial Compressive Force [Del Vecchio, 2002].

The resisting torque produced by this force can be calculated as:

$$\Delta \tau = F_r y = \frac{\sigma t \Delta l y \Delta y}{R} = \frac{E t \Delta l \tan \theta y^2 \Delta y}{R^2} \quad (7-14)$$

$$\tau = \frac{Et\Delta\ell \tan \theta h^3}{12R^2} \quad (7-15)$$

Equating this counter torque with the applied torque and assuming small θ , we get:

$$P_c = \frac{E}{12} \left(\frac{h}{R}\right)^2 \quad (7-16)$$

When the conductor strand has squared ends, there is an additional resistance to tilting because of the ends digging into the key spacers or paper. This results in a tilting pressure of :

$$P_c = \frac{E}{12} \left(\frac{h}{R}\right)^2 + C \frac{N_{ks} W_{ks} t^2}{6h^2 (2\pi R)} \quad (7-17)$$

For a strand with rounded corners of radius R_c , t in the above formula is reduced by $2R_c$ so that only its flat portion is considered. The resulting critical axial pressure is therefore:

$$P_c = \frac{E}{12} \left(\frac{h}{R}\right)^2 + C \frac{N_{ks} W_{ks}}{6(2\pi R)} \left(\frac{t - 2R_c}{h}\right)^2 \quad (7-18)$$

C in the above formula is a constant depending on the spacer material. A value of $C=6.21 \times 10^4$ Mpa (9×10^6 psi) can be used here.

To compare this with the applied maximum axial compressive force, this stress is multiplied by the radial surface area of the strands in one horizontal layer, A_{layer} , that is:

$$A_{layer} = \pi D_m t N_d N_h \left(\frac{N_{st} - 1}{2}\right) \quad (7-19)$$

where N_d is the number of turns in a disk. The term $(N_{st}-1)/2$ yield the number of radial strands that are part of the double layer. For magnet wire, the expression in parentheses is assumed to be 1. Hence, the critical axial force for unbonded cable is:

$$F_{cr} = P_c A_{layer} \quad (7-20)$$

For bonded cable, it is assumed that tilting cannot happen. For a viable design, we should have

$$\frac{F_{cr}}{F_c} > 1$$

In the above process, it was assumed that the compressive force was applied uniformly around the strand ring, whereas in reality it is only applied to the portions of the ring that are in contact with the key spacers. Therefore, the uniformly applied pressure represents an averaging process over the entire ring that is a reasonable approximation [Del Vecchio, 2002].

7.2.2.4 Stress in Tie-Plates

The tie-bars or tie-plates are used to join the upper and lower clamping structures that keep the coils under compression. These are generally long rectangular bars of steel placed along both sides of the core legs. Tie-plates are under mild tension during normal transformer operation. However, the tensile stresses can increase considerably during short circuit. Also, the tie bars support the entire weight of the coils and core when the transformer is lifted [Del Vecchio, 2002].

The short circuit stress in the tie bars is a result of the total end thrust produced by all the coils. This is the sum of all the upward or downward forces acting on the coils and is an output of the

force calculation program. Since this output refers to a single leg, the tie bars carrying this force should only be the ones associated with a single leg. If there is a three-phase fault, all the bars are affected equally. However, if there is a single line to ground fault where the forces are much higher on one leg than the other two, the tie bars along the leg having the greater force will probably sustain the greatest stress. Therefore, as a worst-case scenario, it is assumed that the legs act independently at least for the short duration of the fault [Del Vecchio, 2002].

The total end thrust is calculated from a static force analysis. To account for the dynamic effects, enhancement factors are used based on numerical studies. A force of 1.8 times the end thrust is used if it is larger than 0.8 times the maximum compressive force over all the windings. Else, 0.8 times the maximum compressive force over all the windings is used. However, because the tie bars must support the weight of the core and coils during lifting, the stresses produced in tie bars by lifting are checked. During lifting, it is assumed that only the tie bars go under stress that are associated with the outer legs where the lifting hooks are positioned. Both the short circuit dynamic stresses and the lifting stresses must be within the allowable stress limit. The maximum allowable stress is taken to be 620 MPa (60,000 psi) if a stainless steel used for the tie bar material [Del Vecchio, 2002].

7.2.2.5 Stress in Pressure Rings

The total end thrust of the windings is received by the pressure rings. These rings cover the radial build of the windings with a little overhang. During a fault, it must support the entire dynamic end thrust of the windings, which is the larger of 1.8 times the end thrust and 0.8 times the maximum compressive force in all the windings. The ring is supported on radial blocks and space is provided in between for the leads. Hence, there is an unsupported span of a certain length L_u . This is analogous to the axial bending of a strand discussed before and the same equations can be used with $L=L_u$, $t=0.5(D_{ring,out}-D_{ring,in})$ the radial build of the ring, $h=h_{ring}$ the ring's thickness, and $q=P_{ring}t$ the force/unit length along the unsupported span. Hence:

$$\sigma_{x,max} = \frac{P_{ring}}{2} \left(\frac{L_u}{h_{ring}} \right)^2 = \frac{F_{ring}}{2A_{ring}} \left(\frac{L_u}{h_{ring}} \right)^2 \quad (7-21)$$

$$F_{ring,max} = \sigma_{bend} (\pi/2)(D_{ring,out}^2 - D_{ring,in}^2) \left(\frac{h_{ring}}{L_u} \right)^2 \quad (7-22)$$

For pressboard, $\sigma_{x,max}=103$ Mpa (15,000 psi) is a reasonable maximum allowable bending stress [Del Vecchio, 2002].

7.2.2.6 Hoop Stress

The radial pressure acting on the winding creates a hoop stress in the winding conductor. The hoop stress can be tensile or compressive, depending on whether the pressure acts radially outward or inward respectively. The winding will be treated as an ideal cylinder or ring under radial pressure P_r . R_m being the mean radius of the cylinder, H its axial height, and B the radial dimension of the cylinder, it can be shown that :

$$\sigma_{hoop} = \frac{F}{A} = \frac{P_r H R_m}{A} = \frac{P_r R_m}{B} \quad (7-23)$$

In this formula, it is assumed that the winding is built of homogeneous material. Since this force is primarily supported by the conductor, A should equal the cross sectional area of all the conductors in the winding that is $A=A_t N_t$, where A_t is the cross-sectional area of a turn and N_t is the total number of turns in the winding. This stress shall not exceed the proof stress of the winding material [Del Vecchio, 2002].

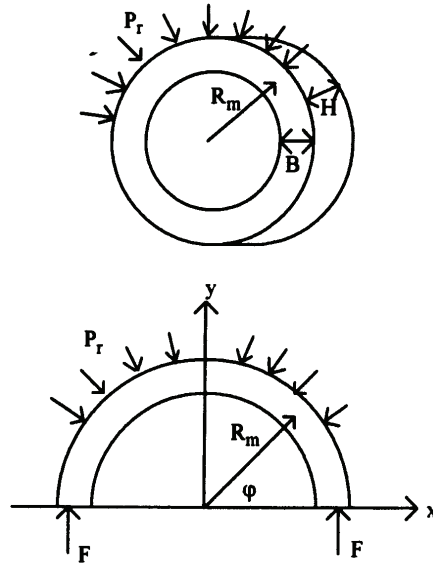


Figure 7-13 Geometry for Determining the Hoop Stress in a Cylinder Acted on by a Radially Inward Pressure [Del Vecchio, 2002].

When the radial pressure acts inward, the winding may buckle before reaching its proof stress. It has been suggested based on limited experimental test that this compressive stress not exceed some fraction of the proof stress, varying from 0.4 to 0.7 depending on the type of cable used and whether it is bonded [Del Vecchio, 2002].

The hoop stress is an average over the disk. However, in reality, the axial magnetic field varies from nearly zero on the inside of the winding to close to its maximum value at the outer radius of the winding for the innermost winding. Because of uniformity of the current density, the force density also varies in the same fashion as the magnetic field. Thus, it is reasonable to expect higher hoop stresses in the outermost turns as compared with the inner turns. Nonetheless, because of the layered structure with paper insulation between turns, the stress tends to be shared more equally by all the turns [Del Vecchio, 2002].

7.2.2.7 Radial Bending Stress

There are inner radial supports for windings such as sticks made of pressboard, which are spaced uniformly along their circumference and extend the height of the winding. In presence of an inward radial pressure acting on the winding, the sections of the winding between supports act

like a curved beam subjected to a uniform load. This is similar to the case of a rotating flywheel with radial spokes that has been analyzed by Timoshenko. Performing an extensive parallel analysis results in:

$$\sigma_{\max} = \sigma_{hoop} \left[\left(\frac{\cos \alpha}{2 \sin \alpha} + \frac{3R}{h} \left(\cos \alpha - \frac{\sin \alpha}{a} \right) \left(\frac{1}{\sin \alpha} \right) \right) \left(f_1(\alpha) + 12 \left(\frac{R}{h} \right)^2 f_2(\alpha) + \frac{EA}{E_{eq} A_{stick}} \right)^{-1} - 1 \right] \quad (7-24)$$

where

$$f_1(\alpha) = \frac{1}{4 \sin^2 \alpha} \left(\alpha + \frac{\sin 2\alpha}{2} \right) \quad (7-25)$$

$$f_2(\alpha) = \frac{1}{4 \sin^2 \alpha} \left(\alpha + \frac{\sin 2\alpha}{2} \right) - \frac{1}{2\alpha} \quad (7-26)$$

$$E_{eq} = \frac{L}{\frac{L_w}{E_w} + \frac{L_s}{E_s} + \frac{L_c}{E_c}} \quad (7-27)$$

α is half the angle between the consecutive supports, L_w is the length of the winding portion and E_w its Young's modulus, and the subtitles s and c referring to stick and core parameters $L=L_w+L_s+L_c$. The innermost winding is not part of the supporting system [Del Vecchio, 2002].

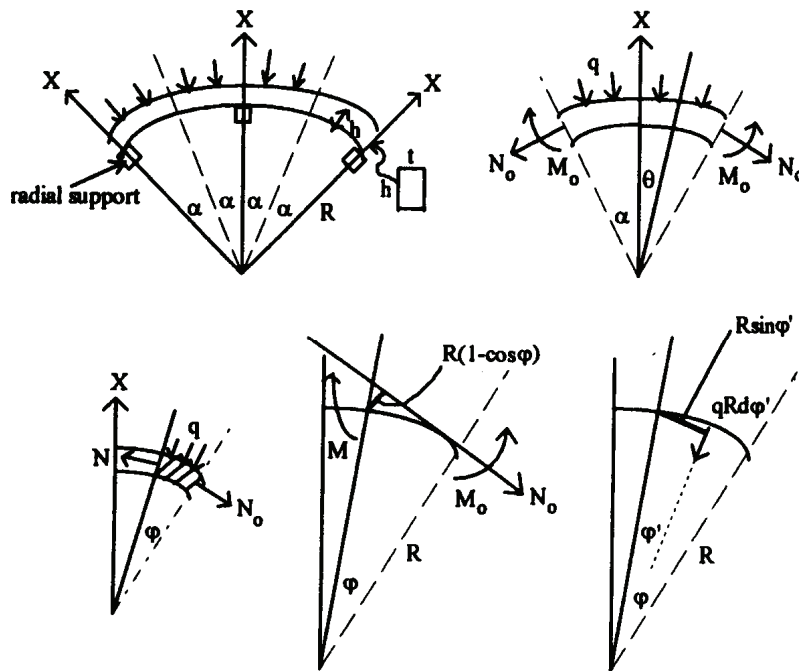


Figure 7-14 Geometry for Determining the Radial Bending Stresses [Del Vecchio, 2002].

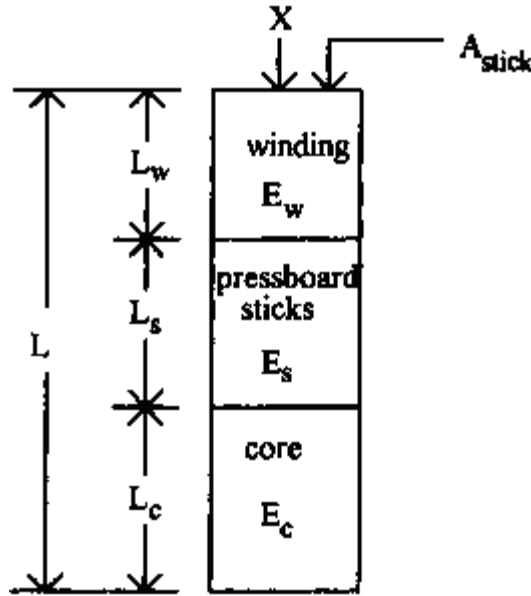


Figure 7-15 Radial Support Structure [Del Vecchio, 2002].

This stress is negative and occurs at the support. These analyses consider a ring that is under a hoop stress. A coil is usually not a monolithic structure, but consists of a number of cables distributed radially. The paper insulation tends to equalize the average hoop stress in the winding in all the cables. The radial thickness h refers to a single cable. For a magnet wire, the radial thickness should be used. In multi-stranded transposed cables, a number less than the radial thickness should be used due to its non-homogeneous nature. For unbonded cables, twice the thickness of an individual strand is used as the effective radial build. If bonded, this value will be 80% of the actual radial thickness [Del Vecchio, 2002].

7.2.3 Radial Buckling Strength

To study the possible buckling of a winding under an inward radial pressure, an individual cable is treated as a closed loop like before, since the cables are not bonded to each other [Del Vecchio, 2002]. In a free buckling analysis, the inner supports can be ignored due to the argument that they are loose enough to have no effect on the onset of the buckling. These effects could be taken into account after the onset of buckling in a forced or constrained buckling analysis. For free buckling:

$$q_{crit} = \frac{3EI}{R^3} \quad (7-28)$$

$$\sigma_{crit} = \frac{qR}{A} = \frac{3EI}{AR^2} = \frac{1}{4}E\left(\frac{h}{R}\right)^2 \quad (7-29)$$

Therefore, the critical hoop stress is only geometrically dependent on the ratio of the radial build to the radius of the ring. The tangent modulus should be used in these equations.

When the supports (sticks) are engaged in the buckling process, there is forced or constrained buckling. Because of some looseness in the supports due to the building tolerance, it is regarded

as a hinged type of attachment for calculation purposes. The lowest-order buckling mode for this case is shown. The corresponding critical force/unit length, q_{crit} , is:

$$q_{crit} = \frac{3EI}{R^3} \left[\left(\frac{2\pi}{\beta} \right)^2 - 1 \right] \quad (7-30)$$

where β is the angle between the supports. Hence, the critical hoop stress is:

$$\sigma_{crit} = \frac{E_t}{12} \left(\frac{h}{R} \right)^2 \left[\left(\frac{2\pi}{\beta} \right)^2 - 1 \right] \quad (7-31)$$

where h is the radial build of the arch. This will exceed the free buckling critical stress if $\beta \leq \pi$, i.e. for only two diametrical supports. However, usually $\beta \ll \pi$, and the constrained buckling stress will be much larger than the free buckling stress. β is taken as the angle between three consecutive inner supports. Arched buckling with this value seems to yield a more realistic value of buckling strength in practice compared to the totally free unsupported buckling [Del Vecchio, 2002].

7.2.4 Points about the Mechanical Design

During a short circuit, the higher fault current in the leads and busbars interact with the higher leakage flux from the main windings and from nearby leads. Hence, the leads must be braced to prevent deformation or large movement during a fault. Although these extra forces could be determined through finite element analysis, past experience has shown that braces usually have sufficient margin so that the extensive analysis will be necessary only for unusual or novel designs [Del Vecchio, 2002].

The weight was neglected except for design of the tie bars. These forces affect the compressive force on the key spacers and the downward end thrust acting on the bottom pressure ring. Similarly, the pre-stressing axial force applying stress in key spacers, the top and bottom thrust on the pressure rings, and the tension in tie bars should be considered. The change in compressive forces acting on the key spacers will also affect the design against conductor tilting [Del Vecchio, 2002].

In addition, the axial and radial stress calculations were done separately whereas in reality there is biaxial stress condition. The combination of the two stresses is what has to be checked at each point along the winding to account for the worst-case situation. However, as long as the materials remain linear, the approach to look at the worst case stresses caused by axial and radial forces separately and apply a failure criterion to each is probably a good approximation to the reality, particularly because the worst case axial and radial forces typically occur at different places along the winding. The radial forces are a result of axial flux that is high in the middle of the winding while the axial forces are produced by radial flux that is high at the ends of the winding [Del Vecchio, 2002].

Some studies on dynamic axial response of the windings subjected to a sudden application of short current found that the prestress level is important. For low levels of prestress, namely about 10% of the normal value, the winding literally bounced against the upper support, resulting in a force much higher than expected. The amplification over the static maximum force was about 4. However, for normal prestress, there was no amplification over the expected maximum force. If

sufficient prestress is applied to clamp the windings in axial direction, there should be little or no amplification of the end thrust over the value determined from static analysis of maximum fault currents. Nonetheless, amplification factor of 1.8 is used in design [Del Vecchio, 2002].

7.3 Behavior of Internal Components under Earthquakes

7.3.1 Possible Failure Modes of Internal Components

The internal components of transformer are mechanically designed to withstand substantial forces caused by fault currents. These forces include radial forces applied to the inner and outer windings and axial forces applied to the windings. Combination of these forces can have different effects like radial stress in windings, radial forces on sticks, buckling of windings under radial stress, compressive stresses in key spacers, bending of strands under axial force, axial stresses in tie bars and pressure rings, and tilting (in a plane normal to winding) of strands under axial key spacer pressure and deformation or movement of leads. The internal components are designed to withstand these forces that give them a considerable resistance. Hence, the internal components are expected to show a good behavior in resisting the earthquake excitations and transferring the loads to their core and avoiding structural damage.

However, the ability of transformers to function depends on keeping the insulation of different parts of the system with substantial difference in electric potential intact. Any damage to the insulation system or anything that causes different components to get closer than their design values produces the possibility of electrical discharge that results in malfunctioning of the transformer with immediate or long-term implications. Based on study of the structure and design of internal components, site visits to inspect opened transformers, and discussions with technical staff of Southern California Edison along with limited information from past performance under earthquakes, the following probable failure modes are identified:

- Sliding of key spacers
- Movement or separation of leads
- Decrease or loss of safe clearance between layers of conductors due to seismic excitations
- Loss of close fitting tolerances between limbs and yokes causing long-term electrical loss

Each of these possible failure modes is explained below.

7.3.1.1 Sliding of Key Spacers

The following picture, taken during a site visit to Southern California Edison, shows key spacers between different layers of windings. Note that in this case spacer consists of a stack of thin pressboards.



Figure 7-16 Key Spacers Separating Different Layers of Winding.

Under normal situation, the key spacers are under compressive pressure due to axial pre-stressing of the winding plus weight of the windings. However, ground motion and oil circulation can cause these spacers to slide. That is, vertical excitations can relieve the normal compressive force. Subsequently, two factors, namely the oil circulation between layers of winding and horizontal excitations caused by the earthquake can result in sliding of the key spacers. The oil used inside transformers has two functions, insulation and cooling. Convection is a source of movement of the oil inside the tank. In large transformers pumping of the oil through transformer might accelerate oil circulation. Hence, it is reasonable to assume that when pre-stressing is relieved, oil movement and/or horizontal vibrations can cause the key spacers to slide.

Loss of key spacers under the above scenario will result in lower spacing between vertically stacked layers of conductors. Closeness or perhaps even attachment of windings from different layers, which have different electric potentials, will interrupt the insulation design and can cause electric discharge.

Sliding of key spacers is the most probable and critical failure mode of transformer internal elements under earthquakes. It will be the main thrust of this study. A simplified model is developed that will be used to determine the level of forces that can result in loss of prestressing. Linear models are employed to determine the level of ground accelerations that can cause total prestressing loss. In light of scarceness of data on transformer designs and the fact that transformer design is very case specific, there is not enough knowledge on the exact amount of prestressing force and exact geometry of the internal components. However, reasonable assumptions based on technical data gathered from different sources are made. Using the analytical model, the behavior for different geometric configurations, material properties and earthquake inputs is calculated and is used to assess the probability of failure under earthquake and also evaluate the effectiveness of base isolation as a rehab scheme.

Similar to static design of the tie plates, only one limb will be modeled. Due to rigidity of the top and bottom clamps it is reasonable to assume that the limbs behave independently. Since there are tie plates on both sides of each limb, the resisting vertical element for each limb will be its tie plates. The winding and key spacers will be simplified into a few alternate segments with the same properties as the winding and the key spacers. There are also two elements representing top and bottom wooden isolation (pressure rings and wooden blockings) and an element representing the vertical spacers, extending between the pressure rings. Thus, the system will be idealized as shown in figure 7-17.

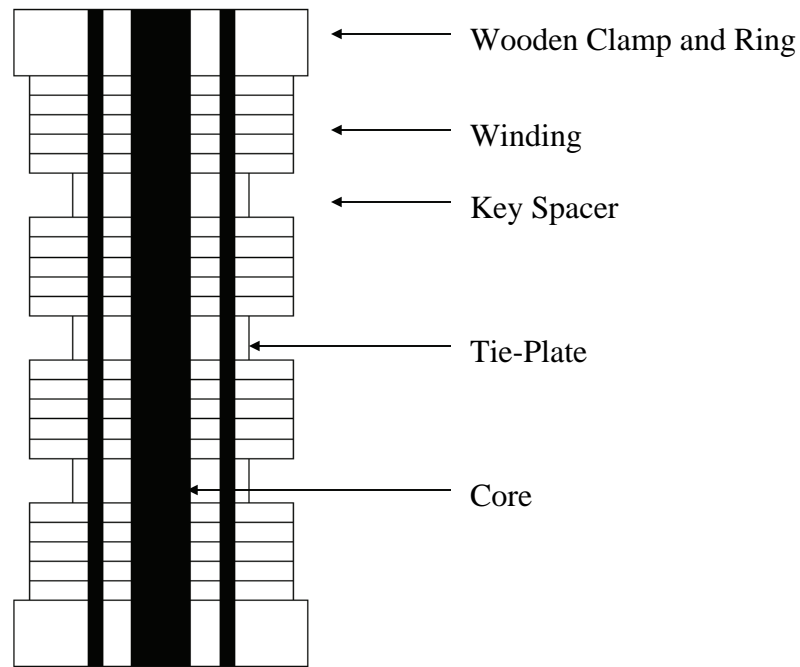


Figure 7-17 Model of Internal Components Used for Analysis.

7.3.1.2 Movement or Separation of Leads

Leads coming from different parts of windings each have their own electric potential. They have differences in potential with all the other elements, and with the steel clamps and the tank that are of ground potential. Hence, they are well insulated and designed in a way to keep sufficient distance from all these other elements. To hold them in place, they are attached to a wooden frame built around the coil clamps. This frame is designed to carry their weight and the loads applied to them during fault currents [Del Vecchio, 2002]. If the connections of leads and the frame are compromised in any way resulting in their movement, the insulation design of the system could be jeopardized. Displacement of the wooden frame relative to the core can happen under seismic excitation due to differences in their frequencies. The core is a relatively stiff structure. The wooden frame, however, is much less stiff and may tend to have excessive displacement, thus, pulling the leads and applying an extra force on the connections.

The following picture shows the leads and their supporting wooden structure.

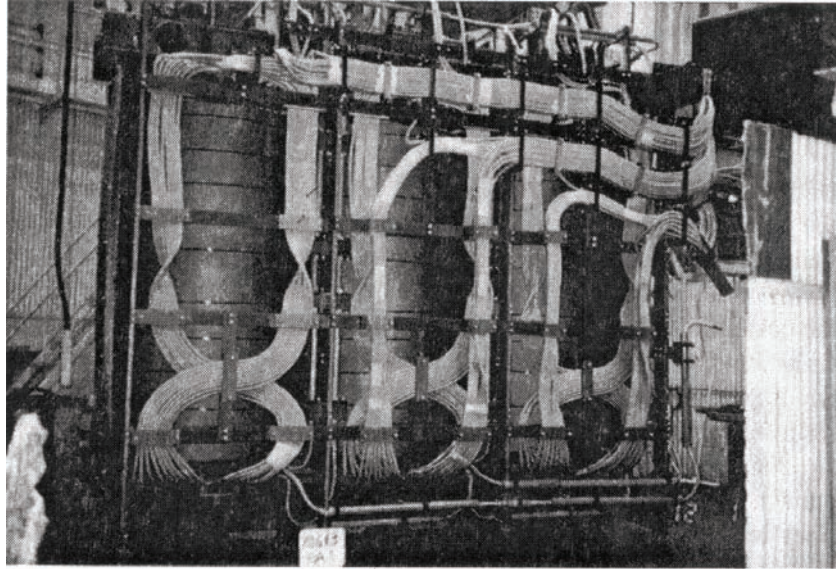


Figure 7-18 Wooden Frame Designed to Support the Leads [Del Vecchio, 2002].

Design of the wooden frames and their connections to the leads is very case specific and depends on various components of the system ranging from its size to its structure and its voltage. For this reason and the fact that designers can easily develop a remedy, no further work on this possible mode of failure is envisioned under this study.

7.3.1.3 Decrease or Loss of Safe Clearance between Layers of Conductors Due to Seismic Excitations

Windings at each level form a horizontal plane supported by key spacers where the distance/clearance between two layers is equal to the height of the key spacers. This clearance can be momentarily reduced due to vertical vibration of the layers of winding behaving as simply supported beams spanning between any two key spacers.

However, for two reasons it is not expected that this mode of possible damage is important. First of all, the winding has the same properties in different layers, except for small differences in the axial and radial electromagnetic forces applied to the winding. Therefore, it can be expected that all windings go through more or less the same response due to seismic excitation, thus, resulting in no relative displacement. The second and more important reason is that unlike the previous cases, even if loss of clearance happens, it is a momentary phenomenon that vanishes after ground motion ceases. It should be noted that the resistance of the insulation system to an electric potential difference is both a function of the magnitude of the potential difference and its duration. Hence, the same insulation that is sufficient for a stationary potential field will also be adequate under a higher potential difference in small fractions of time [Del Vecchio, 2002]. Therefore, it can be expected that the probability of any adverse effect under this situation is non-existent or quite minimal.

7.3.1.4 Loss of Close Fitting Tolerances between Limbs and Yokes Causing Long-Term Electrical Loss

With advance of time, the efficiency of the transformers has increased dramatically. One of the major sources of loss is the core of the transformer. Grain-oriented core steel has been used to increase the electrical efficiency of core. Any factor that requires the flux to deviate from the grain direction will increase the core loss. With modern steels having a very high degree of grain orientation, the loss penalty for such deviation is higher than ever making manufacturers to go through pains to design cores with minimum discontinuity and change of the direction. The most common approach in power transformers is to use mitered corners at the connection of yokes and limbs. This is to limit the extent to which the flux path cuts across of the grain direction at the intersection. The core plates at these mitered corners must be overlapped so that the flux can transfer to the adjacent face rather than cross the air gap which is directly in its path. The fitting should be done to a very close tolerance of order of 0.5 mm to insure the efficiency [Heathcote, 1998].

Because no bolts are used in the joint due to the efficiency considerations, the integrity of core is maintained through the clamps. The top clamps contain the top yoke while the tie-plates connecting the top and bottom clamp apply prestressing force to the core and coil [Heathcote, 1998]. During earthquake, it is possible that the prestressing in the core is temporarily lost. Such loss could results in loss of the close fitting clearance at the yoke-limb joint, hence decreasing the long-term efficiency of transformer. Also, oil might penetrate through these momentary gaps, seriously impeding the electrical functioning of the core. Hence loss of prestressing can be regarded as the critical criteria for this mode of damage. The same model used for studying the axial forces in windings will be used to study this failure mode as well.

7.3.2 The Analytical Model

Finding detailed information on mechanical design and properties of internal elements of a transformer is very hard and challenging. However, different pieces of information gathered from multiple sources have been used to make reasonable assumption about these properties. The details of how different geometric and mechanical properties are selected are given before

7.3.2.1 The Geometric and Mechanical Details

The geometric dimensions of the model are chosen from data from several sources mentioned in the text and a site visit to Southern California Edison. The actual dimensions of the components do not have any real effect on the response and it is just the relative dimension of different parts that is important. Two configurations for the cross section of the system and two configurations for its vertical dimensions are chosen. All the geometric ratios selected are based on study of several pictures in different sources or pictures taken from the visit to Southern California Edison. Figure 5.19 shows the dimension of a cross section. A ratio of 1.5 to 1.8 between the outer radius of windings and the radius of the core is proper.

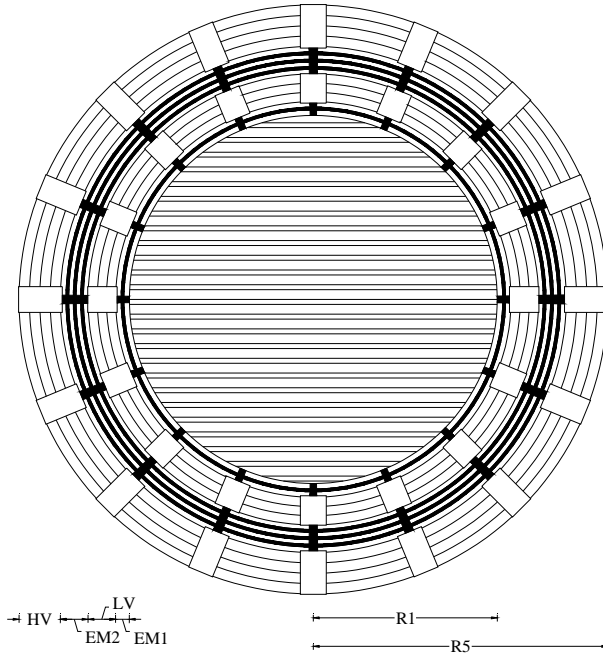


Figure 7-19 Dimensions of a Cross-Section of the Model.

Horizontal Configuration 1:

$$R_5 = 15in$$

$$R_5/R_1 = 1.6$$

$$LV/D = 0.25$$

$$HV/D = 0.375$$

$$EM_1/D = 0.125$$

$$EM_2/D = 0.25$$

Horizontal Configuration 2:

$$R_5 = 15in$$

$$R_5/R_1 = 1.8$$

$$LV/D = 0.25$$

$$HV/D = 0.375$$

$$EM_1/D = 0.125$$

$$EM_2/D = 0.25$$

The ratio of area of key spacers over the winding is assumed to be 24% for the outer winding and 31% and 33% for inner winding of configuration 1 and 2 respectively. The vertical spacers in both configurations are assumed to occupy 25% of the empty area between the windings themselves, and between the windings and the core. In a few cases, the effective area of windings for calculation of stiffness is taken to be equal to that of spacers based on the assumption that not much stress is distributed in it.

For calculating the vertical dimensions, use is made of a reference to a ratio of 40% for the height of the cellulosic material to the height of the winding [Prevost, 2003]. This consists of the wooden pressure rings, blockings, and key spacers. This ratio is used for the vertical configuration 1. The ratio used for vertical configuration 2 is 30%. In both cases, this amount is divided equally between pressure rings and blockings on one hand, and key spacers on the other hand. The height of pressure rings and blockings are also assumed to be equal. However, because the area of blockings is about half of that of the pressure rings, they are both combined into an element having an area equal to 75% of the area of windings. The winding is modeled by four elements between which there are three elements of key spacers. The numerical values of the vertical configurations are as follows:

Vertical Configuration 1:

Height = 45in

Ring = 9in

Spacer = 9in

Winding = 27in

Vertical Configuration 2:

Height = 60in

Ring = 9in

Spacer = 9in

Winding = 42in

7.3.2.2 The Mechanical Properties of Material

The core consists of Cold Rolled Grain Oriented Silicon Steel (CRGO). The density of this material is $\rho=7650 \text{ Kg/m}^3 = 477.146 \text{ lb/ft}^3$ [KRYFS Laminations, 2003] and it has $E=29000 \text{ ksi}$. The steel for tie-plates has very close properties with the same module of elasticity and a density of $\rho = 7874 \text{ Kg/m}^3 = 491.117 \text{ lb/ft}^3$.

The winding itself is made of copper (or aluminum in some cases) and Kraft paper wrapped around it. Based on figures of the winding wires [Prevost, 2003], it is assumed that 12/14 of the height of wire consists of wire while the rest is made of Kraft paper. Having $\rho=8920 \text{ Kg/m}^3 = 556.358 \text{ lb/ft}^3$ and $E=18831 \text{ ksi}$ for copper, and $\rho=1225 \text{ Kg/m}^3 = 76.296 \text{ lb/ft}^3$ and $E=1448.6 \text{ ksi}$ for Kraft paper [Gilani, 1999(a)], the equivalent properties of windings are calculated as $\rho=7820 \text{ Kg/m}^3 = 487.778 \text{ lb/ft}^3$ and $E=16348 \text{ ksi}$.

For properties of pressboard, the data from business material data sheets are used [The Gund Company, 2003]. The pressboard type TX is appropriate for use in pressure rings and blockings. For vertical spacers, the HI-LAM pressboard is used. These material respectively have $\rho=1270 \text{ Kg/m}^3 = 76.212 \text{ lb/ft}^3$ and $\rho=970 \text{ Kg/m}^3 = 60.501 \text{ lb/ft}^3$, and $E=1600 \text{ ksi}$ and $E=500 \text{ ksi}$.

The obtained data suggest a wider range of properties for key spacers. It is suggested that pressboard type 994 be used for key spacers with $\rho=1150 \text{ Kg/m}^3 = 71.728 \text{ lb/ft}^3$ and $E=72.43 \text{ ksi}$ [Dupont, 2002]. However, since it is probable that more stiff material is also used, some analyses with two other sets of properties for key spacers were done as well. In one case, the key spacers are assumed to have the same properties as pressboard TX [The Gund Company, 2003]. In the second set, the intermediate values of $\rho=1270 \text{ Kg/m}^3 = 79.212 \text{ lb/ft}^3$ and $E=200 \text{ ksi}$ are used and it is designated as pressboard type TXX.

7.3.3 The Results

The model for internal components was put under vertical excitations. These excitations include the vertical components of El Centro plus vertical excitations obtained from analyses of primary-secondary systems on FPS. It will be seen that there was no need to use a more extensive collection of earthquake records. All forces including the weight of elements and any prestressing force are excluded from the model and can be added later. Therefore, the results obtained purely show the effect of earthquake. The maximum tensile forces produced in elements in each case are extracted from the results.

Table 7-1 shows the earthquake inputs used. Table 7-2 shows the details of the properties of model and earthquake excitation used for these analyses.

Table 7-1 Characteristics of the Acceleration Time-Histories Used for the Analyses

Case	Input Acceleration	PGA (g)
1	El Centro 05/19/40	0.8
2	Response to Case 1 of isolated Primary system with $f = 14 \text{ Hz}$, bearing secondary system with $f = 10 \text{ Hz}$, $R = 60 \text{ in}$	0.8586
3	Response to Case 1 of isolated Primary system with $f = 8 \text{ Hz}$, bearing secondary system with $f = 8 \text{ Hz}$, $R = 60 \text{ in}$	0.8518
4	Response to Case 1 of isolated Primary system with $f = 8 \text{ Hz}$, bearing secondary system with $f = 11 \text{ Hz}$, $R = 60 \text{ in}$	0.8481
5	Response to Case 1 of isolated Primary system with $f = 11.7 \text{ Hz}$, bearing secondary system with $f = 7 \text{ Hz}$, $R = 60 \text{ in}$	0.8816

Table 7-2 Specifications of the Models Used for Each Analysis

Case	Horizontal Configuration	Vertical Configuration	Key Spacer Material	Input Acceleration
1	1	1	994	1
2	1,LA	1	994	1
3	1	1	TX	1
4	1,LA	1	TX	1
5	1	1	TXX	1
6	1,LA	1	TXX	1
7	2	1	994	1
8	2,LA	1	994	1
9	1	2	994	1
10	1	1	994	2
11	1	1	994	3
12	1	1	994	4
13	1	1	994	5

Figure 7-20 shows the maximum tensile force in the internal elements due to earthquake.

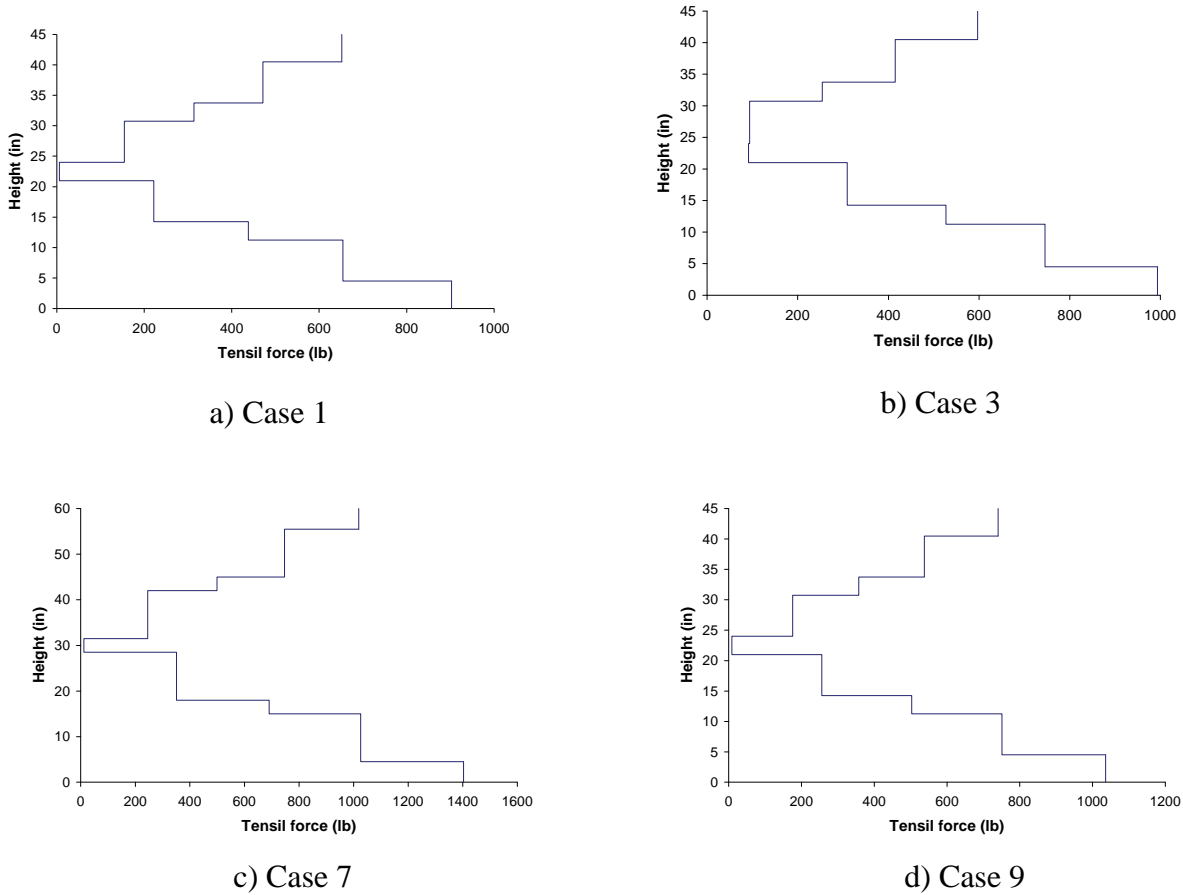
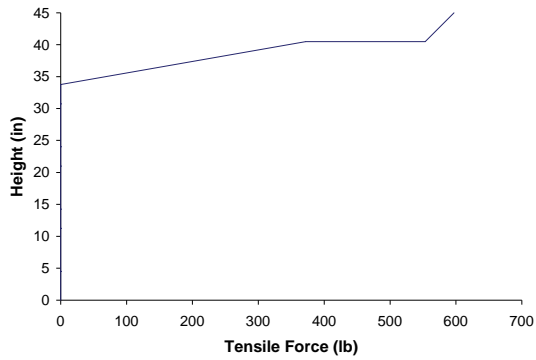
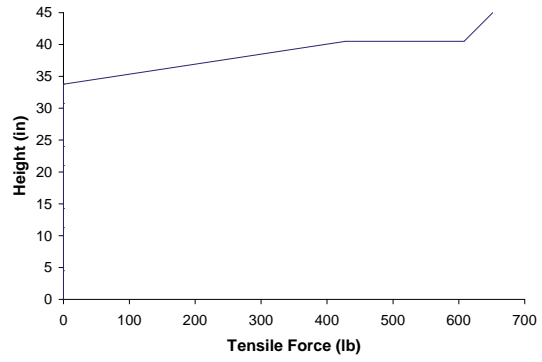


Figure 7-20 Maximum Tensile Force in Coil Due to Earthquake.

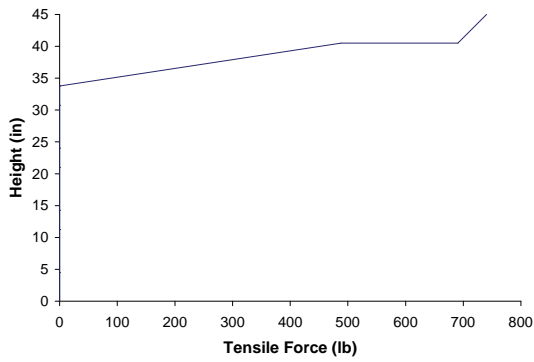
Figure 7-21 shows the same result when the weight is added to these forces.



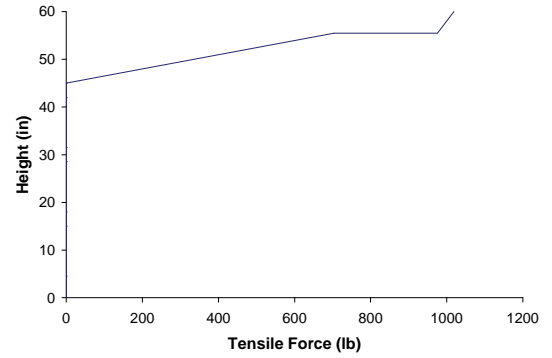
a) Case 1



b) Case 3



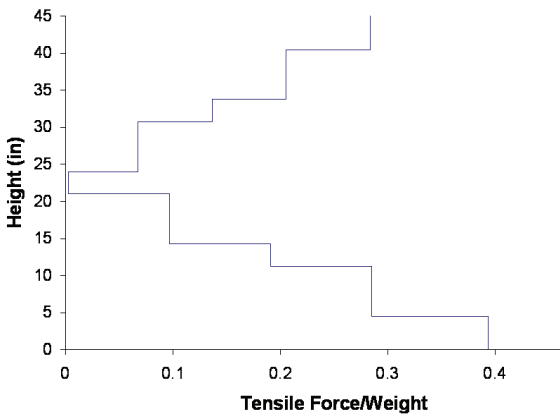
c) Case 7



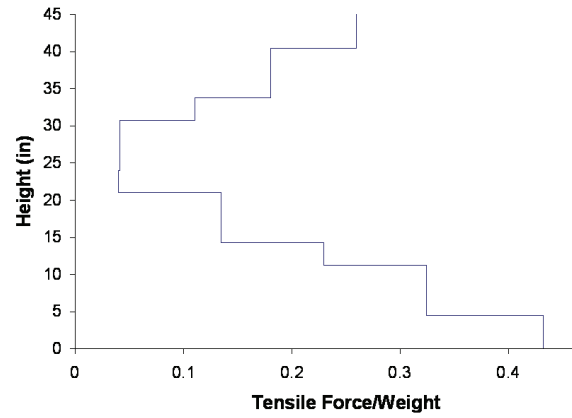
d) Case 9

Figure 7-21 Maximum Tensile Force in Coil Due to Earthquake and Weight.

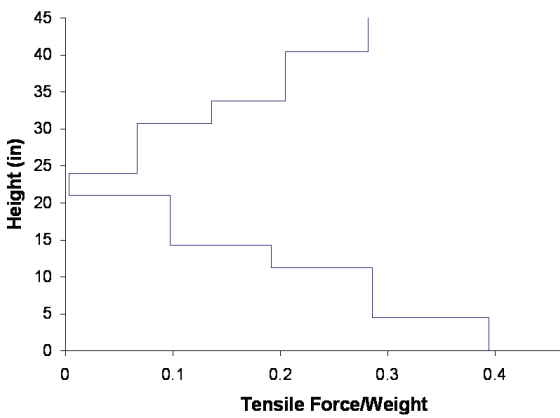
Figure 7-22 shows the maximum tensile force in the internal elements as a percentile of weight due to earthquake. Figure 7-23 shows the same results when the weight is added to the forces.



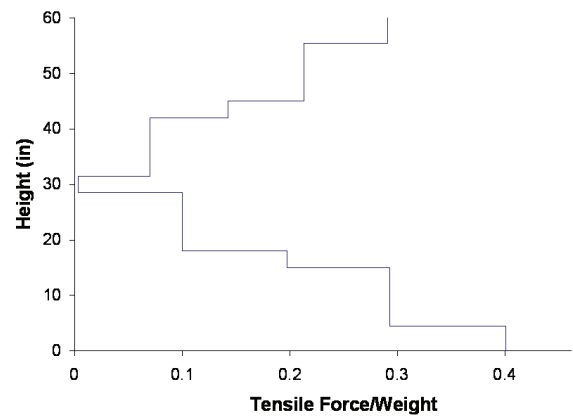
a) Case 1



b) Case 3



c) Case 7



d) Case 9

Figure 7-22 Maximum Tensile Force in Coil Due to Earthquake as a Percentage of Weight.

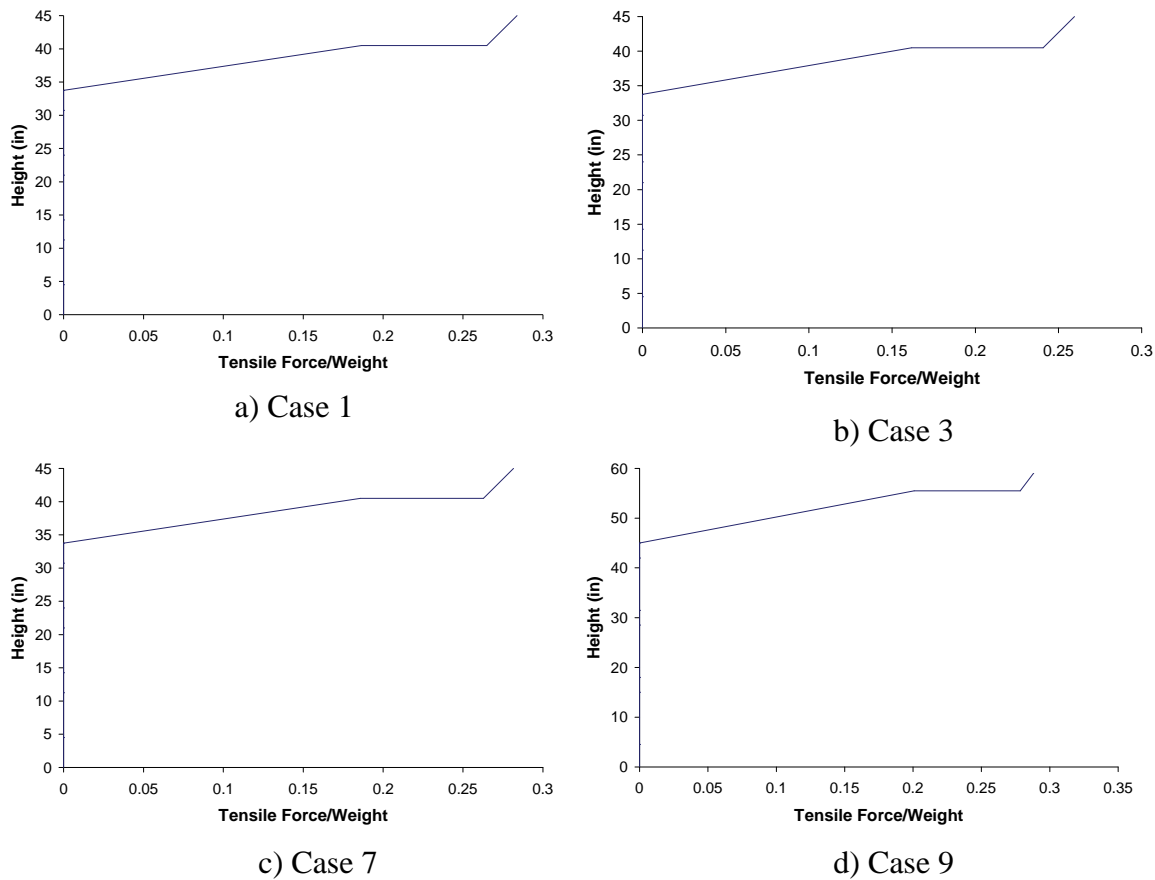
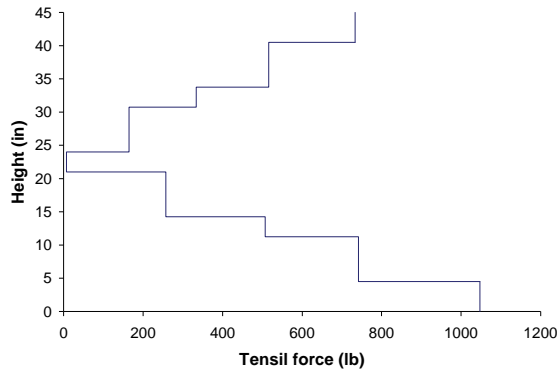


Figure 7-23 Maximum Tensile Force in Coil Due to Earthquake and Weight as a Percentage of Weight.

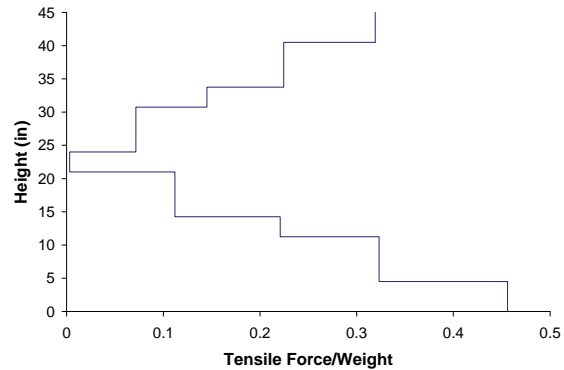
The results show a very low sensitivity to the changes in horizontal and vertical configuration of the system. Also, different properties for the key spacers have not had much of an effect on the internal tensile forces. This is due to immense rigidity of the system in vertical direction. In particular, the presence of a big rigid core in the center gives very high frequency to the system. For example, the first vertical frequency for case 1 is 176Hz (142 Hz for case 9). Hence, response of the system is always in the very rigid side of spectrum, making changes in geometric and mechanical properties almost immaterial. Considering the effect of weight, most of the height of the winding is free from any tensile force during the earthquake, which means there is no possibility of slipping of the key spacers in this region. The maximum net tensile force will be about 30% of the weight of internal elements minus the weight of core and tie-plates. This is a modest force that can be provided through prestressing.

Figure 7-24 shows the same results for an earthquake input equal to the vertical acceleration response of a primary-secondary system on FPS. The input is chosen from analyses of four

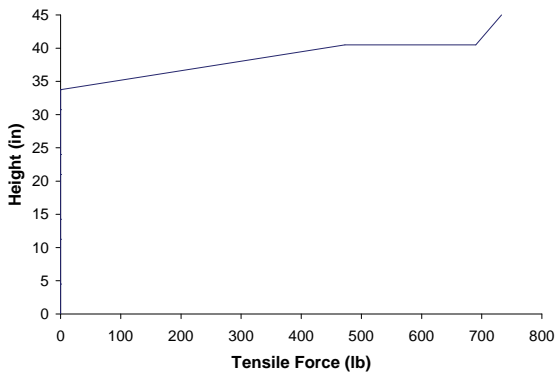
different models with different primary and secondary system properties. The responses are all close, so the one set of results shown can be representative of the response of isolated internal elements in general. These responses are slightly higher compared to the fixed case. This is due to the fact that FPS is primarily a horizontal isolation mechanism, not a vertical one. It is only when the slider in FPS is sliding enough that some effects on vertical direction can be observed; and these effects are not necessarily positive.



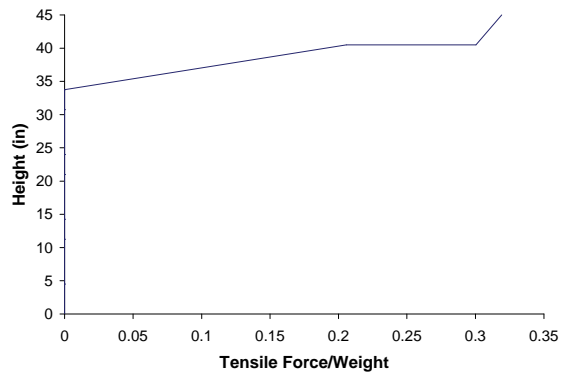
a) Tensile force excluding weight



b) Tensile force excluding weight as a percentage of coil weight



c) Tensile force including weight



d) Tensile force including weight as a percentage of coil weight

Figure 7-24 Maximum Tensile Force in Coil Under Earthquake for Case 10.

Table 7-3 shows the tensile force caused in core and tie-plates for different cases. As seen, most of the force is tolerated by core, because of its high stiffness. These tensile forces are undesirable and will cause loss of close fitting in the yoke to limb joint. Prestressing should be applied to prohibit development of such tensile forces in the core.

Table 7-3 Maximum Tensile Forces in the Core and Tie-Plates for Different Analyses

Case	Core Force (lb)	Core Force/ Core Weight	Tie-plate Force (lb)	Tie-plate Force/ Core Weight
1	1767.30	0.5422	20.2122	0.006201
2	1766.06	0.5418	20.1981	0.006197
3	1698.75	0.5212	19.4282	0.005961
4	1686.50	0.5174	19.2881	0.005918
5	1758.61	0.5396	20.1128	0.006171
6	1760.87	0.5402	20.1387	0.006179
7	1701.59	0.6607	24.6300	0.009564
8	1701.42	0.6607	24.6275	0.009563
9	2532.83	0.5828	28.9675	0.006666
10	2006.99	0.6158	22.9535	0.007042
11	1958.67	0.6009	22.4009	0.006873
12	2101.75	0.6448	24.0373	0.007375
13	1956.81	0.6004	22.3796	0.006866

Table 7-4 shows the maximum tensile force in coil for different cases. It is seen that the force is almost the same in all cases and does not go over 30% of the weight excluding core and tie-plates for fixed cases. In the cases where the response of FPS is considered as the input earthquake, this force is increased to less than 35%. These are very modest forces.

Table 7-4 Maximum Tensile Forces in the Coil for Different Analyses

Case	Maximum Tensile Force in Coil Excluding Weight (lb)	Maximum Tensile Force /Coil Weight	Maximum Tensile Force in Coil Including Weight (lb)	Maximum Tensile Force /Coil Weight
1	902.88	0.3932	651.58	0.2837
2	904.93	0.3941	653.49	0.2846
3	993.70	0.4322	596.85	0.2596
4	983.16	0.4276	607.79	0.2643
5	919.60	0.3999	657.21	0.2858
6	918.90	0.3996	659.26	0.2867
7	1035.91	0.3941	740.31	0.2816
8	1038.18	0.3949	741.21	0.2820
9	1403.35	0.4007	1018.66	0.2909
10	1047.19	0.4560	733.16	0.3193
11	1046.86	0.45587	775.65	0.3378
12	1116.60	0.4862	798.14	0.3476
13	1052.39	0.4583	777.54	0.3386

The proper method used for applying the prestressing force poses an intriguing question. There are two ways to apply the prestressing. It was learned through the visit to the Southern California

Edison that one method of prestressing is through fitting in the wooden blockings that have dimensions larger than the available space. This will require using jacks to increase the available space and then letting the blockings in and letting them to bear the additional load. This will produce tensile forces in tie-plates and core and compressive force in winding. Most of this force is absorbed by core rather than the tie-bar. The second method is to apply the prestressing force through tightening the bolts of the tie-plates [Del Vecchio, 2002]. This will produce compressive forces in both the winding and the core. However, most of this force is absorbed by the core.

The first method has the advantage that it is very effective in the sense that not much force is applied to the tie-bars. The force in winding is almost equal to that in the core. However, it has the effect that it produces tensile forces in core and is counter-productive. Also, this method is practically very hard to apply. The second method has the advantage of simultaneously applying compressive force to both the core and the winding. However, since core absorbs most of the force, a lot of force must be applied to reach the desired level of force in the winding. Therefore, either a combination of methods one or two or just the second method should be used to produce the required compressive force in both the core and winding.

The amount of force in each element required for achieving the specified prestressing force in coil and core is calculated for the cases 1, 7, 9. If all the prestressing is done through the tie-plates, the corresponding force in the tie-plates will be between 80~139 kips. This force will cause a prestressing force of 79~138 kips in the core and the required force of less than 1 kips in the windings. This is a very inefficient since most of the force is taken to produce a prestressing in the core that is much higher than its required value of 2~3 kips.

A better method is to combine the two methods of prestressing to achieve the predefined goals. Since the force in the core in all cases is comfortably less than 3 times that in the winding, the ratio of the goal prestressing force in core to winding is set equal to 3. This assumption leads to a combination of the prestressing methods that will produce the tensile force of less than 4 kips in the tie-plates.

However, for two reasons, it is suggested that an independent prestressing mechanism is used for prestressing the winding by itself to the level required by seismic considerations. The extra prestressing in the winding and core for other considerations can be applied, as they would otherwise be done. The first reason is that finding the right balance between the amount of prestressing applied through tie-plates and blockings is a hard task and its application is practically very hard. Erring on this will result in an insufficiently prestressed core in one side and in a very inefficient design and immense sizes for tie-plates on the other side. The second reason is that the prestressing in a transformer is compromised through its life due to several reasons. The inelasticity in behavior of the key spacers, and their aging precipitated by the amount of heat produced in transformer will result in loss of prestressing after some time. It is a well-known experience that many transformers have not much prestressing left in them when they are opened after their life-cycle [Prevost, 2003]. Having a separate prestressing mechanism for the windings can help insure that the required amount of prestressing needed for seismic reasons is maintained in the winding throughout its life.

A hint to the amount of prestressing force that is actually applied in a typical transformer is found in one of the studies performed on windings [Prevost, 2003]. It is said that a prestressing pressure of about 5 N/mm² (724.29 psi) is the value for a 550 kV BIL 20MVA transformer at 90°. Considering the area of key spacers in the different geometric configurations used, this stress translates into a prestressing force of 53~63 kips in the windings. This value is much higher than the amount needed under seismic considerations to prevent the failure modes. Hence, it seems that the probability of seismic excitations to cause failures in internal components due to structural reasons is very slim, unless the prestressing is lost before earthquake happens. This also suggests that more focus should be put on side reasons for an explanation of the occasional internal damage observed in past earthquakes in the form of slipping of key spacers.

SECTION 8

EFFECT OF ISOLATION ON FOUNDATION DESIGN OF TRANSFORMERS

Transformers are very heavy equipment subject to enormous forces under earthquake. As mentioned in Section 1, failure of foundation of transformers under earthquake is one of the major modes of damage in an electrical substation. Proper design of foundation to withstand large vertical and lateral loads and moments is an integral part of seismic design of the substation.

Enormity of the seismic loads requires very large foundations for transformers that are very costly. Use of FPS can help reduce the loads, hence reducing the cost of foundation. This can be a very considerable saving, justifying use of FPS by itself.

8.1 Seismic Design of Foundations in Electrical Substations

Pile-type foundations supporting equipment in electrical substations should be designed to the loads found in the qualification process for the equipment and support [IEEE, 1998]. Pad-type foundations may be designed using lower loads than required by the qualification of the equipment and support. These types of foundations can be analyzed to the requirements of equation:

$$F_p = ZIC_p W_p \quad (8-1)$$

which comes from the Uniform Building Code (UBC), where $C_p = 0.75$.

The electrical substation equipment is designed based on the seismic performance level expected of them. There are three performance levels (PL) suggested in IEEE. These include high seismic PL, moderate seismic PL, and low seismic PL. Equipment that is shown to perform acceptably in ground shaking up to the desired performance level is said to be seismically qualified to that level. High seismic performance level is chosen for this study [IEEE, 1998].

It is often impractical or not cost-effective to test the equipment to the actual high or moderate performance levels. Hence, the equipment might be tested at 50% of the PL and the analyses are performed at this level as well for consistency. This reduced level is called RRS. The equipment tested or analyzed to the RRS level is expected to have acceptable performance at the required PL. Stresses in brittle components like porcelain and cast aluminum are compared to 50% of their ultimate strength and stresses in ductile materials such as steel and ductile aluminum shall not exceed their allowable stresses. These requirements mean that under PL, the brittle material shall not exceed its ultimate strength and the ductile material may experience some yielding [IEEE, 1998].

The same approach is used for foundation as specified before. These RRS level loads are what the foundation should be designed for so that it does not exceed its capacity under the corresponding PL. This means that the foundation should have an ultimate capacity at least equal

to the loads under PL [IEEE, 1998]. Since use of FPS introduces nonlinear behavior, the loads under PL, rather than twice the loads under RRS, are used to check the design of foundation. Also, to be able to compare the results for pad-type and pile-type foundations, both are designed to carry these loads.

Results of the analysis on the TT1 transformer from Section 3 are used for foundation design. In addition to the high seismic performance level with PGA of 1.0g in horizontal directions and 0.8g in vertical direction, the medium seismic performance level having accelerations half these values is used. The actual transformer used as the base for modeling TT1 has the horizontal frequencies 14.0 and 20.6 Hz. In Section 3, both frequencies were assumed equal to 14.0 Hz. Another set of analysis was performed based on the real frequencies; however, the effects on foundation forces are negligible. Therefore, the same results will represent the forces in the actual transformer.

The 1940 El Centro record is used for the analysis. The record used was recorded on a USGS type C ground [PEER, 2002]. This soil has an allowable stress of $q'_u=1.0 \text{ ksf}$ [ICBO, 1997]. Since the safety factors considered are always higher than 2, an ultimate stress of $q_u=2.0 \text{ ksf}$ is used in the analyses.

It is tried to avoid using piles in the design if possible. However, if the loading demands so, piles are used to make design of a sufficient foundation with reasonable dimensions possible. The foundation is designed in a square shape to be able to withstand the forces if the direction of the earthquake is changed.

To calculate the moment at the level of the bottom of foundation, the moment caused by the lateral loads in this level is calculated. The point of application of this load for transformers is chosen at $2/3$ of height of the transformer, assuming triangular distribution of the load. For isolated transformers, this level is chosen as the middle of the transformer height since the transformer moves as a fairly rigid structure when isolated on FPS. Figure 8-1 shows the load distributions for both cases.

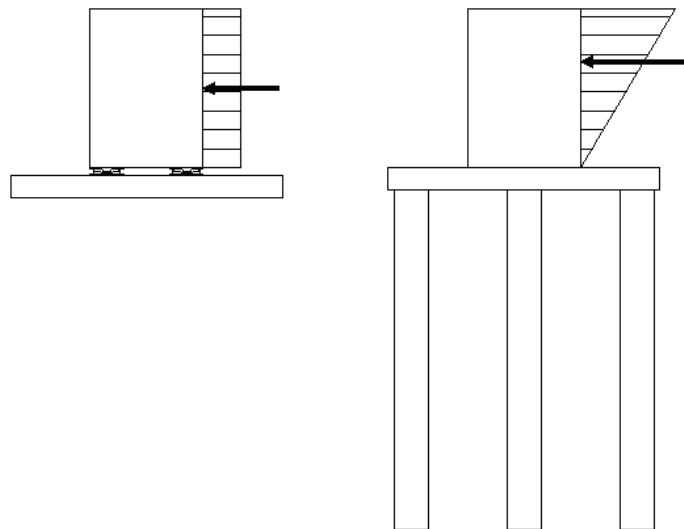


Figure 8-1. Distribution of Lateral Force on Isolated and Fixed Transformers

8.2 Foundation Design Results

Table 8-1 shows the cases used in foundation design. The weight of the transformer is 179 kips.

Table 8-1 Properties of the Cases Considered for Design of Transformer Foundations

Case	Support	PL	F_x (kips)	F_y (kips)	F_z (kips)	M_x (k-ft)	M_y (k-ft)
1	Isolated	High	63.0	141.0	327.5	1280.7	572.3
2	Fixed	High	249.0	194.0	315.7	2220.3	2849.8
3	Isolated	Moderate	35.4	45.9	259.0	416.9	321.6
4	Fixed	Moderate	124.5	97.0	246.0	1110.2	1424.9

The final acceptable design results for all cases are presented in table 8-2.

Table 8-2 The Design Transformer Foundations

Case	B (ft)	L (ft)	D (ft)	Piles	Pile length (ft)	Pile diameter (ft)
1	24	24	2	-	-	-
2	24	24	2	9	30	3
3	17	17	2	-	-	-
4	24	24	2	9	15	3

As observed, a shallow foundation is sufficient to sustain the loads applied to the isolated transformer under moderate and high seismic performance levels. Meanwhile, fixed transformers need 9 piles of diameter 3' and length of 15'~30' to sustain the loads under the same seismic performance levels. The difference is due to higher point of load application for the fixed transformer case in addition to the fact that the value of these loads is also higher. The bigger moment arm puts a higher moment demand on the foundation that necessitates use of piles.

Based on limited data provided by LA Department of Water and Power (LADWP), design and construction of seismic foundation (i.e. piles) will add an additional cost of \$50,000 to \$100,000. Use of four FPS bearings will cost about \$20,000 depending on volume and stroke required. Therefore, it appears that use of FPS bearings can be even justified on an initial cost basis. Further data should be collected in order to make a more accurate initial cost analysis. However, implied life-cycle benefits of FPS isolation are highlighted throughout this research project.

Details of design of a shallow foundation and a pile foundation are given before.

A Shallow Foundation Seismic Design:

A 24'×24'×2' Foundation is selected for Case 1. The eccentricities are calculated as

$$e_x = \frac{M_y}{F_z} = \frac{572.3}{327.5} = 1.7475 \quad ft$$

$$e_y = \frac{M_x}{F_z} = \frac{1280.7}{327.5} = 3.9105 \text{ ft}$$

Since $\frac{e_x}{B} = 0.073 < \frac{1}{6}$, $\frac{e_y}{L} = 0.163 < \frac{1}{6}$, the equivalent area of foundation is calculated using figure 8-2

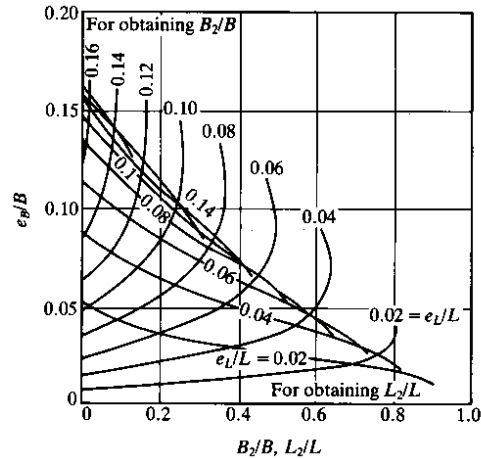


Figure 8-2 Effective Area for Foundation [Das, 1990].

$$\frac{B_2}{B} = 0.42$$

$$\frac{L_2}{L} = 0.0$$

$$A' = L_2 B + \frac{1}{2}(B + B_2)(L - L_2) = 408.96 \text{ ft}^2$$

To account for effect of the lateral load on foundation capacity, the load reduction factor is calculated from figure 8-3.

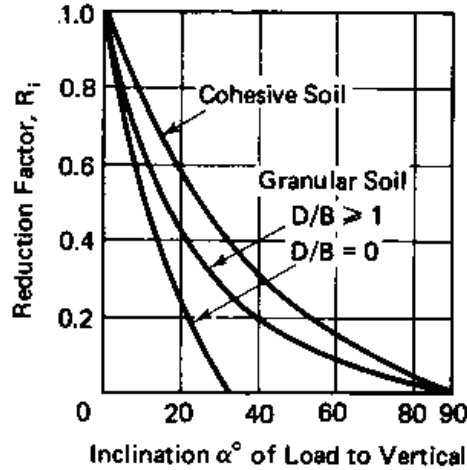
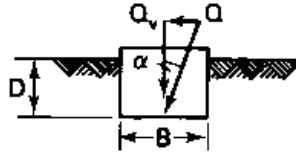


Figure 8-3 Inclined Load Reduction Factors [Liu, 1987].

$$\alpha = \tan^{-1}\left(\frac{\sqrt{F_x^2 + F_y^2}}{F_z}\right) = 25.2^\circ$$

$$R_i = 0.50$$

Hence, the capacity of foundation can be calculated as [Liu, 1987]:

$$Q_{ult} = R_i * A' * q'_u = 0.50 * 408.96 * 2.0 = 408.96 \text{ kips} > 327.5 \text{ kips}$$

A Pile Foundation Seismic Design:

A foundation of dimensions 24' x 24' x 2' with 9 piles of length 30' is used to support the transformer for Case 2. The load in individual piles in the group can be calculated as [Liu, 1987]:

$$Q = \frac{F_z}{n} \pm \frac{M_x y}{\sum y^2} \pm \frac{M_y x}{\sum x^2} \quad (8-2)$$

Using this equation, the maximum compressive and tensile forces can be calculated as 119.6 and 49.4 kips. To account for loss of efficiency in the pile group compared to individual piles, the group efficiency factor G_e is calculated as [Ersoy, 2001]

$$\frac{S}{B} = \frac{10}{3} = 3.33$$

$$G_e = 0.41$$

where S is the center to center distance of piles and D is the pile diameter. Considering this factor, the compressive and tensile capacity of the piles should be at least equal to 291.7 and 120.5 kips, respectively.

The pile capacity can be calculated as [Das, 1990]:

$$Q_u = Q_f + Q_t \quad (8-3)$$

where Q_f is the capacity from friction, and Q_t is the tip load.

$$Q_f = \alpha c_u pL \quad (8-4)$$

$$Q_t = 9c_u A \quad (8-5)$$

where α is chosen from figure 8-4.

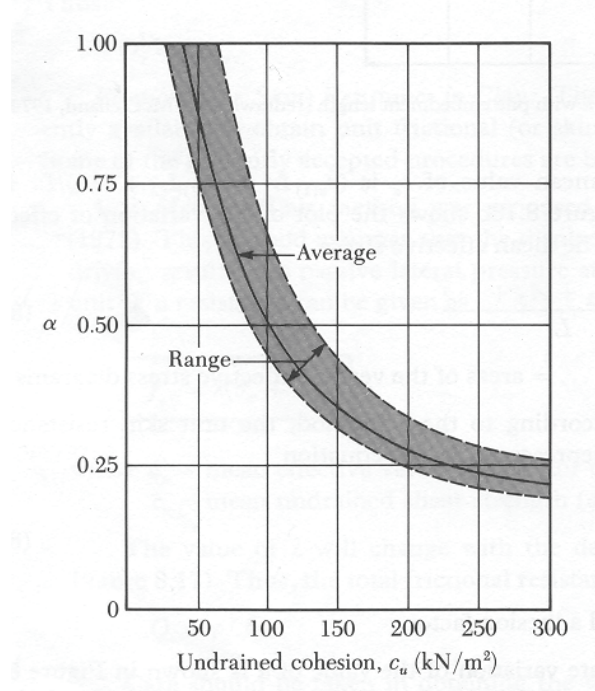


Figure 8-4 Variation of α With Undrained Cohesion of Clay [Das, 1990].

c_u is the cohesion in soil that is half of the value of q'_u for undrained clay, p is the perimeter of the pile, and A is its area.

$$c_u = 1.0 \text{ksf} = 47.94 \text{KN/m}^2$$

$$\alpha = 1.0$$

$$Q_f = 1.0 * 1.0 * (2\pi * 1.5) * 30 = 282.7 \text{ kips}$$

$$Q_t = 9c_u A = 9 * 1.0 * (\pi * 1.5^2) = 42.4 \text{ kips}$$

$$Q_u = 282.7 + 42.4 = 325.1 \text{ kips} > 291.7 \text{ kips}$$

The capacity of piles in tension can be calculated from

$$T_u = \alpha' c_u pL \quad (8-6)$$

$$\alpha' = 0.9 - 0.00625c_u \quad (\text{for } c_u \leq 80 \text{ KN/m}^2) \quad (8-7)$$

where c_u is in KN/m^2 .

$$\alpha' = 0.9 - 0.00625 * 47.94 = 0.600$$

$$T_u = 0.600 * 1.0 * (2\pi * 1.5) * 30 = 169.8 \text{ kips} > 120.5 \text{ kips}$$

The shear capacity of the piles is much higher than the applied load and can be calculated as [Fleming, 1992]:

$$P = 2nc_u SL = 2 * 9 * 1.0 * 10.0 * 30.0 = 5400 \text{ kips} \gg 315.6 \text{ kips}$$

where n is the number of piles and L is the pile depth. Hence, the design is adequate to carry the loads and moments.

For comparison, if the foundation was used without piles, considering the combined effect of vertical and lateral load, the bearing capacity of the foundation would be 17.3 kips that is equal to 5.5% of the actual normal force of 315.7 kips. If the seismic load is reduced until this foundation is sufficient to carry the load, it is found that the seismic load is 0.16 times the original seismic load (0.16g in both horizontal directions, and 0.128g in vertical direction). Both the reduction in lateral load and the consecutive reduction in moment achieved by use of FPS explain such a significant gain in terms of foundation size.

SECTION 9 CONCLUSIONS

Substations, key components of electric power systems, are susceptible to significant damage under seismic events. Rehabilitation of existing substations using advanced technologies and proper design of new systems will reduce the likelihood of failure and/or will enhance the probability of post-earthquake system functionality in a timely manner. Furthermore, it will ensure long-term reliability and longevity of critical equipment, which is essential in light of ever increasing dependence of modern societies on electrical power.

Substation equipment are designed and qualified for a specified level of base excitation. If the design level is exceeded or if their interaction aggravates the seismic response, as in the case of recent strong earthquakes in California and abroad, damage of the equipment is almost certain. This would result in direct and indirect loss and significantly impact the regional economy. Raising the design level is not practical, neither technologically nor economically. Furthermore, the complicated interaction among various electrical components during the dynamic response of the entire system to an event is not well understood. Therefore, raising the design level by itself might not remedy the situation even if it was feasible to do so. To enhance our knowledge of seismic response of substation equipment and develop rehabilitation strategies using advanced technologies a comprehensive study was conducted that included detailed finite element analyses of different types of transformers and bushings as well as parameter and experimental studies of the friction pendulum system as a possible mitigation approach. Furthermore, based on finite element results, simplified models were developed and interaction among transformer-bushing and interconnecting equipment was investigated. Internal packaging of transformers was also evaluated and its seismic performance was qualitatively assessed. Based on the results of this study the following conclusions can be made:

1. The flexibility of the transformer body has an effect on the bushing response. Translational modes of the transformers have the highest effect on the response of the bushing.
2. The dynamic amplification factor specified in IEEE seismic codes is not always conservative.
3. Qualification tests on bushings with twice the response spectra as specified in IEEE should be preceded by a finite element analysis of the transformer model. Qualification tests for bushings should be performed on a semi-rigid stand with a frequency equal to that of the translational mode of the transformer.
4. Rotational degree of freedom due to transformer tank flexibility must be considered in seismic analysis of transformer-bushing system.
5. The frictional pendulum system can be utilized for seismic rehabilitation of transformers where enough slack between bushings and connecting electrical equipment item is provided.

6. The frictional pendulum system provides considerable inertia reductions depending on the peak ground acceleration (PGA) and the bearing radius of curvature. The FPS system is more effective in reducing inertia forces for higher PGAs. Furthermore, both inertia reductions and maximum displacements are affected by the earthquake record used. Records with dominant periods in the vicinity of the isolator period reduce the isolator effectiveness. On the average, FPS bearings can provide 60% inertia reductions within their displacement limits. The amount of inertia reduction is significantly higher compared to the fixed based situation.
7. Proximity of the vertical and horizontal frequencies in transformers can reduce the effectiveness of FPS in terms of bushing response and inertia force reduction. However, for the practical range of frequencies, this adverse effect is limited and will not reduce FPS efficiency significantly.
8. Coupling of responses in two horizontal directions does exist due to dependency of frictional characteristics on total velocity. However, this effect tends to diminish for higher PGAs since at higher velocities frictional constants are less sensitive to the magnitude of the velocity.
9. Interaction between transformer-bushing and interconnecting equipment has adverse effects on different responses, particularly bushing response. This adverse effect exists independent of the relative value of FPS frequency to that of the interconnecting equipment. This phenomenon is even observed when these frequencies are equal.
10. CQC method is recommended for estimating the total resultant displacement of FPS-isolated system for PGAs less than 0.5g. For higher PGAs the average of SRSS and CQC methods could be used for displacements in order to reduce the conservatism of CQC method at higher PGA values. For inertia reductions the average of the two methods is recommended for all PGAs.
11. FPS response is the predominant factor determining the behavior of various interacting components. When the FPS displacement is in the direction away from the interconnecting equipment, it pulls the interconnecting equipment. The resistance of interconnecting equipment to the pulling by FPS will put the connecting cable under enormous tension. The displacements of transformer, bushing, and interconnecting equipment in this condition can be described as vibrations about a center point that is the FPS displacement. This is always the case for the transformer and bushing. The displacement of FPS itself is to some extent shifted toward the direction of interconnecting equipment, whether this is an increase in its maximum displacement or not.
12. Even the slightest interaction has significant adverse effects. Therefore, the interaction of transformer-bushing with interconnecting equipment must be prevented at any cost. One way to insure this is to provide a slack equal to sum of the maximum absolute values of FPS and interconnecting displacements in the connecting cable. Displacement of FPS can be determined from graphs provided under this study.

13. Some of the trends observed in interaction responses when the transformer is isolated are different from those observed for interaction of fixed equipment. Hence, it should be emphasized that results of previous studies on interaction of fixed structures does not automatically hold when base isolation is used.
14. Use of FPS bearings must be avoided where enough slack between bushings and connecting electrical equipment items is not provided. In this case transformers should be anchored to their foundation by use of welds or anchor bolts.
15. The proper radius of FPS that can offer a desirable balance between cost, displacement, and inertia reduction is in the range of 30~60 in. For records on rock, the difference of FPS displacement for different radii is not large. The difference in inertia reduction is particularly high for $PGA > 0.7g$ where the inertia reduction for $R = 30$ in starts to decline. For records on soil, only the displacement for $R = 30$ in is visibly lower than others. The choice of radius is mostly based on cost and inertia reduction balance, because they are more sensitive to FPS radius, compared to displacement. The inertia reductions in soil are less affected by radius compared to those of rock. Hence, it is easier justified for rock ground conditions to pick higher FPS radii compared to soil conditions due to the higher gain in terms of inertia reduction. $R = 45$ in seems to be the radius that combines most of the benefits in general. $R = 60$ in may be preferred if the gain in terms of inertia reduction can balance the increased FPS cost. $R = 30$ in may be chosen in cases where the normal structural design can sustain the increased inertial forces with little or no reinforcement.
16. Among the four modes of damage and failure stipulated for internal components of transformers, sliding of key spacers and loss of close fitting tolerances between limbs and yokes are investigated with the first mode being the most critical one. Both of these damage modes can be attributed to loss of prestressing. The assessments show that the internal components behave as a very rigid body. The tensile forces in windings and core caused by vertical excitation are modest, and are easily offset by the typical prestressing forces. Therefore, it seems that failures of internal components in earthquake due to structural effects are very unlikely, unless the prestressing is lost before earthquake happens. This also suggests that more focus should be put on side reasons for an explanation of the occasional internal damage observed in past earthquakes in the form of slipping of key spacers.
17. FPS is very effective in reducing the foundation size and cost. For the cases studied, use of FPS makes seismic design of foundation possible without use of piles. Hence, it appears that use of FPS bearings can be even justified on an initial cost basis.

Recommendations for further research can be summarized as follow:

1. Finite element model of other substation equipment as well as shake table testing should be performed.

2. It was observed that the effect of vertical motion on the response of FPS is more pronounced on inertia reductions than on displacements. The effect of vertical motion is only significant for records of higher PGAs and of lower frequency contents, based on Section 2 of this report. However, higher vertical accelerations can change the friction force and high frequency vibration of bushing can occur. Further study should be performed to investigate this effect.
3. It is suggested that an independent prestressing mechanism be employed for prestressing the winding by itself to the level required by seismic considerations. Having such an independent prestressing mechanism for the windings can help insure that the required amount of prestressing needed for seismic reasons is not compromised throughout the winding life cycle. This will also facilitate application of proper prestressing to the winding, without jeopardizing practicality and efficiency of design.
4. Develop nonlinear finite element model to accurately represent intricate details of bushing components, particularly rubber gaskets.
5. Perform detailed finite element analyses of bushing considering boundary effects (i.e., transformer flexibility and interconnecting equipment).

SECTION 10 REFERENCES

ADINA (2001) “ADINA Theory and Modeling Guide”, Vol. 1, Report ARD 01-7, ADINA R&D Inc, June

ANSYS, “ANSYS 5.5” A Finite Element Analysis Package, Program developed by ANSYS Inc., Canonsburg, PA.

ASCE, (1998) “Guide to Post Earthquake Investigation of Lifelines,” ASCE Technical Council on Lifeline Earthquake Engineering

ASCE, (1999) “Guide to Improved Earthquake Performance of Electric Power Systems,” ASCE Manuals and Reports on Engineering Practice No. 96

Al-Hussaini, T., Zayas, V., and Constantinou, M. C., (1994) “Seismic Isolation of Multi-Storey Frame Structures Using Spherical Sliding Isolation System,” Report NCEER-94-0007

Almazan, Jose L., De la Llera and Juan C. (2002) ” Analytical Modeling of Structures with Frictional Pendulum Isolators” , Earthquake Engineering and Structural Dynamics, Vol. 31, no 2, pp. 305-332, February

Almazan, J. L., De La Llera, J. C., and Inaudi, J., (1998) “Modeling Aspects of Structures Isolated with the Frictional Pendulum System,” Earthquake Engineering and Structural Dynamics, Vol. 27, pp 845-867

Ashrafi A. (2003), “Issues of Seismic Response and Retrofit for Critical Substation Equipment” M.Sc. Thesis, New Jersey Institute of Technology, August

Bellorini, S., Salvetti, M., Bettinali, F., Zafferani, G., (1998) “Seismic Qualification of Transformer High Voltage Bushings,” IEEE Transactions on Power Delivery, Vol. 13, No. 4, pp 1208-1213

Chopra, A. K., (2000), *Dynamics of Structures, Theory and Applications to Earthquake Engineering*, Prentice Hall, New Jersey

Constantinou, M. C., Mokha, A. S., and Reinhorn, A. M., (1990) “Teflon Bearings in Base Isolation: Modeling,” Journal of Structural Engineering, Vol. 116, pp 455-473

Constantinou, M. C., Tsopelas, P., Kim, and Y-S., Okamoto, S., (1993) “NCEER-Taisei Corporation Research Program on Sliding Isolation Systems for Bridges: Experimental and Analytical Study of a Friction Pendulum System (FPS)” Report NCEER-93-0020

Constantinou, M., Whittaker, A. S., and Velivasakis, E., (2001) “Seismic Evaluation and Retrofit of the Ataturk International Airport Terminal Building,” Proceedings of the 2001 Structures Congress and Exposition, ASCE

Das, Braja M., (1990), *Principle of Foundation Engineering*, PWS Publishing Company, Boston

Der Kiureghian, A., Sackman, J. L., and Hong, K-J. (2001) "Seismic Interaction in Linearly Connected Electrical Substation Equipment" , Earthquake Engineering and Structural Dynamics, Vol. 30, no 3, pp. 327-347, March

Der Kiureghian, A., Sackman, J. L., and Hong, K., (1999) "Interaction in Interconnected Electrical Substation Equipment Subjected to Ground Motions," Report No. PEER 1999/01

Del Vecchio, Robert M., Poulin, Bertrand, Feghali, Pierre T., Shah, Dilipkumar M. and Ahuja, Rajendra, (2002), *Transformer Design Principles, with Application to Core-Form Power Transformers*, Taylor & Francis, New York

DuPont, "NOMEX Pressboard, Technical Information", from <http://Dupont.com/nomex/electapps/pressboard%204%20pager.pdf>, Retrieved June 2003

EERI Newsletter, (1999) "The Izmit (Kocaeli), Turkey Earthquake of August 17, 1999," Vol. 33, No. 10

Earthquake Protection Systems (EPS), "Friction Pendulum Seismic Isolation for Bridges," EPS Inc., Richmond, California 94806

Ersoy S., Saadeghvaziri M. A., (2004), "Seismic Response of Transformer-Bushing Systems" , Vol. 19, no1, IEEE Transactions on Power Delivery, January

Ersoy Selahattin, (2002) "Seismic Response of Transformer Bushing System and Their Rehabilitation Using Friction Pendulum System", Doctoral Dissertation, New Jersey Institute of Technology, January

Ersoy, S., Saadeghvaziri, M. Ala, Liu, K., and Mau, S.T., (2001) "Analytical and Experimental Evaluation of Friction Pendulum System for Seismic Isolation of Transformers", Earthquake Spectra, Vol. 17, No. 4

Fan, Fa-Gung and Ahmadi G., (1990) "Floor Response Spectra for Base-Isolated Multi-Storey Structures", Earthquake Engineering and Structural Dynamics, vol 19, no 3, pp. 377-388, April

Fleming W. G. K., Weltman A. J., Randolph M. F. and Elson W. K., (1992), *Piling Engineering*, Second Edition, John Wiley & Sons Inc., New York

Gilani, A. S., Chavez, J. V., Fenves, G. L. and Whittaker, A. S., (1998) "Seismic Evaluation of 196 kV Porcelain Transformer Bushings," Report No. PEER-98/02, Pacific Earthquake Engineering Research Center

Gilani, A. S., Whittaker, A. S., and Fenves, G. L., (1999) "Seismic Evaluation and Retrofit of 230 kV Porcelain Transformer Bushings," Report No. PEER 1999/14, Pacific Earthquake Engineering Research Center

Gilani, A. S., Whittaker, A. S., and Fenves, G. L., (1999) "Seismic Evaluation of 550 kV Porcelain Transformer Bushings," Report No. PEER 1999/05, Pacific Earthquake Engineering Research Center

- Heathcote Martin J., (1998), *J & P Transformer Book*, Twelfth Edition, Newness, Massachusetts
- Hong K-J., Der Kiureghian A. and Sackman J. L., (2001) “Seismic Interaction in Cable-Connected Equipment Items”, *Journal Engineering Mechanics*, Vol. 127, no 11, pp 1096-1105, November
- ICBO, (1997), *Uniform Building Code*, Volume 2, International Conference of Building Officials
- IEEE, (1998) “IEEE Std. 693-1997, Recommended Practices for Seismic Design of Substations” , Piscataway, New Jersey
- Kim Young-Sang and Lee Dong-Guen, (1993) “Seismic Response of Support-Isolated Secondary Structures in a Multistory Structure”, *Engineering Structures*, Vol. 15, no 5, pp. 335-347, September
- Kohnke P. C., (1989), *ANSYS Engineering Analysis System Theoretical Manual*, Swanson Analysis Systems, August
- Lambrou V. and Constantinou M. C. (1994) “Study of Seismic Isolation Systems for Computer Floors”, Technical Report NCEER 94-0200, National Center for Earthquake Engineering Research, State University of New York , Buffalo, July
- Liu Cheng and Evett Jack B., (1987), *Soils and Foundations*, second edition, Prentice Hall, New Jersey
- MCEER, (2000) “The Marmara, Turkey Earthquake of August 17, 1999: Reconnaissance Report”, Technical Report
- Mokha, A. S., Constantinou, M. C., and Reinhorn, A. M., (1990) “Teflon Bearings in Base Isolation: Testing,” *Journal of Structural Engineering*, Vol. 116, No. 2
- Mokha, A. S., Constantinou, M. C., Reinhorn, A. M., Zayas, V. A., (1991) “Experimental Study of Friction-Pendulum Isolation System,” *Journal of Structural Engineering*, Vol. 117, No. 4
- Mokha, A., Amin, N., Constantinou, M., and Zayas, V., (1996) “Seismic Isolation Retrofit of Large Historic Buildings,” *Journal of Structural Engineering*, Vol. 122, 298-308
- Murota N., Feng M. Q. and Liu G-Y., (2005), “Experimental and Analytical Studies of Base Isolation Systems for Seismic Protection of Power Transformers”, Technical Report MCEER-05-0008, Multidisciplinary Center for Earthquake Engineering Research, State University of New York, Buffalo, September
- Murota N., Feng, M. Q., (2001) “Hybrid Base-Isolation of Bushing-Transformer Systems,” *Proceedings of the 2001 Structures Congress and Exposition*, ASCE
- Naeim, F., Kelly, J. M., (1999), *Design of Seismic Isolation Structures*, John Wiley & Sons Inc., Canada

Nagarajaiah S., Reinhorn A. M. and Constantinou M. C., (1989) “Nonlinear Dynamic Analysis of Three-Dimensional Base Isolated Structures (3D-BASIS)”, Technical Report NCEER 89-0019, National Center for Earthquake Engineering Research, State University of New York, Buffalo, August

Nagarajaiah S., Reinhorn A. M. and Constantinou M. C., (1991) “3D-BASIS Nonlinear Dynamic Analysis of Three-Dimensional Base Isolated Structures: Part II”, Technical Report NCEER 91-0005, National Center for Earthquake Engineering Research, State University of New York, Buffalo, February

Nagarajaiah S., Li C. and Constantinou M. C., (1993) “3D-BASIS-TABS: Computer Program for Nonlinear Dynamic Analysis of Three Dimensional Base Isolated Structures”, Technical Report NCEER 93-0011, National Center for Earthquake Engineering Research, State University of New York, Buffalo, August

Newmark, N. M., Rosenblueth, E., (1971), *Fundamentals of Earthquake Engineering*, Prentice Hall, Englewood Cliffs, New Jersey

Pansini, A. J., (1999), *Electrical Transformer and Power Equipment*, Fairmont Press, Georgia, 1999

PEER, PEER Strong Motion Database, from <http://peer.berkeley.edu/smcat/> , Retrieved August 2007

Prevost Tom, Woodcock David J. and Krause Christoph “ The Effect on Winding Clamping Pressure Due to Changes in Moisture, Temperature and Insulation Age” , WEIDMANN Electrical Technology from <http://www.weidmannb2b.biz/WACT/pdf/WindingClampingPressure.pdf>, Retrieved June, 2003

Reinhorn A. M., Nagarajaiah S., Constantinou M. C. and Tsopelas P. C. , (1994) ,“3D-BASIS-TABS Version 2.0: Computer Program for Nonlinear Dynamic Analysis of Three Dimensional Base Isolated Structures”, Technical Report NCEER 94-0018 National Center for Earthquake Engineering Research, State University of New York, Buffalo, June

Tsai C. S., (1997) “Finite Element Formulation for Friction Pendulum Seismic Isolation Bearings”, Internatinal Journal of Numerical Methods in Engineering, Vol. 40, no 1, pp. 29-49, January

Tsopleas P. C., Nagaraiah S., Constantinou M. C. and Reinhorn A. M., (1994) “3D-BASIS-ME: Computer Program for Nonlinear Dynamics Analysis of Seismically Isolated Single and Multiple Structures and Liquid Storage Tanks”, Technical Report NCEER94-0010, National Center for Earthquake Engineering Research, State University of New York, Buffalo, April

Tsopleas P. C., Constantinou M. C. and Reinhorn A. M., (1991) “3D-BASIS-M: Nonlinear Dynamic Analysis of Multiple Building Base Isolated Structures”, Technical Report NCEER 91-0014, National Center for Earthquake Engineering Research, State University of New York, Buffalo, May

Saadeghvaziri, M. A., Ersoy, S., Mau, S. T., (2000) "Friction Pendulum System for Seismic Isolation for Transformers," PVP-Vol. 402-1, pp 123-134

Villaverde, R., Pardoen, Gerald C., and Carnalla, S., (1999) "Ground Motion Amplification at Base of Bushing Mounted on Electric Substation Transformer," Technical Report PGE-09566

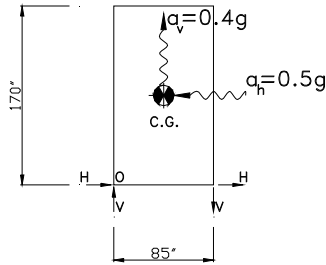
Wilcoski J. and Smith S. J., (1997), "Fragility Testing of a Power Transformer Bushing", USACERL Technical Report 97/57, US Army Corps of Engineers, Construction Engineering Research Laboratories, February

Zayas, V., Low, S., Bozzo, L., Mahin, S., (1989) "Feasibility and Performance Studies on Improving the Resistance of New and Existing Buildings Using the Friction Pendulum System," Technical Report UCB-EERC-89/09

Zayas, V., Low, S., and Mahin, S., (1990) "A Simple Pendulum Technique for Achieving Seismic Isolation," Earthquake Spectra, Vol. 6, pp 317-334

APPENDIX A STATIC CALCULATIONS FOR TRANSFORMERS

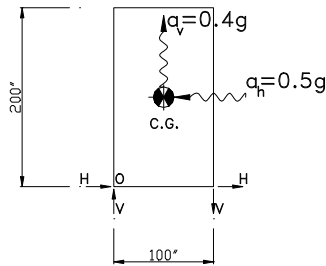
The following are static calculations for transformer tanks (TT1, TT2, TT3).



TT1

$$M_o = 0.5g * \frac{179 \text{ kips}}{g} * \frac{170''}{2} + 0.4g * \frac{179 \text{ kips}}{g} * \frac{85''}{2} = 10650 \text{ kips-in}$$

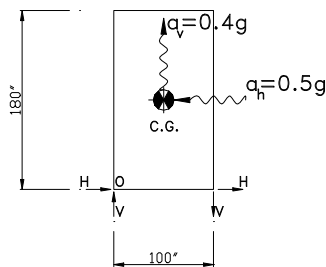
$$V = \frac{1}{2} * \frac{M_o}{85''} = 63 \text{ kips}, H = \frac{1}{4} * 0.5g * \frac{179 \text{ kips}}{g} = 22 \text{ kips}$$



TT2

$$M_o = 0.5g * \frac{300 \text{ kips}}{g} * \frac{200''}{2} + 0.4g * \frac{300 \text{ kips}}{g} * \frac{100''}{2} = 21000 \text{ kips-in}$$

$$V = \frac{1}{2} * \frac{M_o}{100''} = 105 \text{ kips}, H = \frac{1}{4} * 0.5g * \frac{300 \text{ kips}}{g} = 38 \text{ kips}$$



TT3

$$M_o = 0.5g * \frac{512 \text{ kips}}{g} * \frac{180''}{2} + 0.4g * \frac{512 \text{ kips}}{g} * \frac{100''}{2} = 33280 \text{ kips-in}$$

$$V = \frac{1}{2} * \frac{M_o}{100"} = 166 \text{ kips}, H = \frac{1}{4} * 0.5g * \frac{512 \text{ kips}}{g} = 64 \text{ kips}$$

APPENDIX B

FORTRAN CODE FOR FPS

The following is the FORTRAN code for the analysis of FPS with small displacement assumption.

```

INTEGER  NEQ, NPARAM, CCC, GGG, MMM, LLL, NOD, NOTS
CHARACTER *15, FN1, FN2, FN3
PARAMETER (NEQ=6, NPARAM=50)
INTEGER  IDO, IMETH, INORM, NOUT, IATYPE, MTYPE, MITER
REAL  A(1,1), FCN, FCNJ, HINIT, HMAX, PARAM(NPARAM), TOL, X
REAL  XEND, Y(NEQ), MXSTEP, XDISPMAX, XDISPMIN, YDISPMAX
REAL  MAXRESDISP, MAXTOTALACCX, INREDX, INREDY
REAL  MAXTOTALACCY, MAXTOTALACCXY, INREDXY
REAL  YDISPMIN, TOTALACCX(100000), TOTALACCY(100000)
, RESACC(100000)
REAL  TOTALACCXY(100000), GROUNDXY(100000), RESDISP(100000)
REAL  BASESHX(100000), BASESHY(100000), RESBASESH(100000)
REAL  MAXGROUNDX, MAXGROUNDY, MAXGROUNDZ, MAXGROUNDXY
REAL  UGX(10000), UGY(10000), UGUP(10000), DT
COMMON  UGXN(100000), UGYN(100000), UGUPN(100000)
COMMON  C10, C9, C12, C13, C14
COMMON  IEND, ACCX, ACCY
EXTERNAL FCN, IVPAG, SSET, FCNJ
OPEN  (1, FILE='input.txt', STATUS='old')
READ  (1, 100) FN1, FN2, FN3, DT, C10, C9, C12, C13, C14
100   FORMAT (/, A15, //, A15, //, A15, //, F6.3, //, F6.3, //, F6.3
, //, F7.4, //, F7.4, //, F7.4)
PRINT '(A22,A15)', 'INPUT FILE NAME IN X: ', FN1
PRINT '(A22,A15)', 'INPUT FILE NAME IN Y: ', FN2
PRINT '(A22,A15)', 'INPUT FILE NAME IN Z: ', FN3
PRINT '(A17,F6.3,A8)', 'TIME STEP          : ', DT, ' SECONDS'
PRINT '(A17,F6.3,A4)', 'FRICTION           : ', C10
PRINT '(A17,F7.3,A5)', 'RADIUS              : ', C9, ' INCH'
PRINT '(A17,F6.3)', 'X-SCALE FACTOR : ', C12
PRINT '(A17,F6.3)', 'Y-SCALE FACTOR : ', C13
PRINT '(A17,F6.3)', 'Z-SCALE FACTOR : ', C14
C
OPEN OUTPUT FILE
OPEN  (2, FILE='output.dat ', STATUS='REPLACE')
C
FIND THE MAXIMUMS OF THE GROUND INPUTS
OPEN  (22, FILE=FN1, STATUS='OLD')
CCC=0
DO WHILE (.NOT. EOF(22))
CCC = CCC + 1
READ(22, *) UGX(CCC)
IF (CCC.EQ.1) MAXGROUNDX=0.0
IF (ABS(UGX(CCC)).GT.MAXGROUNDX) MAXGROUNDX=ABS(UGX(CCC))
END DO
CLOSE (22)
OPEN  (33, FILE=FN2, STATUS='OLD')
CCC=0
DO WHILE (.NOT. EOF(33))
CCC = CCC + 1
READ(33, *) UGY(CCC)
IF (CCC.EQ.1) MAXGROUNDY=0.0
IF (ABS(UGY(CCC)).GT.MAXGROUNDY) MAXGROUNDY=ABS(UGY(CCC))
END DO
CLOSE (33)

```

```

OPEN (44,FILE=FN3,STATUS='OLD')
CCC=0
DO WHILE (.NOT. EOF(44))
CCC = CCC + 1
READ(44,*) UGUP(CCC)
IF (CCC.EQ.1) MAXGROUNDZ=0.0
IF (ABS(UGUP(CCC)).GE.MAXGROUNDZ) MAXGROUNDZ=ABS(UGUP(CCC))
END DO
CLOSE (44)
C SCALE PGA of GROUND INPUTS TO 1.0g
DO 55 MMM=1,CCC
UGX(MMM)=(UGX(MMM))/MAXGROUNDZ*386.4
UGY(MMM)=(UGY(MMM))/MAXGROUNDZ*386.4
55 UGUP(MMM)=(UGUP(MMM))/MAXGROUNDZ*386.4
CONTINUE
NOD=10
DO 505 LLL=1,CCC-1
UGXN(NOD*(LLL-1)+1)=UGX(LLL)
UGXN(NOD*LLL+1)=UGX(LLL+1)
UGYN(NOD*(LLL-1)+1)=UGY(LLL)
UGYN(NOD*LLL+1)=UGY(LLL+1)
UGUPN(NOD*(LLL-1)+1)=UGUP(LLL)
UGUPN(NOD*LLL+1)=UGUP(LLL+1)
DO 606 GGG=1,NOD-1
UGXN(NOD*(LLL-1)+1+GGG)=UGX(LLL)+GGG*(UGX(LLL+1)-UGX(LLL))/NOD
UGYN(NOD*(LLL-1)+1+GGG)=UGY(LLL)+GGG*(UGY(LLL+1)-UGY(LLL))/NOD
UGUPN(NOD*(LLL-1)+1+GGG)=UGUP(LLL)+GGG*(UGUP(LLL+1)-
606 UGUP(LLL))/NOD
CONTINUE
505 CONTINUE
NOTS=20
HINIT=1.0E-05
HMAX=DT/(NOTS*NOD)
INORM=0
IMETH=2
IATYPE=0
MTYPE=0
MITER=0
MXSTEP=10000000
C SET PARAMETERS FOR SOLVING DIFFERENTIAL EQUATIONS
CALL SSET (NPARAM,0.0,PARAM,1)
PARAM(1)=HINIT
PARAM(4)=MXSTEP
PARAM(10)=INORM
PARAM(12)=IMETH
PARAM(13)=MITER
PARAM(14)=MTYPE
PARAM(19)=IATYPE
IDO=1
X=0.0
Y(1)=0.0
Y(2)=0.0
Y(3)=0.0
Y(4)=0.0
Y(5)=0.0
Y(6)=0.0
TOL=1.0E-07
XDISPMAX=0.0
XDISPMIN=0.0
YDISPMAX=0.0
YDISPMIN=0.0

```

```

MAXRESDISP=0.0
MAXTOTALACCX=0.0
MAXTOTALACCY=0.0
MAXTOTALACCXY=0.0
WRITE (2,99998)
CCC=NOD*(CCC-1)+1
DO 10 IEND=1,CCC
XEND=(IEND)*DT/NOD
CALL IVPAG(IDO,NEQ,FCN,FCNJ,A,X,XEND,TOL,PARAM,Y)
IF ((Y(1)).GT.XDISPMAX) XDISPMAX=Y(1)
IF ((Y(1)).LT.XDISPMIN) XDISPMIN=Y(1)
IF ((Y(3)).GT.YDISPMAX) YDISPMAX=Y(3)
IF ((Y(3)).LT.YDISPMIN) YDISPMIN=Y(3)
RESDISP(IEND)=SQRT((Y(1))**2+(Y(3))**2)
IF (RESDISP(IEND).GT.MAXRESDISP) MAXRESDISP=RESDISP(IEND)
GROUNDXY(IEND)=SQRT((C12*UGXN(IEND))**2+(C13*UGYN(IEND))**2)
TOTALACCX(IEND)=ACCX+C12*UGXN(IEND)
TOTALACCY(IEND)=ACCY+C13*UGYN(IEND)
WRITE (2,99999) X,(Y(II), II=1, 6),TOTALACCX(IEND),
TOTALACCY(IEND)
TOTALACCXY(IEND)=SQRT((TOTALACCX(IEND))**2+
(TOTALACCY(IEND))**2)
IF (MAXGROUNDXY.LT.ABS(GROUNDXY(IEND)))
MAXGROUNDXY=ABS(GROUNDXY(IEND))
(MAXTOTALACCX.LT.ABS(TOTALACCX(IEND)))
MAXTOTALACCX=ABS(TOTALACCX(IEND))
(MAXTOTALACCY.LT.ABS(TOTALACCY(IEND)))
MAXTOTALACCY=ABS(TOTALACCY(IEND))
IF (MAXTOTALACCXY.LT.ABS(TOTALACCXY(IEND)))
MAXTOTALACCXY=ABS(TOTALACCXY(IEND))
IF (IEND.EQ.CCC) THEN
INREDX=(MAXTOTALACCX-C12*386.4)/(C12*386.4)*100
INREDY=(MAXTOTALACCY-C13*386.4)/(C13*386.4)*100
INREDXY=(MAXTOTALACCXY-MAXGROUNDXY)/MAXGROUNDXY*100
END IF
IF (IEND.EQ.CCC) THEN
PRINT '(A27, F6.2,A11)', 'MAXIMUM RESULTANT GROUND : ',
MAXGROUNDXY/386.4, 'g'
PRINT '(A27, F6.2,A5)', 'MAXIMUM X-DISPLACEMENT : ', XDISPMAX,
' INCH'
PRINT '(A27, F6.2,A5)', 'MINIMUM X-DISPLACEMENT : ', XDISPMIN,
' INCH'
PRINT '(A27, F6.2,A5)', 'MAXIMUM Y-DISPLACEMENT : ', YDISPMAX,
' INCH'
PRINT '(A27, F6.2,A5)', 'MINIMUM Y-DISPLACEMENT : ', YDISPMIN,
' INCH'
PRINT '(A37, F6.3,A2)', 'MAXIMUM TOTAL ACCELERATION IN X : ',
MAXTOTALACCX/386.4, ' g'
PRINT '(A37, F6.3,A2)', 'MAXIMUM TOTAL ACCELERATION IN Y : ',
MAXTOTALACCY/386.4, ' g'
PRINT '(A37, F6.2,A5)', 'MAXIMUM RESULTANT DISPLACEMENT : ',
MAXRESDISP, ' INCH'
PRINT '(A37, F6.1,A2)', 'INERTIA REDUCTION IN X DIRECTION : ',
INREDX, ' %'
PRINT '(A37, F6.1,A2)', 'INERTIA REDUCTION IN Y DIRECTION : ',
INREDY, ' %'
PRINT '(A37, F6.1,A2)', 'INERTIA REDUCTION IN X-Y DIRECTION : ',
INREDXY, ' %'
END IF
CONTINUE
IDO=3

```

```

      CALL IVPAG(IDO,NEQ,FCN,FCNJ,A,X,XEND,TOL,PARAM,Y)
99998 FORMAT 11X,'X',14X,'Y(1)',11X,'Y(2)',11X,'Y(3)',11X,'Y(4)',11X,
      'Y(5)',11X,'Y(6)',11X,'TOTALACCX',11X,'TOTALACCY')
99999 FORMAT (9F15.5)
      CLOSE (1)
      CLOSE (2)
      END
      SUBROUTINE FCN (NEQ,X,Y,YPRIME)
      INTEGER NEQ
      REAL X, Y(NEQ), YPRIME(NEQ), C1,C2,C3,C4
      REAL C8(100000)
      COMMON UGXN(100000),UGYN(100000),UGUPN(100000)
      COMMON C10,C9,C12,C13,C14
      COMMON IEND,ACCX,ACCY
      C1=0.005
      C2=0.9
      C3=0.1
      C4=1.0
      C8(IEND)=386.4+C14*UGUPN(IEND)
      YPRIME(1)=Y(2)
      YPRIME(2)=-((C8(IEND))/C9)*Y(1)-(C10*C8(IEND))*Y(5)-
      12*UGXN(IEND)
      YPRIME(3)=Y(4)
      YPRIME(4)=-((C8(IEND))/C9)*Y(3)-(C10*C8(IEND))*Y(6)-
      C13*UGYN(IEND)
      YPRIME(5)=(C4/C1)*Y(2)-(C3/C1)*(Y(4))*(Y(5))*(Y(6))-(C2/C1)*
      (ABS((Y(4))*(Y(6))))*Y(5)-C3/C1*(Y(2))*(Y(5))**2-(C2/C1)
      *(ABS((Y(2))*(Y(5))))*Y(5)
      YPRIME(6)=(C4/C1)*Y(4)-(C3/C1)*(Y(2))*(Y(5))*(Y(6))-(C2/C1)*
      (ABS((Y(2))*(Y(5))))*Y(6)-C3/C1*(Y(4))*(Y(6))**2-(C2/C1)
      *(ABS((Y(4))*(Y(6))))*Y(6)
      ACCX=YPRIME(2)
      ACCY=YPRIME(4)
      RETURN
      END
      SUBROUTINE FCNJ(NEQ, X,Y,DYDPDY)
      INTEGER NEQ
      REAL X,Y(NEQ),DYDPDY(*)
      RETURN
      END

```

APPENDIX C IMPLEMENTATION OF A FPS IN ADINA

The details of calculation of forces in an FPS element in each time step and its implementation in ADINA are presented here. The details of the data about ADINA can be found in the software manuals. ADINA provides a subroutine in Fortran called *CUSERG* that can be used to model a user-supplied element [ADINA, 2001(b)]. The details of the variables used are provided within the subroutine as comments and can be seen in this appendix. This subroutine can be seen in ADINA files under the name *ovl160u.f* [ADINA, 2001(a)]. The calls from ADINA to *CUSERG* are divided into several phases controlled by the integer value *KEY* and include four cases. At the start of the program, *KEY* is equal to 1, where ADINA calls the phase one. In this phase, all the initial values and anything that should be defined once at the beginning of the program are defined. *KEY* = 2 refers to the part of subroutine where the element nodal forces are calculated. *KEY* = 3 refers to the section where the stiffness matrix is defined. In each time step, the program refers repeatedly to phase two and then three and checks for convergence. After the convergence is achieved, the program will refer to the last section with *KEY* = 4. Any action that should be done after the convergence is achieved should be done in this phase. For instance, swapping variables between different time steps that is done after convergence belongs to this section.

The subroutine retains the nodal positions at the last time step. It is for the writer of the element to retain any other variable needed from previous time steps in memory. Temperature-independent and -dependent constants can also be defined and used to describe the behavior of the element. Using these constants and a given nodal position for the element at the next time step, the solution in this time step, including forces and stiffness, should be achieved. The process involves receiving the nodal coordinates at t_{n+1} and calculating forces and stiffness for that displacement. The results are used in time-history analysis and the modified displacement is achieved. This process is repeated until convergence is achieved. Each time step involves the following calculations:

$$dX = X_{n+1} - X_n \tag{C-1}$$

$$\varphi = \tan^{-1} \left(\frac{\sqrt{x_1^2 + x_2^2}}{R} \right)_{n+1} \tag{C-2}$$

$$\theta = \tan^{-1} \left(\frac{x_2}{x_1} \right)_{n+1} \tag{C-3}$$

$$v_1 = \begin{pmatrix} 1/\sqrt{1 + \tan(\phi)^2 * \cos(\theta)^2} \\ 0 \\ \sqrt{1 - v_{11}^2} * \text{sign}(\cos(\theta)) \end{pmatrix} \quad (\text{C-4})$$

$$v_3 = \begin{pmatrix} -\sin(\phi) * \cos(\theta) \\ -\sin(\phi) * \sin(\theta) \\ \cos(\theta) \end{pmatrix} \quad (\text{C-5})$$

$$v_2 = v_3 \times v_1 \quad (\text{C-6})$$

$$z_{surf} = (R - \sqrt{R^2 - x_1^2 - x_2^2})_{n+1} \quad (\text{C-7})$$

$$z_{normal,n+1} = (x_{3,n+1} - z_{surf}) \cos(\phi) \quad (\text{C-8})$$

$$vel_{normal} = \frac{(Z_{normal,n+1} - Z_{normal,n-1})}{2\Delta t} \quad (\text{C-9})$$

$$dX_{v1} = dX \cdot v_1 \quad (\text{C-10})$$

$$dX_{v2} = dX \cdot v_2 \quad (\text{C-11})$$

$$vel = \frac{(X_{n+1} - X_{n-1})}{2\Delta t} \quad (\text{C-12})$$

$$vel_{plane} = \sqrt{|vel|^2 - (vel \cdot v_3)^2} \quad (\text{C-13})$$

$$\mu = \mu_{\max} - \Delta\mu \exp^{-\alpha \cdot vel_{plane}} \quad (C-14)$$

$$\rho = X_{n+1} - C_n \quad (C-15)$$

$$\rho_{v1} = \rho \cdot v_1 \quad (C-16)$$

$$\rho_{v2} = \rho \cdot v_2 \quad (C-17)$$

$$Z_{n+1} = \begin{bmatrix} Z_{1,n+1} \\ Z_{2,n+1} \end{bmatrix} = \begin{bmatrix} \frac{\rho_{v1}}{Y} \\ \frac{\rho_{v2}}{Y} \end{bmatrix} \quad (C-18)$$

$$\text{if } |Z_{n+1}| > 1, \quad Z_{n+1} = \frac{Z_{n+1}}{|Z_{n+1}|} \quad (C-19)$$

$$N = -k_{normal} * z_{normal,n+1} - c * vel_{normal} \quad (C-20)$$

$$\text{if } N < 0, \quad N = 0 \quad (C-21)$$

$$F_{f1} = -\mu N Z_1 \quad (C-22)$$

$$F_{f2} = -\mu N Z_2 \quad (C-23)$$

$$\begin{pmatrix} F_{x1} \\ F_{x2} \\ F_{x3} \end{pmatrix} = - \begin{Bmatrix} v_1 & v_2 & v_3 \end{Bmatrix} \begin{pmatrix} F_{f1} \\ F_{f2} \\ N \end{pmatrix} \quad (\text{C-24})$$

In a model with 12 degrees of freedom, these forces are returned via ADINA subroutine to the main program through:

$$\text{RE}(1) = -F_{x1}$$

$$\text{RE}(2) = -F_{x2}$$

$$\text{RE}(3) = -F_{x3}$$

$$\text{RE}(4) = 0._8$$

$$\text{RE}(5) = 0._8$$

$$\text{RE}(6) = 0._8$$

$$\text{RE}(7) = F_{x1}$$

$$\text{RE}(8) = F_{x2}$$

$$\text{RE}(9) = F_{x3}$$

$$\text{RE}(10) = 0._8$$

$$\text{RE}(11) = 0._8$$

$$\text{RE}(12) = 0._8$$

In the next phase, the stiffness related to these forces should be calculated. This stiffness matrix for the FPS element should satisfy the equation :

$$K\Delta X = \Delta F \quad (\text{C-25})$$

It is defined as a diagonal matrix as follows:

$$K = \begin{bmatrix} T & 0 & -T & 0 \\ 0 & 0 & 0 & 0 \\ -T & 0 & T & 0 \\ 0 & 0 & 0 & 0 \end{bmatrix} \quad (\text{C-26})$$

$$T = \begin{bmatrix} \Delta F_{x1} / \Delta x_1 & 0 & 0 \\ 0 & \Delta F_{x2} / \Delta x_2 & 0 \\ 0 & 0 & \Delta F_{x3} / \Delta x_3 \end{bmatrix} \quad (C-27)$$

However, to achieve convergence, it might be needed that this is smoothed through use of an average value for forces and displacements over a certain number of cycles of the same time step. For example if the current cycle is number j, Equation C-27 can be written as:

$$T = \begin{bmatrix} \sum_{i=j-4}^j \Delta F_{x1,i} / \Delta x_{1,i} & 0 & 0 \\ 0 & \sum_{i=j-4}^j \Delta F_{x2,i} / \Delta x_{2,i} & 0 \\ 0 & 0 & \sum_{i=j-4}^j \Delta F_{x3,i} / \Delta x_{3,i} \end{bmatrix} \quad (C-28)$$

After achieving convergence, all the variables having a time index are scrolled once back and the process of solving for the next time step is started.

The modified subroutine used here for FPS element is shown below:

```

SUBROUTINE CUSERG [DLLEXPORT] (IA,A,NG,NEL,IELD,ND,NOD, &
&      VNI,VNT,IGLOB,THICK, &
&      XYZ,DISP1,DISP2,TEMP1,TEMP2,TREF, &
&      SCP,CTD,CTDD,CTI,ALFA, &
&      TIME,DT,IDEATH,ETIMV,ETIMV2, &
&      NUIPT,NUIT1,NUIT2,NUIT3,XYZIPT, &
&      LGTH1,LGTH2,ARRAY,IARRAY, &
&      RUPLOT,IUPLOT, &
&      RE,AS,REBM,KEY)
!*
!* THIS SUBROUTINE IS TO BE SUPPLIED BY THE USER TO CALCULATE
!* THE FORCES AND STIFFNESS MATRIX OF A GENERAL ELEMENT
!*
!* THIS SUBROUTINE IS CALLED IN USERG FOR EACH GENERAL ELEMENT
!* TO PERFORM THE FOLLOWING OPERATIONS :
!*
!* KEY.EQ.1 INITIALIZE THE WORKING ARRAYS DURING INPUT PHASE
!* PROVIDE THE COORDINATES OF INTERIOR POINTS
!* XYZIPT OF THE ELEMENT, FOR DISPLAYING CALCULATED
!* QUANTITIES
!*
!* KEY.EQ.2 CALCULATE ELEMENT FORCES

```

```

!*|
!*| KEY.EQ.3  CALCULATE THE ELEMENT STIFFNESS
!*|
!*| KEY.EQ.4  PRINT CALCULATED FORCES AND PROVIDE OTHER
!*|           QUANTITIES (STRESSES, STRAINS, ETC)
!*|           FOR POSTPROCESSING
!*|
!*|
!*| THE FOLLOWING VARIABLES ARE PROVIDED TO PERFORM THE ABOVE OPERATIO
!*|
!*| NG           ELEMENT GROUP NUMBER
!*|
!*| NEL           ELEMENT NUMBER
!*|
!*| IELD          NUMBER OF NODES IN THE ELEMENT
!*|
!*| ND            NUMBER OF DEGREES OF FREEDOM
!*|              IN THE ELEMENT
!*|              ND=(5+IGLOB(1))+...+(5+IGLOB(IELD))
!*|              IGLOB() IS EITHER 0 OR 1
!*|
!*| NOD(IELD)     GLOBAL NODE NUMBERS OF THE ELEMENT
!*|
!*| VNI(3,IELD)   INITIAL DIRECTOR VECTORS
!*|
!*| VNT(3,IELD)   DIRECTOR VECTORS AT TIME T
!*|
!*| IGLOB(IELD)   SHELL NODAL D.O.F. FLAG ;
!*|              =0, 6 D.O.F. ASSIGNED FOR THIS NODE
!*|              =1, 5 D.O.F. ASSIGNED FOR THIS NODE
!*|
!*| THICK(IELD)   THICKNESS FOR EACH NODE
!*|
!*| XYZ(3,IELD)   ELEMENT NODAL COORDINATES
!*|
!*| DISP1(ND)     ELEMENT DISPLACEMENTS, AT TIME T
!*|
!*| DISP2(ND)     ELEMENT DISPLACEMENTS, AT TIME+DT
!*|
!*| TEMP1(IELD)   ELEMENT TEMPERATURE AT TIME T
!*|
!*| TEMP2(IELD)   ELEMENT TEMPERATURE AT TIME T+DT
!*|
!*| TREF           REFERENCE TEMPERATURE
!*|
!*| SCP(99)        SOLUTION CONTROL PARAMETERS
!*|              (MAXIMUM 99)
!*|
!*| CTD(98,IELD)  TEMPERATURE-DEPENDENT CONSTANTS
!*|              AT TIME T (MAXIMUM 98),
!*|              AT EACH ELEMENT NODE
!*|
!*| CTDD(98,IELD) TEMPERATURE-DEPENDENT CONSTANTS
!*|              AT TIME T+DT (MAXIMUM 98),
!*|              AT EACH ELEMENT NODE
!*|

```

```

!* CTI(99)      TEMPERATURE-INDEPENDENT CONSTANTS
!*              (MAXIMUM 99)
!*
!* ALFA(IELD)   COEFFICIENT OF THERMAL EXPANSION AT
!*              EACH NODE AT TIME T
!*
!* TIME        TIME AT CURRENT STEP , T+DT
!*
!* DT          TIME STEP INCREMENT , DT
!*
!* IDEATH      ELEMENT BIRTH/DEATH OPTION
!*              EQ.0 OPTION NOT USED
!*              EQ.1 ELEMENTS BECOME ACTIVE
!*              AT TIME OF BIRTH
!*              EQ.2 ELEMENTS BECOME INACTIVE
!*              AT TIME OF DEATH
!*              EQ.3 ELEMENTS BECOME ACTIVE
!*              AT TIME OF BIRTH, THEN
!*              INACTIVE AT TIME OF DEATH
!*
!* ETIMV       BIRTH TIME OF THE CURRENT ELEMENT
!*
!* ETIMV2      DEATH TIME OF THE CURRENT ELEMENT
!*
!* NUIPT       NUMBER OF INTERIOR POINTS OF THE ELEMENT,
!*              (=NUIT1*NUIT2*NUIT3) WHERE THE QUANTITIES TO BE CALCULATED FOR
!*              DISPLAY, INPUT FROM THE ADINA-IN COMMAND
!*              MATRIX USER-SUPPLIED
!*
!* NUIT1       NUMBER OF INTEGRATION POINTS IN THE
!*              FIRST LOCAL AXIS DIRECTION
!*              DEFAULT: NUIT1=1
!*
!* NUIT2       NUMBER OF INTEGRATION POINTS IN THE
!*              SECOND LOCAL AXIS DIRECTION
!*              DEFAULT: NUIT1=1
!*
!* NUIT3       NUMBER OF INTEGRATION POINTS IN THE
!*              THIRD LOCAL AXIS DIRECTION
!*              DEFAULT: NUIT3=1
!*
!* LGTH1       LENGTH OF REAL WORKING ARRAY AT EACH
!*              IPT LOCATION
!*
!* LGTH2       LENGTH OF INTEGER WORKING ARRAY AT
!*              EACH IPT LOCATION
!*
!* THE FOLLOWING VARIABLES ARE TO BE CALCULATED BY THE USER:
!*
!* ARRAY(LGTH1,NUIPT) VARIABLE LENGTH WORKING ARRAY (REAL)
!*              RECEIVED AT TIME T AND UPDATED BY
!*              USER-SUPPLIED CODING TO CORRESPOND TO
!*              TIME T+DT, STORED FOR IPT LOCATIONS
!*              (CF. "AUI" MATERIAL INPUT: LENGTH1)
!*
!* IARRAY(LGTH2,NUIPT) VARIABLE LENGTH WORKING ARRAY (INTEGER)

```

```

!*      RECEIVED AT TIME T AND UPDATED BY
!*      USER-SUPPLIED CODING TO CORRESPOND TO
!*      TIME T+DT, STORED FOR IPT LOCATIONS
!*      (CF. "AUI" MATERIAL INPUT: LENGTH2)
!*
!*      XYZIPT(3,NUIPT)   COORDINATES OF IPT LOCATIONS
!*
!*      RUPLOT(100,NUIPT) USER-CALCULATED REAL QUANTITIES AT IPT
!*      AND MUST BE PLACED IN THE FOLLOWING
!*      ORDER TO BE PROCESSED IN THE ADINA-PLOT,
!*
!*      RUPLOT(1,IPT) :STRESS-XX(-RR)
!*      RUPLOT(2,IPT) :STRESS-YY(-SS)
!*      RUPLOT(3,IPT) :STRESS-ZZ(-TT)
!*      RUPLOT(4,IPT) :STRESS-XY(-RS)
!*      RUPLOT(5,IPT) :STRESS-XZ(-RT)
!*      RUPLOT(6,IPT) :STRESS-YZ
!*      RUPLOT(7,IPT) :STRAIN-XX(-RR)
!*      RUPLOT(8,IPT) :STRAIN-YY(-SS)
!*      RUPLOT(9,IPT) :STRAIN-ZZ(-TT)
!*      RUPLOT(10,IPT):STRAIN-XY(-RS)
!*      RUPLOT(11,IPT):STRAIN-XZ(-RT)
!*      RUPLOT(12,IPT):STRAIN-YZ
!*      RUPLOT(13,IPT):PLASTIC_STRAIN-XX(-RR)
!*      RUPLOT(14,IPT):PLASTIC_STRAIN-YY(-SS)
!*      RUPLOT(15,IPT):PLASTIC_STRAIN-ZZ(-TT)
!*      RUPLOT(16,IPT):PLASTIC_STRAIN-XY(-RS)
!*      RUPLOT(17,IPT):PLASTIC_STRAIN-XZ(-RT)
!*      RUPLOT(18,IPT):PLASTIC_STRAIN-YZ
!*      RUPLOT(19,IPT):CREEP_STRAIN-XX(-RR)
!*      RUPLOT(20,IPT):CREEP_STRAIN-YY(-SS)
!*      RUPLOT(21,IPT):CREEP_STRAIN-ZZ(-TT)
!*      RUPLOT(22,IPT):CREEP_STRAIN-XY(-RS)
!*      RUPLOT(23,IPT):CREEP_STRAIN-XZ(-RT)
!*      RUPLOT(24,IPT):CREEP_STRAIN-YZ
!*      RUPLOT(25,IPT):THERMAL_STRAIN-XX(-RR)
!*      RUPLOT(26,IPT):THERMAL_STRAIN-YY(-SS)
!*      RUPLOT(27,IPT):THERMAL_STRAIN-ZZ(-TT)
!*      RUPLOT(28,IPT):THERMAL_STRAIN-XY(-RS)
!*      RUPLOT(29,IPT):THERMAL_STRAIN-XZ(-RT)
!*      RUPLOT(30,IPT):THERMAL_STRAIN-YZ
!*      RUPLOT(31,IPT):TEMPERATURE
!*      RUPLOT(32,IPT):ACCUM_EFF_PLASTIC_STRAIN
!*      RUPLOT(33,IPT):YIELD STRESS
!*
!*      IUPLOT(50,NUIPT)  USER-CALCULATED INTEGER QUANTITIES
!*      AT IPT POINT
!*      IUPLOT(1,IPT) :STRESS STATE
!*
!*      RE(ND)           ELEMENT NODAL FORCES, TO BE CALCULATED
!*      BY USER-SUPPLIED CODING
!*
!*      AS(ND,ND)        ELEMENT STIFFNESS MATRIX, TO BE
!*      CALCULATED BY USER-SUPPLIED CODING
!*
!*      REBM(ND)         BEAM-SUBTYPE ELEMENT NODAL FORCES IN

```

```

!*|          LOCAL SYSTEM, TO BE CALCULATED
!*|          BY USER-SUPPLIED CODING
!*|
CCCCCCCCCCCCCCCCCCCCCCCCCCCCCCCCCCCCCCCCCCCCCCCCCCCCCCCCCCCCCCCC
CC
!*|          !
!*| THIS SUBROUTINE IS PROVIDED FOR NONLINEAR ANALYSIS.          !
!*| IF THIS NONLINEAR GENERAL ELEMENT IS TO BE USED              !
!*| AS A LINEAR ELEMENT, THEN SET RE=0.0 AND USE                 !
!*| THE OPTION OF NO EQUILIBRIUM ITERATION IN THE ADINA EXECUTION!
!*| E.G. USE AUI COMMANDS: ITERATION METHOD=MODIFIED-NEWTON      !
!*|          EQUILIBRIUM-STEPS / @CLEAR                          !
!*|          STIFFNESS-STEPS  / @CLEAR                          !
!*|          !
!*|
CCCCCCCCCCCCCCCCCCCCCCCCCCCCCCCCCCCCCCCCCCCCCCCCCCCCCCCCCCCCCCCC
CC
!*|
implicit none
!  IMPLICIT DOUBLE PRECISION ( A-H,O-Z )
!

double precision :: x(3,1)=0._8,x1(3,1)=0._8
double precision :: normal_force,normal_force1,R, rigid_slide, all_normal_forces
double precision :: kk(3)=0._8, stiff1(3,3),norm_dx,norm_ro, ro(3,1)= 0._8
double precision :: fb(2,1)=0._8,fb1(2,1)=0._8, norm_fb1, mu= 0.1_8, d_x(3,1), center(3,1)= 0._8
double precision :: z(2,1)=0._8, z1(2,1)=0._8, norm_z1,w,w1
double precision :: real_x3, real_xn1, real_xn=0._8, old_real_xn=0._8, k_vertical,phi=0._8,teta=0._8
double precision :: vector_X(3,1),vector_Y(3,1),normal_direction(3,1)
double precision :: norm_temp,the_sign
double precision :: initial_normal_force
integer :: time_step=0, inside_2=0, inside_3=0
double precision :: mu_max=0.095_8, delta_mu=0.045_8, alpha= 0.9_8, old_x(3,1),vel(3,1),vel_plane,
vel_normal
double precision :: dx_plane(3,1), norm_dx_plane, ro_plane(3,1), norm_ro_plane
integer,parameter :: N_smooth=5
double precision :: damping, sum_dx(3), sum_df(3), all_dx(N_smooth,3), all_dforce(N_smooth,3)

      DIMENSION IA(*),A(*)
      REAL A
integer IA
integer Ield,nuipt,lgth1,lgth2,nd
integer NOD(IELD), IARRAY(LGTH2,NUIPT), IUPLLOT(50,NUIPT),IGLOB(*)
double precision SCP(99), CTI(99), CTD(98,IELD), CTDD(98,IELD)
double precision DISP1(ND), DISP2(ND) !, NOD(IELD)
double precision TEMP1(IELD), TEMP2(IELD)
double precision ARRAY(LGTH1,NUIPT) !, IARRAY(LGTH2,NUIPT)
double precision AS(ND,ND), RE(ND), REBM(ND)
double precision XYZIPT(3,NUIPT), XYZ(3,*), ALFA(IELD)
double precision RUPLLOT(100,NUIPT) !, IUPLLOT(50,NUIPT)
double precision VNI(3,*),VNT(3,*),THICK(*) !,IGLOB(*)
!
double precision xdis1, xdis2, atemp, tref, time, dt, etimv, etimv2, my_stiffness
integer IIN,key,i,j,m,nel,ipt,k,l,ng,ideath,NUIT1,NUIT2,NUIT3
integer IOUT

```

```
integer my_integer
```

```
      IIN=50
      IOUT=46
      R= CTI(1)
      k_vertical= CTI(2)
      mu_max= CTI(3)
      delta_mu= CTI(4)
      alpha= CTI(5)
      damping=CTI(6)

      GO TO (1,2,3,4), KEY
! * |
! * |
! * |  KEY = 1
! * |
! * |  INITIALIZE COMPONENTS OF REAL AND INTEGER WORKING ARRAYS
! * |  ( INITIALIZE ARRAY(LGTH1,NUIPT) AND IARRAY(LGTH2,NUIPT) )
! * |  PROVIDE XYZIPT(3,NUIPT) COORDINATES IF CALCULATED QUANTITIES
! * |  TO BE DISPLAYED INSIDE THE ELEMENT
! * |
      1 CONTINUE

      rigid_slide= 0.005_8
      initial_normal_force= 0._8
      normal_force= initial_normal_force
      normal_force1= initial_normal_force
      w=-normal_force
      w1=-normal_force1
      kk(1)= (mu+rigid_slide/R)*normal_force1/rigid_slide
      kk(2)= normal_force1/R
      kk(3)= normal_force1/2._8/R
      stiff1=0._8
      stiff1(1,1)=kk(1)
      stiff1(2,2)=kk(1)
      stiff1(3,3)= normal_force1/2._8/R

      IELD= 2
      ND= 12
      Ideath=0
      nuipt= 1
      nuit1=1
      nuit2=1
      nuit3=1
      my_stiffness =10000._8

! * |
! * |  * * *  INSERT  USER-SUPPLIED CODING
! * |
      DO 11 I=1,LGTH1
      DO 11 J=1,NUIPT
      11 ARRAY(I,J)=FLOAT(I)*FLOAT(J)*FLOAT(NEL)
      DO 12 I=1,LGTH2
```

```

DO 12 J=1,NUIPT
12 IARRAY(I,J)=I*J*NEL
!
DO 13 IPT=1,NUIPT
DO 13 L=1,3
13 XYZIPT(L,IPT)=0.0D0
!
DO 14 K=1,IELD
DO 14 L=1,3
XYZIPT(L,1)=XYZIPT(L,1)+XYZ(L,K)
14 CONTINUE
!
DO 15 M=1,3
15 XYZIPT(M,1)=XYZIPT(M,1)/IELD
!
IF (NUIPT.LT.2) GO TO 19
DO 16 IPT=2,NUIPT
DO 16 J=1,3
16 XYZIPT(J,IPT)=XYZIPT(J,1)
19 CONTINUE
RETURN
!*
!*
!* K E Y = 2
!*
!* CALCULATIONS OF ELEMENT FORCES, STRESSES, STRAINS
!*
2 CONTINUE
DO 21 I=1,ND
DO 21 J=1,ND
21 AS(I,J)=0.0D0
AS(1,1)=CTDD(1,1)
AS(1,5)=-CTDD(2,1)
AS(1,7)=-CTDD(1,1)
AS(1,11)=-CTDD(2,1)
!
AS(2,2)=CTDD(1,1)
AS(2,4)=CTDD(2,1)
AS(2,8)=-CTDD(1,1)
AS(2,10)=CTDD(2,1)
!
AS(3,3)=CTDD(3,1)
AS(3,9)=-CTDD(3,1)
!
AS(4,2)=AS(2,4)
AS(4,4)=CTDD(4,1)/3.0D0
AS(4,8)=-CTDD(2,1)
AS(4,10)=CTDD(5,1)/3.0D0
!
AS(5,1)=AS(1,5)
AS(5,5)=CTDD(4,1)/3.0D0
AS(5,7)=CTDD(2,1)
AS(5,11)=CTDD(5,1)/3.0D0
!
AS(6,6)=CTDD(6,1)/27.0D0
AS(6,12)=-CTDD(6,1)/27.0D0

```

```

!
AS(7,1)=AS(1,7)
AS(7,5)=AS(5,7)
AS(7,7)=CTDD(1,1)
AS(7,11)=CTDD(2,1)
!
AS(8,2)=AS(2,8)
AS(8,4)=AS(4,8)
AS(8,8)=CTDD(1,1)
AS(8,10)=-CTDD(2,1)
!
AS(9,3)=AS(3,9)
AS(9,9)=CTDD(3,1)
!
AS(10,2)=AS(2,10)
AS(10,4)=AS(4,10)
AS(10,8)=AS(8,10)
AS(10,10)=CTDD(4,1)/3.0D0
!
AS(11,1)=AS(1,11)
AS(11,5)=AS(5,11)
AS(11,7)=AS(7,11)
AS(11,11)=CTDD(4,1)/3.0D0
!
AS(12,6)=AS(6,12)
AS(12,12)=CTDD(6,1)/27.0D0
!
DO 22 I=1,ND
DO 22 J=I,ND
22 AS(J,I)=AS(I,J)
!
ATEMP=0.0D0
DO 295 I=1,IELD
295 ATEMP=ATEMP+TEMP2(I)/IELD
DO 296 I=1,ND
RE(I)=0.0D0
REBM(I)=0.0D0
DO 296 J=1,ND
296 RE(I)=RE(I)+AS(I,J)*DISP2(J)
REBM(1)=RE(3)
REBM(7)=RE(9)
XDIS1=DISP2(2)
XDIS2=DISP2(7)
!
DO 298 IPT=1,NUIPT
RUPLOT(7,IPT)=(XDIS1-XDIS2)
RUPLOT(1,IPT)=CTI(1)*RUPLOT(7,IPT)
IUPLOT(1,IPT)=2
RUPLOT(27,IPT)=ALFA(1)*(ATEMP-TREF)
RUPLOT(3,IPT)=CTI(1)*RUPLOT(27,IPT)
RUPLOT(31,IPT)=ATEMP
RUPLOT(33,IPT)=RUPLOT(1,IPT)
298 CONTINUE
!
DO 299 IPT=1,NUIPT
IARRAY(1,IPT)=IUPLOT(1,IPT)

```



```

DO 299 J=1,33
  ARRAY(J,IPT)=RUPLOT(J,IPT)
299 CONTINUE
!*
!* * * *   INSERT USER-SUPPLIED CODING
!*
!*

inside_2= inside_2 + 1

x1(1:3,1)= DISP2(7:9)- DISP2(1:3)
x(1:3,1)= DISP1(7:9)- DISP1(1:3)
d_x= x1-x

phi= datan2(dsqrt(x1(1,1)**2 + x1(2,1)**2),R)
if ((dabs(x1(1,1)) < 1.d-14) .and. (dabs(x1(2,1)) < 1.d-14)) then
  teta = 0._8
else
  if (x1(2,1) >= 0._8) then
    teta= datan2(x1(2,1),x1(1,1))
  else
    teta= datan2(x1(2,1),x1(1,1)) !+ 3.141592654_8
  end if
end if

! normal_direction always has a positive z component
normal_direction(1,1)= -dsin(phi)*dcos(teta)
normal_direction(2,1)= -dsin(phi)*dsin(teta)
normal_direction(3,1)= dcos(phi)
! vector_X is the tangent vector with no y- component and with always positive x component
vector_X(1,1)= 1._8/dsqrt(1._8+ dtan(phi)**2*dcos(teta)**2)
vector_X(2,1)= 0._8
vector_X(3,1)= dsign(dsqrt(1._8- vector_X(1,1)**2),dcos(teta))
! vector_Y is the other tangent vector and is equal to normal_direction*x1 and always has positive y
component
vector_Y(1,1)= normal_direction(2,1)* vector_X(3,1) - normal_direction(3,1)* vector_X(2,1)
vector_Y(2,1)= normal_direction(3,1)* vector_X(1,1) - normal_direction(1,1)* vector_X(3,1)
vector_Y(3,1)= normal_direction(1,1)* vector_X(2,1) - normal_direction(2,1)* vector_X(1,1)
!
!
real_x3= R- dsqrt(R**2-x1(1,1)**2- x1(2,1)**2) !/(x1(1,1)**2 + x1(2,1)**2)/R
real_xn1= (x1(3,1)-real_x3)*dcos(phi)
vel_normal= (real_xn1-old_real_xn)/2._8/dt

dx_plane(1,1)=d_x(1,1)*vector_X(1,1)+ d_x(2,1)*vector_X(2,1)+ d_x(3,1)*vector_X(3,1)
dx_plane(2,1)=d_x(1,1)*vector_Y(1,1)+ d_x(2,1)*vector_Y(2,1)+ d_x(3,1)*vector_Y(3,1)
dx_plane(3,1)=0._8
norm_dx_plane=dsqrt(dx_plane(1,1)**2 +dx_plane(2,1)**2)

vel=(x1-old_x)/2._8/dt
vel_plane= dsqrt(vel(1,1)**2 + vel(2,1)**2 + vel(3,1)**2 -(vel(1,1)*normal_direction(1,1) +
vel(2,1)*normal_direction(2,1) + vel(3,1)*normal_direction(3,1))**2 )
mu= mu_max- delta_mu*dexp(-alpha*vel_plane)

ro= x1-center

```

```

ro_plane(1,1)=ro(1,1)*vector_X(1,1)+ ro(2,1)*vector_X(2,1)+ ro(3,1)*vector_X(3,1)
ro_plane(2,1)=ro(1,1)*vector_Y(1,1)+ ro(2,1)*vector_Y(2,1)+ ro(3,1)*vector_Y(3,1)
norm_ro_plane=dsqrt(ro_plane(1,1)**2 +ro_plane(2,1)**2)

ro_plane(3,1)=0._8
norm_dx= dsqrt(d_x(1,1)**2 + d_x(2,1)**2 + d_x(3,1)**2)

z1=ro_plane(1:2,1:1)/rigid_slide

norm_z1= dsqrt(z1(1,1)**2 + z1(2,1)**2)

if (norm_z1 > 1._8) then
    z1=z1/norm_z1
    norm_z1= dsqrt(z1(1,1)**2 + z1(2,1)**2)
end if

normal_force1= -(k_vertical*(x1(3,1)-real_x3)*dcos(phi) - initial_normal_force) - damping*vel_normal
if (normal_force1 < 0._8) normal_force1=0._8
all_normal_forces= normal_force1
fb1(1,1)= all_normal_forces* -normal_direction(1,1) + normal_force1* ( mu*z1(1,1)*dabs(vector_X(1,1)) +
mu*z1(2,1)*vector_Y(1,1))
fb1(2,1)= all_normal_forces* -normal_direction(2,1) + normal_force1* ( mu*z1(2,1)*dabs(vector_Y(2,1)))
w1= normal_force1* (mu*z1(1,1)*vector_X(3,1) + mu*z1(2,1)*vector_Y(3,1)) + all_normal_forces* -
normal_direction(3,1)

    RE(7)= fb1(1,1)
    RE(8)= fb1(2,1)
    RE(9)= w1
    RE(10)= 0._8
    RE(11)= 0._8
    RE(12)= 0._8
    RE(1)= -fb1(1,1) !RE(7)
    RE(2)= -fb1(2,1) !RE(8)
    RE(3)= -w1 !RE(9)
    RE(4)= 0._8
    RE(5)= 0._8
    RE(6)= 0._8

    RETURN
!*
!* K E Y = 3
!*
!* FORM GENERAL ELEMENT STIFFNESS
!* ( CALCULATE AS(ND,ND) )
!*
    3 CONTINUE
    DO 31 I=1,ND
    DO 31 J=1,ND
    31 AS(I,J)=0.0D0
    AS(1,1)=CTDD(1,1)
    AS(1,5)=-CTDD(2,1)
    AS(1,7)=-CTDD(1,1)
    AS(1,11)=-CTDD(2,1)

```

```

!
AS(2,2)=CTDD(1,1)
AS(2,4)=CTDD(2,1)
AS(2,8)=-CTDD(1,1)
AS(2,10)=CTDD(2,1)
!
AS(3,3)=CTDD(3,1)
AS(3,9)=-CTDD(3,1)
!
AS(4,2)=AS(2,4)
AS(4,4)=CTDD(4,1)/3.0D0
AS(4,8)=-CTDD(2,1)
AS(4,10)=CTDD(5,1)/3.0D0
!
AS(5,1)=AS(1,5)
AS(5,5)=CTDD(4,1)/3.0D0
AS(5,7)=CTDD(2,1)
AS(5,11)=CTDD(5,1)/3.0D0
!
AS(6,6)=CTDD(6,1)/27.0D0
AS(6,12)=-CTDD(6,1)/27.0D0
!
AS(7,1)=AS(1,7)
AS(7,5)=AS(5,7)
AS(7,7)=CTDD(1,1)
AS(7,11)=CTDD(2,1)
!
AS(8,2)=AS(2,8)
AS(8,4)=AS(4,8)
AS(8,8)=CTDD(1,1)
AS(8,10)=-CTDD(2,1)
!
AS(9,3)=AS(3,9)
AS(9,9)=CTDD(3,1)
!
AS(10,2)=AS(2,10)
AS(10,4)=AS(4,10)
AS(10,8)=AS(8,10)
AS(10,10)=CTDD(4,1)/3.0D0
!
AS(11,1)=AS(1,11)
AS(11,5)=AS(5,11)
AS(11,7)=AS(7,11)
AS(11,11)=CTDD(4,1)/3.0D0
!
AS(12,6)=AS(6,12)
AS(12,12)=CTDD(6,1)/27.0D0
!
!*
!* *** INSERT USER-SUPPLIED CODING
!*
! assigning the stiffnesses

inside_3= inside_3 + 1

do j=1,N_smooth-1
  forall (i=1:3) all_dx(j,i)=all_dx(j+1,i)

```

```

        forall (i=1:3) all_dforce(j,i)=all_dforce(j+1,i)
    end do
    forall (i=1:3) all_dx(N_smooth,i)=d_x(i,1)
    forall (i=1:2) all_dforce(N_smooth,i)=fb1(i,1)-fb(i,1)
    all_dforce(N_smooth,3)=w1-w
    sum_dx=0._8
    sum_df=0._8

    do j=1,N_smooth
        do i=1,3
            sum_dx(i)= sum_dx(i)+ all_dx(j,i)
            sum_df(i)= sum_df(i)+ all_dforce(j,i)
        end do
    end do

    if (inside_3<20) then

        if(dabs(d_x(3,1)) > 1.d-14) then
            kk(3)= (w1-w)/ d_x(3,1)
        end if
        !if (time_step <4)          kk(3)= k_vertical

        do j=1,2
            if (dabs(d_x(j,1)) > 1.d-14 ) then
                kk(j)=(fb1(j,1)- fb(j,1))/ d_x(j,1)
            end if
        end do

    else
        forall (j=1:3) kk(j)=sum_dx(j)/sum_df(j)
    end if

    do j=1,3
        stiff1(j,j)=kk(j)
    end do

    AS(1:3,1:3)= stiff1
    AS(1:3,7:9)= -stiff1
    AS(7:9,7:9)= AS(1:3,1:3)
    AS(7:9,1:3)= AS(1:3,7:9)
    AS(4:6,1:12)= 0._8
    AS(10:12,1:12)= 0._8
    AS(1:12,4:6)= 0._8
    AS(1:12,10:12)= 0._8

    !

    DO 32 I=1,ND
    DO 32 J=I,ND
    32 AS(J,I)=AS(I,J)
    RETURN
    !*
    !*
    !* K E Y = 4

```

```

!*|
!*| PRINTING OF ELEMENT RESPONSE
!*| ( PRINT FORCES, STRESSES, STRAINS )
!*|
  4 CONTINUE
  IF (NEL.EQ.1) WRITE (IOUT,9000)
  DO 499 IPT=1,NUIPT
  IF (IPT.EQ.1) WRITE (IOUT,9002) NEL
  WRITE (IOUT,9003) IPT,(RUPLOT(I,IPT),I=1,12)
499 CONTINUE
!
!*|
!*| *** INSERT USER-SUPPLIED CODING
!*|
time_step=time_step+1
inside_2= 0
inside_3= 0
if (norm_ro_plane > rigid_slide) then
      center(1:3,1) = DISP2(7:9)- DISP2(1:3) - rigid_slide* ro(1:3,1)/ norm_ro_plane
end if

normal_force=normal_force1
w=w1
fb=fb1
old_x=x
x=x1
z=z1
old_real_xn=real_xn
real_xn=real_xn1
!*|
  RETURN
9000 FORMAT (//,4X,3HNEL,2X,3HIPT,6X,9HSTRESS-RR,6X,      &
  & 9HSTRESS-SS,6X,9HSTRESS-TT,6X,9HSTRESS-RS,6X,      &
  & 9HSTRESS-RT,6X,9HSTRESS-ST,/, 20X,9HSTRAIN-RR,6X, &
  & 9HSTRAIN-SS,6X,9HSTRAIN-TT,6X,9HSTRAIN-RS,6X,      &
  & 9HSTRAIN-RT,6X,9HSTRAIN-ST,/)
9002 FORMAT (/ 17 /)
9003 FORMAT (7X,I5,8(2X,E13.6)/102X,2(2X,E13.6)/      &
  & 14X,8(2X,E13.6)/102X,2(2X,E13.6))
!*|FILE END
  END subroutine cuserg

```

This subroutine should be compiled and linked to other subroutines of ADINA existing under the same directory. The steps required are [ADINA, 2002]:

- 1- Run *dfvars.bat* from the compiler you use to make its compiler the active compiler
- 2- Put the compiled version of the subroutine that is *ovl160u.obj* where the original file *ovl160u.f* is installed.
- 3- Run NMAKE (type NMAKE) in that directory.

There are also steps that should be taken to put the relevant information about the model to be analyzed in the ADINA input file. This is achieved through insertion of the commands defining

the user-supplied material group, its associated mass, damping and stiffness matrices, and the element group in the input file (that will have *.in* extension).

The command MATERIAL USER-SUPPLIED defines a material group that will be used for the element [ADINA, 2001(b)]. The characteristics of FPS bearings can be provided here. In this command, $CTI1 = R$, the bearing radius, $CTI2 = k_{normal}$, $CTI3 = \mu_{max}$, $CTI4 = \Delta\mu$, $CTI5 = \alpha$, and $CTI6 = c$, the damping associated with k_{normal} . All these symbols are the same as those defined in Section 2. Dummy values for CTI7~CTI10 and SCP1 ~SCP5 are provided in case that more constants will be required to represent additional parameters. The command EGROUP defines the element group with the specified set of characteristics determined using MATRIXSE=1 [ADINA, 2001(b)]. The command MATRIX USER-SUPP is used to define the element type. Mass, stress, and damping matrices are defined next. There is no internal mass considered for the element and there is no need for any stress calculation inside it. The damping is also taken care of directly inside the subroutine and through the coefficient CTI6. However, these dummy matrices with zero elements should be defined since they are required in the command MATRIXSET that defines the set of characteristics related to the defined element group. The following is an example of this part of the input file. If the bearings have different characteristics, they can be defined under more than one element group.

```

*
MATERIAL USER-SUPPLIED NAME=1 INTEG=FORWARD NSUBD=10,
  TREF=0.0000000000000000 DENSITY=0.0000000000000000 LENGTH1=65,
  LENGTH2=5 OPTION=NONE NCTI=10 NSCP=5 NCTD=0,
  CTI1=60.0000000000000000 CTI2=1.1705000000000000E+07,
  CTI3=0.095000000000000000 CTI4=0.045000000000000000,
  CTI5=0.900000000000000000 CTI6=41914.700000000000,
  CTI7=-5.0000000000000000E+07 CTI8=1.0000000000000000E+08,
  CTI9=-5.0000000000000000E+07 CTI10=1.0000000000000000E+08,
  SCP1=2.0000000000000000E+09 SCP2=100000.000000000000,
  SCP3=10000.000000000000 SCP4=1000.000000000000,
  SCP5=100.00000000000000
*
EGROUP GENERAL NAME=1 MATRIXSE=1 RESULTS=FORCES SKEWSYST=NO,
  USER-SUP=YES
*
MATRIX USER-SUPP NAME=1 ELEMENT-=THREEDSOLID ELNDOF=6 MATERIAL=1,
  NUIPT=1 NUIT1=1 NUIT2=1 NUIT3=1
*
MATRIX MASS NAME=2 ND=12
@CLEAR
1 0.0000000000000000
2 0.0000000000000000
3 0.0000000000000000
4 0.0000000000000000
5 0.0000000000000000
6 0.0000000000000000
7 0.0000000000000000
8 0.0000000000000000
9 0.0000000000000000
10 0.0000000000000000
11 0.0000000000000000

```


The following points regarding the proper choice of values should be considered for the element to work:

- 1- This is a highly nonlinear element. For the simplest cases use of $\Delta t > 0.001s$ is not recommended and for bigger and more complex models, convergence may require $\Delta t = 0.0002s$ or smaller.
- 2- The choice of dimensions and vertical spring constants used for the model should be such that it does not jeopardize accuracy or prevent convergence. The spring used should have stiffness high enough to act rigidly. This may require a frequency of at least 50Hz. The corresponding damping should be high as well to prevent any excessive excitation in this spring so that the value of normal force calculated remains accurate. These considerations mean high values for the stiffness and damping. However, the tolerance chosen for the convergence of the model cannot be outside a certain range. A bigger tolerance will mean loss of accuracy and smaller tolerance will require very large number of cycles that will exceed ADINA limits. The stiffness should be of dimensions that combined with this tolerance describe the behavior with enough accuracy. A Proper choice of dimension units will require some experiments by the user.

MCEER Technical Reports

MCEER publishes technical reports on a variety of subjects written by authors funded through MCEER. These reports are available from both MCEER Publications and the National Technical Information Service (NTIS). Requests for reports should be directed to MCEER Publications, MCEER, University at Buffalo, State University of New York, Red Jacket Quadrangle, Buffalo, New York 14261. Reports can also be requested through NTIS, 5285 Port Royal Road, Springfield, Virginia 22161. NTIS accession numbers are shown in parenthesis, if available.

- NCEER-87-0001 "First-Year Program in Research, Education and Technology Transfer," 3/5/87, (PB88-134275, A04, MF-A01).
- NCEER-87-0002 "Experimental Evaluation of Instantaneous Optimal Algorithms for Structural Control," by R.C. Lin, T.T. Soong and A.M. Reinhorn, 4/20/87, (PB88-134341, A04, MF-A01).
- NCEER-87-0003 "Experimentation Using the Earthquake Simulation Facilities at University at Buffalo," by A.M. Reinhorn and R.L. Ketter, to be published.
- NCEER-87-0004 "The System Characteristics and Performance of a Shaking Table," by J.S. Hwang, K.C. Chang and G.C. Lee, 6/1/87, (PB88-134259, A03, MF-A01). This report is available only through NTIS (see address given above).
- NCEER-87-0005 "A Finite Element Formulation for Nonlinear Viscoplastic Material Using a Q Model," by O. Gyebe and G. Dasgupta, 11/2/87, (PB88-213764, A08, MF-A01).
- NCEER-87-0006 "Symbolic Manipulation Program (SMP) - Algebraic Codes for Two and Three Dimensional Finite Element Formulations," by X. Lee and G. Dasgupta, 11/9/87, (PB88-218522, A05, MF-A01).
- NCEER-87-0007 "Instantaneous Optimal Control Laws for Tall Buildings Under Seismic Excitations," by J.N. Yang, A. Akbarpour and P. Ghaemmaghami, 6/10/87, (PB88-134333, A06, MF-A01). This report is only available through NTIS (see address given above).
- NCEER-87-0008 "IDARC: Inelastic Damage Analysis of Reinforced Concrete Frame - Shear-Wall Structures," by Y.J. Park, A.M. Reinhorn and S.K. Kunnath, 7/20/87, (PB88-134325, A09, MF-A01). This report is only available through NTIS (see address given above).
- NCEER-87-0009 "Liquefaction Potential for New York State: A Preliminary Report on Sites in Manhattan and Buffalo," by M. Budhu, V. Vijayakumar, R.F. Giese and L. Baumgras, 8/31/87, (PB88-163704, A03, MF-A01). This report is available only through NTIS (see address given above).
- NCEER-87-0010 "Vertical and Torsional Vibration of Foundations in Inhomogeneous Media," by A.S. Veletsos and K.W. Dotson, 6/1/87, (PB88-134291, A03, MF-A01). This report is only available through NTIS (see address given above).
- NCEER-87-0011 "Seismic Probabilistic Risk Assessment and Seismic Margins Studies for Nuclear Power Plants," by Howard H.M. Hwang, 6/15/87, (PB88-134267, A03, MF-A01). This report is only available through NTIS (see address given above).
- NCEER-87-0012 "Parametric Studies of Frequency Response of Secondary Systems Under Ground-Acceleration Excitations," by Y. Yong and Y.K. Lin, 6/10/87, (PB88-134309, A03, MF-A01). This report is only available through NTIS (see address given above).
- NCEER-87-0013 "Frequency Response of Secondary Systems Under Seismic Excitation," by J.A. HoLung, J. Cai and Y.K. Lin, 7/31/87, (PB88-134317, A05, MF-A01). This report is only available through NTIS (see address given above).
- NCEER-87-0014 "Modelling Earthquake Ground Motions in Seismically Active Regions Using Parametric Time Series Methods," by G.W. Ellis and A.S. Cakmak, 8/25/87, (PB88-134283, A08, MF-A01). This report is only available through NTIS (see address given above).
- NCEER-87-0015 "Detection and Assessment of Seismic Structural Damage," by E. DiPasquale and A.S. Cakmak, 8/25/87, (PB88-163712, A05, MF-A01). This report is only available through NTIS (see address given above).

- NCEER-87-0016 "Pipeline Experiment at Parkfield, California," by J. Isenberg and E. Richardson, 9/15/87, (PB88-163720, A03, MF-A01). This report is available only through NTIS (see address given above).
- NCEER-87-0017 "Digital Simulation of Seismic Ground Motion," by M. Shinozuka, G. Deodatis and T. Harada, 8/31/87, (PB88-155197, A04, MF-A01). This report is available only through NTIS (see address given above).
- NCEER-87-0018 "Practical Considerations for Structural Control: System Uncertainty, System Time Delay and Truncation of Small Control Forces," J.N. Yang and A. Akbarpour, 8/10/87, (PB88-163738, A08, MF-A01). This report is only available through NTIS (see address given above).
- NCEER-87-0019 "Modal Analysis of Nonclassically Damped Structural Systems Using Canonical Transformation," by J.N. Yang, S. Sarkani and F.X. Long, 9/27/87, (PB88-187851, A04, MF-A01).
- NCEER-87-0020 "A Nonstationary Solution in Random Vibration Theory," by J.R. Red-Horse and P.D. Spanos, 11/3/87, (PB88-163746, A03, MF-A01).
- NCEER-87-0021 "Horizontal Impedances for Radially Inhomogeneous Viscoelastic Soil Layers," by A.S. Veletsos and K.W. Dotson, 10/15/87, (PB88-150859, A04, MF-A01).
- NCEER-87-0022 "Seismic Damage Assessment of Reinforced Concrete Members," by Y.S. Chung, C. Meyer and M. Shinozuka, 10/9/87, (PB88-150867, A05, MF-A01). This report is available only through NTIS (see address given above).
- NCEER-87-0023 "Active Structural Control in Civil Engineering," by T.T. Soong, 11/11/87, (PB88-187778, A03, MF-A01).
- NCEER-87-0024 "Vertical and Torsional Impedances for Radially Inhomogeneous Viscoelastic Soil Layers," by K.W. Dotson and A.S. Veletsos, 12/87, (PB88-187786, A03, MF-A01).
- NCEER-87-0025 "Proceedings from the Symposium on Seismic Hazards, Ground Motions, Soil-Liquefaction and Engineering Practice in Eastern North America," October 20-22, 1987, edited by K.H. Jacob, 12/87, (PB88-188115, A23, MF-A01). This report is available only through NTIS (see address given above).
- NCEER-87-0026 "Report on the Whittier-Narrows, California, Earthquake of October 1, 1987," by J. Pantelic and A. Reinhorn, 11/87, (PB88-187752, A03, MF-A01). This report is available only through NTIS (see address given above).
- NCEER-87-0027 "Design of a Modular Program for Transient Nonlinear Analysis of Large 3-D Building Structures," by S. Srivastav and J.F. Abel, 12/30/87, (PB88-187950, A05, MF-A01). This report is only available through NTIS (see address given above).
- NCEER-87-0028 "Second-Year Program in Research, Education and Technology Transfer," 3/8/88, (PB88-219480, A04, MF-A01).
- NCEER-88-0001 "Workshop on Seismic Computer Analysis and Design of Buildings With Interactive Graphics," by W. McGuire, J.F. Abel and C.H. Conley, 1/18/88, (PB88-187760, A03, MF-A01). This report is only available through NTIS (see address given above).
- NCEER-88-0002 "Optimal Control of Nonlinear Flexible Structures," by J.N. Yang, F.X. Long and D. Wong, 1/22/88, (PB88-213772, A06, MF-A01).
- NCEER-88-0003 "Substructuring Techniques in the Time Domain for Primary-Secondary Structural Systems," by G.D. Manolis and G. Juhn, 2/10/88, (PB88-213780, A04, MF-A01).
- NCEER-88-0004 "Iterative Seismic Analysis of Primary-Secondary Systems," by A. Singhal, L.D. Lutes and P.D. Spanos, 2/23/88, (PB88-213798, A04, MF-A01).
- NCEER-88-0005 "Stochastic Finite Element Expansion for Random Media," by P.D. Spanos and R. Ghanem, 3/14/88, (PB88-213806, A03, MF-A01).

- NCEER-88-0006 "Combining Structural Optimization and Structural Control," by F.Y. Cheng and C.P. Pantelides, 1/10/88, (PB88-213814, A05, MF-A01).
- NCEER-88-0007 "Seismic Performance Assessment of Code-Designed Structures," by H.H-M. Hwang, J-W. Jaw and H-J. Shau, 3/20/88, (PB88-219423, A04, MF-A01). This report is only available through NTIS (see address given above).
- NCEER-88-0008 "Reliability Analysis of Code-Designed Structures Under Natural Hazards," by H.H-M. Hwang, H. Ushiba and M. Shinozuka, 2/29/88, (PB88-229471, A07, MF-A01). This report is only available through NTIS (see address given above).
- NCEER-88-0009 "Seismic Fragility Analysis of Shear Wall Structures," by J-W Jaw and H.H-M. Hwang, 4/30/88, (PB89-102867, A04, MF-A01).
- NCEER-88-0010 "Base Isolation of a Multi-Story Building Under a Harmonic Ground Motion - A Comparison of Performances of Various Systems," by F-G Fan, G. Ahmadi and I.G. Tadjbakhsh, 5/18/88, (PB89-122238, A06, MF-A01). This report is only available through NTIS (see address given above).
- NCEER-88-0011 "Seismic Floor Response Spectra for a Combined System by Green's Functions," by F.M. Lavelle, L.A. Bergman and P.D. Spanos, 5/1/88, (PB89-102875, A03, MF-A01).
- NCEER-88-0012 "A New Solution Technique for Randomly Excited Hysteretic Structures," by G.Q. Cai and Y.K. Lin, 5/16/88, (PB89-102883, A03, MF-A01).
- NCEER-88-0013 "A Study of Radiation Damping and Soil-Structure Interaction Effects in the Centrifuge," by K. Weissman, supervised by J.H. Prevost, 5/24/88, (PB89-144703, A06, MF-A01).
- NCEER-88-0014 "Parameter Identification and Implementation of a Kinematic Plasticity Model for Frictional Soils," by J.H. Prevost and D.V. Griffiths, to be published.
- NCEER-88-0015 "Two- and Three- Dimensional Dynamic Finite Element Analyses of the Long Valley Dam," by D.V. Griffiths and J.H. Prevost, 6/17/88, (PB89-144711, A04, MF-A01).
- NCEER-88-0016 "Damage Assessment of Reinforced Concrete Structures in Eastern United States," by A.M. Reinhorn, M.J. Seidel, S.K. Kunnath and Y.J. Park, 6/15/88, (PB89-122220, A04, MF-A01). This report is only available through NTIS (see address given above).
- NCEER-88-0017 "Dynamic Compliance of Vertically Loaded Strip Foundations in Multilayered Viscoelastic Soils," by S. Ahmad and A.S.M. Israil, 6/17/88, (PB89-102891, A04, MF-A01).
- NCEER-88-0018 "An Experimental Study of Seismic Structural Response With Added Viscoelastic Dampers," by R.C. Lin, Z. Liang, T.T. Soong and R.H. Zhang, 6/30/88, (PB89-122212, A05, MF-A01). This report is available only through NTIS (see address given above).
- NCEER-88-0019 "Experimental Investigation of Primary - Secondary System Interaction," by G.D. Manolis, G. Juhn and A.M. Reinhorn, 5/27/88, (PB89-122204, A04, MF-A01).
- NCEER-88-0020 "A Response Spectrum Approach For Analysis of Nonclassically Damped Structures," by J.N. Yang, S. Sarkani and F.X. Long, 4/22/88, (PB89-102909, A04, MF-A01).
- NCEER-88-0021 "Seismic Interaction of Structures and Soils: Stochastic Approach," by A.S. Veletsos and A.M. Prasad, 7/21/88, (PB89-122196, A04, MF-A01). This report is only available through NTIS (see address given above).
- NCEER-88-0022 "Identification of the Serviceability Limit State and Detection of Seismic Structural Damage," by E. DiPasquale and A.S. Cakmak, 6/15/88, (PB89-122188, A05, MF-A01). This report is available only through NTIS (see address given above).
- NCEER-88-0023 "Multi-Hazard Risk Analysis: Case of a Simple Offshore Structure," by B.K. Bhartia and E.H. Vanmarcke, 7/21/88, (PB89-145213, A05, MF-A01).

- NCEER-88-0024 "Automated Seismic Design of Reinforced Concrete Buildings," by Y.S. Chung, C. Meyer and M. Shinozuka, 7/5/88, (PB89-122170, A06, MF-A01). This report is available only through NTIS (see address given above).
- NCEER-88-0025 "Experimental Study of Active Control of MDOF Structures Under Seismic Excitations," by L.L. Chung, R.C. Lin, T.T. Soong and A.M. Reinhorn, 7/10/88, (PB89-122600, A04, MF-A01).
- NCEER-88-0026 "Earthquake Simulation Tests of a Low-Rise Metal Structure," by J.S. Hwang, K.C. Chang, G.C. Lee and R.L. Ketter, 8/1/88, (PB89-102917, A04, MF-A01).
- NCEER-88-0027 "Systems Study of Urban Response and Reconstruction Due to Catastrophic Earthquakes," by F. Kozin and H.K. Zhou, 9/22/88, (PB90-162348, A04, MF-A01).
- NCEER-88-0028 "Seismic Fragility Analysis of Plane Frame Structures," by H.H-M. Hwang and Y.K. Low, 7/31/88, (PB89-131445, A06, MF-A01).
- NCEER-88-0029 "Response Analysis of Stochastic Structures," by A. Kardara, C. Bucher and M. Shinozuka, 9/22/88, (PB89-174429, A04, MF-A01).
- NCEER-88-0030 "Nonnormal Accelerations Due to Yielding in a Primary Structure," by D.C.K. Chen and L.D. Lutes, 9/19/88, (PB89-131437, A04, MF-A01).
- NCEER-88-0031 "Design Approaches for Soil-Structure Interaction," by A.S. Veletsos, A.M. Prasad and Y. Tang, 12/30/88, (PB89-174437, A03, MF-A01). This report is available only through NTIS (see address given above).
- NCEER-88-0032 "A Re-evaluation of Design Spectra for Seismic Damage Control," by C.J. Turkstra and A.G. Tallin, 11/7/88, (PB89-145221, A05, MF-A01).
- NCEER-88-0033 "The Behavior and Design of Noncontact Lap Splices Subjected to Repeated Inelastic Tensile Loading," by V.E. Sagan, P. Gergely and R.N. White, 12/8/88, (PB89-163737, A08, MF-A01).
- NCEER-88-0034 "Seismic Response of Pile Foundations," by S.M. Mamoon, P.K. Banerjee and S. Ahmad, 11/1/88, (PB89-145239, A04, MF-A01).
- NCEER-88-0035 "Modeling of R/C Building Structures With Flexible Floor Diaphragms (IDARC2)," by A.M. Reinhorn, S.K. Kunnath and N. Panahshahi, 9/7/88, (PB89-207153, A07, MF-A01).
- NCEER-88-0036 "Solution of the Dam-Reservoir Interaction Problem Using a Combination of FEM, BEM with Particular Integrals, Modal Analysis, and Substructuring," by C-S. Tsai, G.C. Lee and R.L. Ketter, 12/31/88, (PB89-207146, A04, MF-A01).
- NCEER-88-0037 "Optimal Placement of Actuators for Structural Control," by F.Y. Cheng and C.P. Pantelides, 8/15/88, (PB89-162846, A05, MF-A01).
- NCEER-88-0038 "Teflon Bearings in Aseismic Base Isolation: Experimental Studies and Mathematical Modeling," by A. Mokha, M.C. Constantinou and A.M. Reinhorn, 12/5/88, (PB89-218457, A10, MF-A01). This report is available only through NTIS (see address given above).
- NCEER-88-0039 "Seismic Behavior of Flat Slab High-Rise Buildings in the New York City Area," by P. Weidlinger and M. Ettouney, 10/15/88, (PB90-145681, A04, MF-A01).
- NCEER-88-0040 "Evaluation of the Earthquake Resistance of Existing Buildings in New York City," by P. Weidlinger and M. Ettouney, 10/15/88, to be published.
- NCEER-88-0041 "Small-Scale Modeling Techniques for Reinforced Concrete Structures Subjected to Seismic Loads," by W. Kim, A. El-Attar and R.N. White, 11/22/88, (PB89-189625, A05, MF-A01).
- NCEER-88-0042 "Modeling Strong Ground Motion from Multiple Event Earthquakes," by G.W. Ellis and A.S. Cakmak, 10/15/88, (PB89-174445, A03, MF-A01).

- NCEER-88-0043 "Nonstationary Models of Seismic Ground Acceleration," by M. Grigoriu, S.E. Ruiz and E. Rosenblueth, 7/15/88, (PB89-189617, A04, MF-A01).
- NCEER-88-0044 "SARCF User's Guide: Seismic Analysis of Reinforced Concrete Frames," by Y.S. Chung, C. Meyer and M. Shinozuka, 11/9/88, (PB89-174452, A08, MF-A01).
- NCEER-88-0045 "First Expert Panel Meeting on Disaster Research and Planning," edited by J. Pantelic and J. Stoyke, 9/15/88, (PB89-174460, A05, MF-A01).
- NCEER-88-0046 "Preliminary Studies of the Effect of Degrading Infill Walls on the Nonlinear Seismic Response of Steel Frames," by C.Z. Chrysostomou, P. Gergely and J.F. Abel, 12/19/88, (PB89-208383, A05, MF-A01).
- NCEER-88-0047 "Reinforced Concrete Frame Component Testing Facility - Design, Construction, Instrumentation and Operation," by S.P. Pessiki, C. Conley, T. Bond, P. Gergely and R.N. White, 12/16/88, (PB89-174478, A04, MF-A01).
- NCEER-89-0001 "Effects of Protective Cushion and Soil Compliancy on the Response of Equipment Within a Seismically Excited Building," by J.A. HoLung, 2/16/89, (PB89-207179, A04, MF-A01).
- NCEER-89-0002 "Statistical Evaluation of Response Modification Factors for Reinforced Concrete Structures," by H.H-M. Hwang and J-W. Jaw, 2/17/89, (PB89-207187, A05, MF-A01).
- NCEER-89-0003 "Hysteretic Columns Under Random Excitation," by G-Q. Cai and Y.K. Lin, 1/9/89, (PB89-196513, A03, MF-A01).
- NCEER-89-0004 "Experimental Study of 'Elephant Foot Bulge' Instability of Thin-Walled Metal Tanks," by Z-H. Jia and R.L. Ketter, 2/22/89, (PB89-207195, A03, MF-A01).
- NCEER-89-0005 "Experiment on Performance of Buried Pipelines Across San Andreas Fault," by J. Isenberg, E. Richardson and T.D. O'Rourke, 3/10/89, (PB89-218440, A04, MF-A01). This report is available only through NTIS (see address given above).
- NCEER-89-0006 "A Knowledge-Based Approach to Structural Design of Earthquake-Resistant Buildings," by M. Subramani, P. Gergely, C.H. Conley, J.F. Abel and A.H. Zaghaw, 1/15/89, (PB89-218465, A06, MF-A01).
- NCEER-89-0007 "Liquefaction Hazards and Their Effects on Buried Pipelines," by T.D. O'Rourke and P.A. Lane, 2/1/89, (PB89-218481, A09, MF-A01).
- NCEER-89-0008 "Fundamentals of System Identification in Structural Dynamics," by H. Imai, C-B. Yun, O. Maruyama and M. Shinozuka, 1/26/89, (PB89-207211, A04, MF-A01).
- NCEER-89-0009 "Effects of the 1985 Michoacan Earthquake on Water Systems and Other Buried Lifelines in Mexico," by A.G. Ayala and M.J. O'Rourke, 3/8/89, (PB89-207229, A06, MF-A01).
- NCEER-89-R010 "NCEER Bibliography of Earthquake Education Materials," by K.E.K. Ross, Second Revision, 9/1/89, (PB90-125352, A05, MF-A01). This report is replaced by NCEER-92-0018.
- NCEER-89-0011 "Inelastic Three-Dimensional Response Analysis of Reinforced Concrete Building Structures (IDARC-3D), Part I - Modeling," by S.K. Kunnath and A.M. Reinhorn, 4/17/89, (PB90-114612, A07, MF-A01). This report is available only through NTIS (see address given above).
- NCEER-89-0012 "Recommended Modifications to ATC-14," by C.D. Poland and J.O. Malley, 4/12/89, (PB90-108648, A15, MF-A01).
- NCEER-89-0013 "Repair and Strengthening of Beam-to-Column Connections Subjected to Earthquake Loading," by M. Corazao and A.J. Durrani, 2/28/89, (PB90-109885, A06, MF-A01).
- NCEER-89-0014 "Program EXKAL2 for Identification of Structural Dynamic Systems," by O. Maruyama, C-B. Yun, M. Hoshiya and M. Shinozuka, 5/19/89, (PB90-109877, A09, MF-A01).

- NCEER-89-0015 "Response of Frames With Bolted Semi-Rigid Connections, Part I - Experimental Study and Analytical Predictions," by P.J. DiCorso, A.M. Reinhorn, J.R. Dickerson, J.B. Radzinski and W.L. Harper, 6/1/89, to be published.
- NCEER-89-0016 "ARMA Monte Carlo Simulation in Probabilistic Structural Analysis," by P.D. Spanos and M.P. Mignolet, 7/10/89, (PB90-109893, A03, MF-A01).
- NCEER-89-P017 "Preliminary Proceedings from the Conference on Disaster Preparedness - The Place of Earthquake Education in Our Schools," Edited by K.E.K. Ross, 6/23/89, (PB90-108606, A03, MF-A01).
- NCEER-89-0017 "Proceedings from the Conference on Disaster Preparedness - The Place of Earthquake Education in Our Schools," Edited by K.E.K. Ross, 12/31/89, (PB90-207895, A012, MF-A02). This report is available only through NTIS (see address given above).
- NCEER-89-0018 "Multidimensional Models of Hysteretic Material Behavior for Vibration Analysis of Shape Memory Energy Absorbing Devices, by E.J. Graesser and F.A. Cozzarelli, 6/7/89, (PB90-164146, A04, MF-A01).
- NCEER-89-0019 "Nonlinear Dynamic Analysis of Three-Dimensional Base Isolated Structures (3D-BASIS)," by S. Nagarajaiah, A.M. Reinhorn and M.C. Constantinou, 8/3/89, (PB90-161936, A06, MF-A01). This report has been replaced by NCEER-93-0011.
- NCEER-89-0020 "Structural Control Considering Time-Rate of Control Forces and Control Rate Constraints," by F.Y. Cheng and C.P. Pantelides, 8/3/89, (PB90-120445, A04, MF-A01).
- NCEER-89-0021 "Subsurface Conditions of Memphis and Shelby County," by K.W. Ng, T-S. Chang and H-H.M. Hwang, 7/26/89, (PB90-120437, A03, MF-A01).
- NCEER-89-0022 "Seismic Wave Propagation Effects on Straight Jointed Buried Pipelines," by K. Elhadi and M.J. O'Rourke, 8/24/89, (PB90-162322, A10, MF-A02).
- NCEER-89-0023 "Workshop on Serviceability Analysis of Water Delivery Systems," edited by M. Grigoriu, 3/6/89, (PB90-127424, A03, MF-A01).
- NCEER-89-0024 "Shaking Table Study of a 1/5 Scale Steel Frame Composed of Tapered Members," by K.C. Chang, J.S. Hwang and G.C. Lee, 9/18/89, (PB90-160169, A04, MF-A01).
- NCEER-89-0025 "DYNA1D: A Computer Program for Nonlinear Seismic Site Response Analysis - Technical Documentation," by Jean H. Prevost, 9/14/89, (PB90-161944, A07, MF-A01). This report is available only through NTIS (see address given above).
- NCEER-89-0026 "1:4 Scale Model Studies of Active Tendon Systems and Active Mass Dampers for Aseismic Protection," by A.M. Reinhorn, T.T. Soong, R.C. Lin, Y.P. Yang, Y. Fukao, H. Abe and M. Nakai, 9/15/89, (PB90-173246, A10, MF-A02). This report is available only through NTIS (see address given above).
- NCEER-89-0027 "Scattering of Waves by Inclusions in a Nonhomogeneous Elastic Half Space Solved by Boundary Element Methods," by P.K. Hadley, A. Askar and A.S. Cakmak, 6/15/89, (PB90-145699, A07, MF-A01).
- NCEER-89-0028 "Statistical Evaluation of Deflection Amplification Factors for Reinforced Concrete Structures," by H.H.M. Hwang, J-W. Jaw and A.L. Ch'ng, 8/31/89, (PB90-164633, A05, MF-A01).
- NCEER-89-0029 "Bedrock Accelerations in Memphis Area Due to Large New Madrid Earthquakes," by H.H.M. Hwang, C.H.S. Chen and G. Yu, 11/7/89, (PB90-162330, A04, MF-A01).
- NCEER-89-0030 "Seismic Behavior and Response Sensitivity of Secondary Structural Systems," by Y.Q. Chen and T.T. Soong, 10/23/89, (PB90-164658, A08, MF-A01).
- NCEER-89-0031 "Random Vibration and Reliability Analysis of Primary-Secondary Structural Systems," by Y. Ibrahim, M. Grigoriu and T.T. Soong, 11/10/89, (PB90-161951, A04, MF-A01).

- NCEER-89-0032 "Proceedings from the Second U.S. - Japan Workshop on Liquefaction, Large Ground Deformation and Their Effects on Lifelines, September 26-29, 1989," Edited by T.D. O'Rourke and M. Hamada, 12/1/89, (PB90-209388, A22, MF-A03).
- NCEER-89-0033 "Deterministic Model for Seismic Damage Evaluation of Reinforced Concrete Structures," by J.M. Bracci, A.M. Reinhorn, J.B. Mander and S.K. Kunnath, 9/27/89, (PB91-108803, A06, MF-A01).
- NCEER-89-0034 "On the Relation Between Local and Global Damage Indices," by E. DiPasquale and A.S. Cakmak, 8/15/89, (PB90-173865, A05, MF-A01).
- NCEER-89-0035 "Cyclic Undrained Behavior of Nonplastic and Low Plasticity Silts," by A.J. Walker and H.E. Stewart, 7/26/89, (PB90-183518, A10, MF-A01).
- NCEER-89-0036 "Liquefaction Potential of Surficial Deposits in the City of Buffalo, New York," by M. Budhu, R. Giese and L. Baumgrass, 1/17/89, (PB90-208455, A04, MF-A01).
- NCEER-89-0037 "A Deterministic Assessment of Effects of Ground Motion Incoherence," by A.S. Veletsos and Y. Tang, 7/15/89, (PB90-164294, A03, MF-A01).
- NCEER-89-0038 "Workshop on Ground Motion Parameters for Seismic Hazard Mapping," July 17-18, 1989, edited by R.V. Whitman, 12/1/89, (PB90-173923, A04, MF-A01).
- NCEER-89-0039 "Seismic Effects on Elevated Transit Lines of the New York City Transit Authority," by C.J. Costantino, C.A. Miller and E. Heymsfield, 12/26/89, (PB90-207887, A06, MF-A01).
- NCEER-89-0040 "Centrifugal Modeling of Dynamic Soil-Structure Interaction," by K. Weissman, Supervised by J.H. Prevost, 5/10/89, (PB90-207879, A07, MF-A01).
- NCEER-89-0041 "Linearized Identification of Buildings With Cores for Seismic Vulnerability Assessment," by I-K. Ho and A.E. Aktan, 11/1/89, (PB90-251943, A07, MF-A01).
- NCEER-90-0001 "Geotechnical and Lifeline Aspects of the October 17, 1989 Loma Prieta Earthquake in San Francisco," by T.D. O'Rourke, H.E. Stewart, F.T. Blackburn and T.S. Dickerman, 1/90, (PB90-208596, A05, MF-A01).
- NCEER-90-0002 "Nonnormal Secondary Response Due to Yielding in a Primary Structure," by D.C.K. Chen and L.D. Lutes, 2/28/90, (PB90-251976, A07, MF-A01).
- NCEER-90-0003 "Earthquake Education Materials for Grades K-12," by K.E.K. Ross, 4/16/90, (PB91-251984, A05, MF-A05). This report has been replaced by NCEER-92-0018.
- NCEER-90-0004 "Catalog of Strong Motion Stations in Eastern North America," by R.W. Busby, 4/3/90, (PB90-251984, A05, MF-A01).
- NCEER-90-0005 "NCEER Strong-Motion Data Base: A User Manual for the GeoBase Release (Version 1.0 for the Sun3)," by P. Friberg and K. Jacob, 3/31/90 (PB90-258062, A04, MF-A01).
- NCEER-90-0006 "Seismic Hazard Along a Crude Oil Pipeline in the Event of an 1811-1812 Type New Madrid Earthquake," by H.H.M. Hwang and C-H.S. Chen, 4/16/90, (PB90-258054, A04, MF-A01).
- NCEER-90-0007 "Site-Specific Response Spectra for Memphis Sheahan Pumping Station," by H.H.M. Hwang and C.S. Lee, 5/15/90, (PB91-108811, A05, MF-A01).
- NCEER-90-0008 "Pilot Study on Seismic Vulnerability of Crude Oil Transmission Systems," by T. Ariman, R. Dobry, M. Grigoriu, F. Kozin, M. O'Rourke, T. O'Rourke and M. Shinozuka, 5/25/90, (PB91-108837, A06, MF-A01).
- NCEER-90-0009 "A Program to Generate Site Dependent Time Histories: EQGEN," by G.W. Ellis, M. Srinivasan and A.S. Cakmak, 1/30/90, (PB91-108829, A04, MF-A01).
- NCEER-90-0010 "Active Isolation for Seismic Protection of Operating Rooms," by M.E. Talbott, Supervised by M. Shinozuka, 6/8/9, (PB91-110205, A05, MF-A01).

- NCEER-90-0011 "Program LINEARID for Identification of Linear Structural Dynamic Systems," by C-B. Yun and M. Shinozuka, 6/25/90, (PB91-110312, A08, MF-A01).
- NCEER-90-0012 "Two-Dimensional Two-Phase Elasto-Plastic Seismic Response of Earth Dams," by A.N. Yiagos, Supervised by J.H. Prevost, 6/20/90, (PB91-110197, A13, MF-A02).
- NCEER-90-0013 "Secondary Systems in Base-Isolated Structures: Experimental Investigation, Stochastic Response and Stochastic Sensitivity," by G.D. Manolis, G. Juhn, M.C. Constantinou and A.M. Reinhorn, 7/1/90, (PB91-110320, A08, MF-A01).
- NCEER-90-0014 "Seismic Behavior of Lightly-Reinforced Concrete Column and Beam-Column Joint Details," by S.P. Pessiki, C.H. Conley, P. Gergely and R.N. White, 8/22/90, (PB91-108795, A11, MF-A02).
- NCEER-90-0015 "Two Hybrid Control Systems for Building Structures Under Strong Earthquakes," by J.N. Yang and A. Daniellians, 6/29/90, (PB91-125393, A04, MF-A01).
- NCEER-90-0016 "Instantaneous Optimal Control with Acceleration and Velocity Feedback," by J.N. Yang and Z. Li, 6/29/90, (PB91-125401, A03, MF-A01).
- NCEER-90-0017 "Reconnaissance Report on the Northern Iran Earthquake of June 21, 1990," by M. Mehrain, 10/4/90, (PB91-125377, A03, MF-A01).
- NCEER-90-0018 "Evaluation of Liquefaction Potential in Memphis and Shelby County," by T.S. Chang, P.S. Tang, C.S. Lee and H. Hwang, 8/10/90, (PB91-125427, A09, MF-A01).
- NCEER-90-0019 "Experimental and Analytical Study of a Combined Sliding Disc Bearing and Helical Steel Spring Isolation System," by M.C. Constantinou, A.S. Mokha and A.M. Reinhorn, 10/4/90, (PB91-125385, A06, MF-A01). This report is available only through NTIS (see address given above).
- NCEER-90-0020 "Experimental Study and Analytical Prediction of Earthquake Response of a Sliding Isolation System with a Spherical Surface," by A.S. Mokha, M.C. Constantinou and A.M. Reinhorn, 10/11/90, (PB91-125419, A05, MF-A01).
- NCEER-90-0021 "Dynamic Interaction Factors for Floating Pile Groups," by G. Gazetas, K. Fan, A. Kaynia and E. Kausel, 9/10/90, (PB91-170381, A05, MF-A01).
- NCEER-90-0022 "Evaluation of Seismic Damage Indices for Reinforced Concrete Structures," by S. Rodriguez-Gomez and A.S. Cakmak, 9/30/90, PB91-171322, A06, MF-A01).
- NCEER-90-0023 "Study of Site Response at a Selected Memphis Site," by H. Desai, S. Ahmad, E.S. Gazetas and M.R. Oh, 10/11/90, (PB91-196857, A03, MF-A01).
- NCEER-90-0024 "A User's Guide to Strongmo: Version 1.0 of NCEER's Strong-Motion Data Access Tool for PCs and Terminals," by P.A. Friberg and C.A.T. Susch, 11/15/90, (PB91-171272, A03, MF-A01).
- NCEER-90-0025 "A Three-Dimensional Analytical Study of Spatial Variability of Seismic Ground Motions," by L-L. Hong and A.H.-S. Ang, 10/30/90, (PB91-170399, A09, MF-A01).
- NCEER-90-0026 "MUMOID User's Guide - A Program for the Identification of Modal Parameters," by S. Rodriguez-Gomez and E. DiPasquale, 9/30/90, (PB91-171298, A04, MF-A01).
- NCEER-90-0027 "SARCF-II User's Guide - Seismic Analysis of Reinforced Concrete Frames," by S. Rodriguez-Gomez, Y.S. Chung and C. Meyer, 9/30/90, (PB91-171280, A05, MF-A01).
- NCEER-90-0028 "Viscous Dampers: Testing, Modeling and Application in Vibration and Seismic Isolation," by N. Makris and M.C. Constantinou, 12/20/90 (PB91-190561, A06, MF-A01).
- NCEER-90-0029 "Soil Effects on Earthquake Ground Motions in the Memphis Area," by H. Hwang, C.S. Lee, K.W. Ng and T.S. Chang, 8/2/90, (PB91-190751, A05, MF-A01).

- NCEER-91-0001 "Proceedings from the Third Japan-U.S. Workshop on Earthquake Resistant Design of Lifeline Facilities and Countermeasures for Soil Liquefaction, December 17-19, 1990," edited by T.D. O'Rourke and M. Hamada, 2/1/91, (PB91-179259, A99, MF-A04).
- NCEER-91-0002 "Physical Space Solutions of Non-Proportionally Damped Systems," by M. Tong, Z. Liang and G.C. Lee, 1/15/91, (PB91-179242, A04, MF-A01).
- NCEER-91-0003 "Seismic Response of Single Piles and Pile Groups," by K. Fan and G. Gazetas, 1/10/91, (PB92-174994, A04, MF-A01).
- NCEER-91-0004 "Damping of Structures: Part I - Theory of Complex Damping," by Z. Liang and G. Lee, 10/10/91, (PB92-197235, A12, MF-A03).
- NCEER-91-0005 "3D-BASIS - Nonlinear Dynamic Analysis of Three Dimensional Base Isolated Structures: Part II," by S. Nagarajaiah, A.M. Reinhorn and M.C. Constantinou, 2/28/91, (PB91-190553, A07, MF-A01). This report has been replaced by NCEER-93-0011.
- NCEER-91-0006 "A Multidimensional Hysteretic Model for Plasticity Deforming Metals in Energy Absorbing Devices," by E.J. Graesser and F.A. Cozzarelli, 4/9/91, (PB92-108364, A04, MF-A01).
- NCEER-91-0007 "A Framework for Customizable Knowledge-Based Expert Systems with an Application to a KBES for Evaluating the Seismic Resistance of Existing Buildings," by E.G. Ibarra-Anaya and S.J. Fennes, 4/9/91, (PB91-210930, A08, MF-A01).
- NCEER-91-0008 "Nonlinear Analysis of Steel Frames with Semi-Rigid Connections Using the Capacity Spectrum Method," by G.G. Deierlein, S-H. Hsieh, Y-J. Shen and J.F. Abel, 7/2/91, (PB92-113828, A05, MF-A01).
- NCEER-91-0009 "Earthquake Education Materials for Grades K-12," by K.E.K. Ross, 4/30/91, (PB91-212142, A06, MF-A01). This report has been replaced by NCEER-92-0018.
- NCEER-91-0010 "Phase Wave Velocities and Displacement Phase Differences in a Harmonically Oscillating Pile," by N. Makris and G. Gazetas, 7/8/91, (PB92-108356, A04, MF-A01).
- NCEER-91-0011 "Dynamic Characteristics of a Full-Size Five-Story Steel Structure and a 2/5 Scale Model," by K.C. Chang, G.C. Yao, G.C. Lee, D.S. Hao and Y.C. Yeh, 7/2/91, (PB93-116648, A06, MF-A02).
- NCEER-91-0012 "Seismic Response of a 2/5 Scale Steel Structure with Added Viscoelastic Dampers," by K.C. Chang, T.T. Soong, S-T. Oh and M.L. Lai, 5/17/91, (PB92-110816, A05, MF-A01).
- NCEER-91-0013 "Earthquake Response of Retaining Walls; Full-Scale Testing and Computational Modeling," by S. Alampalli and A-W.M. Elgamal, 6/20/91, to be published.
- NCEER-91-0014 "3D-BASIS-M: Nonlinear Dynamic Analysis of Multiple Building Base Isolated Structures," by P.C. Tsopelas, S. Nagarajaiah, M.C. Constantinou and A.M. Reinhorn, 5/28/91, (PB92-113885, A09, MF-A02).
- NCEER-91-0015 "Evaluation of SEAOC Design Requirements for Sliding Isolated Structures," by D. Theodossiou and M.C. Constantinou, 6/10/91, (PB92-114602, A11, MF-A03).
- NCEER-91-0016 "Closed-Loop Modal Testing of a 27-Story Reinforced Concrete Flat Plate-Core Building," by H.R. Somaprasad, T. Toksoy, H. Yoshiyuki and A.E. Aktan, 7/15/91, (PB92-129980, A07, MF-A02).
- NCEER-91-0017 "Shake Table Test of a 1/6 Scale Two-Story Lightly Reinforced Concrete Building," by A.G. El-Attar, R.N. White and P. Gergely, 2/28/91, (PB92-222447, A06, MF-A02).
- NCEER-91-0018 "Shake Table Test of a 1/8 Scale Three-Story Lightly Reinforced Concrete Building," by A.G. El-Attar, R.N. White and P. Gergely, 2/28/91, (PB93-116630, A08, MF-A02).
- NCEER-91-0019 "Transfer Functions for Rigid Rectangular Foundations," by A.S. Veletsos, A.M. Prasad and W.H. Wu, 7/31/91, to be published.

- NCEER-91-0020 "Hybrid Control of Seismic-Excited Nonlinear and Inelastic Structural Systems," by J.N. Yang, Z. Li and A. Daniellians, 8/1/91, (PB92-143171, A06, MF-A02).
- NCEER-91-0021 "The NCEER-91 Earthquake Catalog: Improved Intensity-Based Magnitudes and Recurrence Relations for U.S. Earthquakes East of New Madrid," by L. Seeber and J.G. Armbruster, 8/28/91, (PB92-176742, A06, MF-A02).
- NCEER-91-0022 "Proceedings from the Implementation of Earthquake Planning and Education in Schools: The Need for Change - The Roles of the Changemakers," by K.E.K. Ross and F. Winslow, 7/23/91, (PB92-129998, A12, MF-A03).
- NCEER-91-0023 "A Study of Reliability-Based Criteria for Seismic Design of Reinforced Concrete Frame Buildings," by H.H.M. Hwang and H-M. Hsu, 8/10/91, (PB92-140235, A09, MF-A02).
- NCEER-91-0024 "Experimental Verification of a Number of Structural System Identification Algorithms," by R.G. Ghanem, H. Gavin and M. Shinozuka, 9/18/91, (PB92-176577, A18, MF-A04).
- NCEER-91-0025 "Probabilistic Evaluation of Liquefaction Potential," by H.H.M. Hwang and C.S. Lee, 11/25/91, (PB92-143429, A05, MF-A01).
- NCEER-91-0026 "Instantaneous Optimal Control for Linear, Nonlinear and Hysteretic Structures - Stable Controllers," by J.N. Yang and Z. Li, 11/15/91, (PB92-163807, A04, MF-A01).
- NCEER-91-0027 "Experimental and Theoretical Study of a Sliding Isolation System for Bridges," by M.C. Constantinou, A. Kartoum, A.M. Reinhorn and P. Bradford, 11/15/91, (PB92-176973, A10, MF-A03).
- NCEER-92-0001 "Case Studies of Liquefaction and Lifeline Performance During Past Earthquakes, Volume 1: Japanese Case Studies," Edited by M. Hamada and T. O'Rourke, 2/17/92, (PB92-197243, A18, MF-A04).
- NCEER-92-0002 "Case Studies of Liquefaction and Lifeline Performance During Past Earthquakes, Volume 2: United States Case Studies," Edited by T. O'Rourke and M. Hamada, 2/17/92, (PB92-197250, A20, MF-A04).
- NCEER-92-0003 "Issues in Earthquake Education," Edited by K. Ross, 2/3/92, (PB92-222389, A07, MF-A02).
- NCEER-92-0004 "Proceedings from the First U.S. - Japan Workshop on Earthquake Protective Systems for Bridges," Edited by I.G. Buckle, 2/4/92, (PB94-142239, A99, MF-A06).
- NCEER-92-0005 "Seismic Ground Motion from a Haskell-Type Source in a Multiple-Layered Half-Space," A.P. Theoharis, G. Deodatis and M. Shinozuka, 1/2/92, to be published.
- NCEER-92-0006 "Proceedings from the Site Effects Workshop," Edited by R. Whitman, 2/29/92, (PB92-197201, A04, MF-A01).
- NCEER-92-0007 "Engineering Evaluation of Permanent Ground Deformations Due to Seismically-Induced Liquefaction," by M.H. Baziar, R. Dobry and A-W.M. Elgamel, 3/24/92, (PB92-222421, A13, MF-A03).
- NCEER-92-0008 "A Procedure for the Seismic Evaluation of Buildings in the Central and Eastern United States," by C.D. Poland and J.O. Malley, 4/2/92, (PB92-222439, A20, MF-A04).
- NCEER-92-0009 "Experimental and Analytical Study of a Hybrid Isolation System Using Friction Controllable Sliding Bearings," by M.Q. Feng, S. Fujii and M. Shinozuka, 5/15/92, (PB93-150282, A06, MF-A02).
- NCEER-92-0010 "Seismic Resistance of Slab-Column Connections in Existing Non-Ductile Flat-Plate Buildings," by A.J. Durrani and Y. Du, 5/18/92, (PB93-116812, A06, MF-A02).
- NCEER-92-0011 "The Hysteretic and Dynamic Behavior of Brick Masonry Walls Upgraded by Ferrocement Coatings Under Cyclic Loading and Strong Simulated Ground Motion," by H. Lee and S.P. Prawl, 5/11/92, to be published.
- NCEER-92-0012 "Study of Wire Rope Systems for Seismic Protection of Equipment in Buildings," by G.F. Demetriades, M.C. Constantinou and A.M. Reinhorn, 5/20/92, (PB93-116655, A08, MF-A02).

- NCEER-92-0013 "Shape Memory Structural Dampers: Material Properties, Design and Seismic Testing," by P.R. Witting and F.A. Cozzarelli, 5/26/92, (PB93-116663, A05, MF-A01).
- NCEER-92-0014 "Longitudinal Permanent Ground Deformation Effects on Buried Continuous Pipelines," by M.J. O'Rourke, and C. Nordberg, 6/15/92, (PB93-116671, A08, MF-A02).
- NCEER-92-0015 "A Simulation Method for Stationary Gaussian Random Functions Based on the Sampling Theorem," by M. Grigoriu and S. Balopoulou, 6/11/92, (PB93-127496, A05, MF-A01).
- NCEER-92-0016 "Gravity-Load-Designed Reinforced Concrete Buildings: Seismic Evaluation of Existing Construction and Detailing Strategies for Improved Seismic Resistance," by G.W. Hoffmann, S.K. Kunnath, A.M. Reinhorn and J.B. Mander, 7/15/92, (PB94-142007, A08, MF-A02).
- NCEER-92-0017 "Observations on Water System and Pipeline Performance in the Limón Area of Costa Rica Due to the April 22, 1991 Earthquake," by M. O'Rourke and D. Ballantyne, 6/30/92, (PB93-126811, A06, MF-A02).
- NCEER-92-0018 "Fourth Edition of Earthquake Education Materials for Grades K-12," Edited by K.E.K. Ross, 8/10/92, (PB93-114023, A07, MF-A02).
- NCEER-92-0019 "Proceedings from the Fourth Japan-U.S. Workshop on Earthquake Resistant Design of Lifeline Facilities and Countermeasures for Soil Liquefaction," Edited by M. Hamada and T.D. O'Rourke, 8/12/92, (PB93-163939, A99, MF-E11).
- NCEER-92-0020 "Active Bracing System: A Full Scale Implementation of Active Control," by A.M. Reinhorn, T.T. Soong, R.C. Lin, M.A. Riley, Y.P. Wang, S. Aizawa and M. Higashino, 8/14/92, (PB93-127512, A06, MF-A02).
- NCEER-92-0021 "Empirical Analysis of Horizontal Ground Displacement Generated by Liquefaction-Induced Lateral Spreads," by S.F. Bartlett and T.L. Youd, 8/17/92, (PB93-188241, A06, MF-A02).
- NCEER-92-0022 "IDARC Version 3.0: Inelastic Damage Analysis of Reinforced Concrete Structures," by S.K. Kunnath, A.M. Reinhorn and R.F. Lobo, 8/31/92, (PB93-227502, A07, MF-A02).
- NCEER-92-0023 "A Semi-Empirical Analysis of Strong-Motion Peaks in Terms of Seismic Source, Propagation Path and Local Site Conditions, by M. Kamiyama, M.J. O'Rourke and R. Flores-Berrones, 9/9/92, (PB93-150266, A08, MF-A02).
- NCEER-92-0024 "Seismic Behavior of Reinforced Concrete Frame Structures with Nonductile Details, Part I: Summary of Experimental Findings of Full Scale Beam-Column Joint Tests," by A. Beres, R.N. White and P. Gergely, 9/30/92, (PB93-227783, A05, MF-A01).
- NCEER-92-0025 "Experimental Results of Repaired and Retrofitted Beam-Column Joint Tests in Lightly Reinforced Concrete Frame Buildings," by A. Beres, S. El-Borgi, R.N. White and P. Gergely, 10/29/92, (PB93-227791, A05, MF-A01).
- NCEER-92-0026 "A Generalization of Optimal Control Theory: Linear and Nonlinear Structures," by J.N. Yang, Z. Li and S. Vongchavalitkul, 11/2/92, (PB93-188621, A05, MF-A01).
- NCEER-92-0027 "Seismic Resistance of Reinforced Concrete Frame Structures Designed Only for Gravity Loads: Part I - Design and Properties of a One-Third Scale Model Structure," by J.M. Bracci, A.M. Reinhorn and J.B. Mander, 12/1/92, (PB94-104502, A08, MF-A02).
- NCEER-92-0028 "Seismic Resistance of Reinforced Concrete Frame Structures Designed Only for Gravity Loads: Part II - Experimental Performance of Subassemblages," by L.E. Aycaardi, J.B. Mander and A.M. Reinhorn, 12/1/92, (PB94-104510, A08, MF-A02).
- NCEER-92-0029 "Seismic Resistance of Reinforced Concrete Frame Structures Designed Only for Gravity Loads: Part III - Experimental Performance and Analytical Study of a Structural Model," by J.M. Bracci, A.M. Reinhorn and J.B. Mander, 12/1/92, (PB93-227528, A09, MF-A01).

- NCEER-92-0030 "Evaluation of Seismic Retrofit of Reinforced Concrete Frame Structures: Part I - Experimental Performance of Retrofitted Subassemblages," by D. Choudhuri, J.B. Mander and A.M. Reinhorn, 12/8/92, (PB93-198307, A07, MF-A02).
- NCEER-92-0031 "Evaluation of Seismic Retrofit of Reinforced Concrete Frame Structures: Part II - Experimental Performance and Analytical Study of a Retrofitted Structural Model," by J.M. Bracci, A.M. Reinhorn and J.B. Mander, 12/8/92, (PB93-198315, A09, MF-A03).
- NCEER-92-0032 "Experimental and Analytical Investigation of Seismic Response of Structures with Supplemental Fluid Viscous Dampers," by M.C. Constantinou and M.D. Symans, 12/21/92, (PB93-191435, A10, MF-A03). This report is available only through NTIS (see address given above).
- NCEER-92-0033 "Reconnaissance Report on the Cairo, Egypt Earthquake of October 12, 1992," by M. Khater, 12/23/92, (PB93-188621, A03, MF-A01).
- NCEER-92-0034 "Low-Level Dynamic Characteristics of Four Tall Flat-Plate Buildings in New York City," by H. Gavin, S. Yuan, J. Grossman, E. Pekelis and K. Jacob, 12/28/92, (PB93-188217, A07, MF-A02).
- NCEER-93-0001 "An Experimental Study on the Seismic Performance of Brick-Infilled Steel Frames With and Without Retrofit," by J.B. Mander, B. Nair, K. Wojtkowski and J. Ma, 1/29/93, (PB93-227510, A07, MF-A02).
- NCEER-93-0002 "Social Accounting for Disaster Preparedness and Recovery Planning," by S. Cole, E. Pantoja and V. Razak, 2/22/93, (PB94-142114, A12, MF-A03).
- NCEER-93-0003 "Assessment of 1991 NEHRP Provisions for Nonstructural Components and Recommended Revisions," by T.T. Soong, G. Chen, Z. Wu, R-H. Zhang and M. Grigoriu, 3/1/93, (PB93-188639, A06, MF-A02).
- NCEER-93-0004 "Evaluation of Static and Response Spectrum Analysis Procedures of SEAOC/UBC for Seismic Isolated Structures," by C.W. Winters and M.C. Constantinou, 3/23/93, (PB93-198299, A10, MF-A03).
- NCEER-93-0005 "Earthquakes in the Northeast - Are We Ignoring the Hazard? A Workshop on Earthquake Science and Safety for Educators," edited by K.E.K. Ross, 4/2/93, (PB94-103066, A09, MF-A02).
- NCEER-93-0006 "Inelastic Response of Reinforced Concrete Structures with Viscoelastic Braces," by R.F. Lobo, J.M. Bracci, K.L. Shen, A.M. Reinhorn and T.T. Soong, 4/5/93, (PB93-227486, A05, MF-A02).
- NCEER-93-0007 "Seismic Testing of Installation Methods for Computers and Data Processing Equipment," by K. Kosar, T.T. Soong, K.L. Shen, J.A. HoLung and Y.K. Lin, 4/12/93, (PB93-198299, A07, MF-A02).
- NCEER-93-0008 "Retrofit of Reinforced Concrete Frames Using Added Dampers," by A. Reinhorn, M. Constantinou and C. Li, to be published.
- NCEER-93-0009 "Seismic Behavior and Design Guidelines for Steel Frame Structures with Added Viscoelastic Dampers," by K.C. Chang, M.L. Lai, T.T. Soong, D.S. Hao and Y.C. Yeh, 5/1/93, (PB94-141959, A07, MF-A02).
- NCEER-93-0010 "Seismic Performance of Shear-Critical Reinforced Concrete Bridge Piers," by J.B. Mander, S.M. Waheed, M.T.A. Chaudhary and S.S. Chen, 5/12/93, (PB93-227494, A08, MF-A02).
- NCEER-93-0011 "3D-BASIS-TABS: Computer Program for Nonlinear Dynamic Analysis of Three Dimensional Base Isolated Structures," by S. Nagarajaiah, C. Li, A.M. Reinhorn and M.C. Constantinou, 8/2/93, (PB94-141819, A09, MF-A02).
- NCEER-93-0012 "Effects of Hydrocarbon Spills from an Oil Pipeline Break on Ground Water," by O.J. Helweg and H.H.M. Hwang, 8/3/93, (PB94-141942, A06, MF-A02).
- NCEER-93-0013 "Simplified Procedures for Seismic Design of Nonstructural Components and Assessment of Current Code Provisions," by M.P. Singh, L.E. Suarez, E.E. Matheu and G.O. Maldonado, 8/4/93, (PB94-141827, A09, MF-A02).
- NCEER-93-0014 "An Energy Approach to Seismic Analysis and Design of Secondary Systems," by G. Chen and T.T. Soong, 8/6/93, (PB94-142767, A11, MF-A03).

- NCEER-93-0015 "Proceedings from School Sites: Becoming Prepared for Earthquakes - Commemorating the Third Anniversary of the Loma Prieta Earthquake," Edited by F.E. Winslow and K.E.K. Ross, 8/16/93, (PB94-154275, A16, MF-A02).
- NCEER-93-0016 "Reconnaissance Report of Damage to Historic Monuments in Cairo, Egypt Following the October 12, 1992 Dahshur Earthquake," by D. Sykora, D. Look, G. Croci, E. Karaesmen and E. Karaesmen, 8/19/93, (PB94-142221, A08, MF-A02).
- NCEER-93-0017 "The Island of Guam Earthquake of August 8, 1993," by S.W. Swan and S.K. Harris, 9/30/93, (PB94-141843, A04, MF-A01).
- NCEER-93-0018 "Engineering Aspects of the October 12, 1992 Egyptian Earthquake," by A.W. Elgamal, M. Amer, K. Adalier and A. Abul-Fadl, 10/7/93, (PB94-141983, A05, MF-A01).
- NCEER-93-0019 "Development of an Earthquake Motion Simulator and its Application in Dynamic Centrifuge Testing," by I. Krstelj, Supervised by J.H. Prevost, 10/23/93, (PB94-181773, A-10, MF-A03).
- NCEER-93-0020 "NCEER-Taisei Corporation Research Program on Sliding Seismic Isolation Systems for Bridges: Experimental and Analytical Study of a Friction Pendulum System (FPS)," by M.C. Constantinou, P. Tsopelas, Y-S. Kim and S. Okamoto, 11/1/93, (PB94-142775, A08, MF-A02).
- NCEER-93-0021 "Finite Element Modeling of Elastomeric Seismic Isolation Bearings," by L.J. Billings, Supervised by R. Shepherd, 11/8/93, to be published.
- NCEER-93-0022 "Seismic Vulnerability of Equipment in Critical Facilities: Life-Safety and Operational Consequences," by K. Porter, G.S. Johnson, M.M. Zadeh, C. Scawthorn and S. Eder, 11/24/93, (PB94-181765, A16, MF-A03).
- NCEER-93-0023 "Hokkaido Nansei-oki, Japan Earthquake of July 12, 1993, by P.I. Yanev and C.R. Scawthorn, 12/23/93, (PB94-181500, A07, MF-A01).
- NCEER-94-0001 "An Evaluation of Seismic Serviceability of Water Supply Networks with Application to the San Francisco Auxiliary Water Supply System," by I. Markov, Supervised by M. Grigoriu and T. O'Rourke, 1/21/94, (PB94-204013, A07, MF-A02).
- NCEER-94-0002 "NCEER-Taisei Corporation Research Program on Sliding Seismic Isolation Systems for Bridges: Experimental and Analytical Study of Systems Consisting of Sliding Bearings, Rubber Restoring Force Devices and Fluid Dampers," Volumes I and II, by P. Tsopelas, S. Okamoto, M.C. Constantinou, D. Ozaki and S. Fujii, 2/4/94, (PB94-181740, A09, MF-A02 and PB94-181757, A12, MF-A03).
- NCEER-94-0003 "A Markov Model for Local and Global Damage Indices in Seismic Analysis," by S. Rahman and M. Grigoriu, 2/18/94, (PB94-206000, A12, MF-A03).
- NCEER-94-0004 "Proceedings from the NCEER Workshop on Seismic Response of Masonry Infills," edited by D.P. Abrams, 3/1/94, (PB94-180783, A07, MF-A02).
- NCEER-94-0005 "The Northridge, California Earthquake of January 17, 1994: General Reconnaissance Report," edited by J.D. Goltz, 3/11/94, (PB94-193943, A10, MF-A03).
- NCEER-94-0006 "Seismic Energy Based Fatigue Damage Analysis of Bridge Columns: Part I - Evaluation of Seismic Capacity," by G.A. Chang and J.B. Mander, 3/14/94, (PB94-219185, A11, MF-A03).
- NCEER-94-0007 "Seismic Isolation of Multi-Story Frame Structures Using Spherical Sliding Isolation Systems," by T.M. Al-Hussaini, V.A. Zayas and M.C. Constantinou, 3/17/94, (PB94-193745, A09, MF-A02).
- NCEER-94-0008 "The Northridge, California Earthquake of January 17, 1994: Performance of Highway Bridges," edited by I.G. Buckle, 3/24/94, (PB94-193851, A06, MF-A02).
- NCEER-94-0009 "Proceedings of the Third U.S.-Japan Workshop on Earthquake Protective Systems for Bridges," edited by I.G. Buckle and I. Friedland, 3/31/94, (PB94-195815, A99, MF-A06).

- NCEER-94-0010 "3D-BASIS-ME: Computer Program for Nonlinear Dynamic Analysis of Seismically Isolated Single and Multiple Structures and Liquid Storage Tanks," by P.C. Tsopelas, M.C. Constantinou and A.M. Reinhorn, 4/12/94, (PB94-204922, A09, MF-A02).
- NCEER-94-0011 "The Northridge, California Earthquake of January 17, 1994: Performance of Gas Transmission Pipelines," by T.D. O'Rourke and M.C. Palmer, 5/16/94, (PB94-204989, A05, MF-A01).
- NCEER-94-0012 "Feasibility Study of Replacement Procedures and Earthquake Performance Related to Gas Transmission Pipelines," by T.D. O'Rourke and M.C. Palmer, 5/25/94, (PB94-206638, A09, MF-A02).
- NCEER-94-0013 "Seismic Energy Based Fatigue Damage Analysis of Bridge Columns: Part II - Evaluation of Seismic Demand," by G.A. Chang and J.B. Mander, 6/1/94, (PB95-18106, A08, MF-A02).
- NCEER-94-0014 "NCEER-Taisei Corporation Research Program on Sliding Seismic Isolation Systems for Bridges: Experimental and Analytical Study of a System Consisting of Sliding Bearings and Fluid Restoring Force/Damping Devices," by P. Tsopelas and M.C. Constantinou, 6/13/94, (PB94-219144, A10, MF-A03).
- NCEER-94-0015 "Generation of Hazard-Consistent Fragility Curves for Seismic Loss Estimation Studies," by H. Hwang and J-R. Huo, 6/14/94, (PB95-181996, A09, MF-A02).
- NCEER-94-0016 "Seismic Study of Building Frames with Added Energy-Absorbing Devices," by W.S. Pong, C.S. Tsai and G.C. Lee, 6/20/94, (PB94-219136, A10, A03).
- NCEER-94-0017 "Sliding Mode Control for Seismic-Excited Linear and Nonlinear Civil Engineering Structures," by J. Yang, J. Wu, A. Agrawal and Z. Li, 6/21/94, (PB95-138483, A06, MF-A02).
- NCEER-94-0018 "3D-BASIS-TABS Version 2.0: Computer Program for Nonlinear Dynamic Analysis of Three Dimensional Base Isolated Structures," by A.M. Reinhorn, S. Nagarajaiah, M.C. Constantinou, P. Tsopelas and R. Li, 6/22/94, (PB95-182176, A08, MF-A02).
- NCEER-94-0019 "Proceedings of the International Workshop on Civil Infrastructure Systems: Application of Intelligent Systems and Advanced Materials on Bridge Systems," Edited by G.C. Lee and K.C. Chang, 7/18/94, (PB95-252474, A20, MF-A04).
- NCEER-94-0020 "Study of Seismic Isolation Systems for Computer Floors," by V. Lambrou and M.C. Constantinou, 7/19/94, (PB95-138533, A10, MF-A03).
- NCEER-94-0021 "Proceedings of the U.S.-Italian Workshop on Guidelines for Seismic Evaluation and Rehabilitation of Unreinforced Masonry Buildings," Edited by D.P. Abrams and G.M. Calvi, 7/20/94, (PB95-138749, A13, MF-A03).
- NCEER-94-0022 "NCEER-Taisei Corporation Research Program on Sliding Seismic Isolation Systems for Bridges: Experimental and Analytical Study of a System Consisting of Lubricated PTFE Sliding Bearings and Mild Steel Dampers," by P. Tsopelas and M.C. Constantinou, 7/22/94, (PB95-182184, A08, MF-A02).
- NCEER-94-0023 "Development of Reliability-Based Design Criteria for Buildings Under Seismic Load," by Y.K. Wen, H. Hwang and M. Shinozuka, 8/1/94, (PB95-211934, A08, MF-A02).
- NCEER-94-0024 "Experimental Verification of Acceleration Feedback Control Strategies for an Active Tendon System," by S.J. Dyke, B.F. Spencer, Jr., P. Quast, M.K. Sain, D.C. Kaspari, Jr. and T.T. Soong, 8/29/94, (PB95-212320, A05, MF-A01).
- NCEER-94-0025 "Seismic Retrofitting Manual for Highway Bridges," Edited by I.G. Buckle and I.F. Friedland, published by the Federal Highway Administration (PB95-212676, A15, MF-A03).
- NCEER-94-0026 "Proceedings from the Fifth U.S.-Japan Workshop on Earthquake Resistant Design of Lifeline Facilities and Countermeasures Against Soil Liquefaction," Edited by T.D. O'Rourke and M. Hamada, 11/7/94, (PB95-220802, A99, MF-E08).

- NCEER-95-0001 “Experimental and Analytical Investigation of Seismic Retrofit of Structures with Supplemental Damping: Part 1 - Fluid Viscous Damping Devices,” by A.M. Reinhorn, C. Li and M.C. Constantinou, 1/3/95, (PB95-266599, A09, MF-A02).
- NCEER-95-0002 “Experimental and Analytical Study of Low-Cycle Fatigue Behavior of Semi-Rigid Top-And-Seat Angle Connections,” by G. Pekcan, J.B. Mander and S.S. Chen, 1/5/95, (PB95-220042, A07, MF-A02).
- NCEER-95-0003 “NCEER-ATC Joint Study on Fragility of Buildings,” by T. Anagnos, C. Rojahn and A.S. Kiremidjian, 1/20/95, (PB95-220026, A06, MF-A02).
- NCEER-95-0004 “Nonlinear Control Algorithms for Peak Response Reduction,” by Z. Wu, T.T. Soong, V. Gattulli and R.C. Lin, 2/16/95, (PB95-220349, A05, MF-A01).
- NCEER-95-0005 “Pipeline Replacement Feasibility Study: A Methodology for Minimizing Seismic and Corrosion Risks to Underground Natural Gas Pipelines,” by R.T. Eguchi, H.A. Seligson and D.G. Honegger, 3/2/95, (PB95-252326, A06, MF-A02).
- NCEER-95-0006 “Evaluation of Seismic Performance of an 11-Story Frame Building During the 1994 Northridge Earthquake,” by F. Naeim, R. DiSulio, K. Benuska, A. Reinhorn and C. Li, to be published.
- NCEER-95-0007 “Prioritization of Bridges for Seismic Retrofitting,” by N. Basöz and A.S. Kiremidjian, 4/24/95, (PB95-252300, A08, MF-A02).
- NCEER-95-0008 “Method for Developing Motion Damage Relationships for Reinforced Concrete Frames,” by A. Singhal and A.S. Kiremidjian, 5/11/95, (PB95-266607, A06, MF-A02).
- NCEER-95-0009 “Experimental and Analytical Investigation of Seismic Retrofit of Structures with Supplemental Damping: Part II - Friction Devices,” by C. Li and A.M. Reinhorn, 7/6/95, (PB96-128087, A11, MF-A03).
- NCEER-95-0010 “Experimental Performance and Analytical Study of a Non-Ductile Reinforced Concrete Frame Structure Retrofitted with Elastomeric Spring Dampers,” by G. Pekcan, J.B. Mander and S.S. Chen, 7/14/95, (PB96-137161, A08, MF-A02).
- NCEER-95-0011 “Development and Experimental Study of Semi-Active Fluid Damping Devices for Seismic Protection of Structures,” by M.D. Symans and M.C. Constantinou, 8/3/95, (PB96-136940, A23, MF-A04).
- NCEER-95-0012 “Real-Time Structural Parameter Modification (RSPM): Development of Innervated Structures,” by Z. Liang, M. Tong and G.C. Lee, 4/11/95, (PB96-137153, A06, MF-A01).
- NCEER-95-0013 “Experimental and Analytical Investigation of Seismic Retrofit of Structures with Supplemental Damping: Part III - Viscous Damping Walls,” by A.M. Reinhorn and C. Li, 10/1/95, (PB96-176409, A11, MF-A03).
- NCEER-95-0014 “Seismic Fragility Analysis of Equipment and Structures in a Memphis Electric Substation,” by J-R. Huo and H.H.M. Hwang, 8/10/95, (PB96-128087, A09, MF-A02).
- NCEER-95-0015 “The Hanshin-Awaji Earthquake of January 17, 1995: Performance of Lifelines,” Edited by M. Shinozuka, 11/3/95, (PB96-176383, A15, MF-A03).
- NCEER-95-0016 “Highway Culvert Performance During Earthquakes,” by T.L. Youd and C.J. Beckman, available as NCEER-96-0015.
- NCEER-95-0017 “The Hanshin-Awaji Earthquake of January 17, 1995: Performance of Highway Bridges,” Edited by I.G. Buckle, 12/1/95, to be published.
- NCEER-95-0018 “Modeling of Masonry Infill Panels for Structural Analysis,” by A.M. Reinhorn, A. Madan, R.E. Valles, Y. Reichmann and J.B. Mander, 12/8/95, (PB97-110886, MF-A01, A06).
- NCEER-95-0019 “Optimal Polynomial Control for Linear and Nonlinear Structures,” by A.K. Agrawal and J.N. Yang, 12/11/95, (PB96-168737, A07, MF-A02).

- NCEER-95-0020 "Retrofit of Non-Ductile Reinforced Concrete Frames Using Friction Dampers," by R.S. Rao, P. Gergely and R.N. White, 12/22/95, (PB97-133508, A10, MF-A02).
- NCEER-95-0021 "Parametric Results for Seismic Response of Pile-Supported Bridge Bents," by G. Mylonakis, A. Nikolaou and G. Gazetas, 12/22/95, (PB97-100242, A12, MF-A03).
- NCEER-95-0022 "Kinematic Bending Moments in Seismically Stressed Piles," by A. Nikolaou, G. Mylonakis and G. Gazetas, 12/23/95, (PB97-113914, MF-A03, A13).
- NCEER-96-0001 "Dynamic Response of Unreinforced Masonry Buildings with Flexible Diaphragms," by A.C. Costley and D.P. Abrams, 10/10/96, (PB97-133573, MF-A03, A15).
- NCEER-96-0002 "State of the Art Review: Foundations and Retaining Structures," by I. Po Lam, to be published.
- NCEER-96-0003 "Ductility of Rectangular Reinforced Concrete Bridge Columns with Moderate Confinement," by N. Wehbe, M. Saiidi, D. Sanders and B. Douglas, 11/7/96, (PB97-133557, A06, MF-A02).
- NCEER-96-0004 "Proceedings of the Long-Span Bridge Seismic Research Workshop," edited by I.G. Buckle and I.M. Friedland, to be published.
- NCEER-96-0005 "Establish Representative Pier Types for Comprehensive Study: Eastern United States," by J. Kulicki and Z. Prucz, 5/28/96, (PB98-119217, A07, MF-A02).
- NCEER-96-0006 "Establish Representative Pier Types for Comprehensive Study: Western United States," by R. Imbsen, R.A. Schamber and T.A. Osterkamp, 5/28/96, (PB98-118607, A07, MF-A02).
- NCEER-96-0007 "Nonlinear Control Techniques for Dynamical Systems with Uncertain Parameters," by R.G. Ghanem and M.I. Bujakov, 5/27/96, (PB97-100259, A17, MF-A03).
- NCEER-96-0008 "Seismic Evaluation of a 30-Year Old Non-Ductile Highway Bridge Pier and Its Retrofit," by J.B. Mander, B. Mahmoodzadegan, S. Bhadra and S.S. Chen, 5/31/96, (PB97-110902, MF-A03, A10).
- NCEER-96-0009 "Seismic Performance of a Model Reinforced Concrete Bridge Pier Before and After Retrofit," by J.B. Mander, J.H. Kim and C.A. Ligozio, 5/31/96, (PB97-110910, MF-A02, A10).
- NCEER-96-0010 "IDARC2D Version 4.0: A Computer Program for the Inelastic Damage Analysis of Buildings," by R.E. Valles, A.M. Reinhorn, S.K. Kunnath, C. Li and A. Madan, 6/3/96, (PB97-100234, A17, MF-A03).
- NCEER-96-0011 "Estimation of the Economic Impact of Multiple Lifeline Disruption: Memphis Light, Gas and Water Division Case Study," by S.E. Chang, H.A. Seligson and R.T. Eguchi, 8/16/96, (PB97-133490, A11, MF-A03).
- NCEER-96-0012 "Proceedings from the Sixth Japan-U.S. Workshop on Earthquake Resistant Design of Lifeline Facilities and Countermeasures Against Soil Liquefaction, Edited by M. Hamada and T. O'Rourke, 9/11/96, (PB97-133581, A99, MF-A06).
- NCEER-96-0013 "Chemical Hazards, Mitigation and Preparedness in Areas of High Seismic Risk: A Methodology for Estimating the Risk of Post-Earthquake Hazardous Materials Release," by H.A. Seligson, R.T. Eguchi, K.J. Tierney and K. Richmond, 11/7/96, (PB97-133565, MF-A02, A08).
- NCEER-96-0014 "Response of Steel Bridge Bearings to Reversed Cyclic Loading," by J.B. Mander, D-K. Kim, S.S. Chen and G.J. Premus, 11/13/96, (PB97-140735, A12, MF-A03).
- NCEER-96-0015 "Highway Culvert Performance During Past Earthquakes," by T.L. Youd and C.J. Beckman, 11/25/96, (PB97-133532, A06, MF-A01).
- NCEER-97-0001 "Evaluation, Prevention and Mitigation of Pounding Effects in Building Structures," by R.E. Valles and A.M. Reinhorn, 2/20/97, (PB97-159552, A14, MF-A03).
- NCEER-97-0002 "Seismic Design Criteria for Bridges and Other Highway Structures," by C. Rojahn, R. Mayes, D.G. Anderson, J. Clark, J.H. Hom, R.V. Nutt and M.J. O'Rourke, 4/30/97, (PB97-194658, A06, MF-A03).

- NCEER-97-0003 "Proceedings of the U.S.-Italian Workshop on Seismic Evaluation and Retrofit," Edited by D.P. Abrams and G.M. Calvi, 3/19/97, (PB97-194666, A13, MF-A03).
- NCEER-97-0004 "Investigation of Seismic Response of Buildings with Linear and Nonlinear Fluid Viscous Dampers," by A.A. Seleemah and M.C. Constantinou, 5/21/97, (PB98-109002, A15, MF-A03).
- NCEER-97-0005 "Proceedings of the Workshop on Earthquake Engineering Frontiers in Transportation Facilities," edited by G.C. Lee and I.M. Friedland, 8/29/97, (PB98-128911, A25, MR-A04).
- NCEER-97-0006 "Cumulative Seismic Damage of Reinforced Concrete Bridge Piers," by S.K. Kunnath, A. El-Bahy, A. Taylor and W. Stone, 9/2/97, (PB98-108814, A11, MF-A03).
- NCEER-97-0007 "Structural Details to Accommodate Seismic Movements of Highway Bridges and Retaining Walls," by R.A. Imbsen, R.A. Schamber, E. Thorkildsen, A. Kartoum, B.T. Martin, T.N. Rosser and J.M. Kulicki, 9/3/97, (PB98-108996, A09, MF-A02).
- NCEER-97-0008 "A Method for Earthquake Motion-Damage Relationships with Application to Reinforced Concrete Frames," by A. Singhal and A.S. Kiremidjian, 9/10/97, (PB98-108988, A13, MF-A03).
- NCEER-97-0009 "Seismic Analysis and Design of Bridge Abutments Considering Sliding and Rotation," by K. Fishman and R. Richards, Jr., 9/15/97, (PB98-108897, A06, MF-A02).
- NCEER-97-0010 "Proceedings of the FHWA/NCEER Workshop on the National Representation of Seismic Ground Motion for New and Existing Highway Facilities," edited by I.M. Friedland, M.S. Power and R.L. Mayes, 9/22/97, (PB98-128903, A21, MF-A04).
- NCEER-97-0011 "Seismic Analysis for Design or Retrofit of Gravity Bridge Abutments," by K.L. Fishman, R. Richards, Jr. and R.C. Divito, 10/2/97, (PB98-128937, A08, MF-A02).
- NCEER-97-0012 "Evaluation of Simplified Methods of Analysis for Yielding Structures," by P. Tsopelas, M.C. Constantinou, C.A. Kircher and A.S. Whittaker, 10/31/97, (PB98-128929, A10, MF-A03).
- NCEER-97-0013 "Seismic Design of Bridge Columns Based on Control and Repairability of Damage," by C-T. Cheng and J.B. Mander, 12/8/97, (PB98-144249, A11, MF-A03).
- NCEER-97-0014 "Seismic Resistance of Bridge Piers Based on Damage Avoidance Design," by J.B. Mander and C-T. Cheng, 12/10/97, (PB98-144223, A09, MF-A02).
- NCEER-97-0015 "Seismic Response of Nominally Symmetric Systems with Strength Uncertainty," by S. Balopoulou and M. Grigoriu, 12/23/97, (PB98-153422, A11, MF-A03).
- NCEER-97-0016 "Evaluation of Seismic Retrofit Methods for Reinforced Concrete Bridge Columns," by T.J. Wipf, F.W. Klaiber and F.M. Russo, 12/28/97, (PB98-144215, A12, MF-A03).
- NCEER-97-0017 "Seismic Fragility of Existing Conventional Reinforced Concrete Highway Bridges," by C.L. Mullen and A.S. Cakmak, 12/30/97, (PB98-153406, A08, MF-A02).
- NCEER-97-0018 "Loss Assessment of Memphis Buildings," edited by D.P. Abrams and M. Shinozuka, 12/31/97, (PB98-144231, A13, MF-A03).
- NCEER-97-0019 "Seismic Evaluation of Frames with Infill Walls Using Quasi-static Experiments," by K.M. Mosalam, R.N. White and P. Gergely, 12/31/97, (PB98-153455, A07, MF-A02).
- NCEER-97-0020 "Seismic Evaluation of Frames with Infill Walls Using Pseudo-dynamic Experiments," by K.M. Mosalam, R.N. White and P. Gergely, 12/31/97, (PB98-153430, A07, MF-A02).
- NCEER-97-0021 "Computational Strategies for Frames with Infill Walls: Discrete and Smeared Crack Analyses and Seismic Fragility," by K.M. Mosalam, R.N. White and P. Gergely, 12/31/97, (PB98-153414, A10, MF-A02).

- NCEER-97-0022 "Proceedings of the NCEER Workshop on Evaluation of Liquefaction Resistance of Soils," edited by T.L. Youd and I.M. Idriss, 12/31/97, (PB98-155617, A15, MF-A03).
- MCEER-98-0001 "Extraction of Nonlinear Hysteretic Properties of Seismically Isolated Bridges from Quick-Release Field Tests," by Q. Chen, B.M. Douglas, E.M. Maragakis and I.G. Buckle, 5/26/98, (PB99-118838, A06, MF-A01).
- MCEER-98-0002 "Methodologies for Evaluating the Importance of Highway Bridges," by A. Thomas, S. Eshenaur and J. Kulicki, 5/29/98, (PB99-118846, A10, MF-A02).
- MCEER-98-0003 "Capacity Design of Bridge Piers and the Analysis of Overstrength," by J.B. Mander, A. Dutta and P. Goel, 6/1/98, (PB99-118853, A09, MF-A02).
- MCEER-98-0004 "Evaluation of Bridge Damage Data from the Loma Prieta and Northridge, California Earthquakes," by N. Basoz and A. Kiremidjian, 6/2/98, (PB99-118861, A15, MF-A03).
- MCEER-98-0005 "Screening Guide for Rapid Assessment of Liquefaction Hazard at Highway Bridge Sites," by T. L. Youd, 6/16/98, (PB99-118879, A06, not available on microfiche).
- MCEER-98-0006 "Structural Steel and Steel/Concrete Interface Details for Bridges," by P. Ritchie, N. Kauh and J. Kulicki, 7/13/98, (PB99-118945, A06, MF-A01).
- MCEER-98-0007 "Capacity Design and Fatigue Analysis of Confined Concrete Columns," by A. Dutta and J.B. Mander, 7/14/98, (PB99-118960, A14, MF-A03).
- MCEER-98-0008 "Proceedings of the Workshop on Performance Criteria for Telecommunication Services Under Earthquake Conditions," edited by A.J. Schiff, 7/15/98, (PB99-118952, A08, MF-A02).
- MCEER-98-0009 "Fatigue Analysis of Unconfined Concrete Columns," by J.B. Mander, A. Dutta and J.H. Kim, 9/12/98, (PB99-123655, A10, MF-A02).
- MCEER-98-0010 "Centrifuge Modeling of Cyclic Lateral Response of Pile-Cap Systems and Seat-Type Abutments in Dry Sands," by A.D. Gadre and R. Dobry, 10/2/98, (PB99-123606, A13, MF-A03).
- MCEER-98-0011 "IDARC-BRIDGE: A Computational Platform for Seismic Damage Assessment of Bridge Structures," by A.M. Reinhorn, V. Simeonov, G. Mylonakis and Y. Reichman, 10/2/98, (PB99-162919, A15, MF-A03).
- MCEER-98-0012 "Experimental Investigation of the Dynamic Response of Two Bridges Before and After Retrofitting with Elastomeric Bearings," by D.A. Wendichansky, S.S. Chen and J.B. Mander, 10/2/98, (PB99-162927, A15, MF-A03).
- MCEER-98-0013 "Design Procedures for Hinge Restrainers and Hinge Sear Width for Multiple-Frame Bridges," by R. Des Roches and G.L. Fenves, 11/3/98, (PB99-140477, A13, MF-A03).
- MCEER-98-0014 "Response Modification Factors for Seismically Isolated Bridges," by M.C. Constantinou and J.K. Quarshie, 11/3/98, (PB99-140485, A14, MF-A03).
- MCEER-98-0015 "Proceedings of the U.S.-Italy Workshop on Seismic Protective Systems for Bridges," edited by I.M. Friedland and M.C. Constantinou, 11/3/98, (PB2000-101711, A22, MF-A04).
- MCEER-98-0016 "Appropriate Seismic Reliability for Critical Equipment Systems: Recommendations Based on Regional Analysis of Financial and Life Loss," by K. Porter, C. Scawthorn, C. Taylor and N. Blais, 11/10/98, (PB99-157265, A08, MF-A02).
- MCEER-98-0017 "Proceedings of the U.S. Japan Joint Seminar on Civil Infrastructure Systems Research," edited by M. Shinozuka and A. Rose, 11/12/98, (PB99-156713, A16, MF-A03).
- MCEER-98-0018 "Modeling of Pile Footings and Drilled Shafts for Seismic Design," by I. PoLam, M. Kapuskar and D. Chaudhuri, 12/21/98, (PB99-157257, A09, MF-A02).

- MCEER-99-0001 "Seismic Evaluation of a Masonry Infilled Reinforced Concrete Frame by Pseudodynamic Testing," by S.G. Buonopane and R.N. White, 2/16/99, (PB99-162851, A09, MF-A02).
- MCEER-99-0002 "Response History Analysis of Structures with Seismic Isolation and Energy Dissipation Systems: Verification Examples for Program SAP2000," by J. Scheller and M.C. Constantinou, 2/22/99, (PB99-162869, A08, MF-A02).
- MCEER-99-0003 "Experimental Study on the Seismic Design and Retrofit of Bridge Columns Including Axial Load Effects," by A. Dutta, T. Kokorina and J.B. Mander, 2/22/99, (PB99-162877, A09, MF-A02).
- MCEER-99-0004 "Experimental Study of Bridge Elastomeric and Other Isolation and Energy Dissipation Systems with Emphasis on Uplift Prevention and High Velocity Near-source Seismic Excitation," by A. Kasalanati and M. C. Constantinou, 2/26/99, (PB99-162885, A12, MF-A03).
- MCEER-99-0005 "Truss Modeling of Reinforced Concrete Shear-flexure Behavior," by J.H. Kim and J.B. Mander, 3/8/99, (PB99-163693, A12, MF-A03).
- MCEER-99-0006 "Experimental Investigation and Computational Modeling of Seismic Response of a 1:4 Scale Model Steel Structure with a Load Balancing Supplemental Damping System," by G. Pekcan, J.B. Mander and S.S. Chen, 4/2/99, (PB99-162893, A11, MF-A03).
- MCEER-99-0007 "Effect of Vertical Ground Motions on the Structural Response of Highway Bridges," by M.R. Button, C.J. Cronin and R.L. Mayes, 4/10/99, (PB2000-101411, A10, MF-A03).
- MCEER-99-0008 "Seismic Reliability Assessment of Critical Facilities: A Handbook, Supporting Documentation, and Model Code Provisions," by G.S. Johnson, R.E. Sheppard, M.D. Quilici, S.J. Eder and C.R. Scawthorn, 4/12/99, (PB2000-101701, A18, MF-A04).
- MCEER-99-0009 "Impact Assessment of Selected MCEER Highway Project Research on the Seismic Design of Highway Structures," by C. Rojahn, R. Mayes, D.G. Anderson, J.H. Clark, D'Appolonia Engineering, S. Gloyd and R.V. Nutt, 4/14/99, (PB99-162901, A10, MF-A02).
- MCEER-99-0010 "Site Factors and Site Categories in Seismic Codes," by R. Dobry, R. Ramos and M.S. Power, 7/19/99, (PB2000-101705, A08, MF-A02).
- MCEER-99-0011 "Restrainer Design Procedures for Multi-Span Simply-Supported Bridges," by M.J. Randall, M. Saiidi, E. Maragakis and T. Isakovic, 7/20/99, (PB2000-101702, A10, MF-A02).
- MCEER-99-0012 "Property Modification Factors for Seismic Isolation Bearings," by M.C. Constantinou, P. Tsopelas, A. Kasalanati and E. Wolff, 7/20/99, (PB2000-103387, A11, MF-A03).
- MCEER-99-0013 "Critical Seismic Issues for Existing Steel Bridges," by P. Ritchie, N. Kauh and J. Kulicki, 7/20/99, (PB2000-101697, A09, MF-A02).
- MCEER-99-0014 "Nonstructural Damage Database," by A. Kao, T.T. Soong and A. Vender, 7/24/99, (PB2000-101407, A06, MF-A01).
- MCEER-99-0015 "Guide to Remedial Measures for Liquefaction Mitigation at Existing Highway Bridge Sites," by H.G. Cooke and J. K. Mitchell, 7/26/99, (PB2000-101703, A11, MF-A03).
- MCEER-99-0016 "Proceedings of the MCEER Workshop on Ground Motion Methodologies for the Eastern United States," edited by N. Abrahamson and A. Becker, 8/11/99, (PB2000-103385, A07, MF-A02).
- MCEER-99-0017 "Quindío, Colombia Earthquake of January 25, 1999: Reconnaissance Report," by A.P. Asfura and P.J. Flores, 10/4/99, (PB2000-106893, A06, MF-A01).
- MCEER-99-0018 "Hysteretic Models for Cyclic Behavior of Deteriorating Inelastic Structures," by M.V. Sivaselvan and A.M. Reinhorn, 11/5/99, (PB2000-103386, A08, MF-A02).

- MCEER-99-0019 "Proceedings of the 7th U.S.- Japan Workshop on Earthquake Resistant Design of Lifeline Facilities and Countermeasures Against Soil Liquefaction," edited by T.D. O'Rourke, J.P. Bardet and M. Hamada, 11/19/99, (PB2000-103354, A99, MF-A06).
- MCEER-99-0020 "Development of Measurement Capability for Micro-Vibration Evaluations with Application to Chip Fabrication Facilities," by G.C. Lee, Z. Liang, J.W. Song, J.D. Shen and W.C. Liu, 12/1/99, (PB2000-105993, A08, MF-A02).
- MCEER-99-0021 "Design and Retrofit Methodology for Building Structures with Supplemental Energy Dissipating Systems," by G. Pekcan, J.B. Mander and S.S. Chen, 12/31/99, (PB2000-105994, A11, MF-A03).
- MCEER-00-0001 "The Marmara, Turkey Earthquake of August 17, 1999: Reconnaissance Report," edited by C. Scawthorn; with major contributions by M. Bruneau, R. Eguchi, T. Holzer, G. Johnson, J. Mander, J. Mitchell, W. Mitchell, A. Papageorgiou, C. Scaethorn, and G. Webb, 3/23/00, (PB2000-106200, A11, MF-A03).
- MCEER-00-0002 "Proceedings of the MCEER Workshop for Seismic Hazard Mitigation of Health Care Facilities," edited by G.C. Lee, M. Ettouney, M. Grigoriu, J. Hauer and J. Nigg, 3/29/00, (PB2000-106892, A08, MF-A02).
- MCEER-00-0003 "The Chi-Chi, Taiwan Earthquake of September 21, 1999: Reconnaissance Report," edited by G.C. Lee and C.H. Loh, with major contributions by G.C. Lee, M. Bruneau, I.G. Buckle, S.E. Chang, P.J. Flores, T.D. O'Rourke, M. Shinozuka, T.T. Soong, C-H. Loh, K-C. Chang, Z-J. Chen, J-S. Hwang, M-L. Lin, G-Y. Liu, K-C. Tsai, G.C. Yao and C-L. Yen, 4/30/00, (PB2001-100980, A10, MF-A02).
- MCEER-00-0004 "Seismic Retrofit of End-Sway Frames of Steel Deck-Truss Bridges with a Supplemental Tendon System: Experimental and Analytical Investigation," by G. Pekcan, J.B. Mander and S.S. Chen, 7/1/00, (PB2001-100982, A10, MF-A02).
- MCEER-00-0005 "Sliding Fragility of Unrestrained Equipment in Critical Facilities," by W.H. Chong and T.T. Soong, 7/5/00, (PB2001-100983, A08, MF-A02).
- MCEER-00-0006 "Seismic Response of Reinforced Concrete Bridge Pier Walls in the Weak Direction," by N. Abo-Shadi, M. Saiidi and D. Sanders, 7/17/00, (PB2001-100981, A17, MF-A03).
- MCEER-00-0007 "Low-Cycle Fatigue Behavior of Longitudinal Reinforcement in Reinforced Concrete Bridge Columns," by J. Brown and S.K. Kunnath, 7/23/00, (PB2001-104392, A08, MF-A02).
- MCEER-00-0008 "Soil Structure Interaction of Bridges for Seismic Analysis," I. PoLam and H. Law, 9/25/00, (PB2001-105397, A08, MF-A02).
- MCEER-00-0009 "Proceedings of the First MCEER Workshop on Mitigation of Earthquake Disaster by Advanced Technologies (MEDAT-1), edited by M. Shinozuka, D.J. Inman and T.D. O'Rourke, 11/10/00, (PB2001-105399, A14, MF-A03).
- MCEER-00-0010 "Development and Evaluation of Simplified Procedures for Analysis and Design of Buildings with Passive Energy Dissipation Systems, Revision 01," by O.M. Ramirez, M.C. Constantinou, C.A. Kircher, A.S. Whittaker, M.W. Johnson, J.D. Gomez and C. Chrysostomou, 11/16/01, (PB2001-105523, A23, MF-A04).
- MCEER-00-0011 "Dynamic Soil-Foundation-Structure Interaction Analyses of Large Caissons," by C-Y. Chang, C-M. Mok, Z-L. Wang, R. Settgast, F. Waggoner, M.A. Ketchum, H.M. Gonnermann and C-C. Chin, 12/30/00, (PB2001-104373, A07, MF-A02).
- MCEER-00-0012 "Experimental Evaluation of Seismic Performance of Bridge Restrainers," by A.G. Vlassis, E.M. Maragakis and M. Saiid Saiidi, 12/30/00, (PB2001-104354, A09, MF-A02).
- MCEER-00-0013 "Effect of Spatial Variation of Ground Motion on Highway Structures," by M. Shinozuka, V. Saxena and G. Deodatis, 12/31/00, (PB2001-108755, A13, MF-A03).
- MCEER-00-0014 "A Risk-Based Methodology for Assessing the Seismic Performance of Highway Systems," by S.D. Werner, C.E. Taylor, J.E. Moore, II, J.S. Walton and S. Cho, 12/31/00, (PB2001-108756, A14, MF-A03).


- MCEER-01-0001 "Experimental Investigation of P-Delta Effects to Collapse During Earthquakes," by D. Vian and M. Bruneau, 6/25/01, (PB2002-100534, A17, MF-A03).
- MCEER-01-0002 "Proceedings of the Second MCEER Workshop on Mitigation of Earthquake Disaster by Advanced Technologies (MEDAT-2)," edited by M. Bruneau and D.J. Inman, 7/23/01, (PB2002-100434, A16, MF-A03).
- MCEER-01-0003 "Sensitivity Analysis of Dynamic Systems Subjected to Seismic Loads," by C. Roth and M. Grigoriu, 9/18/01, (PB2003-100884, A12, MF-A03).
- MCEER-01-0004 "Overcoming Obstacles to Implementing Earthquake Hazard Mitigation Policies: Stage 1 Report," by D.J. Alesch and W.J. Petak, 12/17/01, (PB2002-107949, A07, MF-A02).
- MCEER-01-0005 "Updating Real-Time Earthquake Loss Estimates: Methods, Problems and Insights," by C.E. Taylor, S.E. Chang and R.T. Eguchi, 12/17/01, (PB2002-107948, A05, MF-A01).
- MCEER-01-0006 "Experimental Investigation and Retrofit of Steel Pile Foundations and Pile Bents Under Cyclic Lateral Loadings," by A. Shama, J. Mander, B. Blabac and S. Chen, 12/31/01, (PB2002-107950, A13, MF-A03).
- MCEER-02-0001 "Assessment of Performance of Bolu Viaduct in the 1999 Duzce Earthquake in Turkey" by P.C. Roussis, M.C. Constantinou, M. Erdik, E. Durukal and M. Dicleli, 5/8/02, (PB2003-100883, A08, MF-A02).
- MCEER-02-0002 "Seismic Behavior of Rail Counterweight Systems of Elevators in Buildings," by M.P. Singh, Rildova and L.E. Suarez, 5/27/02. (PB2003-100882, A11, MF-A03).
- MCEER-02-0003 "Development of Analysis and Design Procedures for Spread Footings," by G. Mylonakis, G. Gazetas, S. Nikolaou and A. Chauncey, 10/02/02, (PB2004-101636, A13, MF-A03, CD-A13).
- MCEER-02-0004 "Bare-Earth Algorithms for Use with SAR and LIDAR Digital Elevation Models," by C.K. Huyck, R.T. Eguchi and B. Houshmand, 10/16/02, (PB2004-101637, A07, CD-A07).
- MCEER-02-0005 "Review of Energy Dissipation of Compression Members in Concentrically Braced Frames," by K.Lee and M. Bruneau, 10/18/02, (PB2004-101638, A10, CD-A10).
- MCEER-03-0001 "Experimental Investigation of Light-Gauge Steel Plate Shear Walls for the Seismic Retrofit of Buildings" by J. Berman and M. Bruneau, 5/2/03, (PB2004-101622, A10, MF-A03, CD-A10).
- MCEER-03-0002 "Statistical Analysis of Fragility Curves," by M. Shinozuka, M.Q. Feng, H. Kim, T. Uzawa and T. Ueda, 6/16/03, (PB2004-101849, A09, CD-A09).
- MCEER-03-0003 "Proceedings of the Eighth U.S.-Japan Workshop on Earthquake Resistant Design of Lifeline Facilities and Countermeasures Against Liquefaction," edited by M. Hamada, J.P. Bardet and T.D. O'Rourke, 6/30/03, (PB2004-104386, A99, CD-A99).
- MCEER-03-0004 "Proceedings of the PRC-US Workshop on Seismic Analysis and Design of Special Bridges," edited by L.C. Fan and G.C. Lee, 7/15/03, (PB2004-104387, A14, CD-A14).
- MCEER-03-0005 "Urban Disaster Recovery: A Framework and Simulation Model," by S.B. Miles and S.E. Chang, 7/25/03, (PB2004-104388, A07, CD-A07).
- MCEER-03-0006 "Behavior of Underground Piping Joints Due to Static and Dynamic Loading," by R.D. Meis, M. Maragakis and R. Siddharthan, 11/17/03, (PB2005-102194, A13, MF-A03, CD-A00).
- MCEER-03-0007 "Seismic Vulnerability of Timber Bridges and Timber Substructures," by A.A. Shama, J.B. Mander, I.M. Friedland and D.R. Allicock, 12/15/03.
- MCEER-04-0001 "Experimental Study of Seismic Isolation Systems with Emphasis on Secondary System Response and Verification of Accuracy of Dynamic Response History Analysis Methods," by E. Wolff and M. Constantinou, 1/16/04 (PB2005-102195, A99, MF-E08, CD-A00).

- MCEER-04-0002 "Tension, Compression and Cyclic Testing of Engineered Cementitious Composite Materials," by K. Kesner and S.L. Billington, 3/1/04, (PB2005-102196, A08, CD-A08).
- MCEER-04-0003 "Cyclic Testing of Braces Laterally Restrained by Steel Studs to Enhance Performance During Earthquakes," by O.C. Celik, J.W. Berman and M. Bruneau, 3/16/04, (PB2005-102197, A13, MF-A03, CD-A00).
- MCEER-04-0004 "Methodologies for Post Earthquake Building Damage Detection Using SAR and Optical Remote Sensing: Application to the August 17, 1999 Marmara, Turkey Earthquake," by C.K. Huyck, B.J. Adams, S. Cho, R.T. Eguchi, B. Mansouri and B. Houshmand, 6/15/04, (PB2005-104888, A10, CD-A00).
- MCEER-04-0005 "Nonlinear Structural Analysis Towards Collapse Simulation: A Dynamical Systems Approach," by M.V. Sivaselvan and A.M. Reinhorn, 6/16/04, (PB2005-104889, A11, MF-A03, CD-A00).
- MCEER-04-0006 "Proceedings of the Second PRC-US Workshop on Seismic Analysis and Design of Special Bridges," edited by G.C. Lee and L.C. Fan, 6/25/04, (PB2005-104890, A16, CD-A00).
- MCEER-04-0007 "Seismic Vulnerability Evaluation of Axially Loaded Steel Built-up Laced Members," by K. Lee and M. Bruneau, 6/30/04, (PB2005-104891, A16, CD-A00).
- MCEER-04-0008 "Evaluation of Accuracy of Simplified Methods of Analysis and Design of Buildings with Damping Systems for Near-Fault and for Soft-Soil Seismic Motions," by E.A. Pavlou and M.C. Constantinou, 8/16/04, (PB2005-104892, A08, MF-A02, CD-A00).
- MCEER-04-0009 "Assessment of Geotechnical Issues in Acute Care Facilities in California," by M. Lew, T.D. O'Rourke, R. Dobry and M. Koch, 9/15/04, (PB2005-104893, A08, CD-A00).
- MCEER-04-0010 "Scissor-Jack-Damper Energy Dissipation System," by A.N. Sigaher-Boyle and M.C. Constantinou, 12/1/04 (PB2005-108221).
- MCEER-04-0011 "Seismic Retrofit of Bridge Steel Truss Piers Using a Controlled Rocking Approach," by M. Pollino and M. Bruneau, 12/20/04 (PB2006-105795).
- MCEER-05-0001 "Experimental and Analytical Studies of Structures Seismically Isolated with an Uplift-Restraint Isolation System," by P.C. Roussis and M.C. Constantinou, 1/10/05 (PB2005-108222).
- MCEER-05-0002 "A Versatile Experimentation Model for Study of Structures Near Collapse Applied to Seismic Evaluation of Irregular Structures," by D. Kusumastuti, A.M. Reinhorn and A. Rutenberg, 3/31/05 (PB2006-101523).
- MCEER-05-0003 "Proceedings of the Third PRC-US Workshop on Seismic Analysis and Design of Special Bridges," edited by L.C. Fan and G.C. Lee, 4/20/05, (PB2006-105796).
- MCEER-05-0004 "Approaches for the Seismic Retrofit of Braced Steel Bridge Piers and Proof-of-Concept Testing of an Eccentrically Braced Frame with Tubular Link," by J.W. Berman and M. Bruneau, 4/21/05 (PB2006-101524).
- MCEER-05-0005 "Simulation of Strong Ground Motions for Seismic Fragility Evaluation of Nonstructural Components in Hospitals," by A. Wanitkorkul and A. Filiatrault, 5/26/05 (PB2006-500027).
- MCEER-05-0006 "Seismic Safety in California Hospitals: Assessing an Attempt to Accelerate the Replacement or Seismic Retrofit of Older Hospital Facilities," by D.J. Alesch, L.A. Arendt and W.J. Petak, 6/6/05 (PB2006-105794).
- MCEER-05-0007 "Development of Seismic Strengthening and Retrofit Strategies for Critical Facilities Using Engineered Cementitious Composite Materials," by K. Kesner and S.L. Billington, 8/29/05 (PB2006-111701).
- MCEER-05-0008 "Experimental and Analytical Studies of Base Isolation Systems for Seismic Protection of Power Transformers," by N. Murota, M.Q. Feng and G-Y. Liu, 9/30/05 (PB2006-111702).
- MCEER-05-0009 "3D-BASIS-ME-MB: Computer Program for Nonlinear Dynamic Analysis of Seismically Isolated Structures," by P.C. Tsopelas, P.C. Roussis, M.C. Constantinou, R. Buchanan and A.M. Reinhorn, 10/3/05 (PB2006-111703).

- MCEER-05-0010 "Steel Plate Shear Walls for Seismic Design and Retrofit of Building Structures," by D. Vian and M. Bruneau, 12/15/05 (PB2006-111704).
- MCEER-05-0011 "The Performance-Based Design Paradigm," by M.J. Astrella and A. Whittaker, 12/15/05 (PB2006-111705).
- MCEER-06-0001 "Seismic Fragility of Suspended Ceiling Systems," H. Badillo-Almaraz, A.S. Whittaker, A.M. Reinhorn and G.P. Cimellaro, 2/4/06 (PB2006-111706).
- MCEER-06-0002 "Multi-Dimensional Fragility of Structures," by G.P. Cimellaro, A.M. Reinhorn and M. Bruneau, 3/1/06 (PB2007-106974, A09, MF-A02, CD A00).
- MCEER-06-0003 "Built-Up Shear Links as Energy Dissipators for Seismic Protection of Bridges," by P. Dusicka, A.M. Itani and I.G. Buckle, 3/15/06 (PB2006-111708).
- MCEER-06-0004 "Analytical Investigation of the Structural Fuse Concept," by R.E. Vargas and M. Bruneau, 3/16/06 (PB2006-111709).
- MCEER-06-0005 "Experimental Investigation of the Structural Fuse Concept," by R.E. Vargas and M. Bruneau, 3/17/06 (PB2006-111710).
- MCEER-06-0006 "Further Development of Tubular Eccentrically Braced Frame Links for the Seismic Retrofit of Braced Steel Truss Bridge Piers," by J.W. Berman and M. Bruneau, 3/27/06 (PB2007-105147).
- MCEER-06-0007 "REDARS Validation Report," by S. Cho, C.K. Huyck, S. Ghosh and R.T. Eguchi, 8/8/06 (PB2007-106983).
- MCEER-06-0008 "Review of Current NDE Technologies for Post-Earthquake Assessment of Retrofitted Bridge Columns," by J.W. Song, Z. Liang and G.C. Lee, 8/21/06 06 (PB2007-106984).
- MCEER-06-0009 "Liquefaction Remediation in Silty Soils Using Dynamic Compaction and Stone Columns," by S. Thevanayagam, G.R. Martin, R. Nashed, T. Shenthan, T. Kanagalingam and N. Ecemis, 8/28/06 06 (PB2007-106985).
- MCEER-06-0010 "Conceptual Design and Experimental Investigation of Polymer Matrix Composite Infill Panels for Seismic Retrofitting," by W. Jung, M. Chiewanichakorn and A.J. Aref, 9/21/06 (PB2007-106986).
- MCEER-06-0011 "A Study of the Coupled Horizontal-Vertical Behavior of Elastomeric and Lead-Rubber Seismic Isolation Bearings," by G.P. Warn and A.S. Whittaker, 9/22/06 (PB2007-108679).
- MCEER-06-0012 "Proceedings of the Fourth PRC-US Workshop on Seismic Analysis and Design of Special Bridges: Advancing Bridge Technologies in Research, Design, Construction and Preservation," Edited by L.C. Fan, G.C. Lee and L. Ziang, 10/12/06 (PB2007-109042).
- MCEER-06-0013 "Cyclic Response and Low Cycle Fatigue Characteristics of Plate Steels," by P. Dusicka, A.M. Itani and I.G. Buckle, 11/1/06 06 (PB2007-106987).
- MCEER-06-0014 "Proceedings of the Second US-Taiwan Bridge Engineering Workshop," edited by W.P. Yen, J. Shen, J-Y. Chen and M. Wang, 11/15/06 (PB2008-500041).
- MCEER-06-0015 "User Manual and Technical Documentation for the REDARSTM Import Wizard," by S. Cho, S. Ghosh, C.K. Huyck and S.D. Werner, 11/30/06 (PB2007-114766).
- MCEER-06-0016 "Hazard Mitigation Strategy and Monitoring Technologies for Urban and Infrastructure Public Buildings: Proceedings of the China-US Workshops," edited by X.Y. Zhou, A.L. Zhang, G.C. Lee and M. Tong, 12/12/06 (PB2008-500018).
- MCEER-07-0001 "Static and Kinetic Coefficients of Friction for Rigid Blocks," by C. Kafali, S. Fathali, M. Grigoriu and A.S. Whittaker, 3/20/07 (PB2007-114767).
- MCEER-07-0002 "Hazard Mitigation Investment Decision Making: Organizational Response to Legislative Mandate," by L.A. Arendt, D.J. Alesch and W.J. Petak, 4/9/07 (PB2007-114768).


- MCEER-07-0003 “Seismic Behavior of Bidirectional-Resistant Ductile End Diaphragms with Unbonded Braces in Straight or Skewed Steel Bridges,” by O. Celik and M. Bruneau, 4/11/07 (PB2008-105141).
- MCEER-07-0004 “Modeling Pile Behavior in Large Pile Groups Under Lateral Loading,” by A.M. Dodds and G.R. Martin, 4/16/07(PB2008-105142).
- MCEER-07-0005 “Experimental Investigation of Blast Performance of Seismically Resistant Concrete-Filled Steel Tube Bridge Piers,” by S. Fujikura, M. Bruneau and D. Lopez-Garcia, 4/20/07 (PB2008-105143).
- MCEER-07-0006 “Seismic Analysis of Conventional and Isolated Liquefied Natural Gas Tanks Using Mechanical Analogs,” by I.P. Christovasilis and A.S. Whittaker, 5/1/07.
- MCEER-07-0007 “Experimental Seismic Performance Evaluation of Isolation/Restraint Systems for Mechanical Equipment – Part 1: Heavy Equipment Study,” by S. Fathali and A. Filiatrault, 6/6/07 (PB2008-105144).
- MCEER-07-0008 “Seismic Vulnerability of Timber Bridges and Timber Substructures,” by A.A. Sharma, J.B. Mander, I.M. Friedland and D.R. Allicock, 6/7/07 (PB2008-105145).
- MCEER-07-0009 “Experimental and Analytical Study of the XY-Friction Pendulum (XY-FP) Bearing for Bridge Applications,” by C.C. Marin-Artieda, A.S. Whittaker and M.C. Constantinou, 6/7/07 (PB2008-105191).
- MCEER-07-0010 “Proceedings of the PRC-US Earthquake Engineering Forum for Young Researchers,” Edited by G.C. Lee and X.Z. Qi, 6/8/07.
- MCEER-07-0011 “Design Recommendations for Perforated Steel Plate Shear Walls,” by R. Purba and M. Bruneau, 6/18/07, (PB2008-105192).
- MCEER-07-0012 “Performance of Seismic Isolation Hardware Under Service and Seismic Loading,” by M.C. Constantinou, A.S. Whittaker, Y. Kalpakidis, D.M. Fenz and G.P. Warn, 8/27/07, (PB2008-105193).
- MCEER-07-0013 “Experimental Evaluation of the Seismic Performance of Hospital Piping Subassemblies,” by E.R. Goodwin, E. Maragakis and A.M. Itani, 9/4/07, (PB2008-105194).
- MCEER-07-0014 “A Simulation Model of Urban Disaster Recovery and Resilience: Implementation for the 1994 Northridge Earthquake,” by S. Miles and S.E. Chang, 9/7/07, (PB2008-106426).
- MCEER-07-0015 “Statistical and Mechanistic Fragility Analysis of Concrete Bridges,” by M. Shinozuka, S. Banerjee and S-H. Kim, 9/10/07, (PB2008-106427).
- MCEER-07-0016 “Three-Dimensional Modeling of Inelastic Buckling in Frame Structures,” by M. Schachter and AM. Reinhorn, 9/13/07, (PB2008-108125).
- MCEER-07-0017 “Modeling of Seismic Wave Scattering on Pile Groups and Caissons,” by I. Po Lam, H. Law and C.T. Yang, 9/17/07 (PB2008-108150).
- MCEER-07-0018 “Bridge Foundations: Modeling Large Pile Groups and Caissons for Seismic Design,” by I. Po Lam, H. Law and G.R. Martin (Coordinating Author), 12/1/07 (PB2008-111190).
- MCEER-07-0019 “Principles and Performance of Roller Seismic Isolation Bearings for Highway Bridges,” by G.C. Lee, Y.C. Ou, Z. Liang, T.C. Niu and J. Song, 12/10/07.
- MCEER-07-0020 “Centrifuge Modeling of Permeability and Pinning Reinforcement Effects on Pile Response to Lateral Spreading,” by L.L. Gonzalez-Lagos, T. Abdoun and R. Dobry, 12/10/07 (PB2008-111191).
- MCEER-07-0021 “Damage to the Highway System from the Pisco, Perú Earthquake of August 15, 2007,” by J.S. O’Connor, L. Mesa and M. Nykamp, 12/10/07, (PB2008-108126).
- MCEER-07-0022 “Experimental Seismic Performance Evaluation of Isolation/Restraint Systems for Mechanical Equipment – Part 2: Light Equipment Study,” by S. Fathali and A. Filiatrault, 12/13/07 (PB2008-111192).

- MCEER-07-0023 "Fragility Considerations in Highway Bridge Design," by M. Shinozuka, S. Banerjee and S.H. Kim, 12/14/07 (PB2008-111193).
- MCEER-07-0024 "Performance Estimates for Seismically Isolated Bridges," by G.P. Warn and A.S. Whittaker, 12/30/07.
- MCEER-08-0001 "Seismic Performance of Steel Girder Bridge Superstructures with Conventional Cross Frames," by L.P. Carden, A.M. Itani and I.G. Buckle, 1/7/08.
- MCEER-08-0002 "Seismic Performance of Steel Girder Bridge Superstructures with Ductile End Cross Frames with Seismic Isolators," by L.P. Carden, A.M. Itani and I.G. Buckle, 1/7/08.
- MCEER-08-0003 "Analytical and Experimental Investigation of a Controlled Rocking Approach for Seismic Protection of Bridge Steel Truss Piers," by M. Pollino and M. Bruneau, 1/21/08.
- MCEER-08-0004 "Linking Lifeline Infrastructure Performance and Community Disaster Resilience: Models and Multi-Stakeholder Processes," by S.E. Chang, C. Pasion, K. Tatebe and R. Ahmad, 3/3/08.
- MCEER-08-0005 "Modal Analysis of Generally Damped Linear Structures Subjected to Seismic Excitations," by J. Song, Y-L. Chu, Z. Liang and G.C. Lee, 3/4/08.
- MCEER-08-0006 "System Performance Under Multi-Hazard Environments," by C. Kafali and M. Grigoriu, 3/4/08.
- MCEER-08-0007 "Mechanical Behavior of Multi-Spherical Sliding Bearings," by D.M. Fenz and M.C. Constantinou, 3/6/08.
- MCEER-08-0008 "Post-Earthquake Restoration of the Los Angeles Water Supply System," by T.H.P. Tabucchi and R.A. Davidson, 3/7/08.
- MCEER-08-0009 "Fragility Analysis of Water Supply Systems," by A. Jacobson and M. Grigoriu, 3/10/08.
- MCEER-08-0010 "Seismic Behavior and Ductile Design of Steel Plate Shear Walls, by B. Qu and M. Bruneau, 3/17/08.
- MCEER-08-0011 "Seismic Evaluation and Rehabilitation of Critical Components of Electrical Power Systems," S. Ersoy, B. Feizi, A. Ashrafi and M. Ala Saadeghvaziri, 3/17/08.



EARTHQUAKE ENGINEERING TO EXTREME EVENTS

University at Buffalo, The State University of New York
Red Jacket Quadrangle ■ Buffalo, New York 14261
Phone: (716) 645-3391 ■ Fax: (716) 645-3399
E-mail: mceer@buffalo.edu ■ WWW Site <http://mceer.buffalo.edu>



University at Buffalo *The State University of New York*

ISSN 1520-295X